

**FORMULATION OF NOVEL BUCCAL
MUCOSAL DRUG DELIVERY SYSTEMS
FOR NICOTINE REPLACEMENT
THERAPY (NRT).**

OBINNA CHIKWADO OKEKE

**A thesis submitted in partial fulfilment of the
requirements of the University of Greenwich for the
Degree of Doctor of Philosophy**

January 2017



DECLARATION

“I certify that this work has not been accepted in substance for any degree, and is not concurrently being submitted for any purpose. I also declare that this work is the result of my own investigations except where otherwise identified by references and that I have not plagiarised another’s work”.

Mr. Obinna C. Okeke (Candidate)

Dr J.S. Boateng (First supervisor)

ACKNOWLEDGEMENTS

I would like to express my sincere gratitude to my supervisor, Dr Joshua Boateng, for his enormous support, encouragement and general guidance throughout my research. His constant support and encouragement has led me to believe in myself and give out my best.

I also appreciate the University of Greenwich for providing the facilities and student support within this period. I would like to acknowledge Dr Ian Slipper for all SEM and XRPD techniques as well as Devyani Amin for HPLC analysis. Thanks to all University staff for supporting my program.

I also want to extend my deepest gratitude to my family. Their support and encouragement have led me to the person I am today. I am grateful to Dr Sam and Samantha Owusu-Ware and family for their support.

Finally, to all my roommates, officemates, library IT and assistance team, project students under my supervision and fellow postgraduate students, I want to say I big thank you for your support.

ABSTRACT

Hydroxypropylmethylcellulose (HPMC) and sodium alginate (SA) were used in the formulation of composite wafers and films for potential nicotine (NIC) replacement therapy via the buccal mucosa route. Composite blank (BK), drug loaded (DL) HPMC-SA films (optimized with 2% w/v plasticizer) and wafers (optimized by freeze drying; annealing) were formulated. Further, nicotine stabilisation using MAS (magnesium aluminium silicate) in optimised composite HPMC-SA films and wafers were undertaken. Formulation characterisation was performed using texture analyser (TA) (mechanical and mucoadhesion properties), scanning electron microscopy (SEM) (surface and internal morphology), X-ray diffractometry (XRD) (physical form), attenuated total reflectance – Fourier transform infrared (ATR-FTIR) spectroscopy (physical interactions), thermo gravimetric analysis (TGA), differential scanning calorimetry (DSC), (thermal profiles) and high-performance liquid chromatography (HPLC) (drug loading efficiency and release). NIC stabilisation was required due to challenges of volatility and oxidative degradation associated with NIC especially for films (<35% drug loading efficiency). The incorporation of magnesium aluminium silicate (MAS) (optimum concentration; 0.25% w/v) was therefore necessary to stabilise NIC in HPMC-SA composite wafers and films. Optimized wafers and films (HPMC-SA, 1.25:0.75% w/v) were selected based on the physicochemical properties including drug loading efficiency of wafers and films (>90% NIC). The optimized formulations were used to demonstrate the effect of constituents of simulated saliva (SS) in mucoadhesion, hydration and swelling, and release of NIC, which was further compared with commercially available NiQuitin® strips. In comparison with NiQuitin® strips, optimized wafers and films containing MAS demonstrated NIC stability and a slower release from a mucoadhesive system suitable for targeted buccal drug delivery. Finally, wafers demonstrated a higher permeation flux ($140.55 \pm 47.55 \mu\text{g}/\text{cm}^2/\text{hr}$) than films ($42.31 \pm 5.22 \mu\text{g}/\text{cm}^2/\text{hr}$), and can be considered safe ($\geq 70\%$ viable cells).

CONTENTS

DECLARATION	i
ACKNOWLEDGEMENTS	ii
ABSTRACT	iii
CONTENTS	iv
FIGURES	xiv
TABLES	xx
ABBREVIATIONS	xxii
CHAPTER 1: GENERAL INTRODUCTION AND LITERATURE REVIEW	1
1.1 Overview	1
1.1.1 Impacts of smoking	3
1.2 Pharmaceutical drug delivery systems and dosage forms	5
1.2.1 Solid dosage forms	6
1.2.2 Liquid dosage forms	8
1.2.3 Semi-solid dosage forms	8
1.3 Routes of administration	9
1.3.1 Oral route	9
1.3.2 Rectal route	9
1.3.3 Parenteral routes	10
1.3.4 Respiratory route	10
1.3.5 Topical routes	11

1.3.6	Transmucosal routes.....	12
1.4	Oral transmucosal routes.....	12
1.4.1	The anatomy and physiology of the oral mucosa.....	13
1.4.2	Drug absorption via the oral mucosa.....	16
1.4.3	Advantages of buccal drug delivery.....	18
1.4.4	Influence of physiological factors on drug absorption.....	19
1.5	Bioadhesion / mucoadhesion.....	20
1.5.1	Theories of mucoadhesion	20
1.5.2	Mucoadhesive mechanisms.....	21
1.5.3	Factors affecting mucoadhesion.....	22
1.5.4	Mucoadhesive polymers.....	25
1.5.5	Ideal characteristics of a buccal mucoadhesive polymer	26
1.6	NIC delivery.....	26
1.6.1	Chemical profile of NIC.....	27
1.6.2	Pharmacokinetics of NIC	27
1.7	NIC replacement therapy (NRT).....	31
1.7.1	Transdermal patch.....	32
1.7.2	Oral NRT.....	32
1.7.3	Electronic NIC delivery systems (ENDS).....	34
1.8	Proposed novel buccal delivery system for NRT.....	35
1.9	Polymers used	36

1.9.1	Hydroxypropylmethylcellulose (HPMC).....	36
1.9.2	Sodium alginate.....	37
1.10	Formulation techniques	42
1.10.1	Solvent casting	42
1.10.2	Lyophilisation/freeze drying	43
1.11	Aim and objectives	43
CHAPTER 2: PREPARATION AND CHARACTERISATION OF HPMC AND SODIUM ALGINATE (SA) BASED BUCCAL FILMS AND WAFERS.....		45
2.1	Introduction	45
2.2	Materials and methods	47
2.2.1	Materials.....	47
2.2.2	Preparation of composite films	47
2.2.3	Preparation of composite wafers	47
2.2.4	Texture analysis (TA).....	50
2.2.5	SEM analysis.....	51
2.2.6	Wafer pore analysis	51
2.2.7	TGA.....	52
2.2.8	DSC analysis	52
2.2.9	XRD analysis.....	52
2.2.10	ATR-FTIR analysis	53
2.2.11	Swelling studies.....	53
2.2.12	Mucoadhesion studies	54

2.2.13	HPLC analysis.....	54
2.2.14	Drug content (% loading and recovery)	55
2.2.15	<i>In vitro</i> drug dissolution	55
2.2.16	Statistical analysis	56
2.3	Results	56
2.3.1	Formulation development	56
2.3.2	TA.....	56
2.3.3	SEM analysis.....	61
2.3.4	Wafers pore analysis	63
2.3.5	TGA.....	63
2.3.6	DSC analysis	66
2.3.7	XRD analysis.....	69
2.3.8	ATR-FTIR analysis.....	71
2.3.9	Swelling studies.....	73
2.3.10	Mucoadhesion studies	75
2.3.11	Drug content (% loading / recovery).....	78
2.3.12	<i>In vitro</i> drug dissolution	79
2.4	Discussion	80
2.5	Conclusions	85

CHAPTER 3: PHYSICOCHEMICAL CHARACTERISATION OF FREEZE-DRIED AND SOLVENT EVAPORATED NICOTINE - MAGNESIUM ALUMINUM SILICATE (MAS) COMPLEXES.	86
---	----

3.1	Introduction	86
3.2	Materials and methods	88
3.2.1	Preparation of composite NIC-MAS complex	88
3.2.2	Particle size analysis.....	88
3.2.3	Zeta potential measurement	88
3.2.4	SEM with energy dispersive X-ray analysis	89
3.2.5	XRD analysis.....	89
3.2.6	ATR-FTIR analysis	89
3.2.7	Nuclear magnetic resonance (NMR) spectroscopy	89
3.3	Results	90
3.3.1	Particle size analysis.....	90
3.3.2	SEM with energy dispersive x-ray analysis	90
3.3.3	XRD analysis.....	94
3.3.4	ATR-FTIR analysis	95
3.3.5	Nuclear magnetic resonance (NMR) spectroscopy	99
3.4	Discussion	101
3.5	Conclusion.....	103

CHAPTER 4: NICOTINE STABILIZATION IN COMPOSITE SODIUM ALGINATE BASED WAFERS AND FILMS FOR NICOTINE REPLACEMENT THERAPY.....	104
---	-----

4.1	Introduction	104
4.2	Materials and methods	106

4.2.1	Materials.....	106
4.2.2	Formulation development	106
4.2.3	Mechanical characterization using TA.....	109
4.2.4	SEM.....	109
4.2.5	Wafer porosity.....	109
4.2.6	XRD	109
4.2.7	ATR-FTIR.....	109
4.2.8	Swelling studies.....	109
4.2.9	Mucoadhesion studies	110
4.2.10	HPLC analysis.....	110
4.2.11	Drug content.....	110
4.2.12	<i>In vitro</i> drug dissolution and release kinetics.....	110
4.2.13	Stability studies of optimized wafers and films	110
4.2.14	Statistical analysis	111
4.3	Results	111
4.3.1	Polymer solution properties	111
4.3.2	TA.....	112
4.3.3	Scanning electron microscopy (SEM).....	114
4.3.4	Wafers porosity	116
4.3.5	XRD analysis.....	117
4.3.6	ATR-FTIR spectroscopy	118

4.3.7	Swelling studies.....	120
4.3.8	Mucoadhesion studies	121
4.3.9	Drug content (% loading / recovery).....	123
4.3.10	<i>In vitro</i> drug dissolution	124
4.3.11	NIC Stability studies	127
4.4	Discussion	128
4.5	Conclusion.....	133
CHAPTER 5: EFFECT OF SIMULATED SALIVA ON MUCOADHESION, SWELLING AND DISSOLUTION CHARACTERISTICS - A COMPARISON OF OPTIMIZED FORMULATIONS WITH COMMERCIALY AVAILABLE NRT PRODUCT (NIQUITIN®).....		
5.1	Introduction	134
5.2	Materials and methods	136
5.2.1	Materials.....	136
5.2.2	Selected optimized formulations.....	136
5.2.3	Swelling studies using SS.	137
5.2.4	<i>In vitro</i> mucoadhesion studies using SS.....	137
5.2.5	<i>In vitro</i> drug dissolution studies using SS.....	138
5.2.6	Swelling profile of commercial strip (NiQuitin®) versus optimized wafers and films	138
5.2.7	<i>In vitro</i> mucoadhesion of commercial strip (NiQuitin®) versus optimized wafers and films.....	138

5.2.8 Drug content (% loading / recovery) of commercial strip (NiQuitin®) versus optimized wafers and films.....	138
5.2.9 <i>In vitro</i> drug dissolution of commercial strip (NiQuitin®) versus optimized wafers and films.....	139
5.2.10 HPLC analysis.....	139
5.2.11 Statistical analysis	139
5.2.12 Comparison of release profiles using difference and similarity factors	139
5.3 Results	140
5.3.1 Swelling studies of optimized wafer using simulated saliva.....	140
5.3.2 <i>In vitro</i> mucoadhesion of optimized wafers and films using SS.....	142
5.3.3 <i>In vitro</i> drug dissolution of optimized wafers and films using SS.....	143
5.3.4 Drug release profiles comparison.....	145
5.3.5 Drug release kinetics in SS and PBS.....	146
5.3.6 Swelling profile of commercial strip (NiQuitin®) versus optimized wafers and films	148
5.3.7 <i>In vitro</i> mucoadhesion of commercial strip (NiQuitin®) versus optimized wafers and films.....	149
5.3.8 Drug content (% loading / recovery) of commercial strip (NiQuitin®) versus optimized wafers and films.....	150
5.3.9 <i>In vitro</i> drug dissolution of commercial strip (NiQuitin®) versus optimized wafers and films in simulated saliva.....	151

5.3.10 Drug release kinetics of commercial strip (NiQuitin®) versus optimized wafers and films.....	152
5.4 Discussion	153
5.5 Conclusion.....	158

CHAPTER 6: *EX VIVO* PERMEATION AND TISSUE VIABILITY STUDIES OF OPTIMIZED WAFERS AND FILMS USING PORCINE BUCCAL TISSUE AND ENGINEERED HUMAN BUCCAL TISSUE (EPIORAL™)..... 159

6.1 Introduction	159
6.2 Materials and methods	161
6.2.1 Materials.....	161
6.2.2 Optimized formulations for permeation studies.....	161
6.2.3 <i>Ex vivo</i> buccal permeation studies (Porcine buccal tissue).....	161
6.2.4 <i>In vitro</i> buccal permeation studies (EpiOral™ buccal tissue).....	162
6.2.5 Permeation correlation between buccal permeation using Porcine and EpiOral™ buccal tissues.....	163
6.2.6 Tissue viability (MTT assay) of EpiOral tissues after permeation studies	163
6.3 Results	164
6.3.1 <i>Ex vivo</i> buccal permeation studies (Porcine buccal tissue).....	164
6.3.2 <i>In vitro</i> buccal permeation studies (EpiOral™ buccal tissue).....	165
6.3.3 Permeation correlation between in vitro porcine buccal tissue and EpiOral™ engineered buccal tissue	166

6.3.4 Tissue viability (MTT assay) of EpiOral™ tissues after permeation studies	168
6.4 Discussion	169
6.5 Conclusion	172
CHAPTER 7: SUMMARY COMMENTS, KEY FINDINGS AND FUTURE WORK	173
7.1 Summary comments	173
7.2 Key research findings	177
7.3 Future work	178
CHAPTER 8: References	179
CHAPTER 9: Appendix	194
APPENDIX A: List of publications	194
APPENDIX B: List of abstract and posters from conference proceedings	195
Conference posters	196

FIGURES

Figure 1.1: Structure of the oral mucosa (Patel et al., 2011)	14
Figure 1.2: Common drug application locations on buccal and sublingual mucosa (Lam et al., 2014)	16
Figure 1.3: Paracellular and transcellular pathway across the epithelia cell (Levendoski et al., 2014).	17
Figure 1.4: Chemical structure of NIC	26
Figure 1.5: Concentration profiles (%) of different NIC species at different pHs (adopted from Djordjevic et al., 1997).	28
Figure 1.6: Pathways of NIC metabolism (Benowitz et al., 2009).	30
Figure 1.7: HPMC structure.....	37
Figure 1.8: Alginate structure showing G and M polymer chain blocks.	38
Figure 1.9: Chemical structure of GLY	41
Figure 2.1: Freeze-drying process chart used to produce wafers with appropriate characteristics.	48
Figure 2.2: Hardness profiles of BK and DL HPMC-SA composite wafers showing the resistance to compression deformation with changing SA content ($n = 3, \pm SD$).	57
Figure 2.3: Mechanical (tensile) profiles of HPMC films showing the effect of GLY concentrations on ($n = 3, \pm SD$): (a) tensile strength, (b) elastic modulus and (c) elongation at break.....	59

Figure 2.4: Mechanical (tensile) properties of BK and DL HPMC-SA composite films showing effect of changing SA content on ($n = 3, \pm SD$) (a) tensile strength (b) elongation at break and (c) elastic modulus.	60
Figure 2.5: SEM images of BK HPMC-SA wafers (a) SA 0.00 (b) SA 0.25 (c) SA 0.50 (d) SA 0.75.....	61
Figure 2.6: (i) Surface morphology of HPMC films at different GLY concentrations: (a) 0.0% w/v, (b) 0.5% w/v, (c) 1.0% w/v, (d) 2.0% w/v, (e) 3.0% w/v and (f) 4.0% w/v. (ii) SEM images of composite HPMC-SA films with different SA content (a) SA 0.00 (b) SA 0.25 (c) SA 0.50 (d) SA 0.75.....	62
Figure 2.7: Wafers pore analysis showing % porosity in BK HPMC-SA wafer formulations ($n = 3, \pm SD$).	63
Figure 2.8: TGA thermal profiles ($n=1$) of (a) BK HPMC-SA wafers and (b) films, and (c) water content (%) of wafers and films.	65
Figure 2.9: DSC thermograms ($n=1$) of (a) BK HPMC-SA wafers (b) DL HPMC-SA wafers (c) BK HPMC-SA films and (d) DL HPMC-SA films.....	67
Figure 2.10: XRD-transmission diffractograms of (a) pure powders, (b) BK HPMC-SA composite wafers, (c) DL HPMC-SA composite wafers, (d) BK HPMC-SA composite films (e) DL HPMC-SA composite films.	70
Figure 2.11: ATR-FTIR spectra of (a) pure polymers, GLY, NIC (b) BK HPMC-SA composite films, (c) DL HPMC-SA composite films (d) BK HPMC-SA composite wafers and (e) DL HPMC-SA composite wafers.....	72

Figure 2.12: Swelling profiles (i.e. % swelling index against time) of ($n = 3, \pm SD$) (a) composite HPMC-SA wafers and (b) composite HPMC-SA films.....	74
Figure 2.13: Mucoadhesive profiles of BK and DL composite wafers ($n = 3, \pm SD$): (a) peak adhesive force (b) total work of adhesion (c) cohesiveness.	76
Figure 2.14: Mucoadhesive profiles of BK and DL composite films ($n = 3, \pm SD$): (a) peak adhesive force (N) (b) total work of adhesion (Nmm) (c) cohesiveness (mm).	77
Figure 2.15: NIC drug content (%) in DL HPMC-SA wafers and films ($n = 3, \pm SD$).	78
Figure 2.16: <i>In vitro</i> drug release profiles of DL HPMC-SA composite wafers ($n = 3, \pm SD$).	79
Figure 3.1: Tetrahedron and octahedron structures of silicate and aluminium/magnesium respectively.	87
Figure 3.2: Morphology of FD MAS-NIC complexes (x150); MAS 0.25 (i), MAS 0.50 (ii) and MAS 0.75 (iii) and surface morphology of SE MAS-NIC complexes (x2500); MAS 0.25 (iv), MAS 0.50 (v) and MAS 0.75 (vi).	91
Figure 3.3: EDX analysis of FD MAS-NIC 0.25 (i), 0.50 (ii) and 0.75 (iii).	92
Figure 3.4: EDX analysis of SE MAS-NIC 0.25 (i), 0.50 (ii) and 0.75 (iii).	93
Figure 3.5: XRD diffractograms of (i) FD (cakes) MAS-NIC complexes and (ii) SE (film) MAS-NIC complexes.....	94
Figure 3.6: ATR-FTIR spectra of (a) FD and (b) SE MAS-NIC complexes.....	96
Figure 3.7: Solid-state ^{29}Si NMR spectra of (a) MAS, (b) MAS-NIC 0.25, (c) MAS-NIC 0.50 and (d) MAS-NIC 0.75 complexes.	100

Figure 4.1: (a) Tensile properties of NIC loaded films ($n = 3, \pm SD$) and (b) hardness profiles showing the resistance of NIC loaded wafers ($n = 3, \pm SD$) to compressive deformation forces. 113

Figure 4.2: SEM images of NIC loaded wafers containing different amounts of MAS: (a) MAS 0.00 (b) MAS 0.25 (c) MAS 0.50 and (d) MAS 0.75. 115

Figure 4.3: SEM images of NIC loaded films containing different amounts of MAS: (a) MAS 0.00 (b) MAS 0.25 (c) MAS 0.50 and (d) MAS 0.75. 115

Figure 4.4: Wafers pore characteristics showing % porosity of the different HPMC-SA-MAS wafer formulations ($n = 3, \pm SD$). 116

Figure 4.5: XRD diffractograms of (a) pure powders, (b) NIC loaded HPMC-SA-MAS wafers and (c) NIC loaded HPMC-SA-MAS films. 117

Figure 4.6: ATR-FTIR spectra of (a) pure polymers, GLY, MAS, and NIC, (b) Drug loaded (DL) MAS wafers and (c) Drug loaded (DL) MAS films. 119

Figure 4.7: Swelling profiles (i.e. swelling index (%) against time) ($n = 3, \pm SD$) of (a) wafers and (b) films. 120

Figure 4.8: Mucoadhesive profiles of HPMC-SA-MAS wafers and films ($n = 3, \pm SD$): (a) peak adhesive force (N) (b) total work done (Nmm) (c) cohesiveness (mm). 122

Figure 4.9: Percentage drug (NIC) assayed content for ($n = 3, \pm SD$) (a) HPMC-SA-MAS wafers and (b) HPMC-SA-MAS films at different MAS concentrations. 123

Figure 4.10: *In vitro* drug release profiles ($n = 3, \pm SD$) of NIC loaded (a) wafers and (b) films containing different MAS concentrations. 125

Figure 4.11: NIC content (%) for (a) MAS wafer (MAS 0.25), (b) MAS film (MAS 0.25) and (c) Non-MAS wafer (MAS 0.00) obtained at accelerated and intermediate stability temperatures ($n = 3, \pm SD$).	127
Figure 5.1: NiQuitin® strips for NRT.	136
Figure 5.2: Swelling profiles (i.e. % swelling index against time) of (a) MAS wafer, (b) MAS film and (c) Non-MAS wafer in SS and PBS ($n = 3, \pm S.D$).	141
Figure 5.3: Mucoadhesive profiles of optimized wafers and films ($n = 3, \pm SD$): (a) peak adhesive force (N) (b) total work done (Nmm) (c) cohesiveness (mm).	142
Figure 5.4: <i>in vitro</i> drug release profile ($n = 3, \pm S.D$) of NIC from optimized formulations; (a) MAS wafer (b) MAS film, and (c) Non-MAS wafer, in SS and PBS.	144
Figure 5.5: Swelling profile (i.e. % swelling index against time) ($n = 3, \pm S.D$) of NiQuitin®, optimized wafers and films.	148
Figure 5.6: Mucoadhesive profiles of NiQuitin® and optimized wafers and films ($n = 3, \pm SD$): (a) peak adhesive force (N) (b) total work done (Nmm) (c) cohesiveness (mm).	149
Figure 5.7: NIC content (%) in NiQuitin® and, optimized wafers and films ($n = 3, \pm SD$).	150
Figure 5.8: <i>In vitro</i> drug release profile of NiQuitin® strip and optimized wafers and films ($n = 3, \pm SD$).	151
Figure 6.1: Cumulative permeation curve of optimized wafers and films using porcine buccal tissue ($n = 3, \pm SD$).	164
Figure 6.2: Cumulative permeation of optimized wafers and films using EpiOral™ engineered buccal tissue ($n = 3, \pm SD$).	166

Figure 6.3: Correlation between porcine and EpiOral™ cumulative permeation curve for (a) MAS wafers, (b) MAS films and (c) Non-MAS wafers..... 167

Figure 6.4: EpiOral™ tissue viability after permeation studies of MAS wafers, MAS films, Non-MAS wafers and negative (non-treated) control ($n = 3, \pm SD$)..... 168

Figure 7.1: Summary of wafers and films mechanisms..... 176

TABLES

Table 1.1: Human carcinogens present in cigarette smoke (adapted from Hecht 2006)	4
Table 1.2: Classification of dosage forms.....	6
Table 1.3. Advantages and disadvantages of solid dosage forms.....	7
Table 1.4: Advantages and disadvantages of oral mucosal delivery (Sankar et al., 2011).....	13
Table 2.3: Peak integration values	68
Table 3.1: Composition of MAS and NIC in solution.	88
Table 3.2: Particle size (μm) and zeta potential (mV) of MAS-NIC complexes dispersed in water.....	90
Table 3.3: ATR-FTIR band assignments of wavelength for FD (cakes) MAS-NIC.....	97
Table 3.4: ATR-FTIR band assignments of wavelength for SE (films) MAS-NIC.....	98
Table 4.1: (a) Concentrations of selected polymers, MAS and mass of NIC used in composite gels for formulating wafers and (b) concentrations of selected polymer, plasticizer, MAS and mass of NIC used in composite gel for film formulation.	107
Table 4.2: Condition for stability studies on optimized wafers and films.	111
Table 4.3: Surface stickiness, stringiness and gel strength of HPMC-SA-MAS gel formulations.	111
Table 4.4: Release parameters of NIC loaded HPMC-SA-MAS wafers developed by fitting experimental drug dissolution (release) data to different kinetic equations.	126
Table 4.5: Release parameters of NIC loaded HPMC-SA-MAS films developed by fitting experimental drug dissolution (release) data to different kinetic equations.	126

Table 5.1: Simulated saliva (SS) compositions used in various studies (Marques et al., 2011)	135
Table 5.2: Optimized wafers and films selected for this study.....	137
Table 5.3: Similarity and difference factors for drug release profiles of optimized wafers and film (a) between optimized wafers and film in SS and (b) between optimized wafers and film in PBS.	145
Table 5.4: Release parameters of optimized wafers and films using PBS developed by fitting experimental drug dissolution (release) data to different kinetic equations.	147
Table 5.5: Release parameters of optimized wafers and films, and NiQuitin® using SS developed by fitting experimental drug dissolution (release) data to different kinetic equations.	147
Table 5.6: Similarity (f_2) and difference factor (f_1) of optimized wafers and films compared to NiQuitin® strips.....	152
Table 6.1: Optimized formulations selected for permeation studies.	161
Table 6.2: Permeation flux (J) for optimized wafers and films from EpiOral™ tissue construct.	165

ABBREVIATIONS

%	Percentage
API	Active pharmaceutical ingredients
ATR-FTIR	Attenuated total reflection – Fourier transform infrared
AUC	Area under the concentration-time curve
BK	Blank
Ca	Calcium
CMC	Carboxymethylcellulose
COOH	Carboxyl
COPD	Chronic obstructive pulmonary disease
DL	Drug loaded
DNA	Deoxyribonucleic acid
DSC	Differential scanning calorimetry
Fe	Iron
F _{max}	Peak adhesive force
g	Gram
GIT	Gastrointestinal tract
GLY	Glycerol
GRAS	Generally recognized as safe
HEC	Hydroxyethylcellulose
Hg	Mercury
HPLC	High-performance liquid chromatography
HPMC	Hydroxypropylmethylcellulose
MAS	Magnesium aluminium silicate

mg	Milligram
Mg	Magnesium
NH ₂	Amine
NIC	Nicotine
NRT	Nicotine replacement therapy
OH	Hydroxyl
PAF	Peak adhesive fore
PAH	Polycyclic aromatic hydrocarbons
Pb	Lead
PBS	Phosphate buffered saline
RH	Relative humidity
rpm	Revolutions per min
SEM	Scanning electron microscopy
Sn	Tin
SO ₄	Sulphate
µm	Micrometre
USP	United States Pharmacopeia
V _g	Geometrical volume
V _p	Pore volume
w/v	Weight per volume
W _f	Final wafer weight
W _g ⁻¹	Watts per gram
W _i	Initial wafer weight
XRD	X-ray diffraction
ρ _e	Ethanol density (0.789 g/cm ³)

CHAPTER 1: GENERAL INTRODUCTION AND LITERATURE REVIEW

1.1 Overview

Tobacco is produced from the dried leaves of a plant belonging to the genus *Nicotiana* and is believed to originate from the early Americans. During the time of Christopher Columbus in 1492, the leaves of tobacco were used as a form of barter. The leaves were offered to him as a gift on his arrival to the new world where it was chewed and smoked by the native Americans. However, by 1500 its use began to spread all over Europe (Britton & Bogdanovica, 2013). The extensively grown tobacco plant *Nicotiana tabacum* and its addictive agent nicotine (NIC) was named after a court physician, Jean Nicot de Villemain who studied the therapeutic properties of tobacco. The commercial cigarette began with the invention of a cigarette rolling machine by James Bonsack in 1880 (O'Brien, 2013). From that moment until now, cigarettes have become a commercial product used by a large proportion of the world's population with more than a billion tobacco smokers worldwide (Rong et al., 2014).

Tobacco smoking can be related to several chronic diseases (U.S. Department of Health and Human Services, 2004), and most of its regular users die as a result of these diseases. Life threatening diseases such as cancer (especially lung cancer), chronic obstructive pulmonary disease (COPD) and cardiovascular diseases (e.g. coronary heart disease and stroke) are usually associated with cigarette smoking (U.S. Department of Health and Human Services, 2014). However, if a regular cigarette user successfully quits smoking, the risks mentioned above are decreased which obviously increases life expectancy. The increase in life expectancy depend on factors such as age, sex, physiology and smoking frequency. For example, the life expectancy of a smoker after cessation at age 35 could increase by 20-24% in men and 17-22% in women. However, the life expectancy of a smoker after cessation at age 65 could increase

by just 2-3% in men and 4-5% in women. It is therefore more beneficial to quit smoking as early as possible (Taylor Jr et al., 2002).

Smoke from a cigarette is made up of two phases: the tar phase and the gas phase (Church & Pryor, 1985). The tar phase contains particles with size above $0.1\mu\text{m}$, which are trapped on the cigarette filter, and contain more than 10^{17} free radicals/g. The gas phase contains particles with sizes below $0.1\mu\text{m}$, which pass through the filter and contain more than 10^{15} free radicals/g. Tar phase radicals have a long life span ranging from hours to months, while the gas phase radicals have a short life span of seconds. Free radicals such as oxygen radicals [(i.e. superoxide anion radical ($\text{O}_2\cdot^-$), singlet oxygen ($^1\text{O}_2$), hydroxyl radical ($\cdot\text{OH}$) and perhydroxyl radical ($\text{HO}_2\cdot$)] have been considered as important agents involved in cancer development (Ahsan et al., 2003). These radicals can lead to oxidative damage of the cellular membrane lipids, proteins, enzymes and DNA, therefore when there is no natural cell death, this can initiate the development of cancer (Dreher & Junod, 1996). An active smoker of tobacco draws a smoke known as a mainstream smoke which comprises 8% of tar and 92% of gaseous components, while the side-stream smoke which is released at the burning tail of a lit cigarette contains an increased proportion of poisonous gaseous components such as nitric oxide and carbon monoxide (Ambrose & Barua, 2004). This contributes to potential health effects as a result of exposure to outdoor tobacco smoke (passive smoking) leading to risks of severe heart diseases (Cho & Lee, 2014).

Over the years, there have been efforts to develop a drug delivery system to help the public withdraw from smoking cigarette due to its health risks. This has resulted in the development of NIC replacement therapy (NRT) as a cessation agent to help people addicted to smoking cigarette to quit (Handa, 2013).

1.1.1 *Impacts of smoking*

1.1.1.1 *Health impact*

Cigarette smoking can be related to several diseases such as cancer (as noted in section 1.1) and other chronic diseases including stroke, rheumatoid arthritis, coronary heart disease and congenital defects. The number of deaths associated with smoking have been estimated to be more than 480,000 deaths each year in United States (U.S. Department of Health and Human Services, 2014) and 81,400 adult (age 35 years and above) deaths in the UK were smoking related (Jones et al., 2015). The impact of smoking on human health has become a major concern for governments and health authorities such that there have been several awareness campaigns to encourage smoking cessation among smokers.

Carcinogenicity of cigarette smoke

A physical, chemical or viral agent that escalates the occurrence of cancer or causes cancer is termed a carcinogen. According to the U.S. Department of Health and Human Service, the combination of the mainstream and the side-stream smoke (termed second-hand smoke) contains more than 7,000 chemicals and about 70 carcinogens (U.S. Department of Health and Human Services, 2006). Hecht (2006) compiled a list of 62 carcinogenic compounds found in cigarette smoke with 15 of these compounds being carcinogenic to humans (Table 1.1). His publication identified strong carcinogenic compounds such as polycyclic aromatic hydrocarbons (PAH), N-nitrosamines and aromatic amines occurring in low amounts, while weak carcinogenic compounds such as acetaldehyde and isoprene were present in high amounts. These carcinogens found in cigarette can be associated with several cancers including the lung, liver, leukaemia, bladder, cervix, pancreas, oesophagus, oral cavity, nasal and larynx (Hecht, 2006).

Table 1.1: Human carcinogens present in cigarette smoke (adapted from Hecht 2006)

<i>Carcinogen</i>	<i>Compounds</i>	<i>Amount in mainstream cigarette smoke</i>	<i>IARC monograph evaluation of carcinogenicity (in human)</i>
<i>Polycyclic aromatic hydrocarbons</i>	Benzo(a)pyrene	8.5–17.6 ng	Limited
<i>N-Nitrosamines</i>	N'-Nitrosornicotine	154–196 ng	Limited
	4-(Methylnitrosamino)-1-(3-pyridyl)-1-butanone	110–133 ng	Limited
<i>Aromatic amines</i>	2-Toluidine	30–200 ng	Limited
	2-Naphthylamine	1–22 ng	Sufficient
	4-Aminobiphenyl	2–5 ng	Sufficient
<i>Aldehydes</i>	Formaldehyde	10.3–25 µg	Sufficient
<i>Volatile hydrocarbons</i>	1,3-Butadiene	20–40 µg	Limited
	Benzene	12–50 µg	Sufficient
<i>Miscellaneous organic compounds</i>	Vinyl chloride	11–15 ng	Sufficient
	Ethylene oxide	7 µg	Limited
<i>Metals and inorganic compounds</i>	Arsenic	40–120 ng	Sufficient
	Beryllium	0.5 ng	Sufficient
	Nickel	ND-600 ng	Sufficient
	Chromium (hexavalent)	4–70 ng	Sufficient
	Cadmium	41–62 ng	Sufficient
	Lead (inorganic)	34–85 ng	Limited

1.1.1.2 Economic impact

Due to the health impact of smoking, health care costs in various countries have become an economic burden. This is the result of smokers developing smoking related chronic illness especially among the elderly. For example, Ruff and co-workers described the economic burden of smoking on the German health care system, where approximately 33.4% of male and 20.4% of female populations are smokers. His publication focused on seven most common diseases associated with smoking which include chronic obstructive pulmonary disease (COPD), lung cancer, stroke, coronary artery disease, cancer of the mouth and larynx, and atherosclerotic occlusive disease, with an estimated total cost of 16.6 billion Euros of smoking related health care costs (Ruff et al., 2000). Furthermore, the daily cost of cigarette can be a financial burden especially for poor smokers and might lead to lack of other basic amenities such as food, clothing and shelter as a result of their cigarette dependency (Steinberg et al., 2004).

1.1.1.3 Social impact

The awareness of health issues related to smoking and second hand smoke has given rise to increases in social stigma as well as isolation among smokers. In addition, there has been an increase of social rejection, with policies which prohibit smokers from smoking in public places and certain environments. These have created a social stigma where employers prefer to employ a non-smoker, landlords would prefer to rent a house to a non-smoker whilst a smoker trying to quit smoking would prefer hanging out around non-smokers. The social impact of smoking has therefore led smokers to quit smoking with the desire to change their social status from being a smoker to non-smoker (Stuber et al., 2008).

1.2 Pharmaceutical drug delivery systems and dosage forms

Drugs or active pharmaceutical ingredients (API) require the use of other substances known as excipients to be able to function effectively in the body. APIs are either small

molecular compounds or larger biological molecules such as peptides, vaccines, antibodies and enzymes. Drug delivery systems, however, involve the development of formulations to enhance the administration and efficiency of therapeutic compounds and molecules (Anselmo & Mitragotri, 2014). These processes have also resulted in formulating APIs into different dosage forms, which are introduced into the body, via different routes. The challenges of overcoming biological barriers within the body should always be considered in the development of any dosage form. Furthermore, drug delivery systems must demonstrate efficiency, safety to the body, patient convenience and ease of manufacturing which must all be considered during the development phase (Allen Jr, 2008).

A dosage form can be defined as the physical form of a drug after formulation and made up of a drug entity and excipients. These forms can be generally categorised based on its physical state as shown in Table 1.2.

Table 1.2: Classification of dosage forms

<i>Classification of dosage forms</i>	<i>Dosage forms</i>
<i>Solid</i>	Tablets, capsules, pellets, beads, spherules.
<i>Liquid</i>	Syrups, lotions, solutions, emulsions, suspensions.
<i>Semi-liquid</i>	Gels, ointments, creams, pastes

1.2.1 *Solid dosage forms*

Conventional solid dosage forms are usually prepared by compression, encapsulation, extrusion and spheronization of APIs with excipients to produce tablets, capsules, pellets and spherules respectively (Hacker et al., 2009, Salústio et al., 2012). They are usually used to achieve a systemic effect after absorption through the gastrointestinal tract (GIT). Excipients

added to a solid dosage form help to enhance disintegration, improve stability, mask or improve taste and increase powder flow.

Table 1.3 summarises the advantages and disadvantages of solid dosage forms. Depending on the delivery requirement, solid dosage forms such as tablets and capsules are designed to perform various functions in the form of controlled release tablet/capsule (Pani & Nath, 2014), chewable tablets (Wu et al., 2012), orally disintegrating tablet (Gryczke et al., 2011), buccal and sublingual tablets, lozenges, pastille, hard and soft gelatine capsules (Conway, 2008).

Table 1.3. Advantages and disadvantages of solid dosage forms

Advantages	Disadvantages
<ul style="list-style-type: none"> • Ease of handling • Flexible selection of manufacturing method • Low cost of mass production • Can be self-administered by the patient • Accurate quality and dosage • More stable compared to other dosage forms • Can be adapted to other profiles e.g. sustained release profile. 	<ul style="list-style-type: none"> • Difficult to swallow particularly in children, elderly or unconscious patients. • Loss of ingredient as a result of several manufacturing unit operations • Physiological factors play a major role in absorption.

1.2.2 *Liquid dosage forms*

Liquid dosage forms are formulations containing one or more solid chemicals dissolved or dispersed in an appropriate solvent. These formulations include solutions, suspensions, emulsions, elixirs, tinctures and syrups. The solubility of the APIs and excipients in the intended solvent is usually considered when developing a one-phase liquid dosage forms. The development of a liquid dosage form as a solution increases the availability of drug for absorption as it by bypass dissolution, can be designed for any route of administration, can be an alternative dosage form when swallowing is difficult and enable flexibility in dosing i.e. can control dose by rationing the amount. The drawbacks of liquid dosage forms include; stability issues, taste challenges, transportation challenges especially for bulky products and drug solubility. However, emulsions and suspensions are usually considered in developing a liquid dosage form where the API is not soluble in the desired solvent (Allen & Popovich, 2005).

1.2.3 *Semi-solid dosage forms*

Semi solid dosage forms include ointments, creams, gels and pastes. They are usually designed for topical use and can be used for either systemic or local effect. The majority of semi-solid drug products are designed for the skin. There are also semi-solid dosage forms designed for local nasal, buccal, rectal, ocular and vaginal drug delivery (Gad, 2008). In the preparation of semi-solid dosage forms for local effect, the formulation is designed to deliver the drug onto the skin, while for systemic absorption, the drug is designed to penetrate the skin and into the bloodstream where it is circulated to the target site (Allen & Popovich, 2005). The therapeutic use of semi-solid products incorporates antibacterial, antifungal, antiviral, astringents, keratolytics and mydriatic agents as API. Non-therapeutic use of semisolid dosage forms are usually designed for protective and lubrication functions such as moisturizing and sun creams (Gad, 2008).

1.3 Routes of administration

A route of administration refers to the site in the human body via which a drug is introduced into the body. The choice of a given route for administering drugs into the body depends on the properties of the drug and the dosage form. The dosage form is therefore designed to present the drug in the most suitable form in order to be absorbed into the body from a particular route of administration (Aulton & Taylor, 2013). The routes of administration of drugs can be classified into three groups: enteral (oral, sublingual and rectum), parenteral (intravascular, intramuscular, subcutaneous and inhalation) and topical (transdermal and transmucosal).

1.3.1 Oral route

The oral /enteral route is the most commonly used route of administration and its popularity is the result of its ease of usage, control of administration process by patients and low production cost (Lam & Gambari, 2014). The dosage forms intended for delivery via the oral route are usually solid (i.e. tablets and capsules) and liquid dosage forms. These dosage forms migrate from the mouth when swallowed, to the gastrointestinal tract (GIT) where absorption takes place. The migration of drugs from the mouth to the GIT can therefore expose susceptible drugs to enzymes, harsh pH and first pass effect in the liver following absorption, which can degrade and eliminate the drug thereby leading to very poor bioavailability (Aulton & Taylor, 2013). As a result, alternative routes have been explored for certain drugs that are particularly sensitive to the above conditions, such as proteins and peptides and these are discussed briefly below.

1.3.2 Rectal route

The rectal route can be utilised for both local and systemic delivery of drugs. Local dosage forms include solutions, suppositories or emulsions. In systemic drug delivery, the rectal route can also serve as an alternative to the oral route of administration especially for

drugs that are affected either by the gastrointestinal fluids or by first pass effect of the liver. This route of administration can also be utilised in a situation when a patient is vomiting or unconscious, or in children and elderly with swallowing difficulties (Jannin et al., 2014). However, the rectal route can be awkward for some patients and its absorption of drugs is unpredictable.

1.3.3 *Parenteral routes*

Parenteral routes usually refer to the administration of drugs by injection and there are three main parenteral routes; intravenous, intramuscular and subcutaneous (Aulton & Taylor, 2013). They are usually the most preferred routes in the case of emergency or in a situation where a patient is not capable of using oral medications. The consideration of parental routes during emergency is because drug is delivered directly to the circulatory system. Parenteral formulations can also be utilised in the delivery of drugs that are poorly absorbed or drugs susceptible to first pass elimination by the liver when administered via the oral route (Date & Nagarsenker, 2008).

1.3.4 *Respiratory route*

The respiratory organ (i.e. the lungs) of the human body offers the most suitable surface for the delivery of drugs in the form of aerosol, mist, gas or as ultra-fine solid particles. For drugs in an aerosol dosage form, the penetration of the site of absorption (i.e. alveolar region) is dependent on its particle size. Particles with diameter ranging from 0.5-1 μm enter the alveolar sac while particles below this range are either exhaled or dumped on the walls of the respiratory airways (Aulton & Taylor, 2013). This route of administration has been utilised in the treatment of pulmonary conditions such as chronic obstructive pulmonary disease as well as in the maintenance therapy of asthma (Newman, 2006) and systemic delivery of drugs such as insulin (Afrezza®)(Yang et al., 2014, Dolovich & Dhand, 2011).

1.3.5 *Topical routes*

Topical routes of administration are usually utilised in the delivery of drugs to the skin and other topical surfaces such as the eye, ear, nose and vagina. The dosage forms for topical routes of administration include creams, pastes and ointments, which are categorized under semi-solid dosage forms. This route is mainly used for local effect, however, novel delivery systems have utilised transdermal patches such as NIC patches and for formulations administered via transmucosal routes, for systemic action of drugs. Such systemic delivery of drugs via the topical route has the advantage of bypassing the first pass metabolism of drugs as well as avoiding elimination of drugs in the gastrointestinal tract (Aulton & Taylor, 2013, Hearnden et al., 2012).

1.3.5.1 *Topical systemic delivery systems (transdermal)*

Among the topical routes of delivery, the transdermal route is the most extensively studied for systemic drug delivery. The skin is the organ with the largest surface area and can easily be accessed. However, permeability of the skin has always been considered a challenge in the development of transdermal delivery systems. The protective nature of the skin is attributed to its keratinised outermost layer called the stratum corneum. The lipids of the stratum corneum form bilayers around the corneocytes (the major composition of the stratum corneum) resulting in a brick and mortar architecture (Moser et al., 2001).

The penetration of drugs through the skin has therefore been limited to low molecular drugs with desirable hydrophilic/ lipophilic properties. However, chemical and physical penetration enhancement have been utilised in the delivery of drugs irrespective of their molecular weight or hydrophilic/lipophilic properties. The use of chemical penetration enhancement especially in cosmetics involve the use of chemical groups such as sulphoxides, fatty acids, alcohols, pyrrolidones and surfactants while physical penetration enhancement involves the design of delivery devices to physically penetrate the skin such as micro-needles,

heating, iontophoresis, electroporation and ultrasound (Azagury et al., 2014, Hearnden et al., 2012, Uddin et al., 2015). Transdermal systemic delivery devices have already been utilised in the delivery of NIC for NRT, contraceptives, analgesics, psycho-stimulants and anti-emetics.

1.3.6 *Transmucosal routes*

Mucosal surfaces including the oral, rectal, vaginal, ocular and nasal mucosa, have been extensively investigated as alternative routes of drug delivery. The advantage of mucosal membranes over the skin is based on the level of keratinisation; hence permeability is higher in mucosal membrane than in the skin's stratum corneum (Hearnden et al., 2012). Patient compliance in the systemic delivery of drugs via the rectal, ocular and vaginal mucosa has always been a limitation, however, they have always been utilised in local drug delivery. Nasal and oral mucosae have been extensively investigated in systemic delivery of drugs (Ugwoke et al., 2005, Lam et al., 2014). For example, NIC has successfully been delivered via the nasal mucosa, calcitonin in treating osteoporosis, oxytocin for nursing mothers, desmopressin in the management of enuresis and butorphanol tartrate for pain relief (Hearnden et al., 2012). Nasal drug delivery limitations include mucociliary clearance of drug from the absorption sites, poor contact between the formulation and the nasal mucosa and less suitable in the delivery of drugs that require regular administration for chronic conditions, as well as drugs that need sustained levels in the blood (Fortuna et al., 2014).

1.4 **Oral transmucosal routes**

The oral route has always been the preferred route of drug administration; however, it faces the problem of first pass hepatic metabolism and drug degradation in the gastrointestinal tract especially for high molecular weight drugs such as peptides and proteins.

The oral transmucosal route offers a solution to this challenge through bypassing the first pass effect in the liver and the degradation within the gastrointestinal tract in addition to

other advantages (Table 1.4). The oral transmucosal route can be utilised in the systemic delivery of drugs, where the drug is delivered directly into the blood stream. This is the result of the high levels of blood flow as well as high permeability of the oral mucosa (Sattar et al., 2014, Hearnden et al., 2012, Sankar et al., 2011).

Table 1.4: Advantages and disadvantages of oral mucosal delivery (Sankar et al., 2011)

<i>Advantages</i>	<i>Disadvantages</i>
<ul style="list-style-type: none"> • Easily accessible • Can be self-administered by patient • Different permeation characteristics between sublingual and buccal regions of the oral cavity • Rapid repair of the oral mucosa • Drug dissolution can be easily achieved by the highly hydrated environment • Suitable for sustained delivery of drugs. • Possible reduction of systemic side effects. 	<ul style="list-style-type: none"> Oral mucosa permeability barrier Washing effect of saliva on the drug Taste is a very important factor in delivery development. Chewing and talking may displace delivery device. Very enzymatic environment Relatively small surface area Possibility of choking or swallowing of delivery device

1.4.1 *The anatomy and physiology of the oral mucosa*

The anatomy and physiology of the oral mucosa have been discussed extensively in several articles (Lam et al., 2014, Patel et al., 2011, Salamat-Miller et al., 2005). However, a brief overview of the anatomy and physiology of the oral mucosa is necessary. The outer surface of the oral mucosa comprises closely packed squamous stratified epithelial cells on the basement membrane, lamina propria (a layer of connective tissues) and the submucosa, which holds the blood vessels and nerves (Figure 1.1). The epithelium serves as a protective

membrane to the tissues underneath it and helps to prevent the invasion of destructive materials (i.e. harsh chemical compounds) or microorganisms into the oral environment.

The epithelial cells are divided into keratinized and non-keratinized cells. The keratinized cells are usually found in the hard palate and the inelastic regions (i.e. dorsum of the tongue and the gingiva) of the oral cavity. The non-keratinized cells are usually found in the surface of the soft palate, alveolar mucosa, and ventral region of the tongue, the lips, the cheeks and floor of the mouth (Salamat-Miller et al., 2005). The non-keratinized cells of the oral mucosa have a higher permeability than the keratinized cells and the difference in permeability is due to the phospholipid composition of the membrane coating particles rather than the presence of keratin (Ganem-Quintanar et al., 1997).

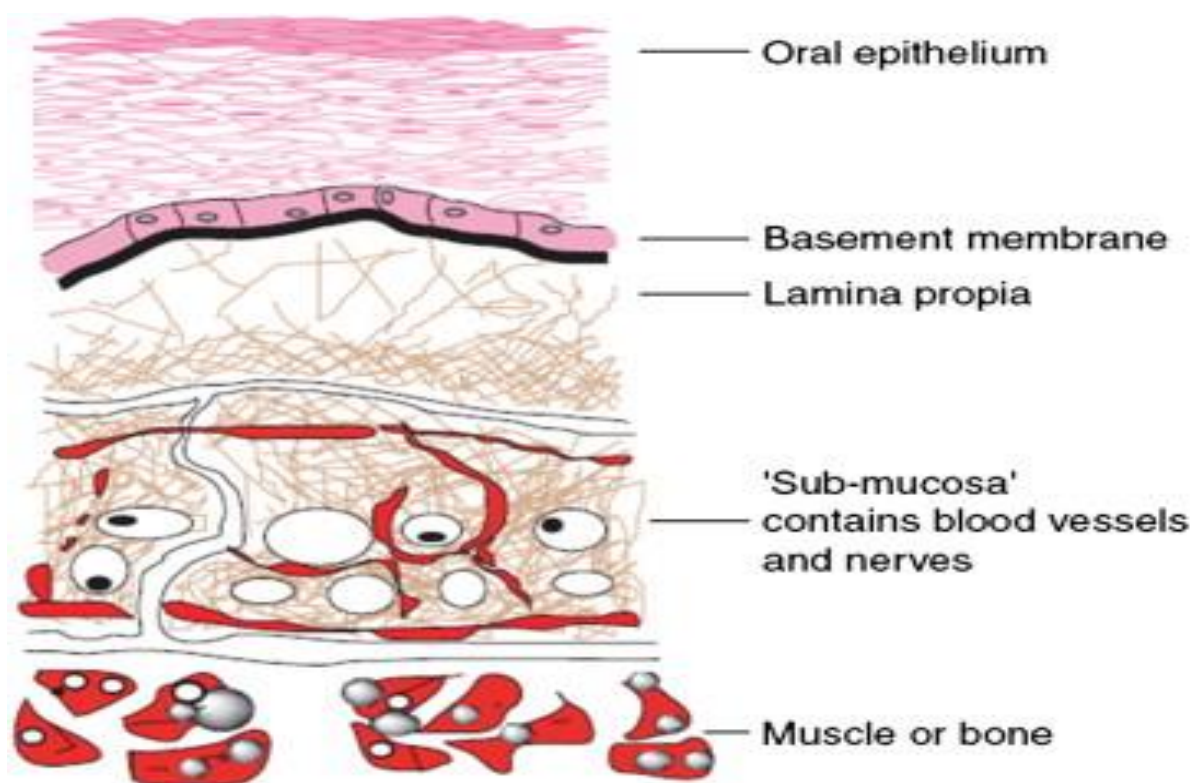


Figure 1.1: Structure of the oral mucosa (Patel et al., 2011)

The mucosa found in the oral cavity can be divided into three types; the lining mucosa, the masticatory mucosa and the specialized mucosa. The lining mucosa includes the non-keratinized cells of the buccal and sublingual tissues of the oral cavity. They comprise

approximately 60% of the total surface area of an adult human oral mucosal lining, followed by the masticatory mucosa making up approximately 25% and the specialized mucosa, which makes up approximately 15%. The outer cells of the masticatory mucosa are keratinized and are found in regions (i.e. the dorsum of the tongue, hard palate and the gingiva) which experience higher levels of stress and strain due to masticatory activities. The specialized mucosa on the other hand has well papillated surfaces with both keratinized and non-keratinized cells and make up the mucosa of the dorsum of the tongue (Patel et al., 2011).

The areas of the oral transmucosal surface, suitable for systemic drug delivery are therefore be classified into (i) buccal and (ii) sublingual routes. The buccal mucosae are in the inner cheek, the pouch between the cheeks and the gum, while that of the sublingual mucosa is usually under the tongue (Figure 1.2). Although both sites are non-keratinized, they still differ in the degree of permeability.

The higher permeability of the sublingual mucosa over the buccal (with moderate permeability) is due to their differences in thickness and epithelial cell composition as well as vascularity. The relative differences in the permeability and bioavailability of buccal and sublingual have served as an advantage in their application in drug delivery. The sublingual route has been utilised in treatment of acute conditions (such as pain, erectile dysfunction, nausea or an allergic reaction) as a result of its rapid onset drug action, while the buccal route has been utilised in sustained drug delivery and chronic systemic therapy such as the management of diabetes using insulin (Lam & Gambari, 2014).

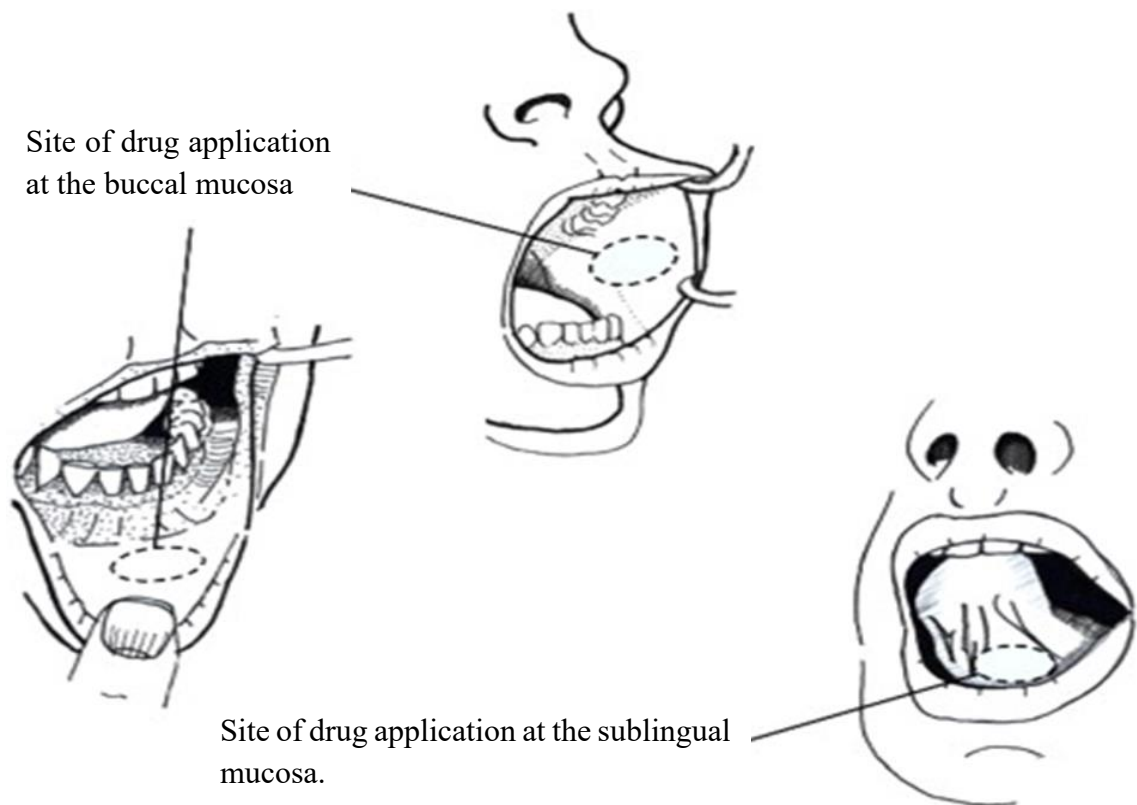


Figure 1.2: Common drug application locations on buccal and sublingual mucosa (Lam et al., 2014)

1.4.2 Drug absorption via the oral mucosa

The permeability of a mucosa surface depends on the membrane thickness, degree of keratinization and physicochemical properties of the drug. As discussed in section 1.4.1, the thickness and composition of the cells of the oral (sublingual and buccal) mucosa membrane can affect the rate of drug absorption. Oral mucosa permeation is reported to be 4-4000 times more than the skin, which can be attributed to the abundance of non-keratinized cells in the oral mucosa and surface hydration (Patel et al., 2011). The transportation of drugs through the epithelial membranes of the oral mucosa can be by passive diffusion, carrier-mediated active transport or other specific mechanism. The means for transportation of drugs can be achieved by both transcellular and paracellular pathways (Figure 1.3) depending on the physicochemical properties of the drug.

The transport of drugs via the transcellular pathway involves the permeation of drug through the cells until they enter the bloodstream. Due to the lipophilic nature of the epithelial cell membrane, the most favoured drug candidates are the highly lipophilic drugs. The paracellular pathway on the other hand involves the permeation of drugs between cells until they reach the bloodstreams. The spaces between the cells are highly hydrophilic, unlike the transcellular pathway; therefore, hydrophilic drugs are favoured during paracellular transport. Drug compounds utilise both transcellular and paracellular pathways simultaneously, however, depending on the physicochemical properties of the drug, one pathway is usually desirable.

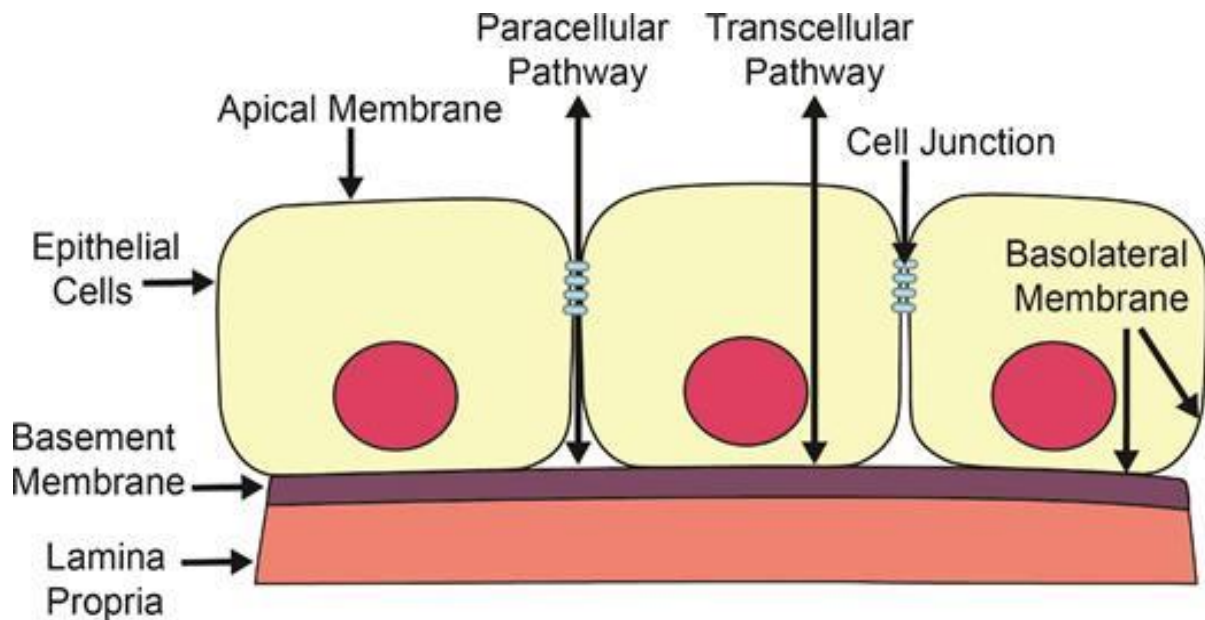


Figure 1.3: Paracellular and transcellular pathway across the epithelia cell (Levendoski et al., 2014).

The flux (J_c) of drug via the membrane in transcellular pathway was described mathematically in equation 1.

$$J_c = \frac{(1-\epsilon)D_c K_c}{h_c} \quad (1)$$

Where, K_c is partition coefficient between lipophilic cell membrane and the aqueous phase, D_c is the diffusion coefficient of the drug in the transcellular spaces, ϵ is the area fraction of the paracellular route and h_c is the path length of the transcellular route.

While the flux (J_p) of drug through the membrane for paracellular route can be described by equation 2.

$$J_p = \frac{D_p \varepsilon}{h_p} C_d$$

(2)

Where, D_p is the diffusion coefficient of the permeant (drug) in the intercellular spaces, h_p is the path length of the paracellular route, ε is the area fraction of the paracellular route and C_d is the donor drug concentration (Sudhakar et al., 2006).

1.4.3 *Advantages of buccal drug delivery*

Generally, oral transmucosal routes such as buccal mucosa offer an advantage of bypassing the hepatic ‘first-pass’ metabolism of susceptible drug after gastrointestinal absorption in conventional oral routes (Şenel & Hıncal, 2001). Drugs delivered via the buccal route can also be absorbed without delay due to the absence of food or gastric disease as well as no exposure to the acid or digestive enzymes. Although the buccal mucosa contains enzymes, there are fewer of them with lower levels of activity compared to the gastric and intestinal mucosae. The buccal cavity is highly vascularised and can also be more permeable to drugs than the skin because of the phospholipid composition of non-keratinized cells of the buccal mucosa membrane (Patel et al., 2011). Furthermore, the buccal mucosa is less prone to damage by harsh drugs as a result of its robust membrane because of its exposure to various physical forces and harsh foreign materials contained in foods and beverages (Gutniak et al., 1996). The buccal route can also be very useful in the administration of drugs to unconscious patients with its ability to mediate systemic delivery of drugs.

The sublingual route also provides similar advantages as the buccal route. In addition to these advantages, the sublingual mucosa is considered more permeable than the buccal mucosa, absorbs drugs more rapidly, it is accessible, convenient and generally acceptable as

an oral transmucosal route for systemic drug delivery. However, the sublingual mucosa possesses less smooth muscle and usually flooded with saliva which is challenging for retention of a delivery system in this region. Furthermore, the high level of permeation and high vascularity provides an immediate onset of action which is less suitable for sustained release formulations (Shojaei, 1998).

1.4.4 *Influence of physiological factors on drug absorption*

There are two major physiological factors that influence drug absorption across the oral mucosa, which are mucus and saliva.

The mucus is a major component of saliva secreted by the salivary glands and made up of glycoproteins known as mucins. The amount of mucin contained in the entire mucus components is about 1-5% (Lam et al., 2014). The mucus forms a negatively charged network at normal oral mucosa pH (6.8) due to the presence of sialic acid and sulphate residues. This negatively charged network forms a strong interconnected gel and binds to the epithelial surface creating a gelatinous layer. The mucus serves as a protective barrier by trapping substances, hence influencing drug penetration. However, the mucus also plays a vital role in the bio-adhesion of mucoadhesives used in oral transmucosal formulations.

Three major glands secrete the saliva: the parotid, the submandibular and the sublingual glands as well as other minor salivary glands. Its function is to lubricate food, assist food mastication, prevent tooth demineralization, moderate the growth of normal flora in the mouth, and contributes to the metabolism of carbohydrates. The major components of saliva are proteins (such as proline-rich proteins), mineral salts (such as sodium chloride), mucus (consisting mainly of mucopolysaccharides and glycoproteins), enzymes (such as α -amylase, lingual lipase, and kallikrein) and antimicrobial agents (such as lysozyme, immunoglobulin A, lactoferrin). Saliva is a weak buffer with a pH of about 5.5-7.0 and the pH is influenced by its ionic composition (due to the presence of electrolytes such as sodium, potassium, bicarbonate,

calcium, magnesium, chloride; as well as, proteins) and flow rate. The flow rate and the ionic composition of saliva depends on the degree of stimulation and time of the day. Its normal flow rate is about 0.5ml/min with an overall secretion of 0.5 to 2 L daily depending on age, sex or presence of disease such as drug induced xerostomia (e.g. hypertensive drugs such as pentolinium, mecamylamine and pempidine) and hypersalivation (e.g. clozapine) (Vinayak et al., 2013). However, with continuous swallowing, the total volume of saliva in the mouth is about 1.1 ml (Sattar et al., 2014). The varying amounts of saliva may influence the release profile of a delivery system designed for prolonged delivery. Excess secretion of saliva can result in saliva washout effect leading to low bioavailability and ultimately reduced therapeutic efficacy of the drug (Lam et al., 2014).

1.5 Bioadhesion / mucoadhesion

When two materials are held together for a prolonged period by interfacial forces and at least one of the materials is biological in nature, the interaction is referred to as bioadhesion. However, in pharmaceutical science, the concept of bioadhesion is usually referred to as mucoadhesion as a result of an adhesive connection to the mucus or the mucosal membrane (Smart, 2015). Mucoadhesive polymers are formulated into a dosage form to adhere to the mucosal tissue within a given time (Smart, 2005). The main benefit of using mucoadhesive polymers in the design of drug delivery systems for oral transmucosal routes such as the buccal mucosa is to enhance drug bioavailability (systemic) through direct interaction with the site of administration by prolonging retention between the mucoadhesive drug delivery system and the mucosa surface (Sosnik et al., 2014).

1.5.1 Theories of mucoadhesion

Adhesion of materials to the mucosal membrane can be explained using six general theories of adhesion, which are briefly discussed.

(a) The *electronic theory* proposes that the differences in electronic structure of adhering surfaces result in electron transfer between the surfaces upon contact, which gives rise to attractive forces (Huang et al., 2000).

(b) The *adsorption theory* suggests that adhesion of materials is based on hydrogen bonding and van der Waals' forces, however; subsection theory of adsorption (the chemisorption theory) also assumes that the interaction across their point of contact is due to strong covalent bonding (Smart, 2005).

(c) The *wetting theory* suggests that when two surfaces with high affinity of liquid to solid are brought together in the presence of a liquid, the liquid serves as an adhesive agent. The affinity of the liquid can be determined by measuring its contact angle using techniques such as contact angle goniometry (Rahamatullah Shaikh et al., 2011).

(d) The *diffusion theory* suggests that mucoadhesion occurs as the result of chain entanglement of mucoadhesive polymer with glycoproteins present in mucus. The process of diffusion theory is determined by concentration gradient and influenced by factors such as molecular mobility and chain length (Agarwal & Aggarwal, 2015).

(e) The *fracture theory* like the other five describes the force required to detach two systems after adhesion from their adhesive strength, which suggests that adhesive bond breakage occurs at the interface (Smart, 2005).

(f) The *mechanical theory* describes adhesion of a liquid adhesive on a rough surface postulating that the liquid adhesive forms an interlock with a rough surface because of the irregularities on the rough surface (Smart, 2005, Salamat-Miller et al., 2005).

1.5.2 *Mucoadhesive mechanisms*

The mechanism of mucoadhesion involves two stages: the contact stage and the consolidation stage. The contact stage involves an initial interaction between the mucoadhesive material and mucous membrane. In exposed mucosal surfaces such as the oral cavity, the ocular

and vagina mucous membranes, the contact stage can be initiated by mechanical means where the delivery system is placed and held on the mucosal membrane (Smart, 2005). In the consolidation stage, the presence of moisture stimulates a stronger adhesion of mucoadhesive material to a solid dry surface especially for larger formulations that are susceptible to stress when administered to a site where there are constant movements such as the oral cavity (mouth movements) and/or the eye (constant blinking). The molecules of mucoadhesive material become free upon hydration, adjust to the shape of the surface and bond mainly by weaker van der Waal forces and hydrogen bonding as moisture plasticizes the system. Smart (2005) has described the consolidation stage with diffusion and hydration theory. As described in Section 1.5.1(d) of mucoadhesion diffusion theory, the chains of the polymer which interpenetrate with the glycoprotein of mucus form a secondary bond at the consolidation stage (Smart, 2005).

1.5.3 *Factors affecting mucoadhesion*

The factors that affect the degree of polymer-mucus interactions with reference to the theories of mucoadhesion are usually polymer related factors. The properties of a polymer used as mucoadhesive delivery system have a direct relationship with the degree of adhesion and are briefly discussed below.

1.5.3.1 *Polymer concentration*

The degree of mucoadhesion of polymer has been demonstrated to be influenced by its concentration (Andrews et al., 2009). At optimal concentration of the mucoadhesive polymer, the degree of mucoadhesion between the polymer and the mucosal surface is increased. This phenomenon also depends on the physical state of the drug delivery device. For semi-solids, the adhesion properties of the polymer beyond the optimum concentration, are reduced due to reduced availability of chains necessary for polymer-mucus interpenetration, due to the instability created from polymer chain entanglement. However, in solid delivery systems, an increase in mucoadhesive polymer concentration will lead to increase in adhesion with readily

available polymer chains. At low concentration, the number of polymer chains available for interpenetration is low whereas at high concentration the amount of polymer chains available for interpenetration is high. (Andrews et al., 2009, Boddupalli et al., 2010).

1.5.3.2 Functional group contribution

For most mucoadhesive polymers (such as hydroxypropylmethylcellulose - HPMC and sodium alginate - SA), the attachment and bonding between the polymer and mucus is the result of interpenetration followed by secondary bonding (usually non-covalent) that occurs usually by hydrogen bonding. The presence of hydrophilic functional groups such as hydroxyl (OH), carboxyl (COOH), amide (NH₂) and sulphate (SO₄) plays a vital role during secondary bonding. Increase in hydrogen bonding groups will result in an increase in bonding strength between the mucoadhesive polymer and mucin glycoproteins (Andrews et al., 2009).

1.5.3.3 Degree of hydration

The degree to which a mucoadhesive polymer hydrates is an important factor that affects the strength of mucoadhesion. In situations where the surface environment contains limited amounts of water, polymers tend to exhibit low mucoadhesive properties. During hydration of a mucoadhesive polymer, the polymer expands to form a suitable macromolecular mass with an appropriate size. It also induces the mobility of the polymer chains, which increases inter-penetration between the polymer and mucin glycoproteins. Swollen polymer functional group sites for hydrogen and/or electrostatic bonding are also exposed. However, there is a critical degree of hydration where optimum swelling and mucoadhesion of mucoadhesive polymer occurs. Excessive hydration could lead to a wash-away effect of the polymer chain while under hydration of mucoadhesive polymer results in lower polymer expansion/swelling and hence reduced mobility of polymer chains (Boddupalli et al., 2010).

1.5.3.4 Charge

The charge of a bioadhesive polymer has been shown to play a vital role in the degree of adhesion to mucosal surfaces (Grabovac et al., 2005). The degree of adhesion in non-ionic polymers such as HPMC, is relatively low compared to anionic and cationic polymers due to the surface charge of mucin. Polymers with strong anionic charge such as polyacrylic acids, have been shown to possess strong mucoadhesive properties. However, some cationic polymers with high molecular weight such as chitosan have demonstrated superior mucoadhesive properties in a neutral or slightly alkaline medium, especially when improved by substituting the free amino groups with short alkyl chains which increases the pKa and hence results in ionization of these groups at increased pH (Boddupalli et al., 2010).

1.5.3.5 Molecular weight

The increase in molecular weight of a mucoadhesive polymer can result in an increase in the strength of adhesion as lower molecular weight polymers form weak gels and dissolve rapidly. However, for most mucoadhesive polymers, there is an optimum molecular weight, that can yield maximum mucoadhesive properties. This is because excessively high molecular weight polymers take a long time to hydrate and hence can lead to lower interaction of binding groups with a substrate. The optimum molecular weight depends on polymer type which can be up to 100,000 (Gurny et al., 1984).

1.5.3.6 Degree of cross-linking

In a polymer network, the degree of cross-linking determines the rate at which a solvent diffuses into the polymer network, which is related to the degree of swelling of a hydrophilic mucoadhesive polymer. The hydration and swelling of a mucoadhesive polymer is favourable such that there is availability of polymer chains, which increases interpenetration between the chains and mucus glycoprotein (i.e. mucin). Increase in cross-link density will lead to a decrease in hydration and swelling rate and consequent reduction in availability of chains for

interpenetration between polymer and mucus glycoprotein (Andrews et al., 2009, Boddupalli et al., 2010).

1.5.4 *Mucoadhesive polymers*

Mucoadhesive polymers have been widely used in the development of pharmaceutical formulations. The routes of administration which have been exploited include nasal, ocular, oral mucosal and other mucosal routes. Sosnik *et al.*, (2014) have classified mucoadhesive polymers into three groups based on their sources; natural, synthetic and semi-synthetic. For natural polymers, their sources are usually biological materials, for example, those obtained from shrimps and other crustacean shells such as chitosan, brown algae as in alginates and ground endosperms of guar beans as in guar gum. However, natural polymers can also be modified to obtain desirable characteristics through chemical means and are grouped under semi-synthetic mucoadhesive polymers. Semi-synthetic polymers are usually obtained through the semi-synthesis of different ether and ester derivatives using cellulose obtained from fibrous plants e.g. hydroxyethylcellulose (HEC), hydroxypropylmethylcellulose (HPMC), carboxymethyl cellulose (CMC) salts i.e. NaCMC and CaCMC. Synthetic polymers on the other hand are fully synthesized in the laboratory such as poly(ethylene glycol), poly(ethylene oxide), poly(acrylic acid) and poly(methacrylic acid) derivatives and poly(vinyl pyrrolidone) (Sosnik et al., 2014).

One of the characteristics for optimal retention of mucoadhesive polymers upon application to targeted sites include charge potential with charged polymers demonstrating more adhesion than uncharged polymers (Khutoryanskiy, 2011). Mucoadhesive polymers have also been sub-divided into four based on their charged groups; anionic (e.g. poly (acrylic acid) and sodium alginate), cationic (e.g. chitosan) (Martin et al., 2003, Ayensu et al., 2012a, Costa et al., 2014, Boateng & Okeke, 2014), non-ionic (e.g. HPMC) (Perioli et al., 2004, Morales & McConville, 2011) and amphoteric polymers (gelatin) (Abruzzo et al., 2012).

1.5.5 *Ideal characteristics of a buccal mucoadhesive polymer*

Polymers used for buccal drug delivery should possess the following characteristics to qualify as an ideal mucoadhesive polymer (Dixit & Puthli, 2009, Mamatha et al., 2012):

- Should be non-toxic, non-irritant and with no leachable impurities.
- Biocompatible pH with good viscoelastic properties.
- Should possess a good spreadability, wetting, swelling and solubility.
- Should possess good buccal mucoadhesive property with an adhesively active group and suitable mechanical properties.
- Must be readily available at relatively low cost.
- Should be able to exhibit local enzyme inhibition with penetration enhancement properties.
- Should exhibit a suitable shelf life.
- Should possess an optimum molecular weight.
- Should be appropriately crosslinked and not suppress bond forming groups as a result of high degree of crosslinking.

1.6 **NIC delivery**

Nicotine (NIC) has been utilised as an active ingredient in the development of NIC replacement therapy that can be absorbed via the oral mucosa (chewing gum, sublingual tablets, lozenges), nasal mucosa (nasal spray and inhalers) and skin (transdermal patch).

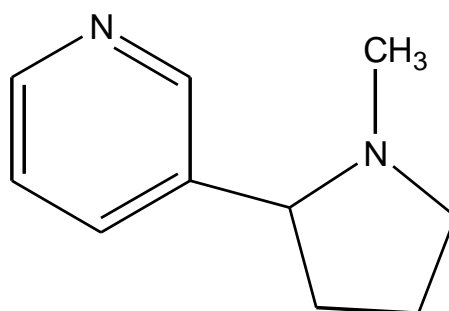


Figure 1.4: Chemical structure of NIC

1.6.1 *Chemical profile of NIC*

Nicotine (NIC) (Figure 1.4) is a tertiary amine consisting of a pyridine and pyrrolidine ring. It is also known as ‘nicotin’ or ‘nikotin’, however its name based on IUPAC is 3-(1-methylpyrrolidin-2-yl)pyridine. It is composed of 74.03% of carbon, 8.7% of hydrogen and 17.27% nitrogen (molecular formula: $C_{10}H_{14}N_2$) and can exist in two different stereoisomers i.e. (S)-NIC and (R)-NIC. The pharmaceutically active form of NIC is the (S)-NIC which is found in tobacco. NIC is a volatile, alkaline and colourless liquid (vapour pressure; 0.006kPa at 20°C) with two well separated pKa values of 3.04 and 7.84 which can form diprotonated, mono-protonated and neutral NIC species in an acid, neutral or basic solvent respectively (Pongjanyakul & Suksri, 2009). These different NIC species can readily permeate mucosa membranes such as nasal, buccal and sublingual mucosa. However, un-ionized species demonstrate higher permeation in the buccal membrane than ionized species (Nair et al., 1997). The challenges posed by NIC in the formulation of drug delivery systems are its volatility (0.006 kPa at 20°C) and oxidative degradation of the free base form.

1.6.2 *Pharmacokinetics of NIC*

1.6.2.1 *Absorption*

The absorption of NIC in the buccal mucosa is dependent on the environmental pH (Figure 1.5). This is due to the two well-separated pKa of NIC (i.e. 3.04 and 7.84) which implies that at acidic pH, it is ionised (diprotonated) and hence does not cross the membranes of the buccal mucosa cell, which is more lipophilic in nature. However, it can cross the cell membrane at physiological pH (7.4) where 31% of NIC is non-ionised. The advantage of the ready absorption of NIC in the buccal region (with higher bioavailability) is related to the thin epithelium and rich blood supply, compared to NIC which is swallowed. The swallowed portion is absorbed by the small intestines into the portal venous circulation where it undergoes

pre-systemic metabolism by the liver resulting in low bioavailability (30-40%) (Lorist & Snel, 2013, Nair et al., 1997).

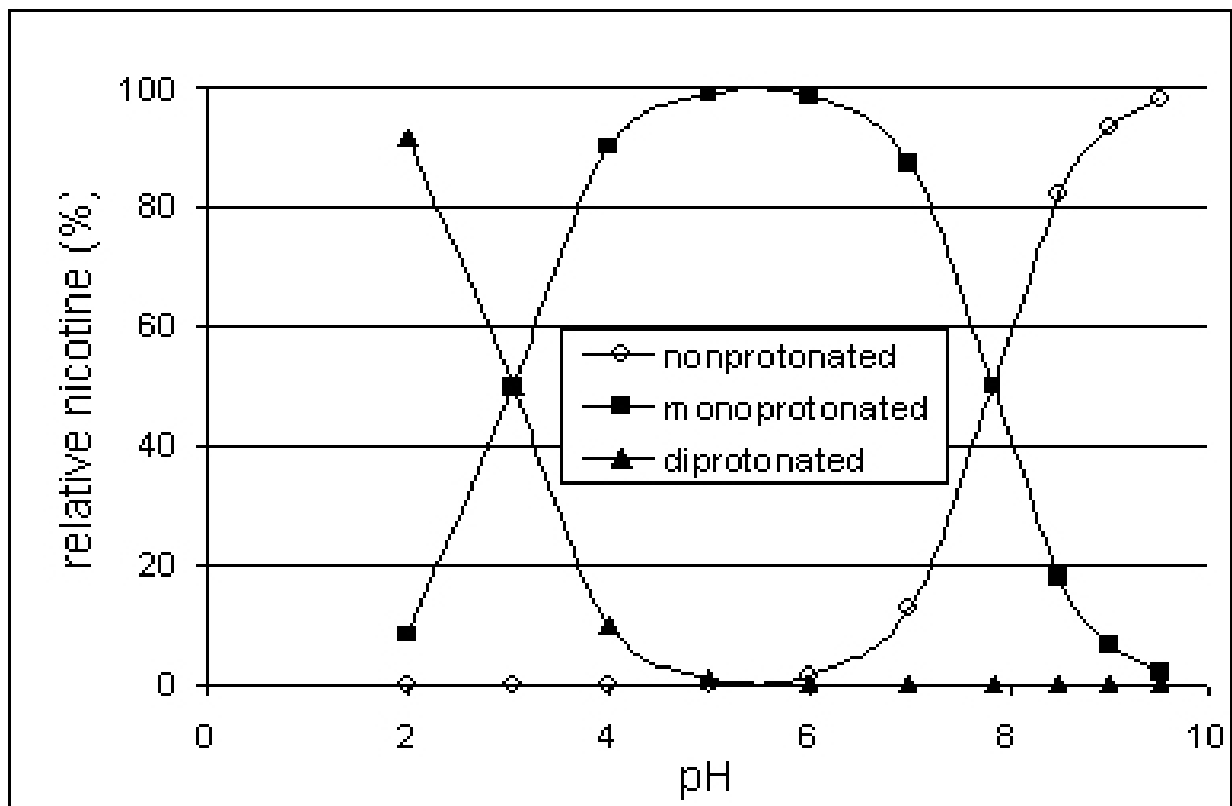


Figure 1.5: Concentration profiles (%) of different NIC species at different pHs (adopted from Djordjevic et al., 1997).

Most cigarettes containing flue-cured tobacco (most popular tobacco type) have an acidic smoke with little absorption in the buccal region even when held in the mouth. However, the absorption of NIC in cigarette smoke is possible through inhalation and then absorption via the alveolar epithelium into the systemic circulation. The rapid bioavailability is a result of the high blood flow in the pulmonary capillary with the passage of the entire blood volume in the lungs per minute. The concentration of NIC in the blood rises rapidly during cigarette smoking and reaches ultimate concentration at completion making the absorbed NIC reach different parts of the body as well as the brain (Benowitz et al., 1988).

The dose of NIC is complex in both cigarette smoking and chewing gum. Smoking is dependent on the intensity, duration and frequency/number of puffs, depth of inhalation, and the degree of intermingling of smoke with air. In the case of chewing gum, the dose of NIC is dependent on the rate of chewing, degree of swallowing and other local buccal factors (Lorist & Snel, 2013). However, NIC is readily absorbed through the oral and nasal mucosa, as well as the skin (NIC patches). NIC absorption through the skin can be slow and takes 6-8 hrs to attain maximum blood levels but can be effective in sustained delivery of NIC over a 24-hrs period. Nasal and buccal drug delivery, can however, be effective in mimicking the absorption of NIC via cigarette smoking with a more rapid absorption via the oral and nasal routes (Cheng et al., 2002, Keane, 2013).

1.6.2.2 Distribution of NIC

The blood carries absorbed NIC with 69% ionised and 31% unionised as a result of the physiological pH of the blood (pH 7.4), with less than 5% of NIC usually bound to plasma protein (Benowitz et al., 1982). NIC is widely distributed into body tissues at a steady state volume of distribution at around 2.6L/kg with the highest affinity in the liver, kidney, spleen and lung, and lowest in adipose tissue (fat). There is also high affinity of NIC in the brain with higher percentage of nicotinic cholinergic receptors in a smoker's brain. NIC can also accumulate in the gastric fluids and saliva via ion-trapping of NIC and can also accumulate in breast milk. In pregnant women, NIC can easily cross the placental barrier and accumulate in foetal serum showing higher concentration in comparison to maternal serum (Benowitz et al., 2009, Dempsey & Benowitz, 2001). The duration of NIC accumulation in the brain and/or various organs in the body to induce a pharmacological effect depends on the route and dosing rate. For delivery of NIC via cigarette smoking, it takes 10-20 seconds after a puff for NIC to reach the brain (Benowitz et al., 2009).

1.6.2.3 Elimination of NIC

The metabolism of NIC by the liver can lead to several metabolites (Figure 1.6).

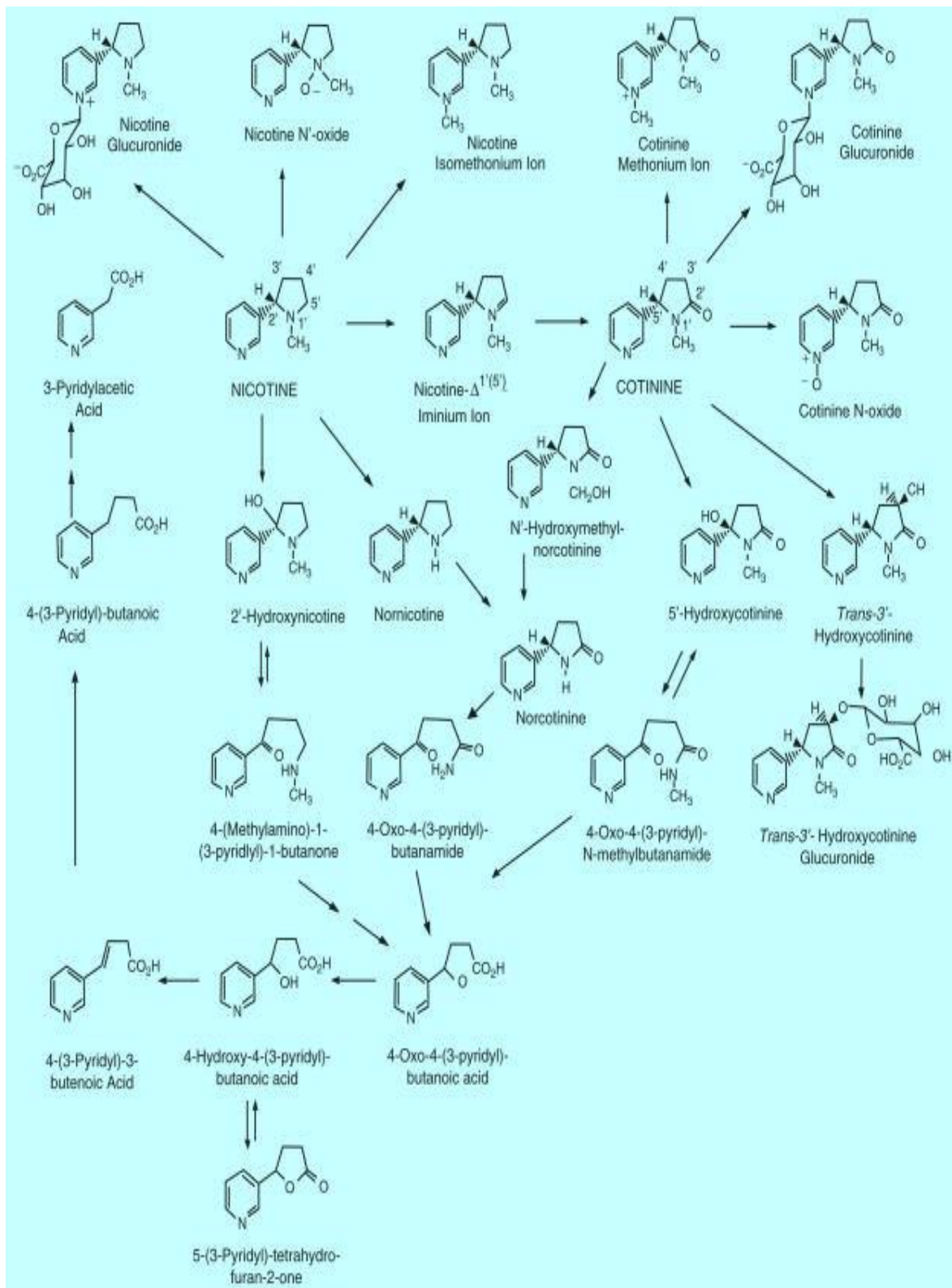


Figure 1.6: Pathways of NIC metabolism (Benowitz et al., 2009).

The most important metabolite of NIC in humans is the lactam derivative (cotinine) with 70-80% of NIC converted to cotinine. Other important metabolites include NIC- $\Delta^{1(5)}$ -iminium ion, NIC *N'*-oxide, NIC glucuronides, nornicotine and 2-hydroxynicotine. In a smoker's urine, although 70-80% of NIC is metabolised to cotinine, only 10-15% of NIC appears as uncharged cotinine, with the rest appearing as metabolites of cotinine. The half-life of NIC in the body is approximately 2 hours while the half-life of cotinine (16 hrs) is much longer. In acidic urine, NIC is ionised with low tubular reabsorption, resulting in a high renal clearance of about 600 ml min⁻¹ while in alkaline urine, NIC is unionised with high tubular reabsorption with a low renal clearance of about 17 ml min⁻¹. The urinary excretion of NIC therefore depends on urine pH with increased excretion in acidic urine (Benowitz et al., 2009).

1.7 NIC replacement therapy (NRT)

An attempt by a smoker to stop smoking instantly, can lead to several physiological and psychomotor withdrawal symptoms. These withdrawal symptoms include irritability, sleepiness, sleeplessness, unsteadiness, regular coughing, mouth blisters, constipation, chest stiffness and continuous cigarette craving (Cummings et al., 1985). According to researchers, the withdrawal symptoms can last between 2-12 hours (Shiffman et al., 2002, Hughes et al., 1994). The physiological and psychomotor symptoms associated with smoking cessation have been managed using NRTs with NIC as the active pharmaceutical ingredient. NIC cannot be developed as an oral pill due to its susceptibility to first pass metabolism in the liver which can retard bioavailability (Stead et al., 2008). As a result, different drug delivery strategies as well as drug delivery routes have been explored for NRT. Several NRT products have been developed to increase NIC absorption and to avoid the withdrawal symptoms of smoking and these include chewing gums, lozenges, mouth sprays, nasal sprays and transdermal patches. These products have been licensed in several countries including the UK and Canada to help

reduce withdrawal symptoms in the temporary abstinence periods which can usually arise in places where smoking is prohibited e.g. in airplanes, trains or hospitals (Brown et al., 2013).

1.7.1 *Transdermal patch*

NIC transdermal patches are adhesive sheets worn either based on their dose or over a period depending on the design and brand. Most transdermal patches are worn over a 24 hrs period, however, a few are worn for 16 hours per day (Stead et al., 2012). Usually, the 24 hour patch contains 21 mg of NIC while the 16 hours patch contains 15 mg of NIC. These dosing parameters are important in reducing withdrawal symptoms with peak symptoms at initial abstinence period (usually first 2 weeks). Shiffman et al. demonstrated that 21 mg/24 hour patch can be effective in reducing craving and withdrawal symptoms during the first 2 weeks of abstinence (Shiffman et al., 2000). The NIC patch is applied on the upper arm with less hair for the period according to manufacturer instructions. Examples of commercially available NRT for transdermal application include Nicoderm®, Nicorette® and Habitrol®. These products deliver between 5 to 25mg of NIC per day (Pastore et al., 2015). This form of NRT differs from other products by its slow and sustained release of NIC, however, does not match the fast delivery of NIC by cigarette which on average delivers between 1-3mg of NIC per puff and 20 to 40mg per day for a pack/day smoker (Stead et al., 2012). Itching, oedema, erythema have also been associated with transdermal patches (Ghulaxe & Verma, 2015).

1.7.2 *Oral NRT*

1.7.2.1 *Chewing gum*

NIC chewing gum was the first commercially available NRT. The formulation was developed by the formation of a NIC resin complex in a buffered chewing gum which enabled the absorption of NIC via the buccal mucosa and achieves approximately half of the plasma concentration achieved through cigarette smoking (Silagy et al., 2004). The NIC chewing gum

releases NIC upon compression by the teeth leading to absorption through the buccal mucosa and gums. The commercially available (e.g. Nicorette®) NIC gum usually comes in two separate doses of 2mg and 4mg, which can be recommended depending on the individual's smoking frequency and intention. For every piece of gum (e.g. 4mg dose), there is a slow rise in blood NIC levels and approximately 6 ng/ml is reached after 10 minutes and maximum levels within 30 minutes (Benowitz et al., 1988). NIC chewing gum can however, sometimes result in slow onset and prolonged plasma NIC levels which cannot be matched with the rapid pharmacological effect as well as high and quick maximum arterial NIC levels required for relief (Cheng et al., 2002). The concentration of NIC from the chewing gum available for buccal absorption can also be reduced by swallowing in the mouth during chewing. Other limitations include the fact that people with dental issues or who wear dentures find it difficult to use.

1.7.2.2 Lozenges

Lozenges are small tablets similar to NIC gum that dissolve slowly in the mouth over a 20-30mins duration. Lozenges release NIC in the mouth and absorbed through the buccal mucosa to reach the systemic circulation. Contrary to NIC gum which is based on the amount of cigarettes, lozenges are based on how soon in the morning (after sleeping) a smoker takes his first smoke which can be considered a powerful index of NIC dependency (Henningfield et al., 2005). Choi et al. demonstrated in their study a better pharmacokinetic profile of lozenges than NIC chewing gums with 8-10% higher maximal plasma concentration and 25-27% higher area under the concentration-time curve (AUC) at 2 and 4mg dose levels. The findings showed lozenges are effective and safe compared to NIC gum (Choi et al., 2003).

1.7.2.3 Spray

Oral sprays have been commercially developed for NRT and are liquid formulations stored in specifically designed containers that release a mist dispersed in air into an individual's

mouth and are absorbed via the buccal route. A typical example of a commercially available NRT oral spray is Nicorette® QuickMist mouth spray with a dosage of 1-2 sprays (1mg/spray) every 30 – 60 mins. The design of the dosage form enables it to absorb NIC more rapidly. The NRT oral spray has been reported to achieve its highest plasma concentrations after 10 minutes with variable blood levels compared to NIC chewing gum and lozenge (Chaplin, 2011). In spite of its ability to achieve rapid bioavailability, oral sprays still requires constant administration hence the bioavailability at the therapeutic level is not sustained.

1.7.2.4 Strips

NRT strips are commercially developed film formulations that dissolve upon contact with the mouth. The most common NRT strip formulation is NiQuitin® designed by GlaxoSmithKline. NiQuitin® strip is a fast dissolving oral formulation that releases NIC within 3 minutes of contact with the tongue (GlaxoSmithKline, 2016). This formulation deals with the challenge of chewing gum for people with dental issues or who wear dentures. However, it still faces the limitation of lower absorption of NIC due to the effect of swallowing (Bruce & Manning, 2009).

1.7.3 Electronic NIC delivery systems (ENDS)

Electronic cigarette or ENDS is an electronic device used for NRT and first became commercially available in the US in 2007 (Regan et al., 2013). An e-cigarette is made up of three parts; the battery, heating component and container or reservoir where NIC solution is stored. The mechanism by which it delivers NIC is by heating NIC solution as the user puffs, with the inhalation of the vapour produced into the lungs (Czogala et al., 2014). Though e-cigarettes can be used as NRT and smokers can easily migrate to its use, it can be misused as a substitute for cigarette especially in environments with smoking ban policies. This can encourage significant population of smokers not to quit smoking (Beaglehole et al., 2015). Furthermore, a recent study has demonstrated the presence of free radicals (although in a lower

concentration) in e-cigarettes which can possibly cause harm to human cells (Choices, 2015). Lerner *et al.*, also demonstrated the presence of a potential cytotoxic metal and oxidants (such as copper and perhydroxyl radical (HO₂·)) normally found in conventional cigarette, in e-cigarettes (Lerner *et al.*, 2015).

1.8 Proposed novel buccal delivery system for NRT

The buccal mucosa can provide a moderately rapid onset of action and also provide a sustained systemic delivery of the drug (Paderni *et al.*, 2012). The major challenge associated with developing an effective oral NRT formulation is to by-pass first pass metabolism in the liver and provide fast but prolonged bioavailability. Most of the commercially available NRT formulations discussed above either produce a rapid bioavailability but poor sustained NIC plasma levels (e.g. oral spray) or sustained NIC release but slow rate of plasma bioavailability (e.g. chewing gum and lozenges) (Cheng *et al.*, 2002). Furthermore, depending on the individual, a high content of NIC can mix with saliva and be swallowed upon administration of NRT formulations. For chewing gums, a correct chewing technique which involves gradual chewing of the gum is required and might not be suitable for older patients who tend to have fewer teeth (Tang *et al.*, 1994).

Mucoadhesive buccal NRT can however, provide a formulation with lower swallowing effect and can be modified to provide a balance between sustained NIC release and quick bioavailability as a result of close contact of the dosage form with the buccal mucosal surface. In the past, buccal films have been formulated as NRT using individual mucoadhesive polymers such as chitosan (Pongjanyakul *et al.*, 2013), HPMC (İkinci *et al.*, 2004) and SA (Pongjanyakul & Suksri, 2010). Following the challenge of volatility posed by the base form of NIC, the temperature involved in the drying process required during film formation can lead to loss of NIC. Therefore NIC freebase forms are either stabilised in film formulations using stabilizers such as magnesium aluminium silicate (MAS) (Pongjanyakul & Suksri, 2010), or

substituted with a more stable salt form such as NIC hydrogen tartrate (İkinci et al., 2004). However, the salt form is more hydrophilic and therefore its transport across the mucosa membrane can be poor (İkinci et al., 2006). As an alternative approach, the use of a freeze-dried wafer formulations for NRT in comparison with previously reported solvent cast film has been adopted as a novel approach in the current project to overcome the limitation associated with the liquid base form of NIC considering the lower temperatures involved during freeze-drying to obtain wafer formulations.

1.9 Polymers used

1.9.1 *Hydroxypropylmethylcellulose (HPMC)*

HPMC is a hydrophilic, biocompatible and semi-synthetic polymer derived from cellulose, which is a naturally occurring polysaccharide. They are commonly used as hydrophilic carriers in the development of controlled drug delivery systems in oral formulations (Colombo, 1993). They usually demonstrate high water-uptake when used as excipients in formulations and therefore affect the drug release mechanism. Drug release from HPMC based matrix is the result of polymer chain relaxation with volume expansion as water/biological fluid diffuses into the system, resulting in drug release by diffusion from the swollen matrix (Siepmann & Peppas, 2012).

1.9.1.1 *Properties of HPMC*

HPMC is a cellulose ether with a hydroxypropyl group substituting three hydroxyl groups for every anhydroglucose ring of a naturally occurring cellulose. Depending on the type and degree of substitution, various varieties of HPMC with different properties can be produced. The water soluble HPMC can be synthesized by substituting two hydroxyl group per anhydroglucose ring with hydroxypropyl group while non-water soluble HPMC substitute's three hydroxyl groups per anhydroglucose ring with hydroxypropyl group (Swamy & Ramaraj,

2009). The chemical structure (Figure 1.7) containing substituents such as $-\text{CH}_3$, $-\text{CH}_2\text{CH}(\text{CH}_3)\text{OH}$ which replace the hydrogen atom to form a methoxyl and hydroxypropyl groups. The percentage of hydroxypropyl and methoxyl groups and molecular weight determines the physicochemical properties of the polymer e.g. hydration and viscosity. According to the USP, the types of HPMC are classified based on $-\text{OCH}_3$ and $-\text{OCH}_2\text{CH}(\text{CH}_3)\text{OH}$ content which are HPMC 1828, HPMC 2208, HPMC 2906 and HPMC 2910, with the first two numbers indicating the percentage of methoxyl groups while the last two indicate the percentage of hydroxypropyl groups (Siepmann & Peppas, 2012).

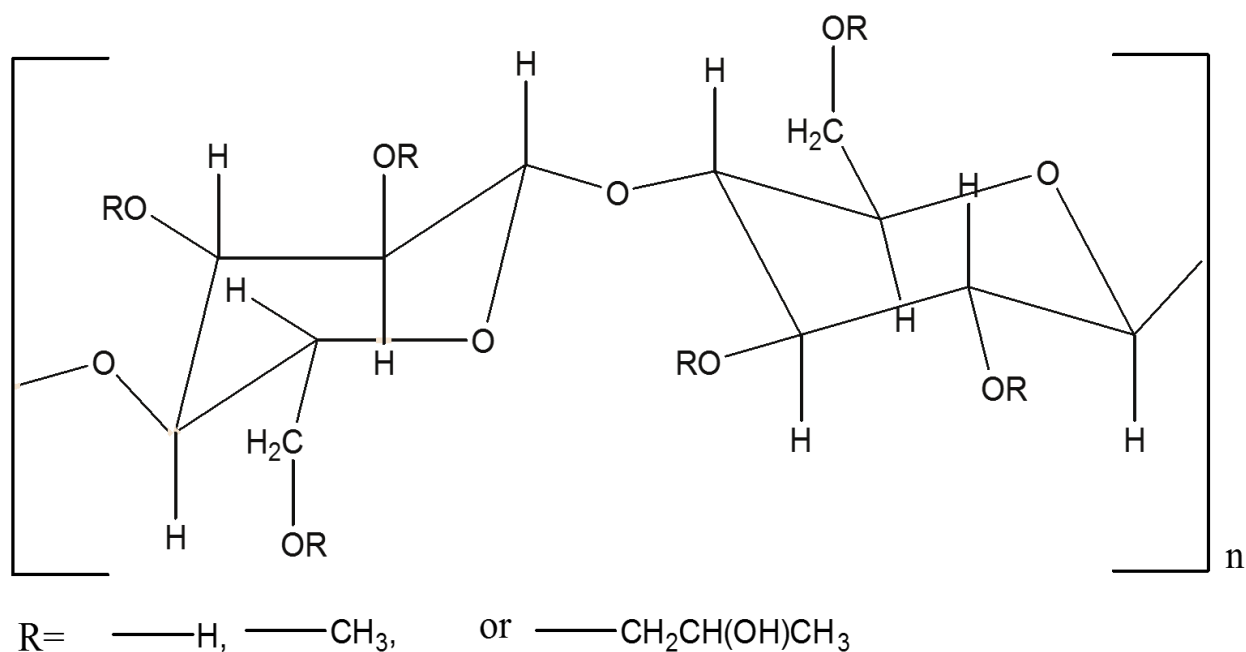


Figure 1.7: HPMC structure

1.9.2 Sodium alginate

Alginates are natural polysaccharides extracted from brown seaweed (Rioux et al., 2007). Sodium alginate is a salt of alginic acid commonly used for pharmaceutical products such as suspensions, gels and emulsions, as a thickener, emulsifier or stabilizer; they are non-toxic, biocompatible and biodegradable. They are hydrophilic polymers in nature and contain a carboxyl group which gives them their anionic property (Rhim, 2004) and provide the ability to demonstrate mucoadhesive properties as they can interact with mucin glycoprotein chains.

1.9.2.1 Structure of sodium alginate

Alginates are made up of D-mannuronic (M) and L-guluronic (G) acid residues arranged in the polymer chain blocks. The polymer chain blocks (homopolymer) made up of either M or G acid residues alone are separated by a combination of polymer chains (copolymer) of M and G which could either alternate or be completely random (Figure 1.8).

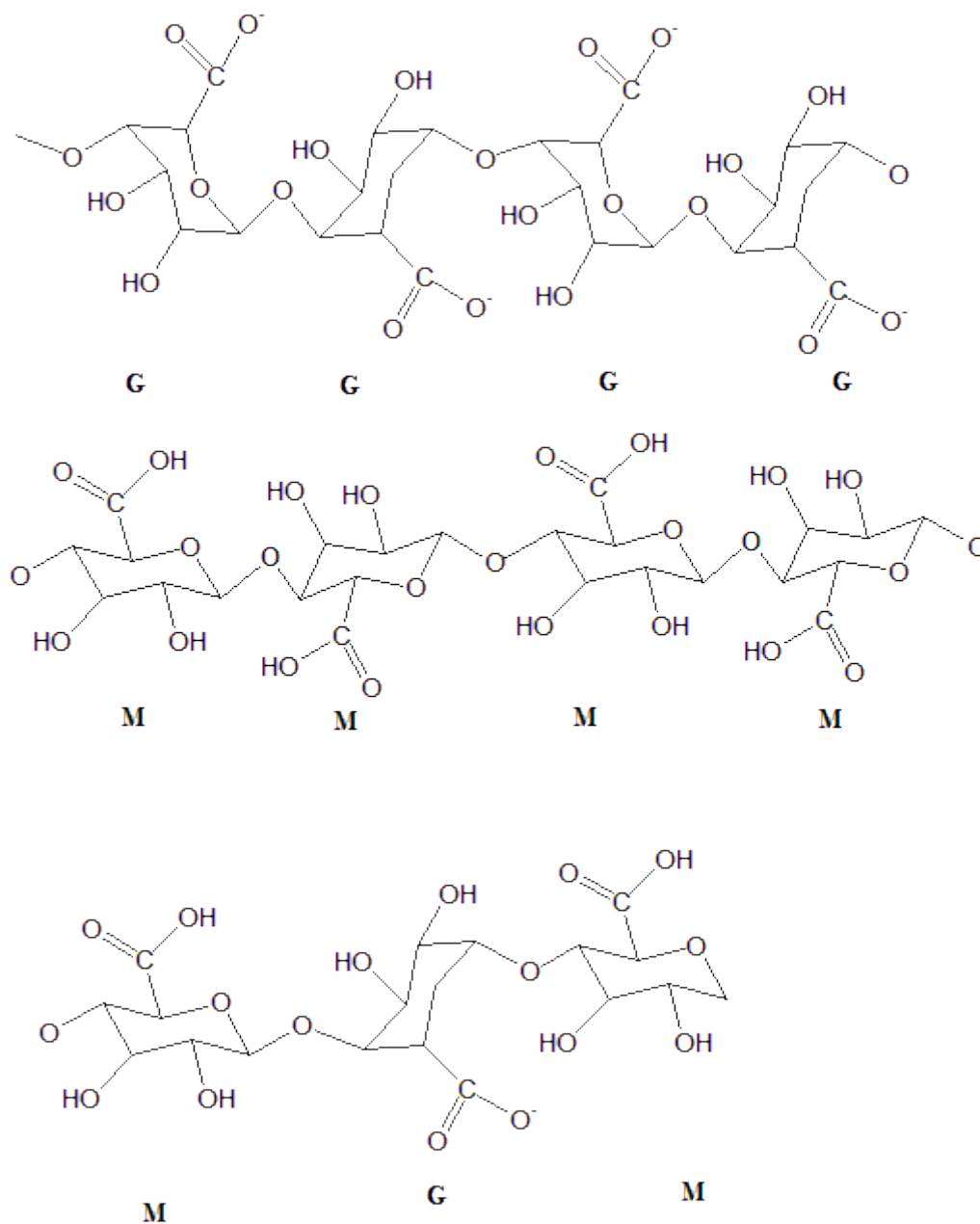


Figure 1.8: Alginate structure showing G and M polymer chain blocks.

Alginate forms gels or precipitates in the presence of divalent (Ca^{2+} , Fe^{2+} and Hg_2^{2+}) cations except for Mg^{2+} and multivalent cations (Fe^{3+} , Pb^{4+} and Sn^{4+}), but can form salts with monovalent ions such as sodium. The M and G content plays a vital role in gel formation as higher G blocks in polymer chain will result in the formation of stronger gels while lower G blocks in polymer chain produces flexible gels (Tønnesen & Karlsen, 2002).

1.9.3 *Rational for polymer selection*

HPMC and SA were selected in this study because they are non-toxic, biocompatible, biodegradable and relatively cheap polymers. HPMC can be effective as a release delaying polymer which makes it a suitable polymer for the controlled release of NIC in buccal formulations. The grade used i.e. Methocel K100 premium LV is a low viscosity HPMC grade with 22% methoxyl groups and 8% hydroxypropyl groups (HPMC 2208). The rationale for selecting a low viscosity HPMC grade was based on the rate of diffusion, as increase in HPMC viscosity decreases the rate of diffusion of incorporated drug. In addition to the viscosity, the K-chemistry grade of Methocel contains high ratio of hydroxypropyl (hydrophilic) to methoxyl (hydrophobic) group which contribute significantly to the degree of hydration of the HPMC grade (Dow, 2000). Although both polymers are mucoadhesive polymers, SA is more mucoadhesive than HPMC due its anionic properties which means that it can interact better with mucin glycoprotein chains which possess with both anionic and cationic properties. SA was therefore incorporated into the formulation to enhance mucoadhesion as well as interact with positively charged amine group of NIC. In addition to the above, G to M ratio of SA (1.06) was selected for appropriate mechanical properties as high G proportion can result in stronger gels (Mitchell and Blanshard, 1976).

1.10 Plasticizer

According to the council of the IUPAC (International Union of Pure and Applied Chemistry) a plasticizer can be defined as any substance introduced into a material with the aim of increasing its flexibility, workability or distensibility (Vieira et al., 2011). The aim of introducing a plasticizer to the formulation was to modify the mechanical properties of HPMC-SA films intended to improve elasticity and to overcome brittleness and stiffness. They decrease hardness, resistance to fracture, tension of deformation and amount of crystallinity in polymeric chain by reducing the intermolecular forces between the polymer chains and increasing the free volume hence improving handling of film formulation (Riggleman et al., 2007).

In selecting an appropriate plasticizer, physicochemical properties such as hydrogen bonding capability, polarity and solubility are considered. Other factors considered during selection of plasticizer for formulation development of film include compatibility with selected polymer/polymers, concentration of plasticizer-polymer ratio, formulation process characteristics, anticipated thermal behaviour and mechanical properties of finished film formulation. However, phase separation can occur with increased concentration of plasticizer (Vieira et al., 2011).

1.10.1 *Glycerol as selected plasticizer*

Glycerol (GLY) is a polyol compound with a colourless, clear, viscous and miscible with water and alcohol. It can absorb moisture from the atmosphere at room temperature and has a low vapour pressure, hence producing a plasticizing effect on films by reducing brittleness and stiffness with increased elasticity (Vieira et al., 2011). GLY can be classified as a natural plasticizer of polyols (including ethylene glycol (EG), polyethylene glycol (PEG), diethylene glycol (DEG), triethylene glycol (TEG) and propylene glycol (PG)). It comprises of three hydroxyl groups (Figure 1.9), which contribute to its hydrogen bonding capabilities as

well as its solubility in water. The rationale for the use of GLY in this research project include its plasticizing properties which improves film handling as well as increase in film solubility which increases dissolution rate. Other rationale for selecting GLY include cost, availability, non-toxic and optical quality (glossy).

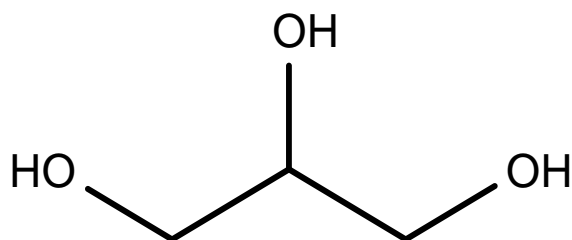


Figure 1.9: Chemical structure of GLY

1.11 Silicate clays

Silicate clays are used mainly in cosmetics as adsorbent, anticaking and as bulking agents (Elmore, 2002). They are also used in pharmaceutical industries as excipients in the manufacture of various dosage forms including tablets, ointments, capsules, suspensions, drops, syrups and lotions. They also possess therapeutic function as actives in the treatment of gastrointestinal and topical diseases (López-Galindo *et al.*, 2007).

Silicate clays can either be synthesized e.g. lithium magnesium silicate or refined from naturally occurring minerals e.g. magnesium aluminium silicate (MAS). Other silicate clays include kaolinite, bentonite, talc and magnesium trisilicate. In general, clay structures are made up of atomic networks (lattices) with two structural units. The first unit is made up of two sheets of oxygen closely packed together with aluminium, iron or magnesium inserted within these sheets in an octahedral coordination in such a way that the aluminium, iron or magnesium are in the centre of the oxygen or hydroxyl groups. The second unit is made up of a silicon atom which is also at the centre of 4 oxygen or hydroxyls arranged in the form of a tetrahedron.

A sheet with chemical composition, $\text{Si}_4\text{O}_6(\text{OH})_4$ is formed from a repeated silica tetrahedron groups arranged in a hexagonal network (Grim, 1968).

1.11.1 *Magnesium aluminium silicate*

MAS ($\text{Al}_2\text{MgO}_8\text{Si}_2$) silicate clay was used in this research as an excipient in the formulation of a NRT wafers and films. It is a pharmaceutical group of natural clays consisting of montmorillonite and saponite. It has been used as an adsorbent in improving the loading capacity of propranolol (a β -blocking agent) as well as the release patterns (Rojtanatanya and Pongjanyakul, 2008). Pongjanyakul (2010) also demonstrated the effect of MAS on NIC loaded film formulation with increase in NIC loading capacity with addition of MAS (Pongjanyakul *et al.*, 2010), which was the basis for its selection in the current research.

1.12 Formulation techniques

Film forming techniques include solvent casting, hot-melt extrusion and spray coating. Wafers on the other hand are formulated by freeze-drying also known as lyophilisation.

1.12.1 *Solvent casting*

Among the methods used in film preparation, solvent casting is the most reported in the literature. Its popularity is due to the simplicity in the development process as well as low cost of production on a research laboratory scale (Morales & McConville, 2011). The process involves gel (or polymeric solution) preparation, transfer of gel to an adequate casting container, drying process at a given temperature, cutting to final dosage form and packaging. Boateng *et al.*, demonstrated the use of the solvent casting technique in film formulation for buccal drug delivery system (Boateng *et al.*, 2009). Both aqueous and organic solvents can be used in the formulation of films (Kianfar *et al.*, 2014, Boateng *et al.*, 2009).

1.12.2 *Lyophilisation/freeze drying*

Freeze-drying of polymeric gels or solutions produces porous sponge-like wafers. Wafers have been utilised in pharmaceutical formulations such as fast dissolving tablets (Ganguly et al., 2014), wound healing drug delivery dressings (Pawar et al., 2014) and buccal formulations (Ayensu et al., 2012a). Freeze-drying utilises the mechanism of sublimation to remove solvent from a solid frozen system. The process is therefore grouped into three stages based on its mechanism: the formation of solid by freezing (freezing step), sublimation of solvent (usually water) from solid to gas (primary drying step) and final drying (secondary drying) (Kasper & Friess, 2011).

1.13 Aim and objectives

The aim of this project is to develop two composite dosage forms (wafers and films) and successfully loading NIC on the dosage forms for NRT via the buccal mucosa. The development of the NRT dosage forms will involve the combination of two mucoadhesive polymers (HPMC and SA), together with plasticizer (GLY) and drug stabilizer MAS. These components will be vital in the optimisation of the dosage forms to enable effective NIC loading as well as achieve expected functional physicochemical properties.

Objectives of the study:

- i. To formulate optimized composite solvent cast films and freeze-dried wafers for NIC replacement therapy via the oral buccal mucosa for NRT.
- ii. To show the effectiveness of the use of mucoadhesive GRAS polymers (HPMC and SA) in the delivery of NIC via the buccal mucosa.
- iii. To stabilise NIC in both wafers and films using MAS in order to achieve therapeutically effective and reproducible drug content, and investigate the possible mechanism of NIC stabilization by MAS.
- iv. To evaluate stability of films and freeze-dried wafers at different storage conditions.

- v. To compare the functional physicochemical characteristics such as hydration (swelling), mucoadhesion and drug release from the two different formulations (wafers and films) as well as with commercially available NIC oral strip.
- vi. To evaluate the permeation of NIC across the buccal mucosa tissue using both *in vitro* and *ex vivo* models.

CHAPTER 2: PREPARATION AND CHARACTERISATION OF HPMC AND SODIUM ALGINATE (SA) BASED BUCCAL WAFERS AND FILMS.

2.1 Introduction

Various researchers have demonstrated the potential use of the buccal mucosa in the delivery of poorly bioavailable drugs as well as drugs susceptible to first pass metabolism including proteins and peptides (Boateng & Okeke, 2014, Ayensu et al., 2012b, Hirlekar & Kadam, 2009, Kianfar et al., 2012). The key advantage of buccal drug delivery over conventional oral drug delivery through the gastrointestinal tract is its ability to bypass the hepatic metabolic effect of drug degradation in the liver by direct absorption of drug into the bloodstream. This route can also be an alternative to the parental route which can be inconvenient to patients as it requires skin piercing using injection needle and also requires trained medical personnel for the procedure (Sattar et al., 2014, Hearnden et al., 2012).

The buccal mucosa can be utilised as a potential route for nicotine (NIC) replacement therapy (NRT) as NIC is susceptible to degradation when delivered via oral-gastrointestinal tract. It can also be an alternative to transdermal patches which takes an extended time period after administration for a smoker to achieve a saturation peak (Cheng et al., 2002).

NIC is the major component of tobacco used in cigarette production and is an alkaline, colourless and volatile liquid that is soluble in both water and other organic solvents including alcohol. As discussed in the previous chapter, the well-separated pKa of NIC (3.04 and 7.84) enables it to exist as either protonated, diprotonated or neutral species in neutral, acidic or alkaline conditions respectively. However, all species of NIC can readily be absorbed across the skin and mucosal surfaces (Pongjanyakul & Suksri, 2009), but can differ in permeability, which is pH dependent with unionised NIC species being 10 times more permeable than protonated species (Adrian et al., 2006).

The use of mucoadhesive polymers such as HPMC and sodium alginate (SA) in film and/or wafers formulation will impart adhesive characteristics to the final dosage form. These mucoadhesive polymers can possess functional properties such as surface charge and solubility that play a vital part in mucoadhesion. The ability to form a strong electrostatic interaction with the charged surface of mucin gives charged polymers such as SA an advantage of higher adhesion than non-ionic polymers (e.g. HPMC) (Khutoryanskiy, 2011). Therefore, composite polymeric systems can be adopted to enhance the functional properties of a mucoadhesive dosage form. HPMC is very effective in designing controlled drug delivery systems while SA can be used to improve functional properties such as mucoadhesion of a given polymeric dosage form. Furthermore, the charged property (anionic) of SA can be utilised as a potential means of interaction with drugs with charged group such as the charged species (i.e. protonated and diprotonated) of NIC. The interaction of the carboxylic acid side chain of SA and the charged amine group of protonated or diprotonated NIC species can improve drug stability and provide further control in the release of drug from the polymer matrix (Pongjanyakul & Suksri, 2009, Siepmann & Peppas, 2012).

Wafers and films have been investigated extensively as buccal delivery dosage forms. Films are usually prepared by the solvent evaporation method (Salamat-Miller *et al.*, 2005; Chinna *et al.*, 2011) while wafers are prepared by sublimation process known as freeze-drying (Boateng *et al.*, 2010). Elasticity, flexibility and toughness are essential properties to be considered in film formulation due to stress from mouth motions (Gilhotra *et al.*, 2014) as films have to show adequate mechanical characteristics (such as moderate toughness, low brittleness and high elasticity) to tolerate such stress. In the case of wafers, porosity plays a vital role in determining the hardness of wafers, which affects ease of handling (Boateng *et al.*, 2010).

This chapter describes the formulation development of freeze-dried wafers and solvent evaporated films, and comparing their physicochemical characteristics as mucoadhesive

systems for NIC replacement therapy. The formulations have been characterised using texture analysis, scanning electron microscopy, X-ray diffraction (XRD), attenuated total reflection – Fourier transform infrared (ATR-FTIR) spectroscopy differential scanning calorimetry (DSC) and high-performance liquid chromatography (HPLC) for mechanical/hardness, surface/internal morphology, crystallinity, chemical interactions, thermal, drug content/release properties respectively. The swelling profiles were also determined by calculating the swelling index for hydration and water holding capacity. The characterisation data was used to compare the properties of different HPMC-SA composite films. The selected optimized formulation (wafer) was then further characterised for drug dissolution behaviour.

2.2 Materials and methods

2.2.1 *Materials*

The materials used in this study included; HPMC (Methocel K100 premium LV) obtained as a gift from Colorcon Limited (Dartford, UK). Sodium hydroxide, potassium dihydrogen phosphate and gelatine were all purchased from Fluka Analytical (Buchs, Switzerland); Nicotine (liquid form), sodium alginate, and mucin from porcine stomach were obtained from Sigma-Aldrich (Dorset, UK). Sodium acetate, trimethylamine and glycerol were purchased from Fisher Scientific (Loughborough, UK).

2.2.2 *Preparation of composite wafers*

Viscous polymeric solutions for BK and DL wafers were prepared in similar manner as for the films but without using GLY. The polymeric solutions (1g) were poured into each well of a 24 well plate (diameter 15.5mm). The concentrations of polymers and drug present in each polymeric solution are summarised in °C to 25°C (12hrs 30mins).

Table 2.1. The freeze-dried wafers were prepared using an automated lyophilisation cycle on a Virtis Advantage XL 70 freeze-dryer (Biopharma process systems, Winchester, UK). The well plates containing the polymeric solutions were loaded onto the shelves of the freeze-dryer and programmed for freezing, primary drying and secondary drying steps (Figure 2.1).

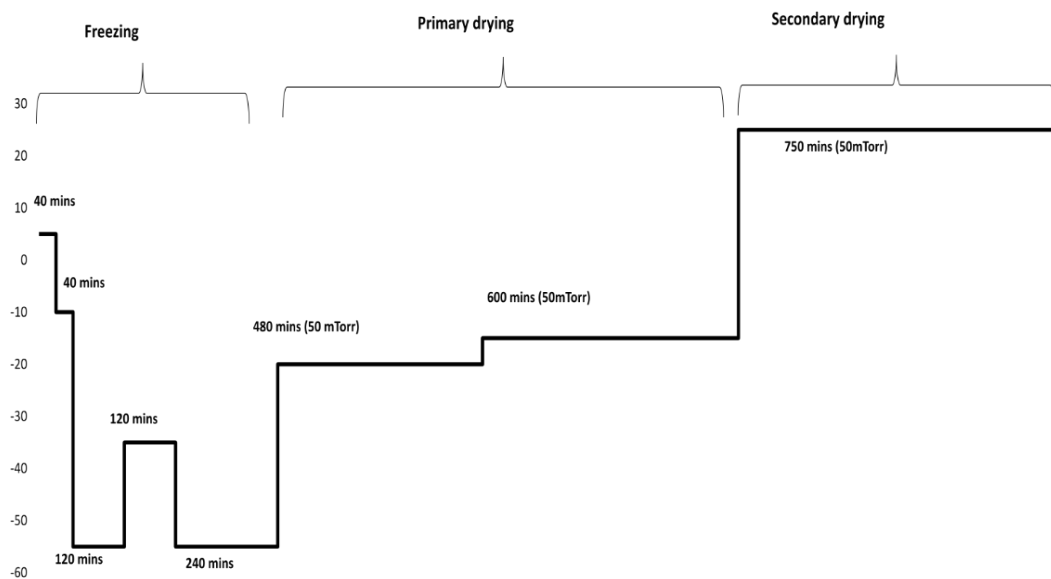


Figure 2.1: Freeze-drying process chart used to produce wafers with appropriate characteristics.

The freezing step involved cooling the sample from room temperature to 5°C (40mins), 5°C to -10°C (40mins), and then from -10°C to -55°C (120mins). An annealing step was incorporated into the freezing cycle in order to improve pore size distribution by increasing the temperature from -55°C to -35°C (2hrs) and then cooling back down to -55°C (3hrs). Additional freezing was performed to ensure uniformity by freezing at -55°C (1hr) with a condenser temperature of -55°C and pressure of 200mTorr. The primary drying occurred under high pressure of 50mTorr, with temperature raised from -55°C to -20°C (8hrs) and further increased from -20°C to -15°C (10hrs). Secondary drying occurred at the same pressure as primary drying but increasing the temperature from -15°C to 25°C (12hrs 30mins).

Table 2.1: Composition of selected polymers and drug used in polymeric solutions for freeze-dried composite wafer formulations.

<i>Sample name</i>	<i>HPMC</i> (% w/v)	<i>SA</i> (% w/v)	<i>NIC</i> (g)	<i>Total excipient content in</i> <i>final solution (% w/v)</i>
<i>BK SA 0.00</i>	2.00	0.00	0.00	2.00
<i>BK SA 0.25</i>	1.75	0.25	0.00	2.00
<i>BK SA 0.50</i>	1.50	0.50	0.00	2.00
<i>BK SA 0.75</i>	1.25	0.75	0.00	2.00
<i>DL SA 0.00</i>	2.00	0.00	0.20	2.00
<i>DL SA 0.25</i>	1.75	0.25	0.20	2.00
<i>DL SA 0.50</i>	1.50	0.50	0.20	2.00
<i>DL SA 0.75</i>	1.25	0.75	0.20	2.00

2.2.3 Preparation of composite films

Blank (BK) viscous polymeric solutions were prepared by dissolving HPMC, sodium alginate (SA) and glycerol (GLY) in 100ml of distilled water at 25°C. The resulting polymeric solutions were left to stand overnight to remove all air bubbles, 30g was poured into a Petri dish (90mm diameter) and dried in an oven at 30°C for 18-20hrs. Drug loaded (DL) films were prepared as above with the addition of NIC to the polymeric solutions before drying in the oven. The concentrations of polymers, plasticizer and drug used in each viscous polymeric solution have been summarised in Table 2.2.

Table 2.2: Composition of selected polymers, plasticizer and drug used in composite polymeric solutions for film formulations.

Sample name	HPMC (% w/v)	SA (% w/v)	GLY (% w/v)	NIC (g)	Total excipient content in final solution (% w/v)
BK SA 0.00	2.00	0.00	2.00	0.00	4.00
BK SA 0.25	1.75	0.25	2.00	0.00	4.00
BK SA 0.50	1.50	0.50	2.00	0.00	4.00
BK SA 0.75	1.25	0.75	2.00	0.00	4.00
DL SA 0.00	2.00	0.00	2.00	0.20	4.00
DL SA 0.25	1.75	0.25	2.00	0.20	4.00
DL SA 0.50	1.50	0.50	2.00	0.20	4.00
DL SA 0.75	1.25	0.75	2.00	0.20	4.00

2.2.4 *Texture analysis (TA)*

2.2.4.1 *Mechanical properties of wafers (hardness)*

The resistance to compressive deformation (hardness) of the freeze-dried wafers was determined using a texture analyser (HD plus, Stable Micro System, Surrey, UK) equipped with a 5kg load cell. The BK and DL wafers were compressed at 5 different locations of each wafer ($n = 3$), using a 2mm cylinder stainless steel probe to a depth of 2mm at a speed of 1mm/sec with the instrument in compression mode.

2.2.4.2 *Tensile properties of films*

The tensile properties of the films were analysed using a texture analyser (HD plus, Stable Micro System, Surrey, UK) equipped with a 5kg load cell. Prior to obtaining tensile data, the BK and DL films were cut into dumb-bell shaped strips and the thickness of films was measured using a micrometre screw gauge. The films were fixed in between two tensile grips

of the TA instrument and then stretched at a test speed of 2mm/s till breaking point. The elongation at break (%), tensile strength and elastic modulus was determined using equations (1), (2) and (3) respectively ($n = 3$) (Morales & McConville).

$$\text{Elongation at break}(\%) = \frac{\text{Distance travelled}}{\text{initial film length}} \times 100 \quad (1)$$

$$\text{Tensile strength} = \frac{\text{peak force at break}}{\text{cross - sectional area of the film}} \quad (2)$$

$$\text{Elastic modulus} = \frac{\text{slope of stress - strain curve}}{\text{thickness (film)} \times \text{cross head speed}} \quad (3)$$

2.2.5 Scanning electron microscopy (SEM) analysis

The surface morphology of both BK and DL wafers and films were analysed using a Hitachi SU8030 (Hitachi High-Technologies, Krefeld, Germany) scanning electron microscope. The wafers and films were cut into small strips and placed on Agar Scientific G301 aluminium pin-type stubs using an Agar Scientific G3347N double-sided adhesive carbon tape. The wafers were gold coated for clearer pore image, while films were chromium coated using a Sputter Coater (Edwards 188 Sputter Coater S1508). Wafers were analysed at 5.0kV accelerating voltage while films were analysed at 2.0kV accelerating voltage.

2.2.6 Wafer pore analysis

Wafer pore analysis was used to evaluate the porosity of HPMC-SA wafer structure. The wafers were initially weighed and then immersed in 5ml of ethanol in a glass vial and left to stand for 10mins. The vials with ethanol and wafers were degassed to remove air bubbles trapped inside the wafers for 10mins. After degassing, the wafers were carefully removed from the solvent, wiped to remove excess solvent and immediately weighed to avoid loss of ethanol due to its volatility (0.006 kPa at 20°C).

The percentage porosity of wafers was calculated using equation (4) below:

$$P = \frac{V_p}{V_g} \times 100 = \frac{W_f - W_i}{\rho_e V_g} \quad (4)$$

Where

V_p = pore volume

V_g = wafers geometrical volume

W_f = final weight of wafer

W_i = initial weight of wafer

ρ_e = ethanol density (0.789 g/cm³)

2.2.7 *Thermogravimetric Analysis (TGA)*

TGA studies were performed using a Q5000 (TA Instruments Thermal Analysis) thermogravimetric analyser (TGA). Samples of wafers and films were weighed (1-3mg) and placed on an aluminium sample pans. Samples were heated under nitrogen (N₂) gas with a flow rate of 25ml/min, from ambient temperature 25°C to 100°C at a heating rate of 10°C/min to evaluate the water content of wafers and films after preparation. The experiment was performed once considering the weight accuracy ($\pm 0.1\%$) and precision ($\pm 0.01\%$) of Q5000 TGA.

2.2.8 *Differential scanning calorimetry (DSC) analysis*

A TA Instrument's DSC was used to thermally analyse pure samples as well as BK and DL wafers and films. Wafers and films were weighed (1-3mg), placed in Tzero pans and covered with Tzero hermetic lids. The samples were heated from -50°C to 150°C at the rate of 10°C/min under constant purge of nitrogen. The experiment was performed once considering the temperature accuracy ($\pm 0.025^\circ\text{C}$) and precision ($\pm 0.005^\circ\text{C}$) of TA Instrument's DSC.

2.2.9 *X-ray diffraction (XRD) analysis*

The physical (crystalline/amorphous) form of both BK and DL wafers and films was investigated using a D8 Advantage X-ray diffractometer. Wafers were compressed using two

clean cover glasses whilst films were cut into small pieces, placed on the holder and mounted onto the sample cell. For pure starting materials, Mylar was used to hold the powders before placing on the sample cell. The samples were analysed in transmission mode at a diffraction angle ranging from 5° to 50° 2θ, step size 0.04°, and scan speed of 0.4s/step.

2.2.10 *Attenuation total reflectance Fourier transform infrared (ATR-FTIR) analysis*

ATR-FTIR spectra were obtained using a Perkin Elmer Spectrum instrument which was equipped with a diamond universal ATR-unit. The composite wafers and films were cut into strips, placed on the ATR diamond crystal and force applied using a pressure clamp to allow adequate contact between the sample and diamond crystal. Pure solid samples (i.e. HPMC and SA) were also examined in a similar way as the wafers and films. For NIC, there was no force applied as the liquid could form intimate contact with the diamond crystal without any applied force. The resolutions of the samples were recorded at 4 cm⁻¹ within the range of 450-4000 cm⁻¹. Background spectra were subtracted in order to obtain a reliable absorbance of each sample.

2.2.11 *Swelling studies*

The swelling capacities of both BK and DL wafers and films were determined by immersing each formulation into 5ml of phosphate buffer (pH 6.8; ionic strength, 0.07M). The percentage swelling index was investigated by recording change in weight at time intervals of 2 mins up to 30 mins. For every time point, the medium was carefully removed to obtain an accurate weight of the sample and replaced with fresh medium. Three replicates were performed for each sample and swelling index (%) was calculated using equation (5) (Nair et al., 2013)

$$\text{Swelling index} = \frac{W_s - W_d}{W_d} \times 100 \quad (5)$$

Where W_d = dry weight of polymeric wafer/film.

W_s = weight of wafer/film after swelling.

2.2.12 *Mucoadhesion studies*

Adhesion test was performed on BK and DL wafers and films using a TA. HD *plus* Texture Analyser (Stable micro systems, Surry, UK) in tensile mode and fitted with a 5kg load cell. Films were cut considering the mathematical area of wafers (a circle with diameter = 15.5mm). The wafers and films were attached to an adhesive probe (75mm diameter) of the TA instrument using a double-sided adhesive tape. Gelatine gel [6.67% (w/v)] was prepared by dissolving gelatine in water at 70°C, poured into a Petri dish (86mm diameter) and placed in a fridge overnight to set into a solid gel to represent the buccal mucosa surface. Mucin solution (2% w/v) was prepared by dissolving mucin powder from porcine stomach in a phosphate buffer (pH 6.8; ionic strength, 0.07M) and 0.5ml evenly spread on the surface of the set gelatine gel. Using the TA analyser, the probe with film or wafer attached was lowered to make contact with the model buccal mucosa surface and was detached after the contact time of 60 sec with an applied force of 1.0N. Mucoadhesive strength was determined by the maximum adhesive force (F_{\max}) required to detach the sample from the model buccal surface, work of adhesion was determined by the area under the force-distance curve, while cohesiveness represents the distance the wafers/films travelled till they detached from the model buccal surface. Texture Exponent 32[®] software was used in collecting and processing the data from the texture analyser.

2.2.13 *HPLC analysis*

NIC was analysed by HPLC using an Agilent 1200 HPLC instrument (Agilent Technologies, Cheshire, UK) with an auto sampler. The stationary phase used was a C-18 reverse-phase column, 4.6 x 250mm (Phenomenex HPLC column, Cheshire, UK). Sodium acetate solution, methanol and trimethylamine, (88:12:0.5 v/v) were used as mobile phase with pH adjusted to 4.2 using glacial acetic acid, at a flow rate of 1ml/min and UV detection at 259nm (Pongjanyakul & Suksri, 2010). The retention time of NIC was detected at

approximately 4.5 min. A calibration curve was plotted using standards with NIC concentration ranging from 40µg/ml to 400µg/ml ($R^2=0.9994$).

2.2.14 *Drug content (% loading and recovery)*

The content of NIC in DL wafers and films was assayed, by accurately weighing both DL wafers and films and dissolving in 10ml of distilled water. The resulting wafer/film solution was collected into a syringe, filtered through a 0.45µm cellulose acetate membrane, transferred into HPLC vials and placed in HPLC sample chamber and analysed as described above ($n = 3$).

2.2.15 *In vitro drug dissolution*

In vitro drug dissolution of DL wafers was performed with the help of a Franz-diffusion cell apparatus. The receptor compartment was filled with 8ml of phosphate buffer (pH 6.8) with a mesh on the receptor surface. The donor and receptor compartments were sealed with paraffin, to limit evaporation and held together by a pinch clamp. The system was placed on a water bath at 37°C with magnetic stirring at approximately 200rpm. The wafer samples were weighed and placed on the mesh between the donor and receptor compartments. At predetermined time intervals, 0.5ml aliquots of the dissolution media were withdrawn using a 1ml syringe, filtered through a 0.45µm cellulose acetate membrane, transferred into HPLC vials and analysed using HPLC. Each aliquot withdrawn at each time point, was replaced with fresh buffer solution, in order to maintain a constant volume of dissolution media. The percentage drug released from wafers was calculated and plotted against time ($n = 3$).

2.2.16 *Statistical analysis*

Statistical analysis was performed using student t-test and / or one-way ANOVA to compare the results. The results were expressed as mean \pm standard deviation and significant differences were determined at a level of $p < 0.05$.

2.3 **Results**

2.3.1 *Formulation development*

2.3.1.1 *Wafers*

HPMC wafers formulated by lyophilisation were easily removed from well plates, easy to handle and were intact, therefore there was no need to use plasticizer to enhance their physical and handling properties unlike the films.

2.3.1.2 *Films*

BK unplasticised HPMC film with no SA was highly brittle and therefore was difficult to remove from the Petri dish. As a result, GLY was added to the polymeric solutions to reduce brittleness and increase flexibility of the final films. The optimum concentration of GLY (2% w/v) present in the polymeric solutions for the BK HPMC film was selected based on texture analysis and SEM analysis. Polymeric solutions of plasticised composite HPMC-SA films were easy to pour and were easy to remove from the Petri dish after oven drying. DL HPMC-SA films were much easier to remove from Petri dishes than BK HPMC-SA film. All HPMC-SA films were transparent but as concentration of SA increased, the film showed a light yellowish colour imparted by pure SA powder.

2.3.2 *Texture analysis*

2.3.2.1 *Mechanical properties of wafer (hardness)*

Texture analysis was used to determine the resistance to compressive deformation (hardness) of the BK and DL HPMC-SA wafers. Figure 2.2 showed the hardness profiles of

BK and DL HPMC-SA wafers containing different ratios of both polymers. DL HPMC wafer (SA 0.00) demonstrated higher resistance to compression with a peak force of $1.50 \pm 0.13\text{N}$ than BK HPMC (SA 0.00) wafers with a peak resistance force of $1.27 \pm 0.10\text{N}$. The BK HPMC-SA wafers demonstrated a slight decrease in the hardness for HPMC-SA composite wafer containing the lowest amount of SA (i.e. SA 0.25) when compared to HPMC alone (i.e. SA 0.00), but started to increase for subsequent HPMC-SA composite wafers containing SA 0.50 and 0.75. On the other hand, DL HPMC-SA wafers showed a decrease in hardness with increase in SA concentration from $1.50 \pm 0.13\text{N}$ for HPMC only wafer (i.e. SA 0.00) to $1.06 \pm 0.06\text{N}$ for DL composite wafers containing SA 0.75. The comparison between BK and DL HPMC-SA wafers, however, did not demonstrate any significant difference ($p = 0.775$).

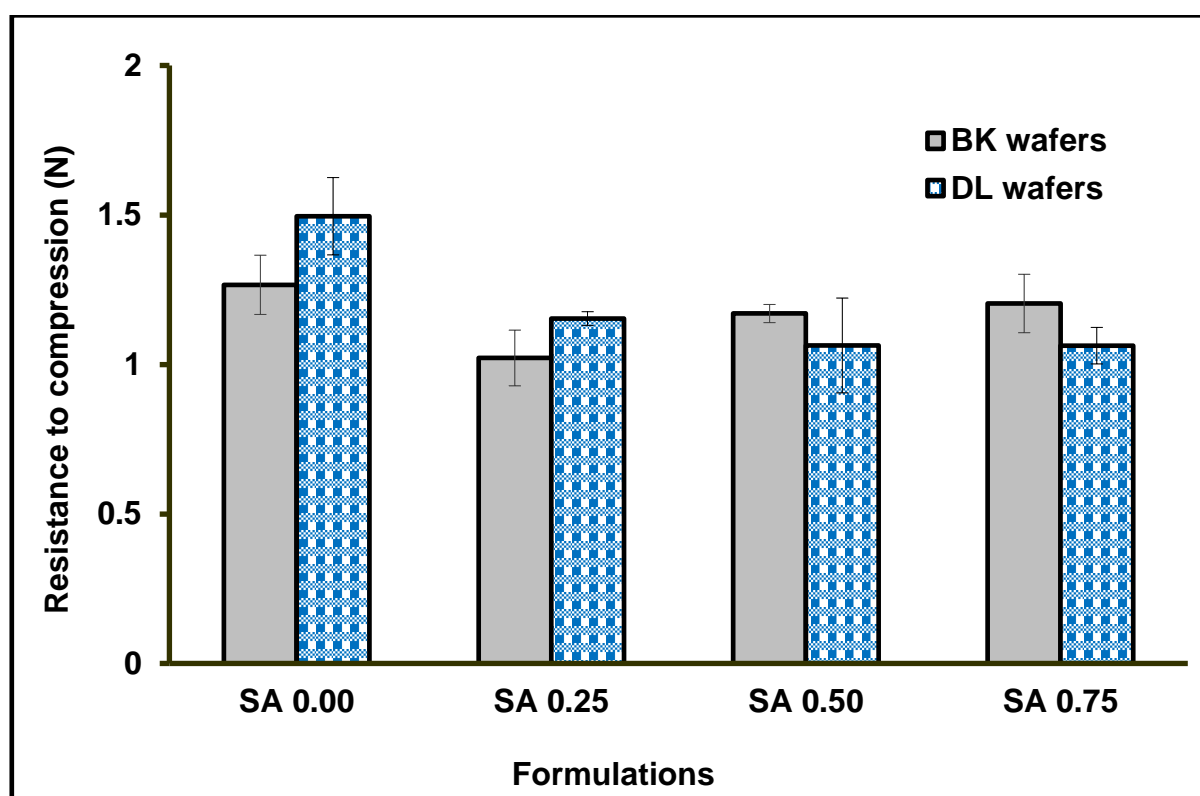


Figure 2.2: Hardness profiles of BK and DL HPMC-SA composite wafers showing the resistance to compression deformation with changing SA content ($n = 3, \pm SD$).

2.3.2.2 Tensile properties of films

Texture analysis was used to analyse the mechanical properties of the films. The effect of GLY is demonstrated in Figure 2.3. As concentration of GLY in the original HPMC solution

increased from 0% w/v to 4% w/v there was a decrease in brittleness and stiffness, as well as increase in elasticity which are related to tensile strength in Figure 2.3(a), elastic modulus Figure 2.3(b) and elongation at break (%) Figure 2.3(c) respectively. Highly plasticised BK HPMC films prepared from polymeric solutions containing more than 2% w/v GLY demonstrated very low tensile strength and elastic modulus as well as very high elongation at break, which are undesirable and can result in difficulty in handling of the film due to their sticky nature.

Figure 2.4 also shows the tensile strength (brittleness), elastic modulus (stiffness) and % elongation at break (elasticity) results of BK and DL composite HPMC-SA films. The tensile strength of both BK and DL composite HPMC-SA films (Figure 2.4a) remained constant as the amount of SA increased. This implies that there is no effect of SA concentration on the brittleness of BK and DL HPMC-SA composite films. However, DL HPMC-SA composite film showed significantly ($p = 0.0028$) higher tensile properties than BK HPMC-SA composite film.

BK composite HPMC-SA films showed a decrease in elastic modulus (Figure 2.4b) as SA content increased from 0.25 to 0.75, however, the elastic modulus for BK films with no SA (SA 0.00) ($12.42 \pm 1.46\text{N/mm}^2$) and BK SA 0.25 ($12.42 \pm 1.20\text{N/mm}^2$) remained the same in BK HPMC-SA composite films. On the contrary DL HPMC-SA composite films showed a significantly ($p=0.0334$) lower elastic modulus than BK HPMC-SA composite film as well as an increase in elastic modulus as SA concentration increased. A significant difference ($p=0.0019$) was also observed between the elongation at break (%) of BK HPMC-SA films and DL HPMC-SA films (Figure 2.4c) with the highest elongation at break (%) observed for films containing SA 0.75 in both BK ($39.62 \pm 2.99\%$) and DL ($52.63 \pm 4.27\%$) HPMC-SA composite films.

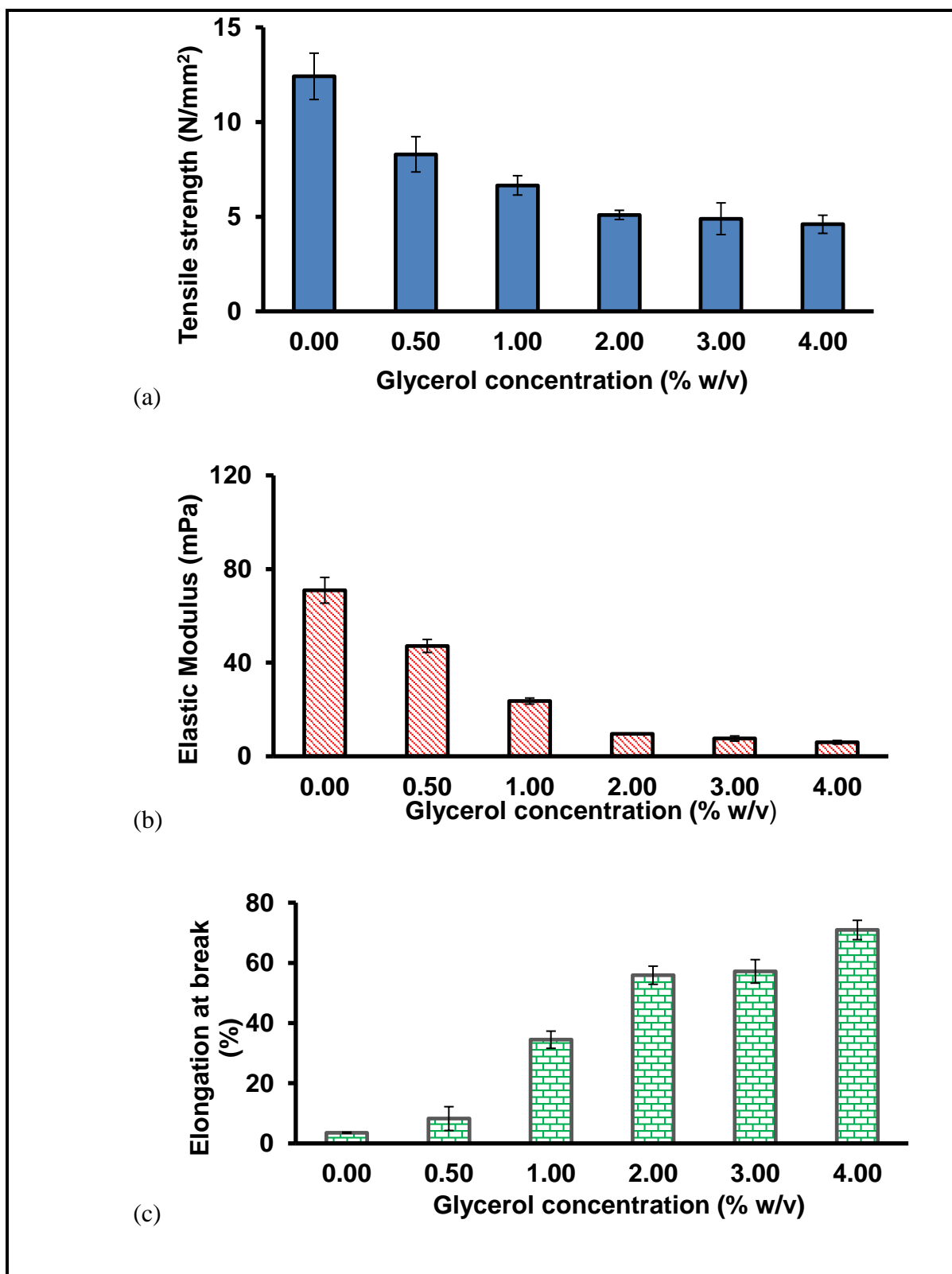


Figure 2.3: Mechanical (tensile) profiles of HPMC films showing the effect of GLY concentrations on ($n = 3, \pm SD$): (a) tensile strength, (b) elastic modulus and (c) elongation at break.

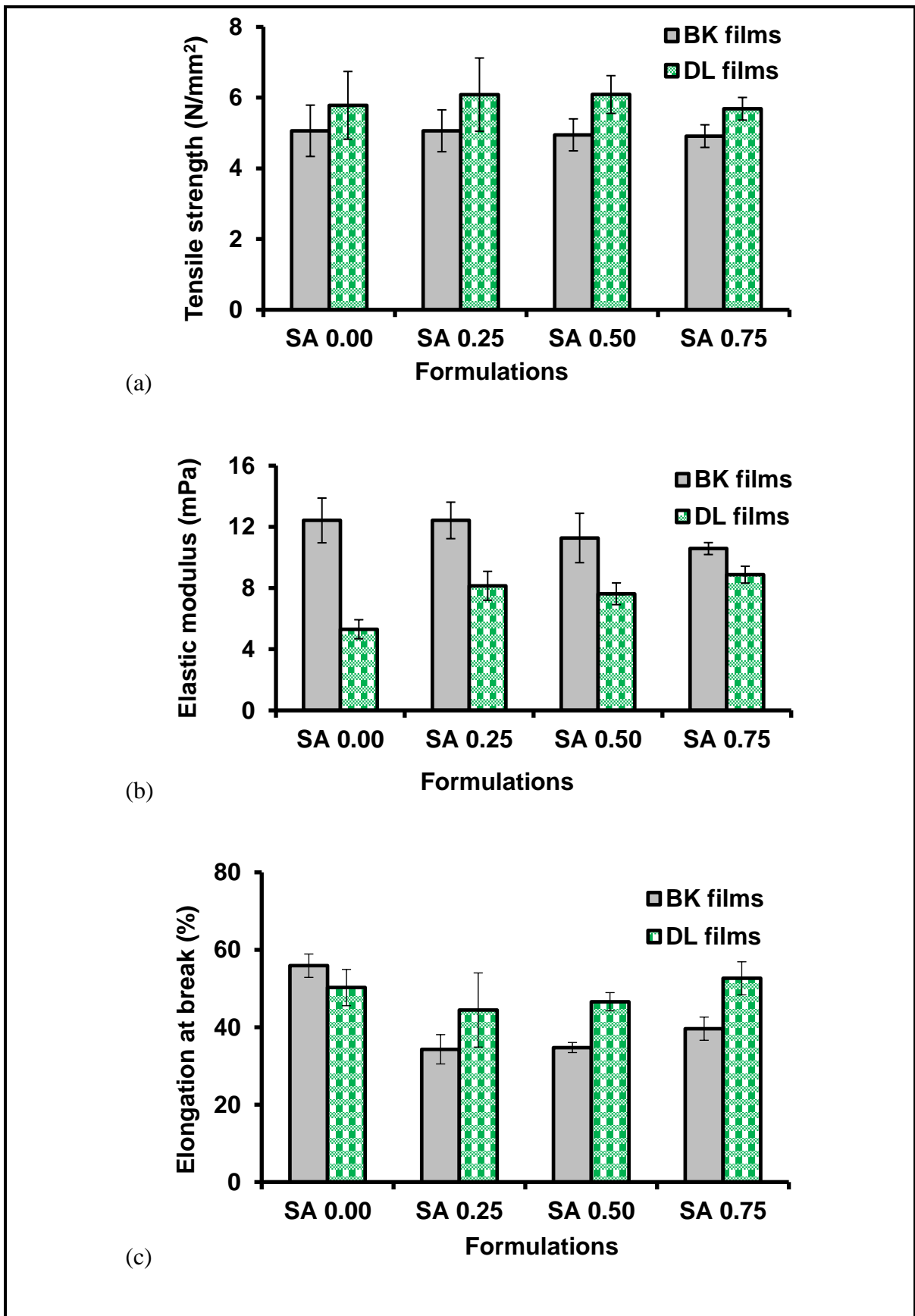


Figure 2.4: Mechanical (tensile) properties of BK and DL HPMC-SA composite films showing effect of changing SA content on ($n = 3, \pm SD$) (a) tensile strength (b) elongation at break and (c) elastic modulus.

2.3.3 SEM analysis

SEM images showing internal structure of composite BK wafers and surface morphology of composite BK films are shown in Figure 2.5 and Figure 2.6(ii) respectively. BK wafers showed a sponge-like and porous internal morphology due to ice nucleation formed during freeze-drying Figure 2.5). HPMC-SA composite wafers with low SA concentration (SA 0.25) in Figure 2.5(b) showed collapsed pores but as SA concentration increased, the wafers appeared less collapsed as shown in Figure 2.5 (c) and (d). This is due to increase in molecular interaction between COO^- groups and OH groups of SA and HPMC respectively.

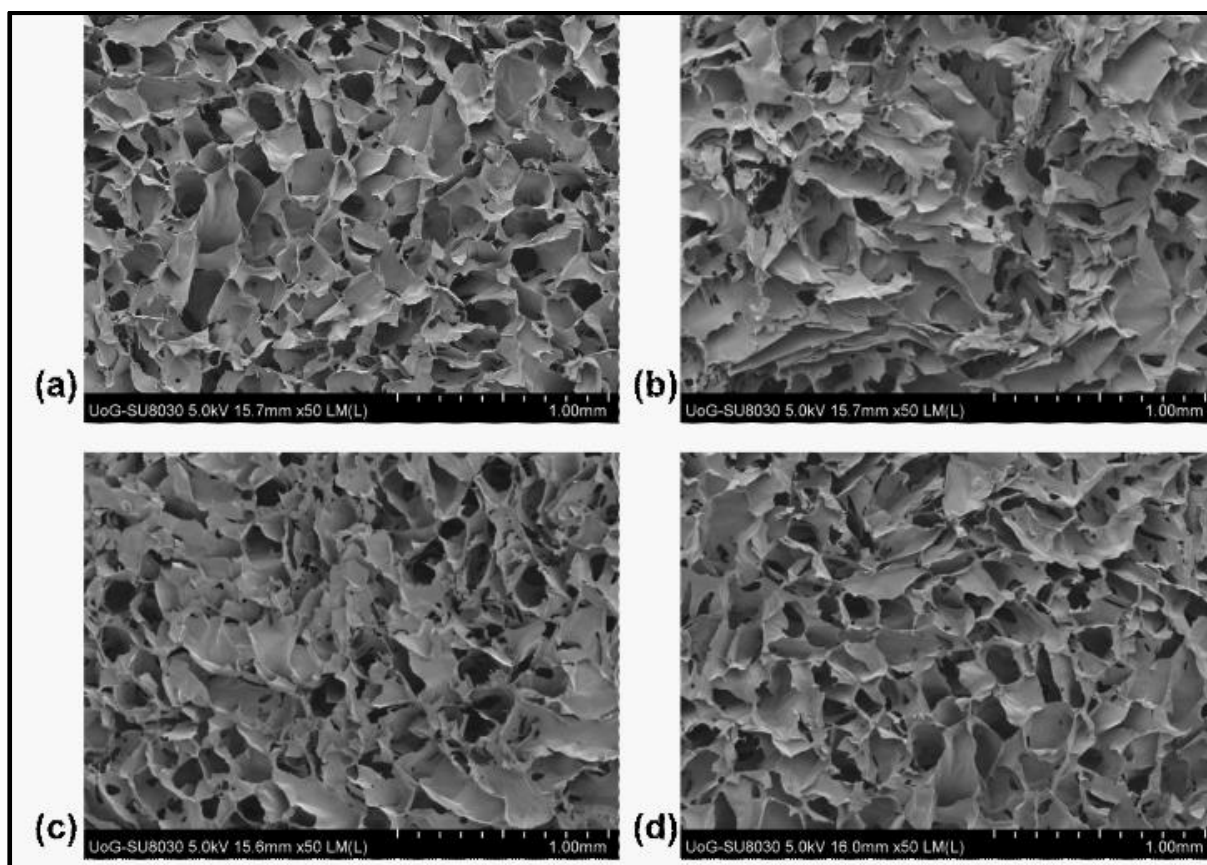


Figure 2.5: SEM images of BK HPMC-SA wafers (a) SA 0.00 (b) SA 0.25 (c) SA 0.50 (d) SA 0.75

The surface morphology of BK HPMC only films with different concentrations of GLY are shown in Figure 2.6(i), confirming that the surface structures of the film demonstrated an undesired observed stickiness at highly plasticised BK HPMC films.

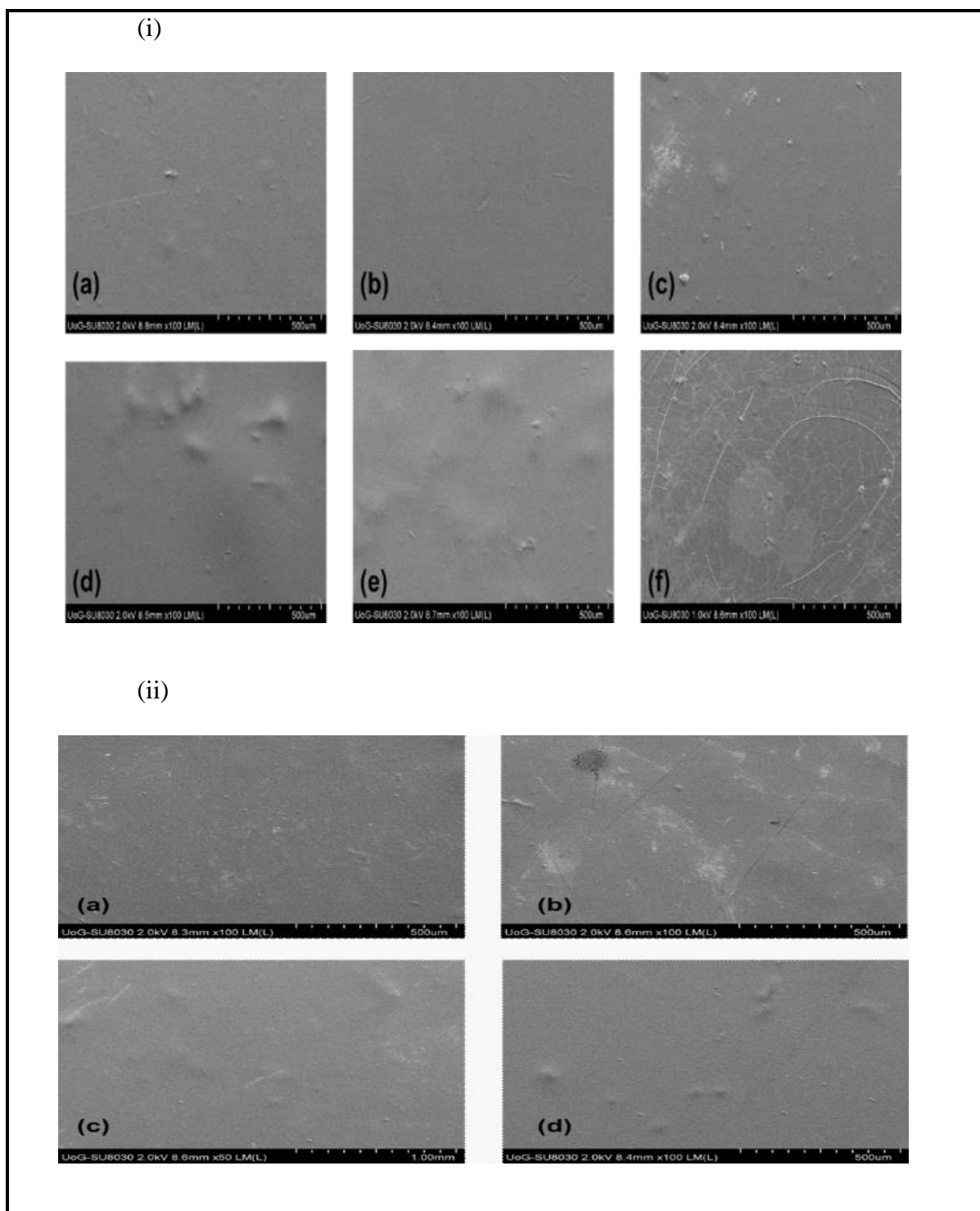


Figure 2.6: (i) Surface morphology of HPMC films at different GLY concentrations: (a) 0.0% w/v, (b) 0.5% w/v, (c) 1.0% w/v, (d) 2.0% w/v, (e) 3.0% w/v and (f) 4.0% w/v. (ii) SEM images of composite HPMC-SA films with different SA content (a) SA 0.00 (b) SA 0.25 (c) SA 0.50 (d) SA 0.75.

A GLY concentration of 2% w/v within the polymeric solutions was therefore selected as the optimum to prepare BK HPMC films. Films showed smooth topography especially for HPMC-SA films with higher SA concentration (Figure 2.6(ii)(c) and (d)), however, films with

lower SA (Figure 2.6(ii)(a)) showed a rough surface. SA 0.25 films (Figure 2.6(ii) (b)) showed cracks on the surface and could be due to a lack of proper blending and hence low molecular interaction between SA and HPMC as well as poor mechanical properties.

2.3.4 *Wafers pore analysis*

Wafer pore analysis was performed to complement the SEM analysis with the aim of semi-quantitatively analysing the porosity of the wafers with different SA content in composite HPMC-SA formulations. The result of the porosity (%) (Figure 2.7) ranged from 61 – 74%, with the porosity increasing as SA content increased within the formulations. The porosity results however, confirms the less collapsed pores of wafers containing higher amounts of SA (SA 0.50 and 0.75) and can be attributed to hydrogen bonding interaction between SA and HPMC.

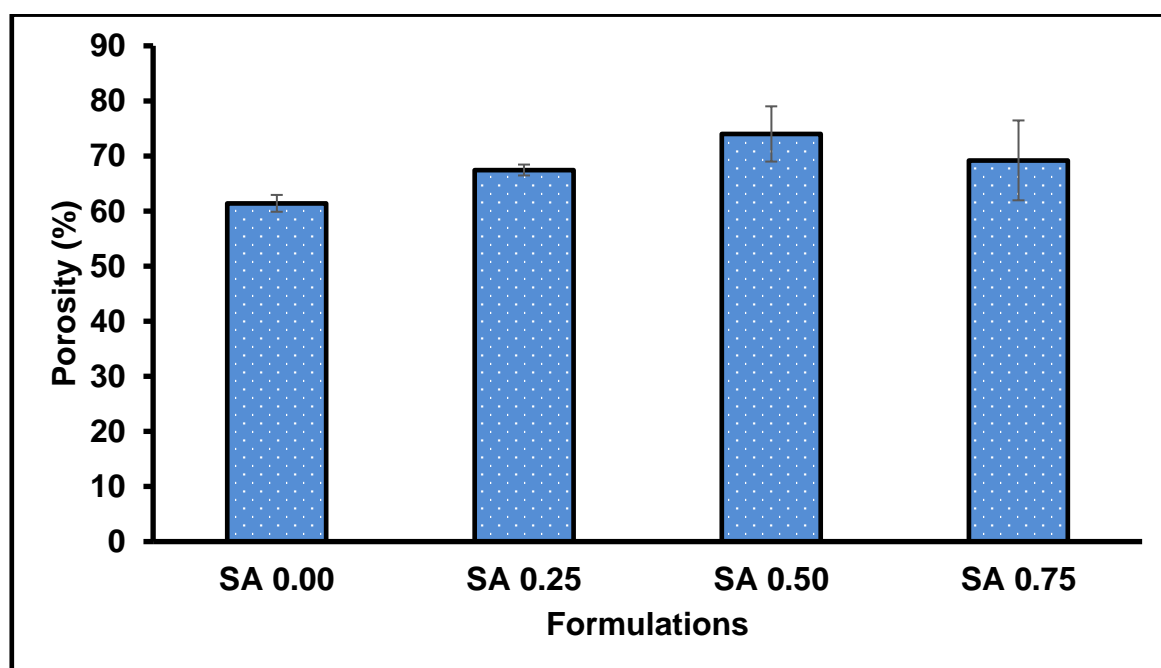


Figure 2.7: Wafers pore analysis showing % porosity in BK HPMC-SA wafer formulations ($n = 3, \pm SD$).

2.3.5 *TGA*

TGA was used in the determination of residual moisture/water content (%) of HPMC-SA composite wafers and films. Figure 2.8 showed the TGA thermal profiles and water content

(%) of HPMC-SA wafers and films at different SA concentration. HPMC-SA composite film demonstrated a higher water content (between 10% - 14%) than HPMC-SA wafers (4% - 9%). This is due to the presence of GLY plasticizer which can absorb and trap water within the polymer matrix and also the inefficiency of solvent evaporation method under proposed conditions to reduce water content to less than 10%. In HPMC-SA composite wafers, water content increases with increase in SA concentration. While in HPMC-SA composite films, formulations with SA concentration demonstrated lower water content (SA 0.25, 0.50 and 0.75) than HPMC only film formulation (SA 0.00).

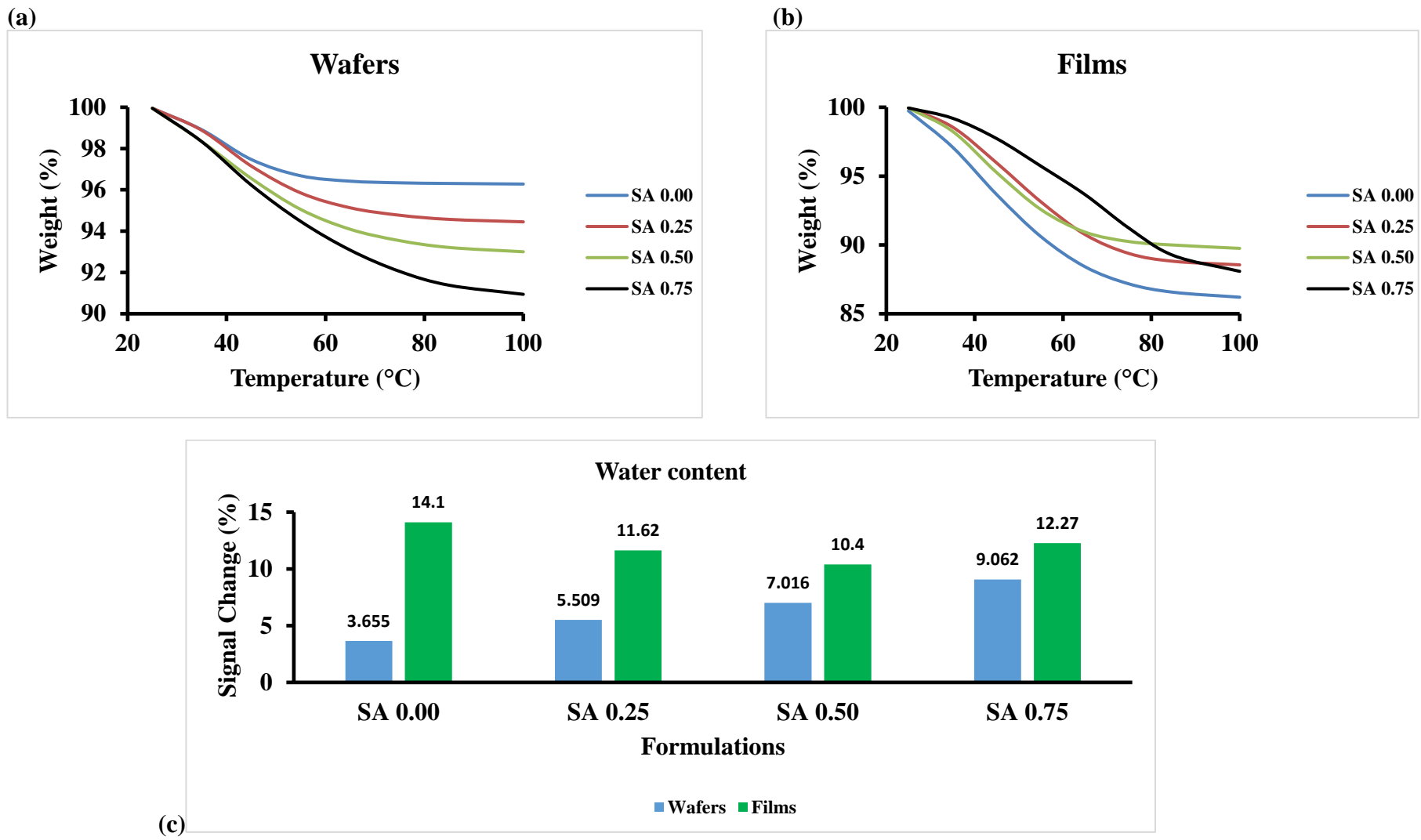


Figure 2.8: TGA thermal profiles (n=1) of (a) BK HPMC-SA wafers and (b) films, and (c) water content (%) of wafers and films.

2.3.6 DSC analysis

DSC analysis was used to investigate the thermal properties of pure polymer powders, and the HPMC-SA composite wafers and films. Figure 2.9 shows the thermal profiles of BK HPMC-SA wafers, DL HPMC-SA wafers, BK HPMC-SA films and DL HPMC-SA films at different SA concentrations. There were no glass transition peaks in the thermograms for both pure polymers (Figure 2.9) or HPMC-SA wafers and films within the temperature range analysed. However, endothermic transitions were observed between 50-90°C in the pure powders and HPMC-SA wafers and films, attributed to the loss of residual water from the polymer matrix. SA demonstrated a higher peak endothermic temperature in with a maximum peak temperature of 109.91°C (Table 2.1) than HPMC powder with a maximum peak temperature of 81.16°C.

BK and DL wafers (Figure 2.9a and b) demonstrated an increase in endothermic peak temperature as SA concentration increased. BK and DL HPMC wafer (SA 0.00) showed the lowest peak temperature at 54.94 and 53.3°C respectively. Both BK and DL HPMC-SA wafers showed maximum peak temperature between 60-72°C.

On the other hand, BK HPMC films (i.e. BK SA 0.00) in Figure 2.9b showed the higher peak temperature at 89.63°C. However, subsequent BK HPMC-SA films decreased in peak temperature (between 76-80°C) as SA concentration increased (i.e. SA 0.25, 0.50 and 0.75). Similar to BK HPMC-SA films, DL HPMC films (DL SA 0.00) in Figure 2.9b also demonstrated endothermic peak temperature at 65.83°C but this increased (64-66°C) as SA concentration increased at SA 0.25, 0.50 and 0.75 DL HPMC-SA films. In general, BK HPMC-SA films (Figure 2.9a) showed higher peak temperature compared to DL HPMC-SA films (Figure 2.9b).

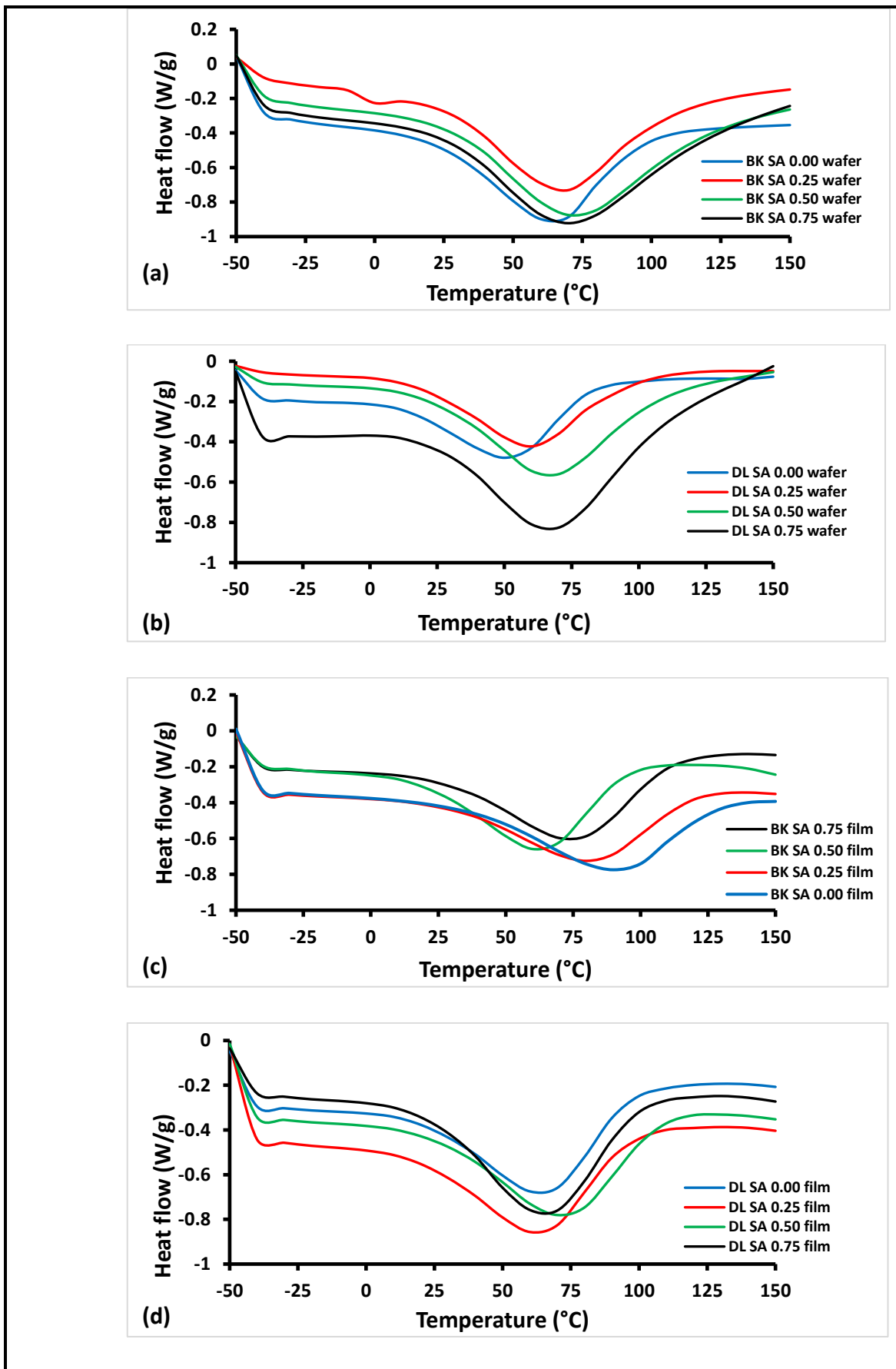


Figure 2.9: DSC thermograms ($n=1$) of (a) BK HPMC-SA wafers (b) DL HPMC-SA wafers (c) BK HPMC-SA films and (d) DL HPMC-SA films.

Table 2.1: Peak integration values ($n=1$) of (a) pure powders, (b) BK wafers, (c) DL wafers, (d) BK films and (e) DL films.

		Peak (°C)
BK wafers	HPMC (pure)	81.16
	SA (pure)	109.91
DL wafers	BK SA 0.00	54.94
	BK SA 0.25	66.48
	BK SA 0.50	71.98
	BK SA 0.75	65.46
	DL SA 0.00	53.30
BK films	DL SA 0.25	59.00
	DL SA 0.50	67.45
	DL SA 0.75	70.81
	BK SA 0.00	89.63
DL films	BK SA 0.25	79.90
	BK SA 0.50	61.35
	BK SA 0.75	75.61
	DL SA 0.00	65.83
	DL SA 0.25	63.71
	DL SA 0.50	71.87
	DL SA 0.75	65.71

2.3.7 XRD analysis

Figure 2.10(a) shows XRD transmission diffractograms of pure polymers (SA and HPMC) and Mylar (used in pure powder preparation to hold the powder and prevent it from spilling). The results show the amorphous nature of SA with a broad peak at 2θ 14° and 22° , whilst HPMC also showed a broad peak at 2θ 20° . Figure 2.10(b) and (c) showed the XRD transmission diffractograms of BLK HPMC-SA and DL HPMC-SA wafers, while Figure 2.10(d) and (e) showed that of BLK HPMC-SA and DL HPMC-SA films respectively. Both BK and DL HPMC-SA wafers and films exhibited an amorphous nature, with a broad peak around 2θ of 20° . However, the wafers also showed a small crystalline shoulder peak at 2θ of 23° . Given that this peak was not present in the films, it could be attributed to false peak detection arising from compression of the wafers which causes the leafy networks to be piled up on top of each other and detected as a false crystalline peak. However, this might require further investigation to rule out possibility of trace amounts of other material naturally present in one of the polymers.

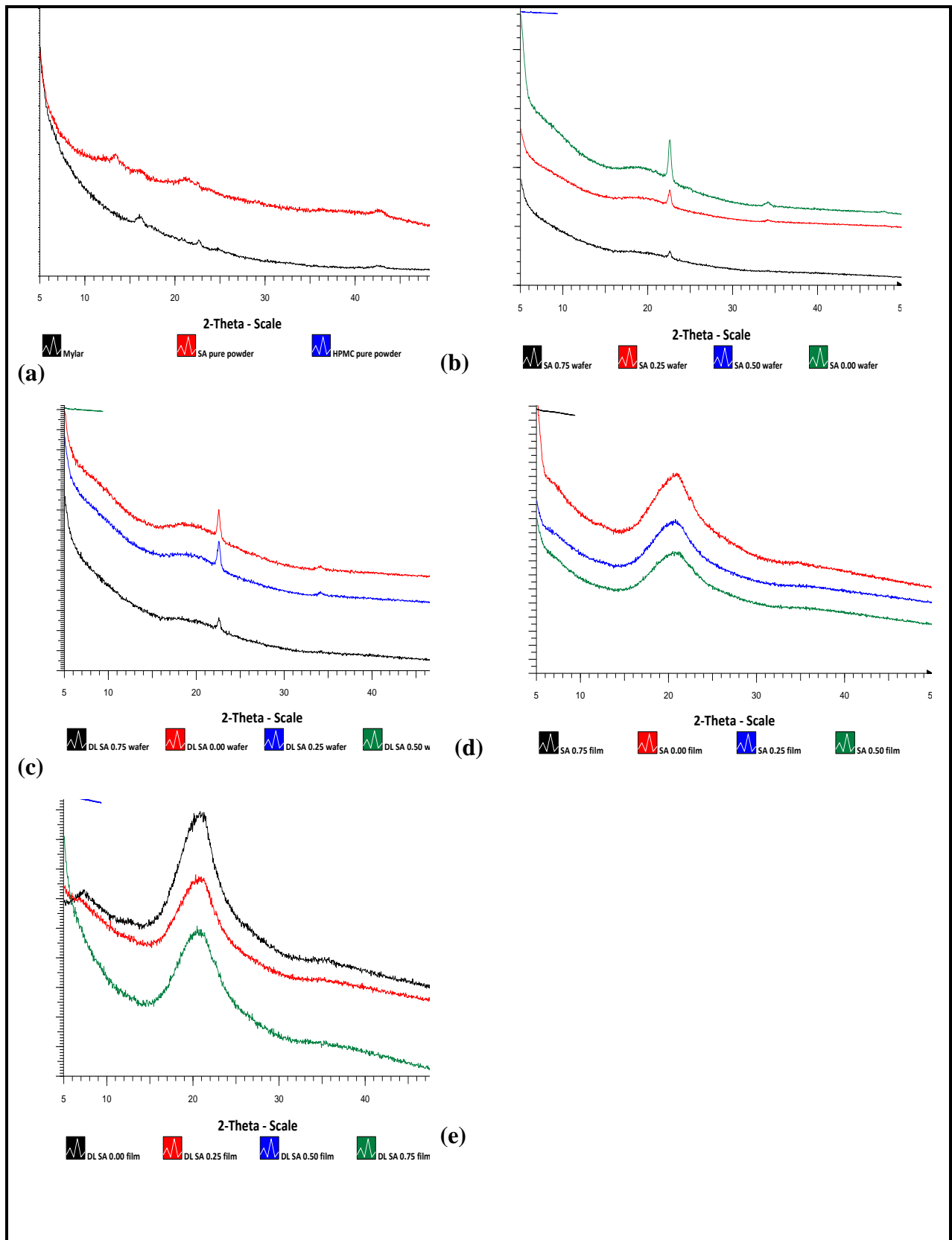


Figure 2.10: XRD-transmission diffractograms of (a) pure powders, (b) BK HPMC-SA composite wafers, (c) DL HPMC-SA composite wafers, (d) BK HPMC-SA composite films (e) DL HPMC-SA composite films.

2.3.8 *ATR-FTIR analysis.*

The major peaks from the ATR-FTIR spectra of pure powders, BK and DL HPMC-SA composite films and BK and DL HPMC-SA composite wafers are summarised in Figure 2.11. The characteristic peaks of SA, HPMC and GLY can be seen in Figure 2.11a. BK HPMC-SA composite films (Figure 2.11b) showed a shift to lower wavenumbers for OH stretching vibration as SA concentration increased except for BK SA 0.25 film, which showed a much higher OH stretching vibration band at 3370cm^{-1} . Hydrogen bonding in COO groups was also observed at higher SA concentration as evidenced by shifting to lower wavenumber from 1647cm^{-1} to 1607cm^{-1} for COO- asymmetric stretching and the disappearance of the peak for COO-symmetric stretching (composite BK HPMC: SA 0.50 films) at 1455cm^{-1} present from the spectra of the composite BK HPMC: SA 0.75 films. The shift in C-CH₃ bending was a result of GLY present in the HPMC-SA composite films. DL HPMC-SA films (Figure 2.11c) also showed a shift in OH stretching vibration to lower bands as SA concentration increased except for SA 0.50 film at 3340cm^{-1} which showed similar OH vibration with HPMC only film (i.e. SA 0.00).

Characteristic peaks for BK HPMC-SA composite wafers are summarised in Figure 2.11d. The results showed a shift to lower wavenumber, with increase in SA concentration, for OH stretching (SA 0.00: 3414cm^{-1} ; SA 0.25: 3402cm^{-1} ; SA 0.50: 3401cm^{-1} and SA 0.75: 3393cm^{-1}). There was also a shift to lower wavenumbers for COO- asymmetric vibrations (SA 0.00: 1647cm^{-1} ; SA 0.25: 1615cm^{-1} ; SA 0.50: 1607cm^{-1} and SA 0.75: 1605cm^{-1}). The COO-symmetric stretching vibrations were only present in SA 0.00 (1456cm^{-1}) and SA 0.25 (1456cm^{-1}) wafers. However, these were absent at higher concentrations of SA (SA 0.50 and 0.75). In addition, there was absence of COO- symmetric stretching vibration peaks in SA 0.00 wafers but present in SA 0.25, 0.50 and 0.75 wafers at 1413 , 1412 and 1412cm^{-1} respectively. DL HPMC-SA wafers exhibited similar changes in OH stretching (SA 0.00: 3414cm^{-1} ; SA

0.25: 3401 cm^{-1} ; SA 0.50: 3401 cm^{-1} and SA 0.75: 3393 cm^{-1}) and COO- asymmetric stretching bands (SA 0.00: 1647 cm^{-1} ; SA 0.25: 1616 cm^{-1} ; SA 0.50: 1607 cm^{-1} and SA 0.75: 1604 cm^{-1}) as noticed in BK HPMC-SA wafers.

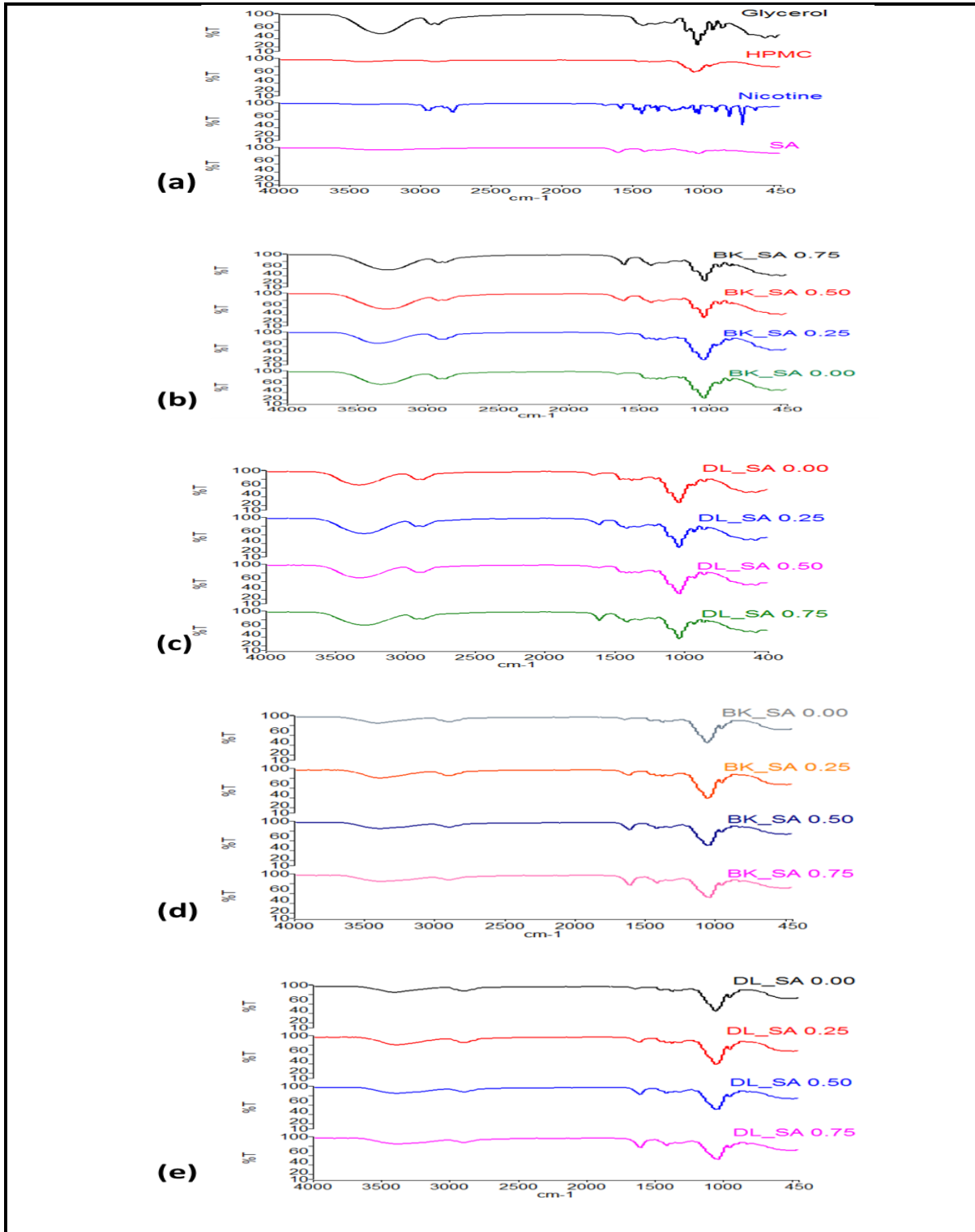


Figure 2.11: ATR-FTIR spectra of (a) pure polymers, GLY, NIC (b) BK HPMC-SA composite films, (c) DL HPMC-SA composite films (d) BK HPMC-SA composite wafers and (e) DL HPMC-SA composite wafers.

However, DL HPMC-SA wafers (Figure 2.11e) demonstrated changes in C-CH₃ bending with absence of C-CH₃ bending peak in wafers containing higher SA concentrations (SA 0.50 and 0.75 wafers).

2.3.9 *Swelling studies*

Figure 2.12(a) and (b) show changes in swelling index of DL HPMC-SA wafers and films respectively with time.

The swelling profile in Figure 2.12(a) demonstrate an increase in swelling index as SA increased for HPMC-SA wafers, while the swelling profile in Figure 2.12(b) demonstrate a decrease in swelling index (%) with increase in SA content within HPMC-SA films. However, there was no statistically significant difference between the different wafers formulations ($p = 0.355$, one-way ANOVA) as well as between the films ($p = 0.726$, one-way ANOVA). In addition, it can also be observed that while HPMC-SA films showed a gradual increase in swelling index (%) with time, HPMC-SA wafers showed a more rapid increase in swelling index (%) within a short time (2mins) and then remained constant over the duration of the study.

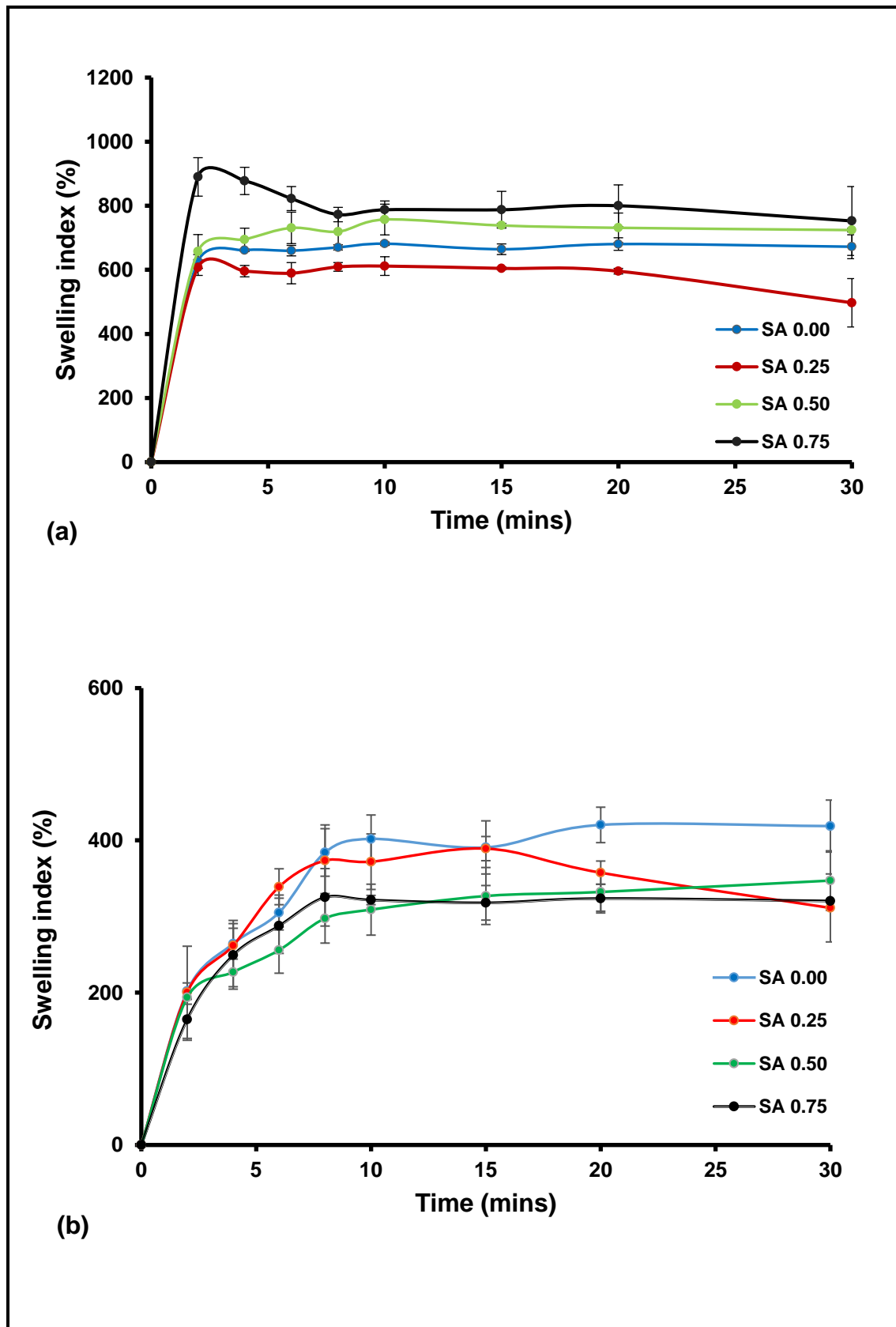


Figure 2.12: Swelling profiles (i.e. % swelling index against time) of (n = 3, \pm SD) (a) composite HPMC-SA wafers and (b) composite HPMC-SA films.

2.3.10 *Mucoadhesion studies*

Figure 2.13 and Figure 2.14 show the mucoadhesion profiles of BK and DL HPMC-SA wafers, and BK and DL HPMC-SA films respectively obtained from the TA curves during the analysis. The peak adhesion force (PAF) or F_{\max} of BK HPMC-SA wafers remained constant (Figure 2.13a) as SA concentration increased while F_{\max} for DL HPMC-SA wafers increased as SA concentration increased. Further, BK HPMC-SA wafers showed lower F_{\max} than DL HPMC-SA wafers though the difference was not statistically significant ($p=0.109$). The TWA (Figure 2.13b) and cohesiveness (Figure 2.13c) of DL HPMC-SA showed an increase with initial SA concentration (SA 0.25), but decreased at maximum SA concentration (SA 0.75) while BK HPMC-SA wafers showed an increase in TWA and cohesiveness at maximum SA concentration (SA 0.75). The increase in the F_{\max} and decrease in cohesiveness resulted in similar values of TWA for both BK and DL HPMC-SA wafers at maximum SA concentration (SA 0.75). In addition, the F_{\max} , TWA and cohesiveness of BK and DL HPMC-SA wafers showed no statistically significant difference with p values of 0.109, 0.151 and 0.902 respectively.

The F_{\max} of BK and DL HPMC-SA films (Figure 2.14a) increased as SA concentration increased with a maximum value of $2.78 \pm 0.09\text{N}$ for BK HPMC-SA films and $1.94 \pm 0.13\text{N}$ for DL HPMC-SA films, containing SA 0.75. The TWA (Figure 2.14b) and the cohesiveness (Figure 2.14c) of DL HPMC-SA films did not show a consistent profile for SA 0.25 and 0.50 formulation respectively, with higher error bars in both TWA and cohesiveness for SA 0.25 films and lower error bars in TWA and cohesiveness for SA 0.50 films.

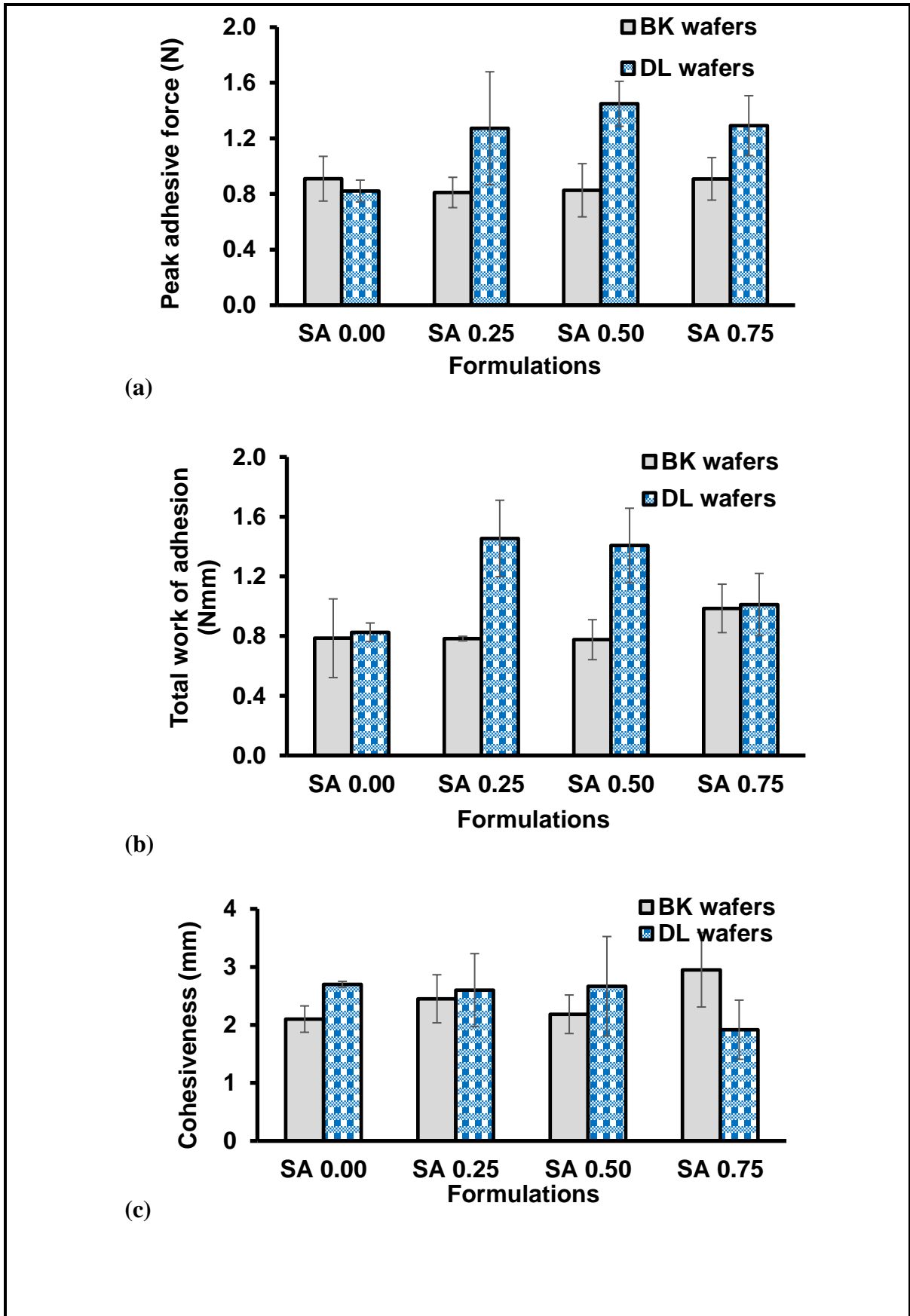


Figure 2.13: Mucoadhesive profiles of BK and DL composite wafers ($n = 3, \pm SD$): (a) peak adhesive force (b) total work of adhesion (c) cohesiveness.

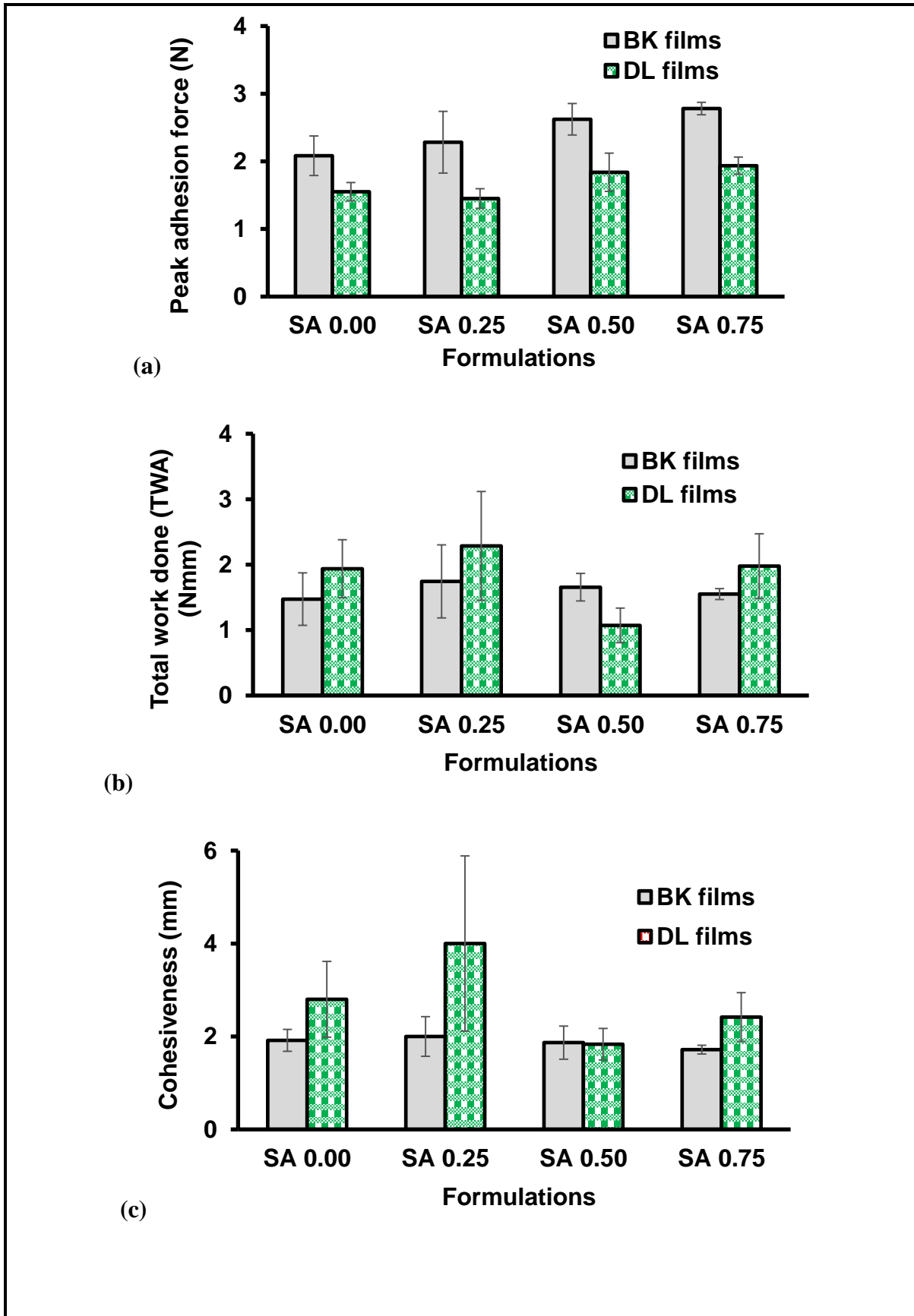


Figure 2.14: Mucoadhesive profiles of BK and DL composite films ($n = 3, \pm SD$): (a) peak adhesive force (N) (b) total work of adhesion (Nmm) (c) cohesiveness (mm).

This suggests that the SA 0.25 formulation has poor interaction of HPMC and SA in the composite formulation and therefore not very reliable to take forward. However, DL HPMC-SA film with higher SA concentration i.e. SA 0.75 film showed lower variability in TWA ($1.98 \pm 0.50\text{Nmm}$) and relatively high cohesion ($2.42 \pm 0.53\text{mm}$) than SA 0.50. Generally, films demonstrated higher mucoadhesive values than wafers.

2.3.11 Drug content (% loading / recovery)

Films showed a very low percentage of NIC (Figure 2.15) with a maximum assayed content below 35% (SA 0.75, $28 \pm 4.09\%$).

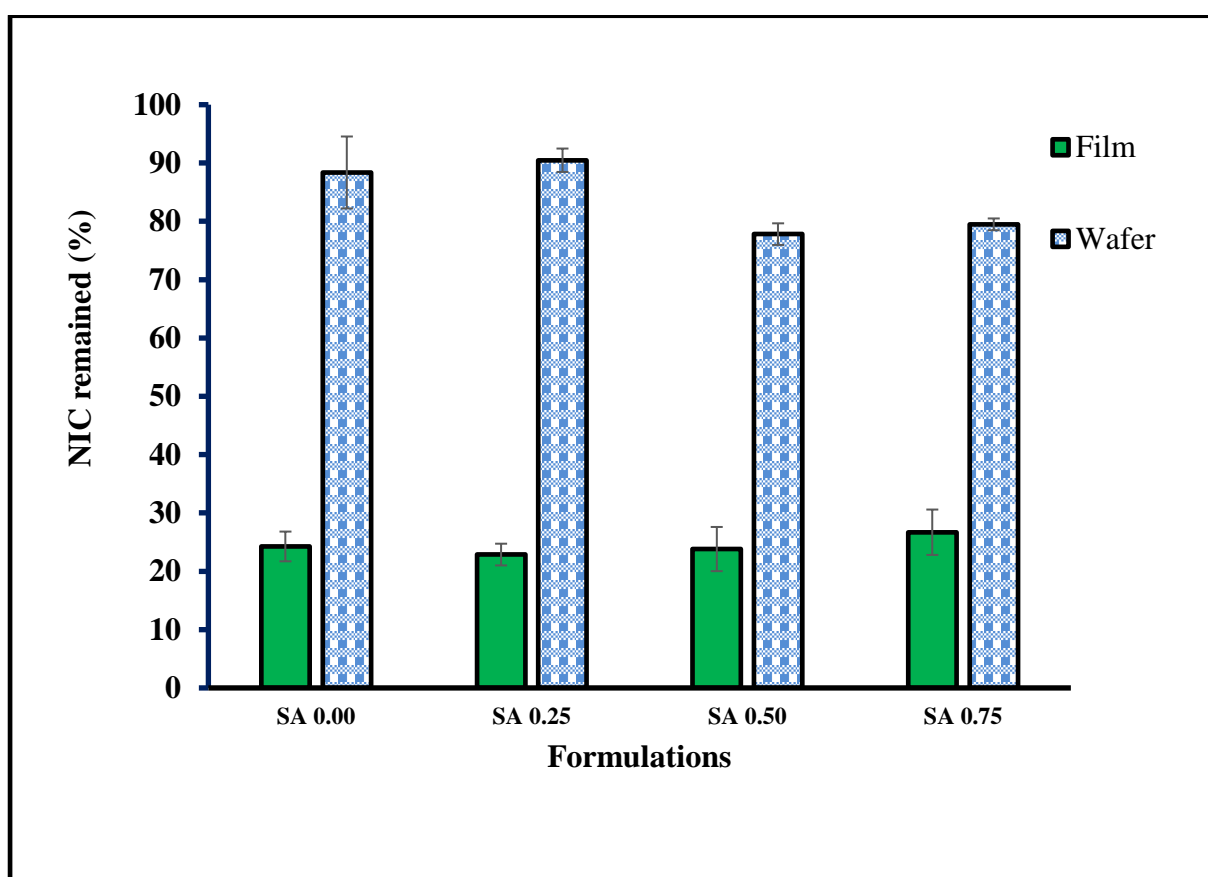


Figure 2.15: NIC drug content (%) in DL HPMC-SA wafers and films ($n = 3, \pm SD$).

On the other hand, the composite wafers yielded significantly higher NIC content above 75% (i.e. SA 0.00, $88 \pm 6.17\%$; SA 0.25, $90 \pm 2.01\%$; SA 0.50, $78 \pm 1.854\%$ and SA 0.75, $79 \pm 1.011\%$) attributed to the formulation technique of wafers (freeze drying) which allowed low temperature compared to solvent evaporation. However, increase in effective SA concentration

resulted in a decrease in the percentage NIC content in the respective formulations (i.e. SA 0.50, 78 ± 1.854 and SA 0.75, $79 \pm 1.011\%$) as compared to DL HPMC-SA composite wafer with low SA concentration (i.e. SA 0.25, $90 \pm 2.01\%$) and DL HPMC wafer with no SA present (i.e. SA 0.00, $88 \pm 6.17\%$).

2.3.12 *In vitro drug dissolution*

Due to the very low drug contents observed in all the films, DL HPMC-SA films were discontinued from further analysis. Figure 2.16 shows the dissolution profiles of DL HPMC-SA composite wafers. DL HPMC-SA composite wafers with the highest SA concentration (SA 0.75) showed the highest % cumulative drug release within 4 hrs as compared to other composite wafers with a significant difference ($p = 0.041$, one-way ANOVA). The DL HPMC-SA composite wafers with the highest SA concentration released $92 \pm 8\%$ within the first 30mins and up to a 100% in 4 hrs in comparison with other HPMC-SA composite wafers, which released less than 60% within 4hrs.

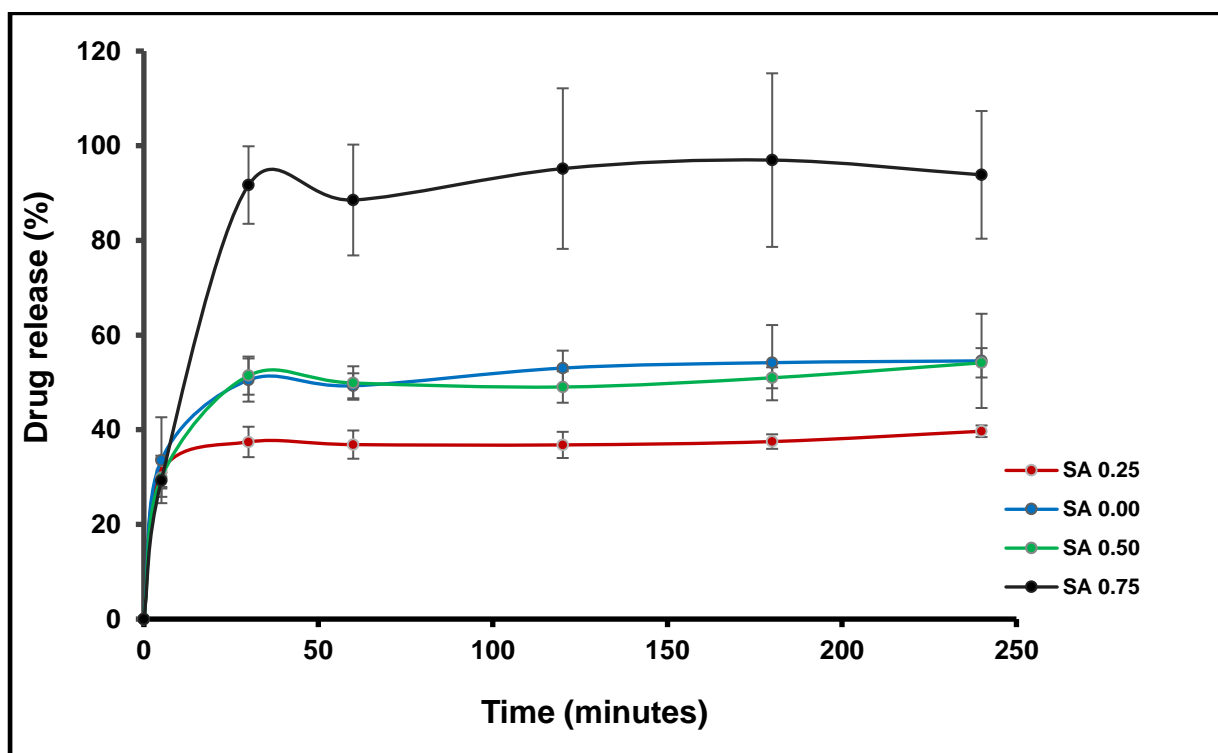


Figure 2.16: *In vitro drug release profiles of DL HPMC-SA composite wafers (n = 3, ± SD).*

2.4 Discussion

The polymers used to prepare the composite wafers and films, were selected based on their mucoadhesive characteristics as well as their classification as GRAS. HPMC was selected based on its ability to control the release of drugs incorporated within a delivery system as well as its accessibility in regards to low cost of production (Siepmann & Peppas, 2012). SA on the hand was considered based on its mucoadhesive property as an anionic material, usually considered a better mucoadhesive polymer than non-ionic polymers such as HPMC (Wittayaarekul et al., 2006, Xiao et al., 2014). SA was also considered based on its ability to form ionic interactions by interacting with the positive charge of protonated NIC (Pongjanyakul & Suksri, 2010).

The dosage forms (i.e. freeze-dried wafers and solvent cast films) were compared to determine drug loading efficiency due to the challenges posed by incorporating NIC, which is volatile, into drug delivery systems. Wafers were easy to handle, due to the ability to control the thermal events during the freeze-drying cycle. The thermal programme used was essential in achieving a cake-like structure that can be easy to handle by improving the freezing, primary and secondary drying stages. Using a controlled freezing process incorporating an annealing step, the ice crystal size and distribution was improved leading to better sponge-like pores preceding sublimation via primary and secondary drying (Kasper & Friess, 2011).

The consideration of plasticizer in films was the result of the brittleness and poor handling of unplasticised films during preliminary formulation development. The incorporation of plasticizer aids in increasing the free volume between the polymer chains (HPMC and SA) with the ability to slip past each other, resulting in more flexible films which are easy to handle (Riggleman et al., 2007). The effect of plasticizer therefore decreased brittleness (tensile strength) and stiffness (elastic modulus) but increased elasticity (percentage elongation at break) in HPMC films shown in Figure 2.3. It also increased the water content of

films as it absorbs and traps moisture in the polymeric matrix of SA and HPMC films as demonstrated in TGA results (Figure 2.8). However, an excess of plasticizer could result in higher free volumes between polymers that are highly slippery and difficult to handle (very sticky) as shown in mechanical properties (Figure 2.3) and SEM images (Figure 2.6) of BK HPMC films obtained from polymeric solution with GLY above 2% w/v. Therefore a balance between flexibility and toughness with an optimum elongation ideally between 30-50% is desirable (Boateng et al., 2009). Optimized concentration of GLY at 2% w/v within the original polymeric solution met the criteria of an ideal film based on its elongation and was therefore the concentration of choice in DL films.

Handling of wafers is important during application and therefore optimized mechanical properties are necessary. The resistance of the wafers to compressive deformation (hardness) data allows the assessment of the reliability of wafer structure (Boateng & Areago, 2014). The increase in hardness of BK wafers at higher SA concentration (Figure 2.2) was possible due to hydrogen bonding existing between the COO⁻ group of SA and the OH group of HPMC, which may interrupt the polymeric matrix of HPMC and hence increased the resistance to compression forces but was limited for wafers with lower SA concentration (SA 0.25). Wafers loaded with NIC decreased in resistance to deformation, which can be attributed to the NIC causing a slight increase in free volume between HPMC and SA polymeric chains in the composite wafers as observed in HPMC-SA composite films where there was increase in elasticity and decrease in stiffness.

HPMC and SA composite formulations formed a network polymeric matrix with a non-ionic interaction between the polymers. SA showed no plasticising effect on HPMC-SA composite films as the brittleness (tensile strength) of the films remained constant. However, NIC in the formulation increased the elongation but decreased the stiffness of the film while

interacting with SA via ionic and hydrogen bonding. By this interaction, NIC increases the free volume between SA and HPMC thereby exhibiting a plasticizing effect on the film.

The formulation techniques used in formulating wafers and films influenced the properties of the dosage forms. HPMC-SA wafers demonstrated a lower water content as demonstrated in the signal change (%) of the TGA result (Figure 2.8) compared to films. The low water content in wafers is as a result of a combination of primary and secondary drying process. This ensure the removal of free water in primary drying and bound water in secondary drying, hence resulting to a significant reduction in water content of wafers in comparison to films. Two factors were responsible for the high water content of film compared to wafers. First the drying process was not sufficient for the removal of significant bound water within the polymer matrix, and secondly the presence of plasticizer which adsorb moisture from the environment. DSC results (Figure 2.9) also demonstrated the presence of bound water within the polymer matrix as the endothermic transition showed loss of water residual from the polymer matrix. The pure dry SA and HPMC demonstrated residual water within the polymeric networked with an endothermic transition on the thermal profile of the pure powder with a higher endothermal transition in SA compared to HPMC. This explained the increase in endothermic peak temperature with increase in SA in both HPMC-SA wafers and films. The thermal profile of SA and HPMC lacked a glass transition due to a broad endothermic peaks of water evaporation which has an effect on DSC thermal profile (Dhawade and Jagtap, 2012).

Hydration and swelling behaviour of a dosage form can influence the drug dissolution profile, since diffusion, swelling and erosion are the mechanisms by which drug release is controlled (Siepmann & Peppas, 2012). The amorphous properties of wafers and films as demonstrated in XRD results (Figure 2.10) played a role in swelling, as amorphous materials are more mobile and hence improve the rate of dissolution (Blagden et al., 2007). The high swelling property of HPMC explains the higher swelling index of HPMC only films (i.e. SA

0.00) compared to other formulations containing different amounts of SA (i.e. SA 0.25, 0.50 and 0.75), with the composite films showing a decrease in swelling as SA concentration increased. The higher swelling index of HPMC-SA wafers in comparison to HPMC-SA films can be attributed to the sponge-like pores in the internal structure as shown in SEM image (Figure 2.5) and by the pore analysis data (Figure 2.7), with increase in porosity as SA increased in the formulations, which permits rapid ingress of buffered solution into the polymer matrix (Boateng et al., 2010). The rapid ingress upon contact with buffered solution explains the rapid increase of swelling index (%) within 2 mins and then constant swelling index (%) with time. This also explains the increase in swelling index as SA increased in wafers but with an opposite effect in the films. This difference in swelling behaviour of wafers and films, has been previously reported (Ayensu et al., 2012a, Boateng et al., 2009).

The mucoadhesion results of HPMC-SA wafers and films demonstrate increase in adhesive properties as SA increased and with the addition of NIC in all HPMC-SA wafers and films. This can be attributed to hydrogen bonding (SA) and electrostatic interaction (NIC) with mucin (Boddupalli et al., 2010). Charged bioadhesive polymers have been shown to increase mucoadhesion as the polymer charge interacts with the surface charge of mucin thereby leading to stronger bonding (Grabovac et al., 2005). However, HPMC-SA films demonstrated higher adhesive properties than HPMC-SA wafers due to better initial contact, which could enable better hydrogen bonding and high affinity of liquid to solid (wetting theory) (Jannin et al., 2014). HPMC-SA films also contained GLY with hydrogen bonding OH groups group, which can further improve the interaction of both BK and DL HPMC-SA films with the model buccal mucosal surface (i.e. gelatine equilibrated with mucin).

HPMC-SA wafers demonstrated more diffusion of solvent (swelling) and therefore expected to follow diffusion theory, than hydrogen bonding which is the result of limited contact surface area from its sponge-like nature leading to liquid to solid affinity. However,

introduction of NIC improved bonding during mucoadhesion by introducing electrostatic ionic groups, which enhanced interaction of the formulations with mucin, resulting in an increase in mucoadhesion of DL HPMC-SA film and wafers (Smart, 2005).

NIC loading efficiency is important in selecting optimized dosage form (films/wafers) for NRT. The main challenge of dealing with the free base (liquid) form of NIC is its volatility (0.006 kPa at 20°C). The drug loading efficiency of NIC demonstrated in the drug content result (Figure 2.15) was higher in HPMC-SA wafers than films. This is because in the case of films, NIC experienced evaporation during the drying process in the oven at higher temperature (Pongjanyakul & Suksri, 2010). The improved drug loading efficiency in HPMC-SA wafers is due the freeze-drying cycle, which allowed use of lower temperatures below 25°C compared to HPMC-SA films with a drying temperature of 30°C. Therefore, in this study HPMC-SA films were not considered further for *in vitro* drug dissolution.

The rapid drug release shown in the dissolution profiles (Figure 2.16) of HPMC-SA wafers could be due to water-uptake by diffusion of dissolution media into HPMC-SA wafers due to the sponge-like porous internal structure of the wafers. The rate of drug release in the composite HPMC-SA wafers was higher in wafers containing highest SA concentration and could be explained using the swelling results of HPMC-SA wafers which demonstrated a higher swelling index for wafers with maximum SA concentration. The HPMC-SA wafers demonstrated the highest swelling index at SA 0.75 and the lowest swelling index at SA 0.25. This can be correlated to the drug release as SA 0.75 showed rapid drug release while SA 0.25 formulation showed the slowest rate of release of drug from the polymer matrix. The relationship between the release and the swelling profiles can be attributed to the porosity of the polymer matrix as shown in the SEM images and pore analysis because SA 0.75 formulation showed the highest porosity. Furthermore, the porosity can be explained by the mechanical properties of the wafer as increase in porosity decreased the resistance to

compression. The release of more than 90% of NIC within 30 mins is expected to be effective in rapid delivery of NIC to brain receptors and hence increase dopamine levels resulting in a pleasurable feeling similar to that of smoking (Weidner, 2002).

2.5 Conclusions

HPMC-SA composite wafers and films have been optimized and compared as potential dosage forms for NRT via the buccal route. The two dosage forms demonstrated different characteristics in their physical properties (mechanical, surface/internal morphology and thermal properties), swelling index, mucoadhesion, drug loading capacity and drug release. HPMC-SA composite wafers showed a porous internal morphology, higher mucoadhesion, swelling index and drug loading capacity than HPMC-SA composite films. SA polymer used in the development of HPMC-SA composite wafers modified and improved properties of HPMC at optimum SA concentration and hence can be utilised as a drug delivery system for NRT. The composite polymeric system comprising HPMC and SA can be effective in enhancing the functional properties of buccal NRT to achieve desired optimum characteristics as an improvement over the currently used chewing gum, which is difficult to control in terms of drug release.

CHAPTER 3: PHYSICOCHEMICAL CHARACTERISATION OF FREEZE-DRIED AND SOLVENT EVAPORATED NICOTINE - MAGNESIUM ALUMINUM SILICATE (MAS) COMPLEXES.

3.1 Introduction

As stated in previous chapters NIC is a volatile liquid, which is highly soluble in both water and organic solvents. Its volatility and oxidative degradation are critical challenges, which require consideration when developing a NIC dosage form and this has resulted in the use of NIC stabilisers. Cation exchange resins, cellulose powder and magnesium aluminium silicate (MAS) have been utilised as NIC stabilisers (Rakić et al., 2010, Mihranyan et al., 2004, Pongjanyakul et al., 2009, Pongjanyakul & Suksri, 2009). NIC stabilisers adsorb NIC onto its surface, hence preventing NIC evaporation and improving stability (Pongjanyakul et al., 2009).

MAS is obtained from the combination of natural smectites (montmorillonite and saponite clays) that form a layered structure (Rowe et al., 2006, López-Galindo et al., 2007, Carretero & Pozo, 2009). The layered structure of MAS comprises three lattice layers of octahedral alumina or magnesia and two tetrahedral silica. Upon hydration, the MAS layered structure separates, exposing the weakly positively charged edges and negatively charged faces (Figure 3.1). These can readily interact with amine drugs such as NIC as well as demonstrate electrostatic interaction, which contributes to its controlled release effect in formulations (Rowe et al., 2006, Pongjanyakul & Suksri, 2010).

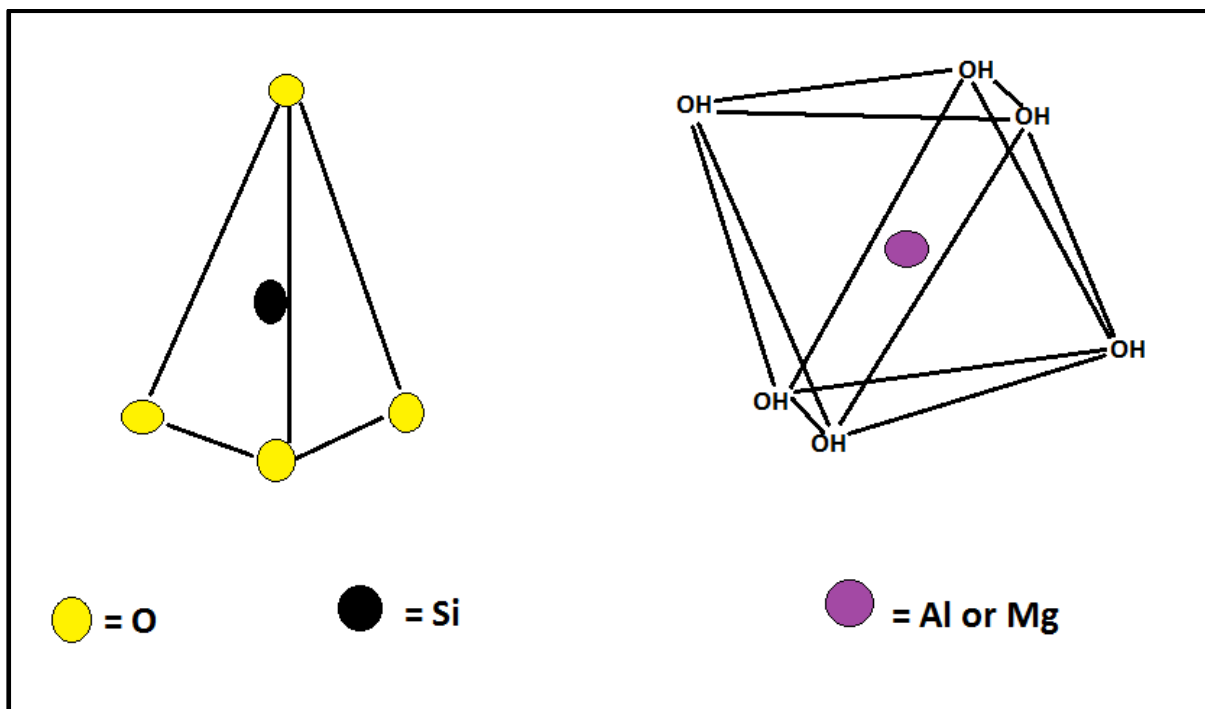


Figure 3.1: Tetrahedron and octahedron structures of silicate and aluminium/magnesium respectively.

In this chapter, the interaction between MAS and NIC in aqueous dispersions at different concentrations were investigated to determine changes in physical properties such as particle size and zeta potential of NCT-MAS flocculates as NIC is adsorbed onto MAS. Furthermore, NIC-MAS complexes at different concentrations were dried using both solvent evaporation (SE) and freeze drying methods. This was followed by further investigation for changes in physicochemical properties such as thermal behaviour, solid-state crystallinity, surface morphology and elemental surface analysis using DSC, XRD, and SEM with energy dispersive X-ray analysis respectively. Further, ATR-FTIR and ^{29}Si NMR spectroscopy were used to examine the molecular interaction of NIC-MAS complexes.

3.2 Materials and methods

3.2.1 Preparation of composite NIC-MAS complex

Various concentrations of MAS (as shown in Table 1) were prepared by dispersed in 20ml of hot distilled water (50°C) for 30mins at 500rpm and allowed to cool to room temperature for 30mins. NIC was added to the MAS dispersion at low stirring speed (100-200 rpm) for 30mins. The prepared MAS-NIC complexes were poured into glass vials and dried in the oven at 30°C for 18-20 hrs for solvent evaporated (SE) (films) and/or freeze dried (FD) (cakes) in a freeze drier using the freeze dryer settings described in chapter 2 (section 2.2.3).

Table 3.1: Composition of MAS and NIC in solution.

<i>Sample name</i>	<i>MAS (% w/v)</i>	<i>NIC (g)</i>
<i>MAS-NIC 0.25</i>	1.25	0.2
<i>MAS-NIC 0.50</i>	2.50	0.2
<i>MAS-NIC 0.75</i>	3.75	0.2

3.2.2 Particle size analysis

The particle size of MAS and NIC-MAS complexes was measured using a laser diffraction particle size analyser (Mastersizer2000 model Hydro2000SM, Malvern Instrument Ltd., UK). The samples were dispersed in 70ml of deionised water in sample dispersion unit and stirred at a rate of 50Hz for 30s before measurement. The particle sizes (volume weighted mean diameter) were reported as a mean of three replicates ($n = 3$).

3.2.3 Zeta potential measurement

The zeta potential of MAS and NIC-MAS complexes was measured using a Malvern Zetasizer Nano ZS (Zetasizer) equipment. The temperature of the samples was controlled at 25°C. The samples were diluted prior to the measurement to an appropriate concentration ($n = 3$).

3.2.4 *SEM with energy dispersive X-ray analysis*

The surface morphology FD and SE NIC-MAS complexes were analysed using the SEM method described in Section 2.2.5. Energy dispersive X-ray (EDX) analysis was used for surface chemical analysis of the samples. The characteristic X-rays emitted and elemental information of the samples were recorded.

3.2.5 *XRD analysis*

The physical (crystalline/amorphous) form of both FD and SE MAS-NIC complexes was investigated using a D8 Advantage X-ray diffractometer. The SE MAS-NIC complexes were crushed into powders whilst FD MAS-NIC complexes were compressed using two clean cover glasses, placed on the holder and mounted onto the sample cell. For SE MAS-NIC complexes, Mylar was used to hold the powders before placing on the sample cell. The samples were analysed in transmission mode at a diffraction angle ranging from 5° to 50° 2θ , step size 0.04° , and scan speed of 0.4s/step.

3.2.6 *ATR-FTIR analysis*

ATR-FTIR spectra were obtained from a Perkin Elmer Spectrum instrument which was equipped with a diamond universal ATR-unit. The FD and SE MAS-NIC complexes were crushed into powders and were analysed based on the method described in section 2.2.10 of chapter 2.

3.2.7 *Nuclear magnetic resonance (NMR) spectroscopy*

^{29}Si NMR spectra of both FD and SE MAS-NIC complexes were measured using a solid-state ^{29}Si cross-polarization magic angle spinning NMR spectrometer. The spectral parameters used are as follows: 1600 spins, a relaxation delay of 30sec, a pin rate of 5 kHz, and a spectral size of 4 K with 2 K time domain size.

3.3 Results

3.3.1 Particle size analysis

The particle size distribution of MAS and MAS-NIC complexes are shown in

Table 3.2. MAS dispersion showed a particle size of $45.99 \pm 4.17\mu\text{m}$. Increase in particle size was observed upon addition of NIC at low MAS concentration (MAS-NIC 0.25) with a particle size of $80.02 \pm 10.20\mu\text{m}$, but particle size decreased at subsequent higher MAS concentration (MAS-NIC 0.50) with particle size of $57.09 \pm 0.60\mu\text{m}$. Finally, MAS-NIC complex with the highest MAS concentration (0.75 MAS-NIC) showed the highest particle size ($141.58 \pm 21.04\mu\text{m}$).

The zeta potential of MAS and MAS-NIC complexes at different MAS concentrations are shown in

Table 3.2. The zeta potential of MAS dispersion and 0.50 MAS-NIC had similar zeta potential with values of $-28.2 \pm 0.78\text{mV}$ and $-28.0 \pm 2.23\text{mV}$ respectively. However, the zeta potential of MAS-NIC complex at lowest concentration (0.25 MAS-NIC) demonstrated the lowest zeta potential ($-21.0 \pm 1.29\text{mV}$) while the MAS-NIC complex at highest concentration (0.75 MAS-NIC) demonstrated the highest zeta potential ($-31.0 \pm 0.379\text{mV}$).

Table 3.2: Particle size (μm) and zeta potential (mV) of MAS-NIC complexes dispersed in water.

<i>Sample</i>	<i>Particle size (μm)</i>	<i>Zeta potential (mV)</i>
<i>MAS dispersion</i>	45.99 ± 4.17	-28.2 ± 0.78
<i>MAS-NIC 0.25</i>	80.02 ± 10.20	-21.0 ± 1.29
<i>MAS-NIC 0.50</i>	57.09 ± 0.60	-28.0 ± 2.23
<i>MAS-NIC 0.75</i>	141.58 ± 21.04	-31.0 ± 0.379

3.3.2 SEM with energy dispersive x-ray analysis

The images showing surface morphology of FD and SE MAS-NIC complexes are shown in Figure 3.2. MAS-NIC complexes dried using FD technique showed a sponge-like

cake and more visual porous structure than MAS-NIC complexes dried using SE method. The porosity of the freeze-dried cake structure decreased with increase in MAS concentration in MAS-NIC complexes. The cake of FD MAS-NIC complexes at higher MAS concentration (Figure 3.2 (iii)) showed a more collapsed structure with less pores on the surface. MAS-NIC complexes dried using SE method showed no pores or sponge-like structure, rather they showed some aggregated flocculates that increased with increase in MAS concentration.

Elemental surface analysis of MAS and MAS-NIC complexes was studied using energy dispersive x-ray analysis (EDX) to study the elements on the surface of MAS-NIC complexes particularly the main element of NIC (C- Carbon). The main component of MAS; C, O, Mg, Al and Si was found to be 0.9 ± 0.1 , 63.4 ± 0.3 , 4.7 ± 0.1 , 4.5 ± 0.5 and $22.4 \pm 0.1\%$ w/w.

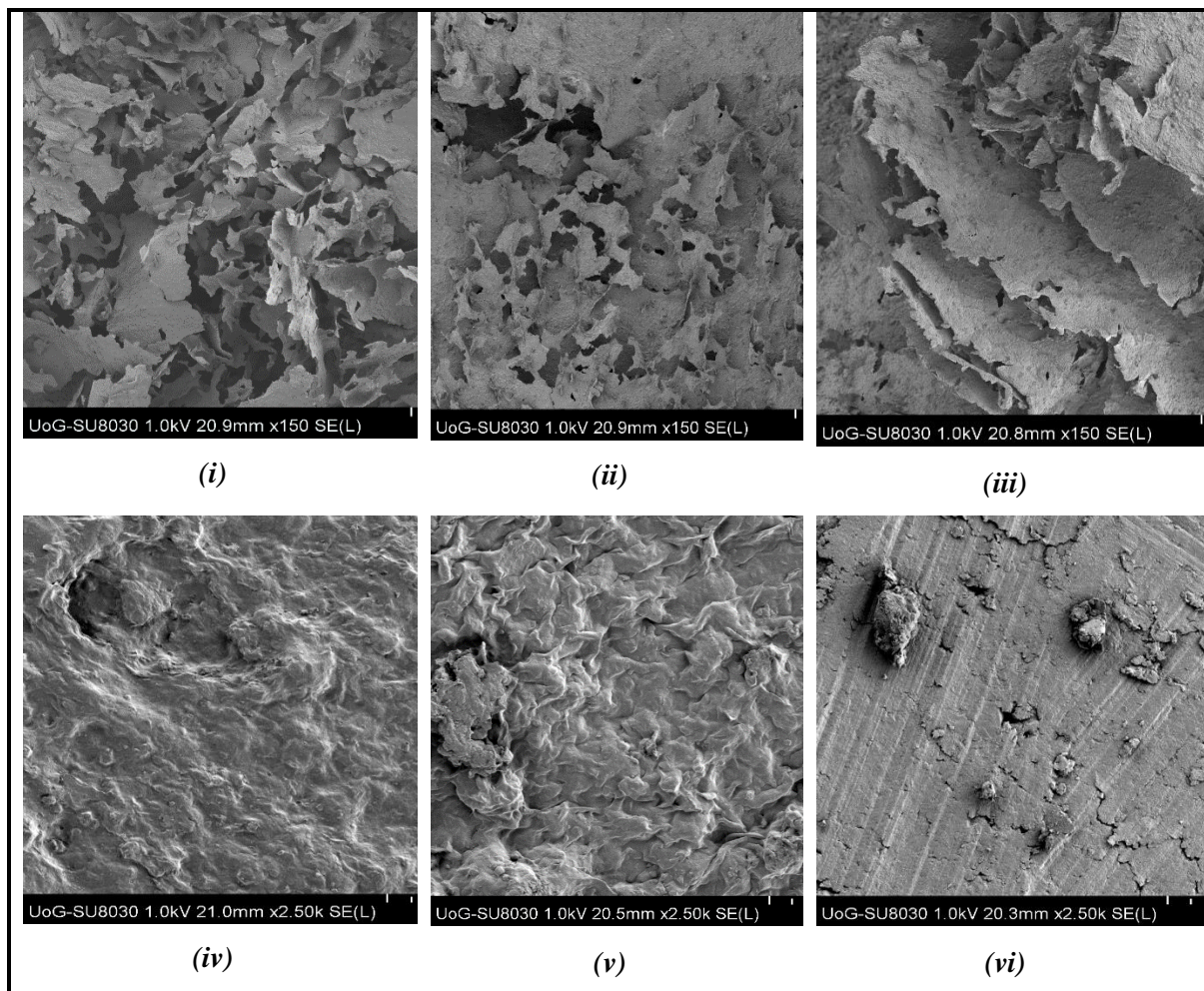


Figure 3.2: Morphology of FD MAS-NIC complexes (x150); MAS 0.25 (i), MAS 0.50 (ii) and MAS 0.75 (iii) and surface morphology of SE MAS-NIC complexes (x2500); MAS 0.25 (iv), MAS 0.50 (v) and MAS 0.75 (vi).

The elemental surface composition of both FD and SE MAS-NIC complexes demonstrated a prominent C peak. This was found to be 4.3 ± 0.1 , 3.3 ± 0.1 and $2.6 \pm 0.2\%$ w/w for 0.25, 0.50 and 0.75 for FD MAS-NIC respectively (Figure 3.3); and 4.2 ± 0.1 , 4.1 ± 0.1 and $3.4 \pm 0.1\%$ w/w for 0.25, 0.50 and 0.75 for SE MAS-NIC respectively (Figure 3.4). The C peak decreased with increase in MAS concentration in MAS-NIC complexes with the highest C element found in 0.25 MAS-NIC complexes in both FD ($4.3 \pm 0.1\%$ w/w) and SE ($4.2 \pm 0.1\%$ w/w).

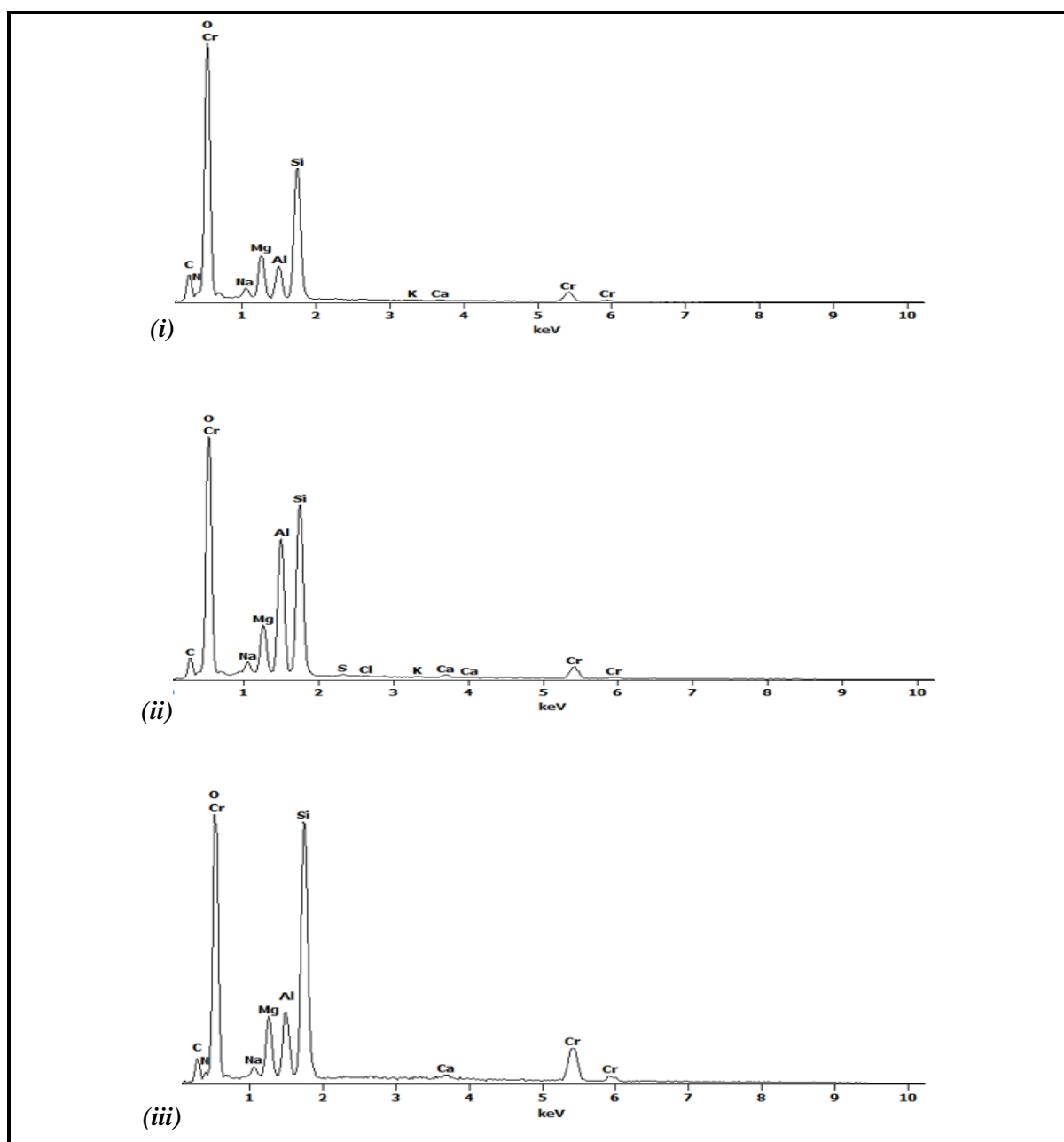


Figure 3.3: EDX analysis of FD MAS-NIC 0.25 (i), 0.50 (ii) and 0.75 (iii).

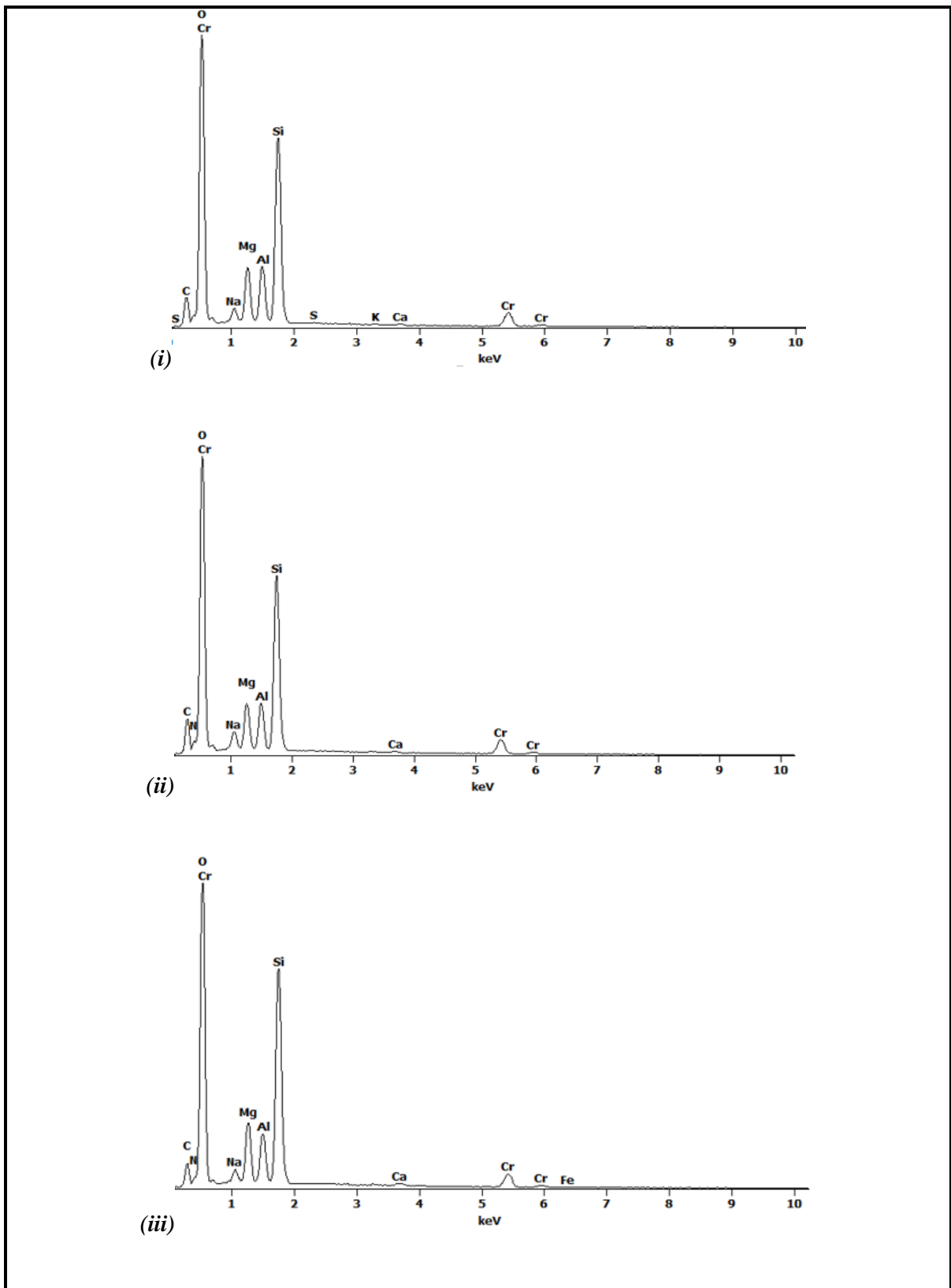


Figure 3.4: EDX analysis of SE MAS-NIC 0.25 (i), 0.50 (ii) and 0.75 (iii).

3.3.3 XRD analysis

MAS pure powder was analysed with both FD (cake) and SE (film) MAS-NIC complexes to be able to identify shifts in peaks.

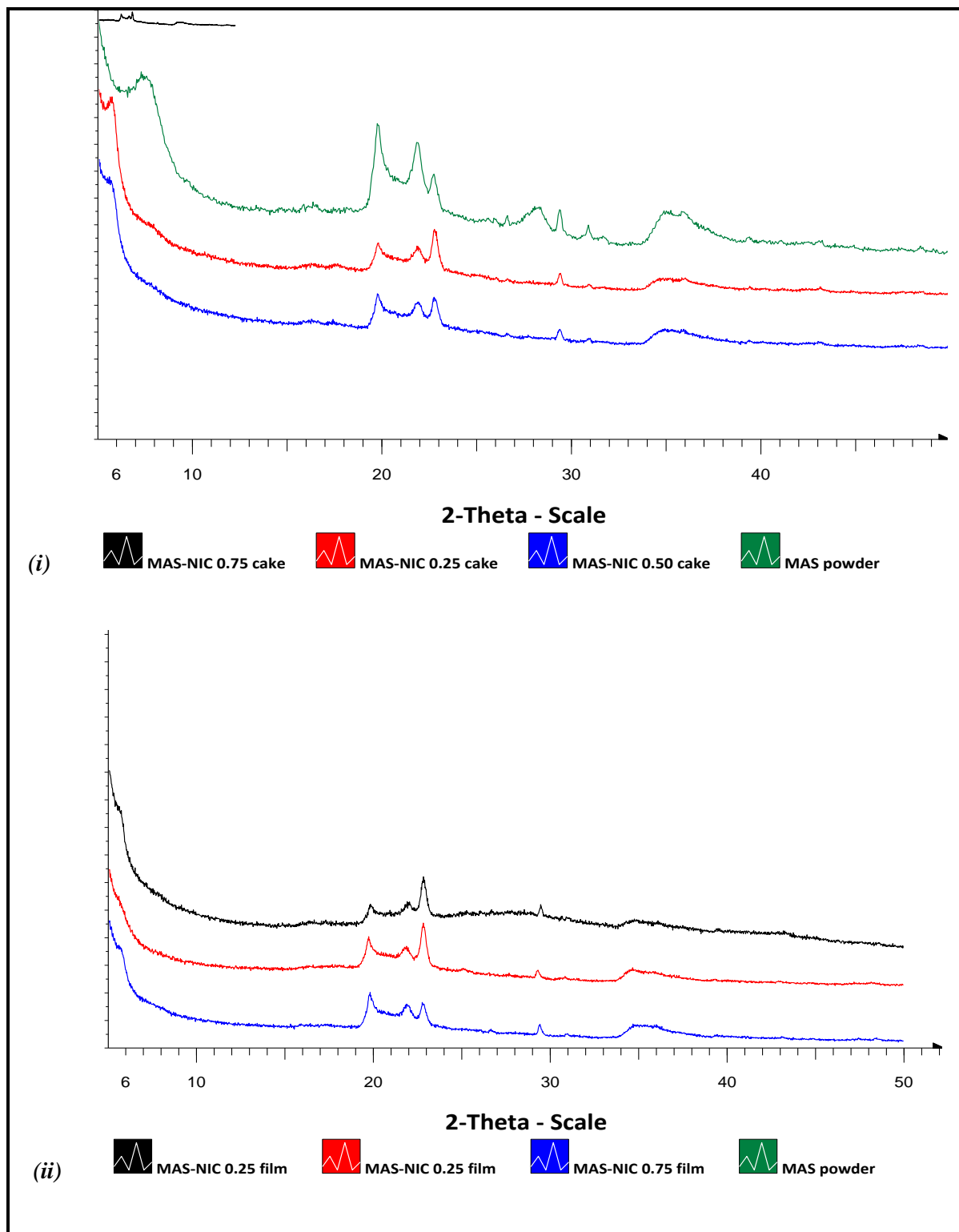


Figure 3.5: XRD diffractograms of (i) FD (cakes) MAS-NIC complexes and (ii) SE (film) MAS-NIC complexes.

Figure 3.5 demonstrates the X-ray diffraction patterns of MAS powder together with that of FD and SE MAS-NIC complexes. MAS-NIC complexes (Figure 3.5 (i) and (ii)) (both FD and SE) demonstrated a crystalline form with diffraction peaks at 2θ values of 20° , 22° , 23° and 29° , and a broad amorphous peak from 2θ of $34^\circ - 38^\circ$ which is similar to the MAS powder XRD pattern. However, MAS powder demonstrated a different reflection at 8.00° (2θ) in comparison with the MAS-NIC complexes, which demonstrated a shift to $5.95-6.00^\circ$ (2θ).

3.3.4 ATR-FTIR analysis

The ATR-FTIR spectra of FD and SE MAS-NIC complexes are summarised in Figure 3.6. The characteristic peak of NIC showed OH stretching vibration band at 3434cm^{-1} , C-H stretching vibration band at 2943cm^{-1} , C=C stretching vibration band at 1477cm^{-1} and N-H wagging vibration band at 715cm^{-1} (Table 3.4 and 3.5). MAS showed characteristic bands of OH stretching vibration at 3626cm^{-1} , SiOH stretching band at 983cm^{-1} , Si-O (amorphous) stretching vibration at 794cm^{-1} and Si-O-Al (octahedral Al) stretching vibration band at 517cm^{-1} . FD MAS-NIC complexes demonstrated a shift of OH stretching vibration band at 3626cm^{-1} to lower wavenumber at $3618 - 3624\text{cm}^{-1}$ and a shift of Si-OH stretching vibration band at 983cm^{-1} to higher wavelength at $987-1000\text{cm}^{-1}$ (Table 3.4). SE MAS-NIC complexes also demonstrated a similar shift of OH stretching vibration band at 3626cm^{-1} to lower wavenumber at $3339 - 3524\text{cm}^{-1}$ and a shift of Si-OH stretching vibration band at 983cm^{-1} to higher wavelength at $983-1004\text{cm}^{-1}$ (Table 3.5). FD and SE MAS-NIC demonstrated a major shift in MAS-NIC 0.25 than in MAS-NIC 0.50 and 0.75.

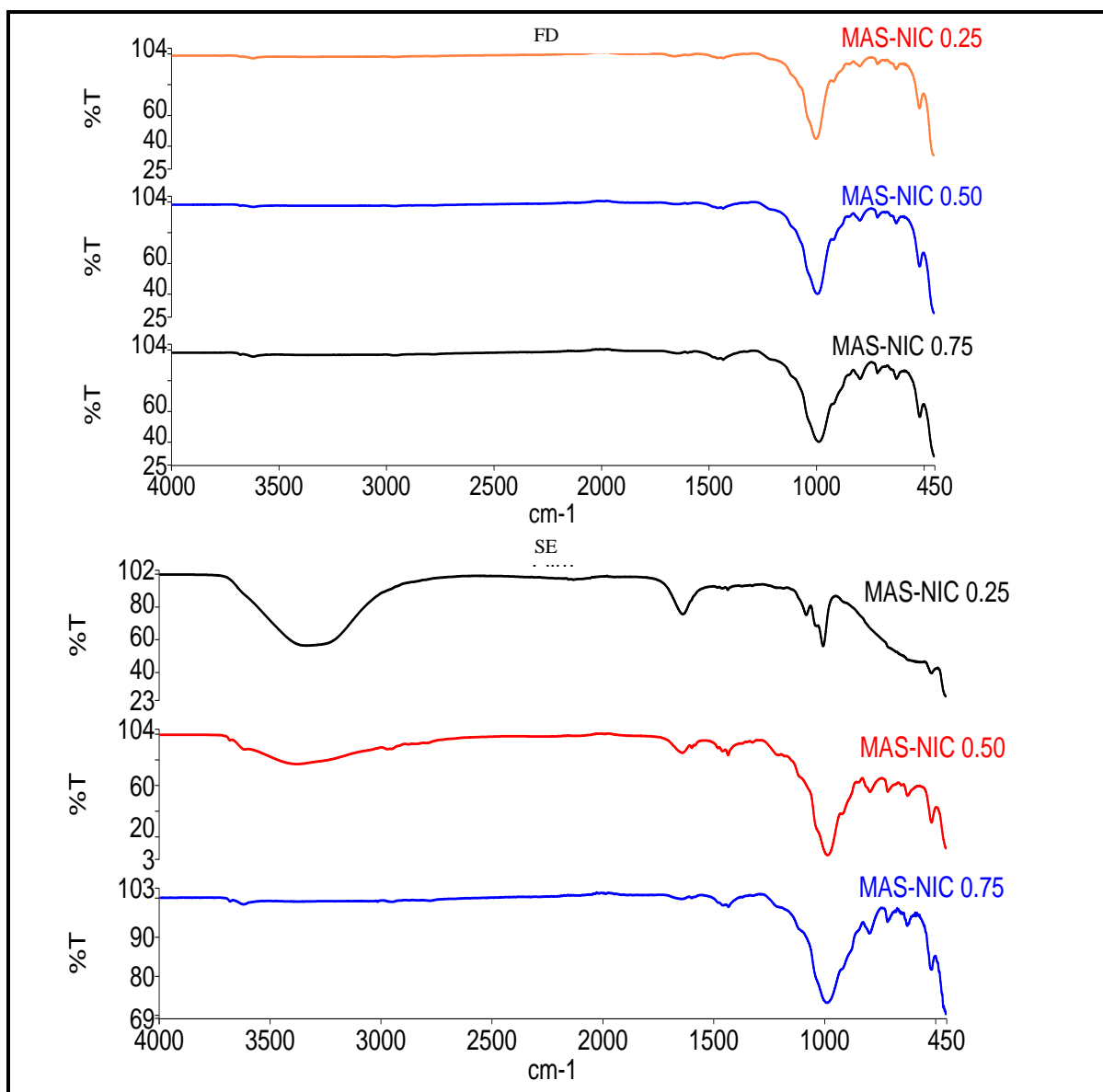


Figure 3.6: ATR-FTIR spectra of (a) FD and (b) SE MAS-NIC complexes.

Table 3.3: ATR-FTIR band assignments of wavelength for FD (cakes) MAS-NIC.

<i>Band assignments</i>						
MAS-NIC complex FD cakes		<i>MAS-NIC 0.25 (cm^{-1})</i>	<i>MAS-NIC 0.50 (cm^{-1})</i>	<i>MAS-NIC 0.75 (cm^{-1})</i>	<i>Pure MAS (cm^{-1})</i>	<i>Pure NIC (cm^{-1})</i>
	O-H band stretching	3618	3619	3624	3626	3434
	C-H stretching				-	2943
	C=N stretching					1692
	Aromatic C=N stretching					1577
	C=C stretching	1433	1433	1432	-	1477
	Si-OH	1000	992	987	983	
	Si-O (amorphous)	796	796	794	794	
	N-H wagging	713	713	713	-	715
	Si-O-Al (octahedral Al), Si- O	517	516	516	517	

Table 3.4: ATR-FTIR band assignments of wavelength for SE (films) MAS-NIC.

<i>Band assignments</i>						
MAS-NIC complex SE films		<i>MAS-NIC 0.25 (cm⁻¹)</i>	<i>MAS-NIC 0.50 (cm⁻¹)</i>	<i>MAS-NIC 0.75 (cm⁻¹)</i>	<i>MAS pure (cm⁻¹)</i>	<i>MAS-NIC 0.25 (cm⁻¹)</i>
	O-H band stretching	3339	3391		3626	3434
	C-H stretching	2133			-	2943
	C=N stretching	1639	1640		-	1692
	Aromatic C=N stretching				-	1577
	C=C stretching	1435	1434		-	1477
	Si-OH	1004	984		983	-
	Si-O (amorphous)		792		794	-
	N-H wagging		712		-	715
	Si-O-Al (octahedral Al), Si-O	515	514		517	-

3.3.5 *Nuclear magnetic resonance (NMR) spectroscopy*

^{29}Si NMR spectra of all samples were measured using a solid-state ^{29}Si cross-polarization magic angle spinning NMR spectrometer. Figure 3.7 demonstrates the ^{29}Si NMR spectra of MAS and MAS-NIC complexes.

^{29}Si chemical shift from -94.38ppm of MAS ^{29}Si NMR spectra to -95.85ppm was observed in all MAS-NIC complexes ^{29}Si NMR spectra. The chemical shift in the ^{29}Si indicate interaction between the silicate layer of MAS and NIC.

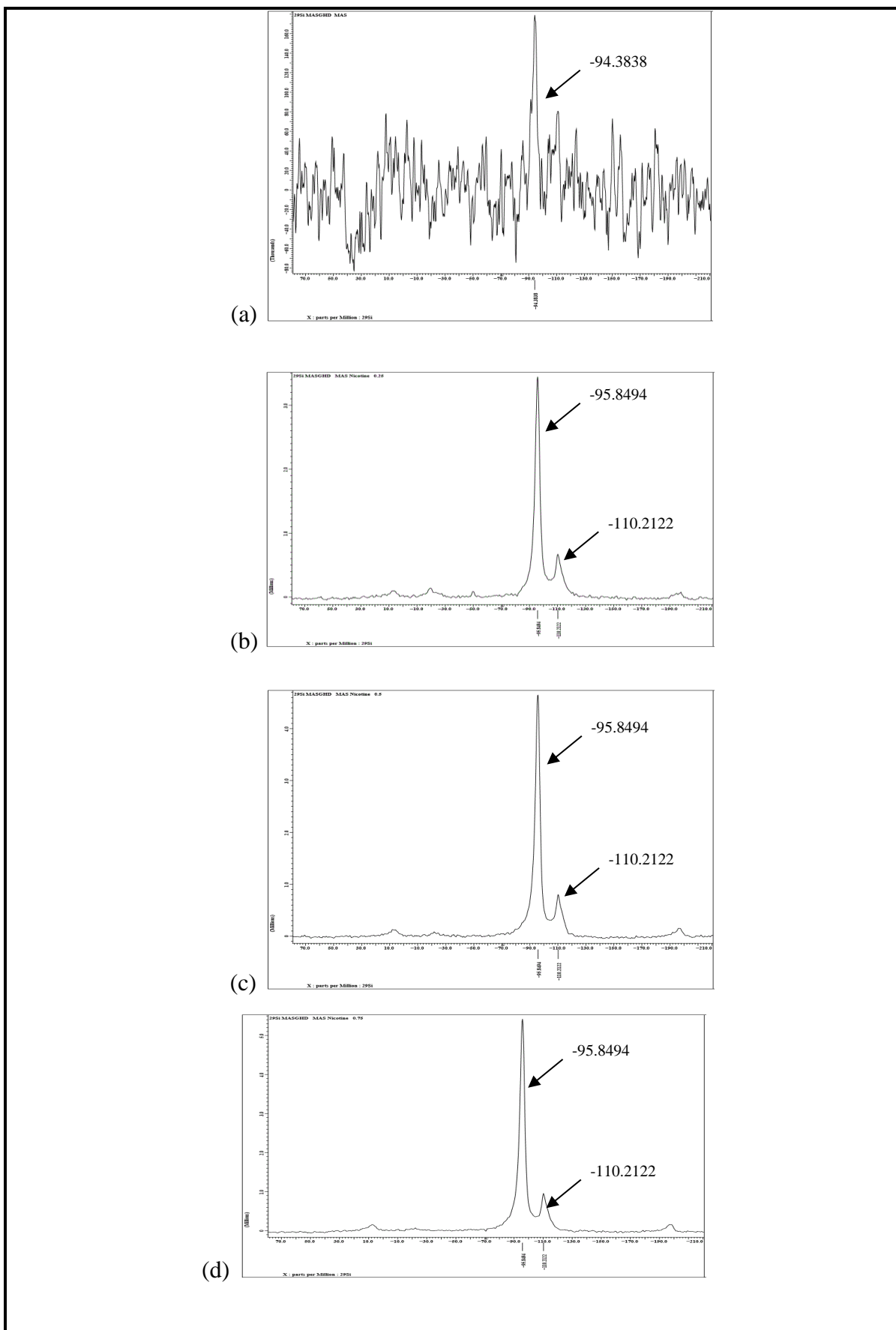


Figure 3.7: Solid-state ^{29}Si NMR spectra of (a) MAS, (b) MAS-NIC 0.25, (c) MAS-NIC 0.50 and (d) MAS-NIC 0.75 complexes.

3.4 Discussion

The increase in particle size (μm) in MAS-NIC complex compared to control (MAS) can be attributed to the adsorption of NIC on the exposed negatively charged surfaces of MAS upon hydration during the preparation of MAS-NIC complex (Pongjanyakul & Suksri, 2009, Rowe et al., 2006). Although MAS-NIC 0.75 demonstrated the highest particle size (μm) (Table 3.2) compared to MAS-NIC 0.25 and 0.50, MAS-NIC interaction was lower than MAS-NIC 0.25 and 0.50 with the MAS-NIC 0.75 demonstrating a higher negative surface charge (zeta potential (mV)). This suggested that the increase in particle size (μm) was the result of flocculation of MAS rather than increased MAS-NIC interaction as the surface charge (zeta potential (mV)) showed a higher negative charge ($-31.0 \pm 0.38\text{mV}$) compared to the pure MAS ($-28.2 \pm 0.78\text{mV}$). The flocculation of MAS-NIC complex was a result of high concentration of MAS leading to entanglement, which formed larger particles with higher surface charge as NIC competes for site of cationic exchange interaction and hydrogen bonding. MAS 0.25 demonstrated an optimum MAS-NIC interaction with an increase in particle size (μm) compared to MAS (control) and decrease in negative surface charge of silicate in MAS. This suggested that the increase in particle size was the result of NIC adsorption onto the exposed negatively charged surface thereby increasing the particle size ($80.02 \pm 10.20\mu\text{m}$) and decreasing the negative surface charge ($-21.0 \pm 1.29\text{mV}$).

The soft porous cake with micro particles on FD MAS-NIC complexes suggested that the MAS-NIC complex structures were retained without disruption during the freeze-drying process. However, SE MAS-NIC complexes demonstrated aggregated flocculates, which increased as MAS concentration increased. This suggests a disruption in the structure of the complex as water evaporated from the mixture. However, the elemental surface structure of MAS-NIC complexes prepared both by freeze-drying and solvent evaporation demonstrated an increase in carbon elemental composition in the structure compared to MAS (control). This

increase could be attributed to the adsorption of NIC to the surface of MAS and thereby increasing the percentage of carbon present in the MAS-NIC structure. The maximum carbon percentage in MAS-NIC complexes was demonstrated in MAS-NIC 0.25, which relates to optimum MAS-NIC interaction as shown in its increased particle size (μm) and decreased negative surface charge when dispersed in water.

The separate reflection demonstrated in MAS powder (control) at 8.00° (2θ) represents the thickness of the silicate layer of MAS. The diffraction showed a shift to $5.95\text{-}6.00^\circ$ (2θ) in MAS-NIC complexes which confirms that NIC adsorbed into the MAS which increased the basal spacing from an initial thickness of 1.22nm to approximately 1.47nm (Pongjanyakul et al., 2009). This suggests that all MAS-NIC complexes showed adsorption of NIC to the exposed negative charges of the silicate layer of MAS. Clay minerals such as MAS with cationic exchange properties interact by ion exchange with basic drugs (NIC) when dissolved in solution (Aguzzi et al., 2007, Pongjanyakul et al., 2009). The interaction between NIC and MAS was demonstrated in the FTIR and NMR analysis results. The shift in OH stretching to a lower wavenumber in FD and SE MAS-NIC complexes can be attributed to the hydrogen bonding between the silicate group of MAS and the amine group of NIC as well as water molecules which act as a bridging mechanism (Aguzzi et al., 2007). The shift to higher wavenumber of SiOH band observed in FD and SE MAS-NIC complex can be attributed to cationic exchange between the negatively charged Si and protonated amine group of NIC. Although the interaction showed weak intensity which is the result of the weakly protonated NIC at pH 9, there is enough protonated NIC which can demonstrate an ionic interaction (Pongjanyakul et al., 2009).

The chemical shift of MAS-NIC complexes in solid state ^{29}Si NMR spectra to a higher ppm indicate an ionic interaction with a decreased MAS layer charged structure as observed in the surface charge (zeta potential) of MAS silicate. Therefore the interaction between MAS

and NIC was formed with a combination of hydrogen bonding, water bridges and ionic bonding (Pongjanyakul et al., 2009).

3.5 Conclusion

The possible mechanism of MAS and NIC interaction for NIC formulation stability was investigated in order to deal with the challenges posed by NIC as observed in chapter two. MAS-NIC complexes showed cationic exchange, hydrogen bonding and water bridging in all MAS-NIC complexes (both FD and SE). MAS-NIC complexes when dispersed in water demonstrated an increase in particle size with decrease in negative surface charge (especially MAS 0.25) compared to MAS alone. This suggested cationic exchange upon dispersion in water. However, concentration of MAS played a role in the extent of interaction. MAS-NIC complexes with higher MAS concentration demonstrated flocculation when dispersed in water as NIC competes for site of interaction with MAS entanglement which limited cationic exchange interaction and hydrogen bonding. Dried (FD and SE) MAS-NIC complexes demonstrated cationic, hydrogen bonding and water bridging interaction as shown in ATR-FTIR and NMR results, with cationic exchange between the negatively charged silicate in MAS and the amine group of NIC.

**CHAPTER 4: NICOTINE STABILIZATION IN COMPOSITE SODIUM
ALGINATE BASED WAFERS AND FILMS FOR NICOTINE
REPLACEMENT THERAPY.**

4.1 Introduction

In chapter one (section 1.6), the use of NIC as an active pharmaceutical ingredient in the development of NRT formulations was discussed. Important properties of NIC such as its pKa (3.04 and 7.84), which potentially forms di-protonated, mono-protonated and neutral species in acid, neutral or basic solutions respectively (Pongjanyakul & Suksri, 2009) were also highlighted. The above mentioned species are capable of permeating biological membranes such as buccal, nasal and sublingual mucosae, however, NIC permeation varies with the unionized species demonstrating a higher permeation than ionized species (i.e. mono-protonated and di-protonated) (Nair et al., 1997).

The oral mucosa drug delivery has gained increased interest because of its ability to avoid gastric acid, enzymes in the small intestine and first pass metabolism in the liver, common with the conventional oral route (Sattar et al., 2014). The buccal mucosa is highly vascular, less vulnerable to irritation and has a lower amount of enzyme activity compared to intestinal, rectal, vaginal and nasal mucosae (Boateng & Okeke, 2014). Though the use of the buccal mucosa for NIC delivery has been demonstrated in NIC chewing gum, Nicorette®, a large percentage of the drug is swallowed before achieving complete absorption (Nair et al., 1997, Adrian et al., 2006, Benowitz et al., 1987).

In developing NRT formulations using the free NIC base (liquid), volatility and oxidative degradation pose major challenges in terms of the physical and chemical stability of NIC in the final dosage form. There has been several research in the past where excipients such as cellulose powder (Mihrianyan et al., 2004), cation exchange resins (Rakić et al., 2010) and inorganic clays such as magnesium aluminium silicate (MAS) (Pongjanyakul & Suksri, 2009)

were introduced into the formulation to address these challenges with NIC stability. Furthermore, these excipients in addition to stabilising NIC, form a polymer-clay/resins composites (complexes) that improve the mechanical, thermal behaviour and modified drug release properties of the formulation (Aguzzi et al., 2007, Gilman, 1999, Pavlidou & Papaspyrides, 2008).

In this research, MAS was selected as an excipient for NIC stabilization. MAS comprises of two natural smectites (montmorillonite and saponite clays) which form a layered structure (Rowe et al., 2006, Pongjanyakul & Suksri, 2009), made up of three-lattice layers of octahedral alumina or magnesia and two tetrahedral silica. The hydration of MAS results in the separation of the layered structure, which exposes the weakly positively charged edge and negatively charged faces. The charged edges of the exposed MAS layered structure can readily interact with NIC, which can result in NIC stabilization as well as influence drug release from the formulation (Pongjanyakul & Suksri, 2009, Rowe et al., 2006). Pongjanyakul & Suksri demonstrated the interaction of MAS with NIC in a SA based film which resulted in increase in NIC retention within the film (Pongjanyakul & Suksri, 2010).

In this chapter, composite HPMC-SA based wafers and films containing different concentrations of MAS, loaded with NIC were characterised and compared for the first time. The hypothesis is that the presence of SA and MAS within a composite formulation will stabilize NIC and result in high drug loading suitable for NRT via the buccal mucosa.

4.2 Materials and methods

4.2.1 *Materials*

Hydroxypropylmethylcellulose - HPMC (Methocel K100 Premium LV) and Magnesium aluminium silicate (MAS) were gifts from Colorcon Limited (Dartford, UK) and R.T. Vanderbilt Company Inc (Norwalk, CT, USA) respectively. Sodium hydroxide, potassium dihydrogen phosphate and gelatine were purchased from Fluka Analytical (Buchs, Switzerland). Nicotine (liquid form), sodium alginate –SA (molecular weight 120,000 – 190,000 g/mol, mannuronate/guluronate ratio 1.56), and mucin from porcine stomach were all obtained from Sigma Aldrich (Dorset, UK); sodium acetate, trimethylamine and glycerol were purchased from Fisher Scientific (Loughborough, UK).

4.2.2 *Formulation development*

4.2.2.1 *Preparation of composite films*

NIC loaded MAS films were prepared in different ratios with a total polymer (HPMC-SA) concentration of 2% w/v. The concentrations of polymers, MAS, plasticizer and drug used in each polymer solution have been summarised in Table 4.1b. The polymeric solutions for film formulation were prepared by dissolving glycerol (GLY) in 80ml of distilled water while stirring at of 25°C before gradually adding HPMC and SA powder one after the other and stirred between 500-700rpm for 2hrs. MAS on the other hand was dissolved in 20ml of hot distilled water (50°C) for 30mins, and mixed with the dispersed polymeric solution. The resulting final solutions were left overnight (16-20hrs) to eliminate air bubbles, NIC added to the MAS composite mixture and stirred at low rpm (100-200rpm) for 30mins. 30g of the NIC loaded MAS solutions were poured into a Petri dish (90mm diameter) and dried in an oven at 30°C for 18-20hrs.

Table 4.1: (a) Concentrations of selected polymers, MAS and mass of NIC used in composite gels for formulating wafers and (b) concentrations of selected polymer, plasticizer, MAS and mass of NIC used in composite gel for film formulation.

(a) Wafers					
Sample name	HPMC (% w/v)	SA (% w/v)	MAS (% w/v)	NIC (g)	
MAS 0.00	1.25	0.75	0.00	0.20	
MAS 0.25	1.25	0.75	0.25	0.20	
MAS 0.50	1.25	0.75	0.50	0.20	
MAS 0.75	1.25	0.75	0.75	0.20	
(b) Films					
Sample name	HPMC (% w/v)	SA (% w/v)	GLY (% w/v)	MAS (% w/v)	NIC (g)
MAS 0.00	1.25	0.75	2.00	0.00	0.20
MAS 0.25	1.25	0.75	2.00	0.25	0.20
MAS 0.50	1.25	0.75	2.00	0.50	0.20
MAS 0.75	1.25	0.75	2.00	0.75	0.20

4.2.2.2 *Preparation of composite wafers*

NIC loaded HPMC-SA-MAS solutions were prepared in a similar manner to films but without using GLY. The solutions (1g) were poured into each well of a 24 well plate (diameter 15.5mm). The concentrations of polymers, MAS and drug present in each solution are summarised in Table 4.1a. The freeze-dried wafers were prepared using an automated lyophilisation cycle, Virtis Advantage XL 70 freeze-dryer (Biopharma process systems, Winchester, UK). The well plates containing the gels were loaded onto the shelves of the freeze-dryer and programmed for freezing, primary drying and secondary drying steps. The freezing step involved cooling the sample from room temperature to 5°C (40mins), 5°C to -10°C (40mins), and then from -10°C to -55°C (120mins). An annealing step was incorporated into the freezing cycle by increasing the temperature from -55°C to -35°C (2hrs) and then cooling back down to -55°C (3hrs). Additional freezing was performed at -55°C (1hr) with a condenser temperature of -55°C under pressure (200mTorr). The primary drying occurred under high pressure of 50mTorr. The temperature was raised from -55°C to -20°C (8hrs) and further increased from -20°C to -15°C (10hrs). Secondary drying occurred at 50mTorr, from -15°C to 25°C (12.5hrs).

4.2.2.3 *Polymer solution properties*

The polymeric solutions were analysed for surface stickiness, stringiness and ‘gel’ strength using a texture analyser (HD Plus, Stable Micro System, Surrey, UK) equipped with a 5kg load cell. A 25mm probe was lowered onto the solution at a speed of 1mm/sec, held for 2secs, and then withdrawn at a speed of 8mm/sec. The maximum force at withdrawal of probe from sample was recorded as surface stickiness while the distance from the onset and offset of force while moving the probe away from the sample was recorded as stringiness. The viscous ‘gel’ strength was recorded as the maximum force as the probe penetrated the polymeric solution to the required depth.

4.2.3 ***Mechanical characterization using TA***

4.2.3.1 ***Tensile properties of films***

The tensile properties of the films were analysed using method and equations described in chapter 2; section 2.2.4.1.

4.2.3.2 ***Mechanical properties of wafers (hardness)***

The resistance to compressive deformation (hardness) of the freeze-dried wafers was determined using method described in chapter 2; section 2.2.4.2.

4.2.4 ***SEM***

The surface morphology of wafers and films was analysed using the method described in chapter 2; section 2.2.5.

4.2.5 ***Wafer porosity***

Pore analysis was performed to evaluate the porosity of wafer structure. Wafers were analysed using the method and equations described in chapter 2; section 2.2.6.

4.2.6 ***XRD***

The physical (crystalline/amorphous) form of NIC loaded MAS wafers and films was investigated using the method described in chapter 2; section 2.2.9.

4.2.7 ***ATR-FTIR***

Wafers and films were analysed using the method described in chapter 2; section 2.2.10.

4.2.8 ***Swelling studies***

The swelling capacities of wafers and films were determined using the method and equation described in chapter 2.2.10.

4.2.9 *Mucoadhesion studies*

Adhesion test was performed on wafers and films using the method described in chapter 2; section 2.2.12.

4.2.10 *HPLC analysis*

The HPLC method used for NIC analysis was described in chapter 2; section 2.2.13.

4.2.11 *Drug content*

The drug content of wafers and films was performed using the methods described in chapter 2; section 2.2.14.

4.2.12 *In vitro drug dissolution and release kinetics*

In vitro drug dissolution of NIC loaded wafers and films was performed using the method described in chapter 2; section 2.2.15.

Experimental release data was fitted to various kinetic models using representative plots to determine the drug release kinetics and mechanisms. These plot profiles include: cumulative % drug release vs time (zero order kinetic model); log cumulative of % drug remaining vs time (first order kinetic model); cumulative % drug release vs square root of time (Higuchi model); cube root of drug % remaining in matrix vs time (Hixson-Crowell cube root law), and log cumulative % drug release vs log time (Korsmeyer-Peppas model), ((Dash et al., 2010, Singhvi & Singh, 2011).

4.2.13 *Stability studies of optimized wafers and films*

NIC stability studies in optimized wafers (MAS 0.25, MAS 0.00) and films (MAS 0.25) were determined by high performance liquid chromatography (HPLC). Accelerated and intermediate stability studies were performed on the optimized wafers and films (Table 4.2) in accordance to ICH and FDA guideline for stability testing of new drug substances and products

for general cases (i.e. for substance not intended for storage in the refrigerator, freezer or below -20°C (Guideline, 2003) . Table 4.2 demonstrates the stability studies and conditions.

Table 4.2: Condition for stability studies on optimized wafers and films.

<i>Study</i>	<i>Storage condition</i>	<i>Time</i>
<i>Intermediate</i>	25°C ± 2°C/60% RH ± 5% RH	6 months
<i>Accelerated</i>	40°C ± 2°C/75% RH ± 5% RH	6 months

4.2.14 *Statistical analysis*

The results were expressed as mean ± standard deviation and statistical analysis was performed using student t-test and / or one-way ANOVA to compare results. The significant differences of data were determined at a level of $p < 0.05$.

4.3 **Results**

4.3.1 *Polymer solution properties*

The pH of the HPMC-SA solutions was neutral but increased to between pH 9-10 upon addition of NIC. NIC loaded HPMC-SA-MAS solutions were less viscous and therefore flowed easily when poured into both the well plates and Petri-dishes for wafers and films respectively.

Table 4.3: Surface stickiness, stringiness and gel strength of HPMC-SA-MAS gel formulations.

<i>Formulations</i>	<i>Surface stickiness (g)</i>	<i>Stringiness (mm)</i>	<i>Gel strength (g)</i>
<i>MAS 0.00</i>	15.51 ± 9.30	0.80 ± 0.27	804.42 ± 268.81
<i>MAS 0.25</i>	18.98 ± 1.64	0.88 ± 0.08	981.45 ± 111.59
<i>MAS 0.50</i>	4.15 ± 0.39	0.53 ± 0.07	184.09 ± 10.30
<i>MAS 0.75</i>	20.91 ± 0.71	0.85 ± 0.05	541.51 ± 153.24

The HPMC-SA-MAS solutions (Table 4.3) also demonstrated increase in surface stickiness, stringiness and 'gel' strength with initial increase in MAS concentration from MAS 0.00 to MAS 0.25, but a decrease in stickiness, stringiness and gel strength for MAS 0.50 formulation and a subsequent increase in stickiness, stringiness and 'gel' strength for the MAS 0.75 formulation. Overall, the MAS 0.25 formulation demonstrated the highest value of stringiness and 'gel' strength compared to other formulations, while MAS 0.75 formulation demonstrated the highest value of surface stickiness. However, MAS 0.50 formulation demonstrated the lowest value of stickiness, stringiness and 'gel' strength compared to the other MAS loaded formulations. NIC loaded solutions were transparent with light brown colour but transparency decreased as MAS concentration increased.

4.3.2 TA

4.3.2.1 Tensile properties of films

Figure 4.1a shows the tensile profiles of NIC loaded SA based composite films at different MAS concentrations. The tensile strength of NIC loaded SA based composite films ranged from $4.98 \pm 0.55\text{N/mm}$ to $6.58 \pm 0.15\text{N/mm}$. There was a gradual increase in tensile strength as the concentration of MAS increased. Films with the lowest concentration of MAS (0.25) showed the lowest tensile strength ($4.98 \pm 0.55\text{N/mm}$) while those with the maximum MAS concentration (0.75) showed the highest tensile strength ($6.58 \pm 0.15\text{N/mm}$). There was also a significant difference ($p < 0.05$) between MAS 0.25 and MAS 0.75 tensile strength. A gradual increase in elastic modulus was also observed as MAS concentration increased with the highest concentration of MAS (MAS 0.75) exhibiting the highest value ($28.04 \pm 1.2327\text{N/mm}^2$) of elastic modulus. A decrease in elongation at break (%) was observed as MAS concentration increased which was most pronounced at the highest concentration of MAS (MAS 0.75) with a value of $16 \pm 0.58\%$. Composite films with no MAS demonstrated the

highest elongation at break (%) of $53 \pm 4.27\%$ followed by MAS 0.50 ($30 \pm 1.85\%$). In general, the concentration of MAS influenced the mechanical properties of NIC loaded composite films.

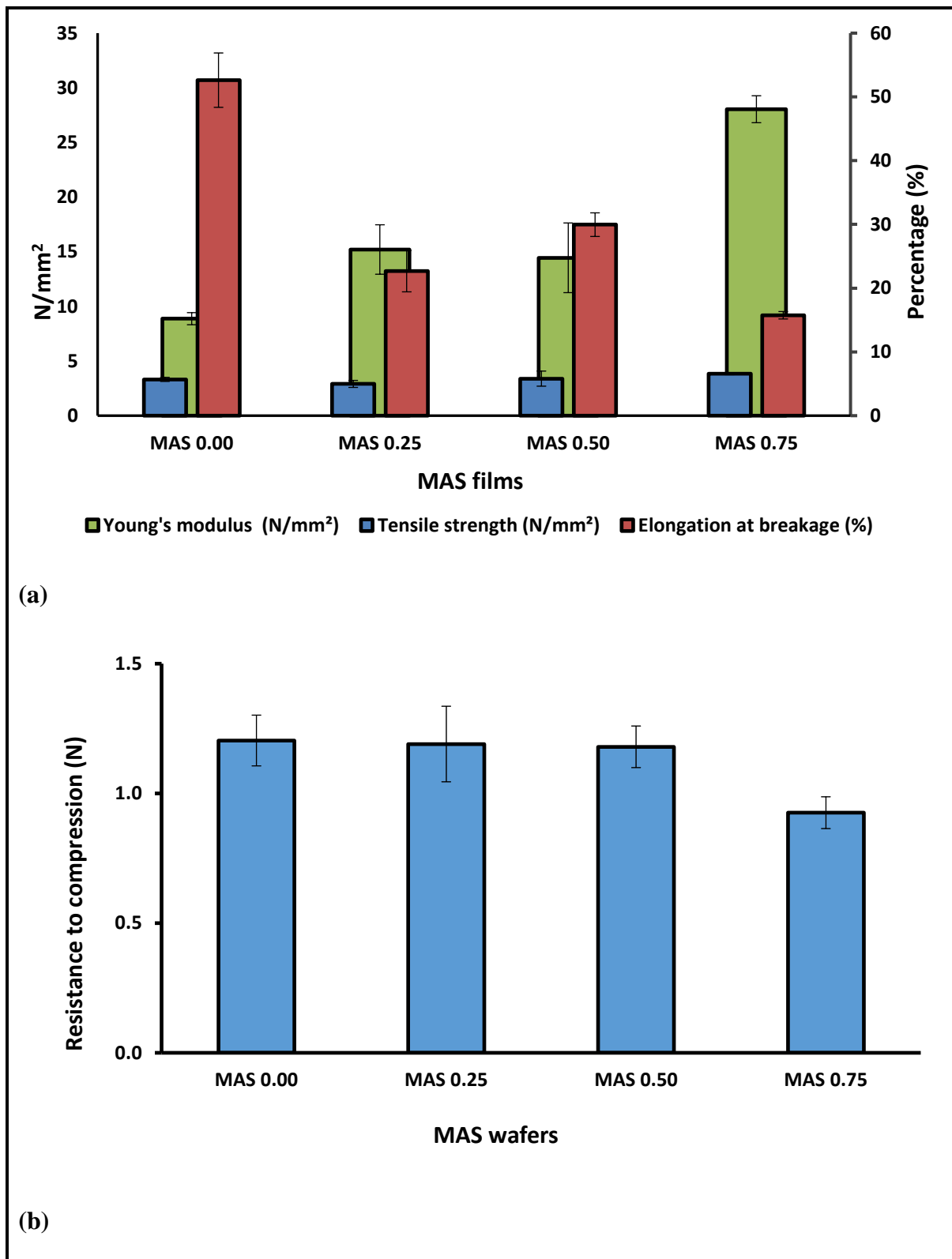


Figure 4.1: (a) Tensile properties of NIC loaded films ($n = 3, \pm SD$) and (b) hardness profiles showing the resistance of NIC loaded wafers ($n = 3, \pm SD$) to compressive deformation forces.

4.3.2.2 *Mechanical properties of wafer (hardness)*

Figure 4.1b shows the hardness profiles of NIC loaded SA based composite wafers at different MAS concentrations. The results showed similar hardness values of 1.20 ± 0.10 , 1.19 ± 0.15 and $1.18 \pm 0.08\text{N}$ for MAS 0.00, 0.25 and 0.50 wafers respectively, but decreased ($0.93 \pm 0.06\text{N}$) for wafers containing the highest amounts of MAS (0.75). The results show that increase in the concentration of MAS up to MAS 0.50 did not affect the resistance of wafer to compression deformation force until the concentration exceeded MAS 0.50 (i.e. MAS 0.75) as demonstrated in Figure 4.1b.

4.3.3 *Scanning electron microscopy (SEM)*

The internal structures and surface morphology of wafers and films, are shown in Figure 4.2 and Figure 4.3 respectively. Wafers demonstrated a sponge-like and porous internal structure while the films showed a continuous polymer sheet. The wafers showed collapsed pore walls as MAS concentration increased with a highly-collapsed wall observed at MAS 0.75. The films also demonstrated a rough surface morphology as MAS concentration increased with MAS 0.75 film showing the most uneven surface compared to other films.

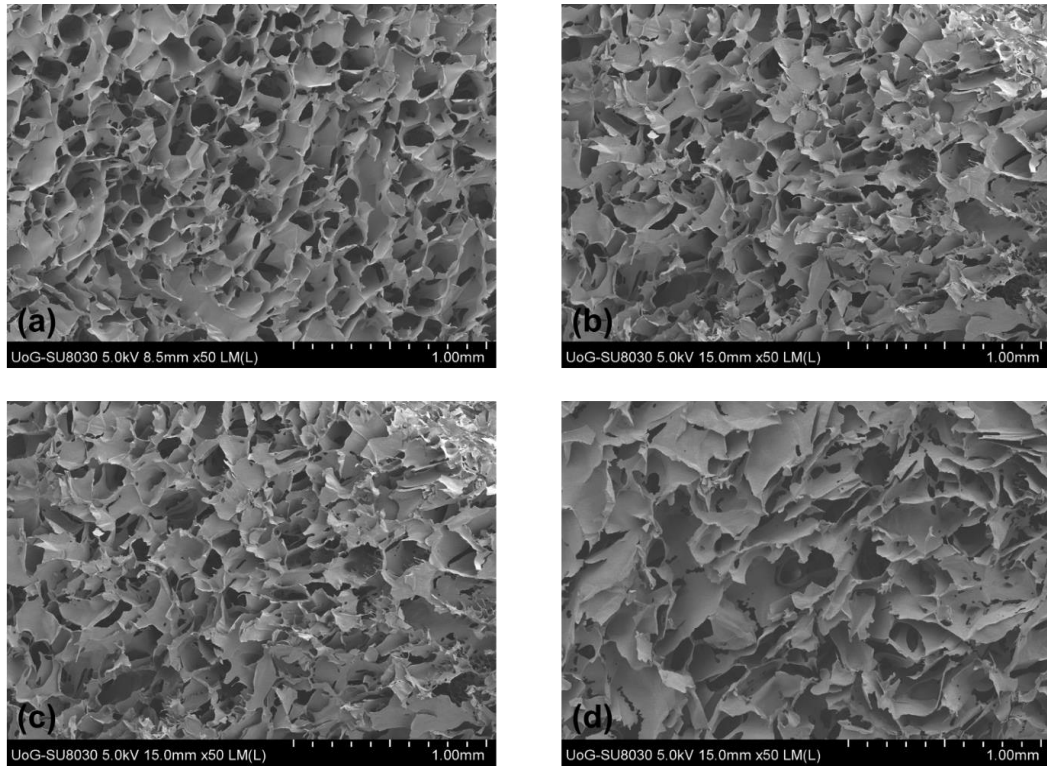


Figure 4.2: SEM images of NIC loaded wafers containing different amounts of MAS: (a) MAS 0.00 (b) MAS 0.25 (c) MAS 0.50 and (d) MAS 0.75.

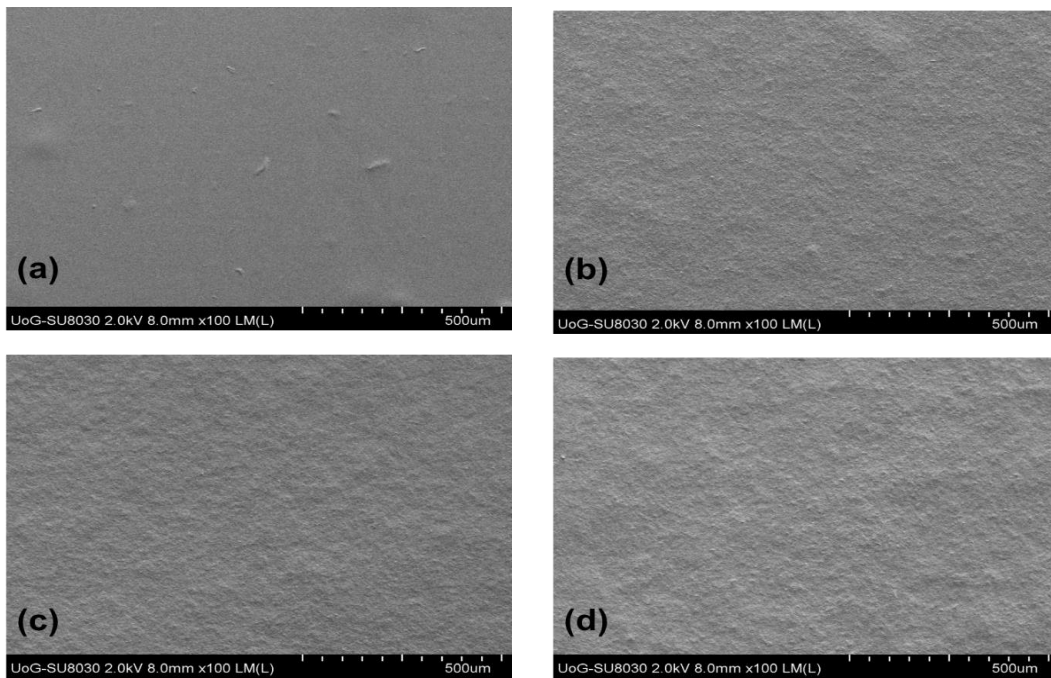


Figure 4.3: SEM images of NIC loaded films containing different amounts of MAS: (a) MAS 0.00 (b) MAS 0.25 (c) MAS 0.50 and (d) MAS 0.75.

4.3.4 *Wafers porosity*

Figure 4.4 shows the porosity (%) of SA based composite wafers at different MAS concentrations. The results demonstrated a decrease in porosity as MAS concentration in the formulation increased from MAS 0.00 to 0.50, but showed a sudden increase at maximum MAS concentration (MAS 0.75). However, this cannot be conclusive because of the degree of error observed between MAS 0.50 and 0.75. Generally, the porosity data supports SEM results for wafers with a better pore structure (less collapsed pores) and pore size homogeneity observed for HPMC-SA wafer with no MAS present (i.e. MAS 0.00).

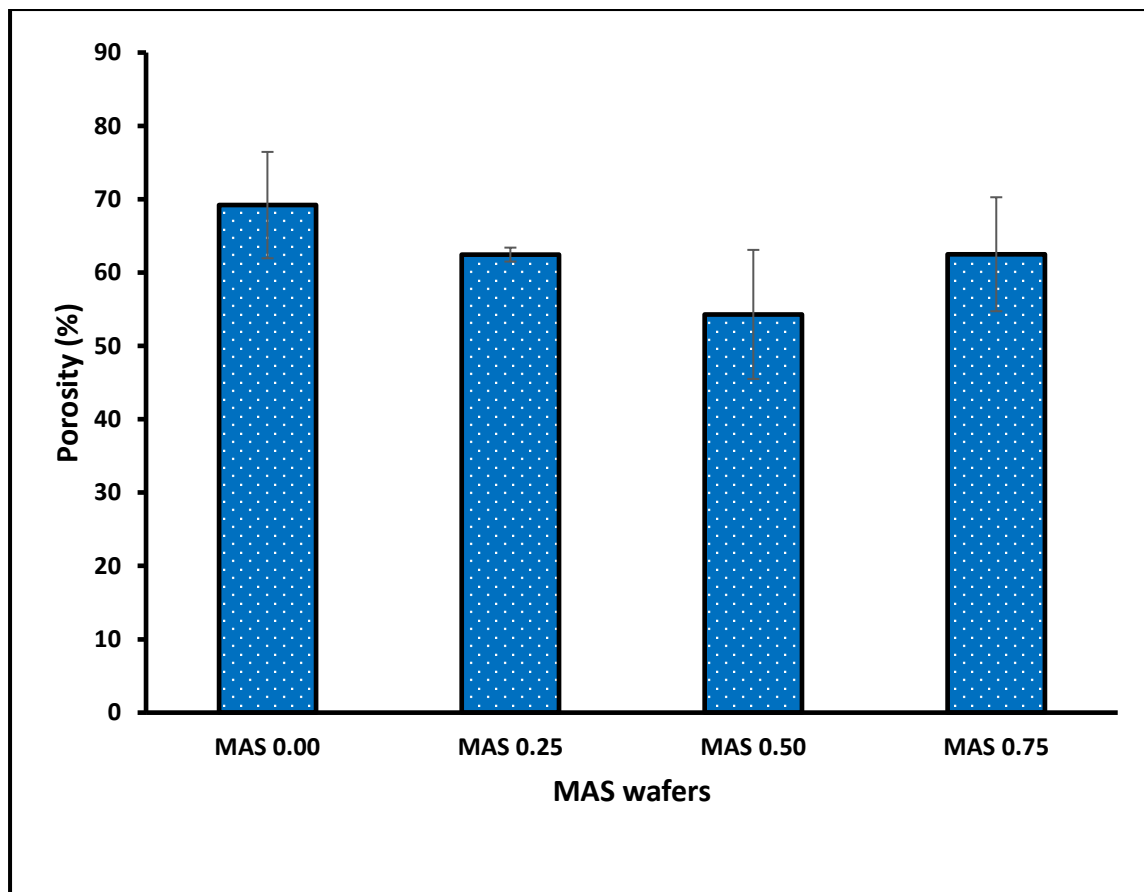


Figure 4.4: Wafers pore characteristics showing % porosity of the different HPMC-SA-MAS wafer formulations ($n = 3$, $\pm SD$).

4.3.5 XRD analysis

Figure 4.5(a) shows XRD transmission diffractograms of pure SA, HPMC, MAS and Mylar (Okeke and Boateng, 2016).

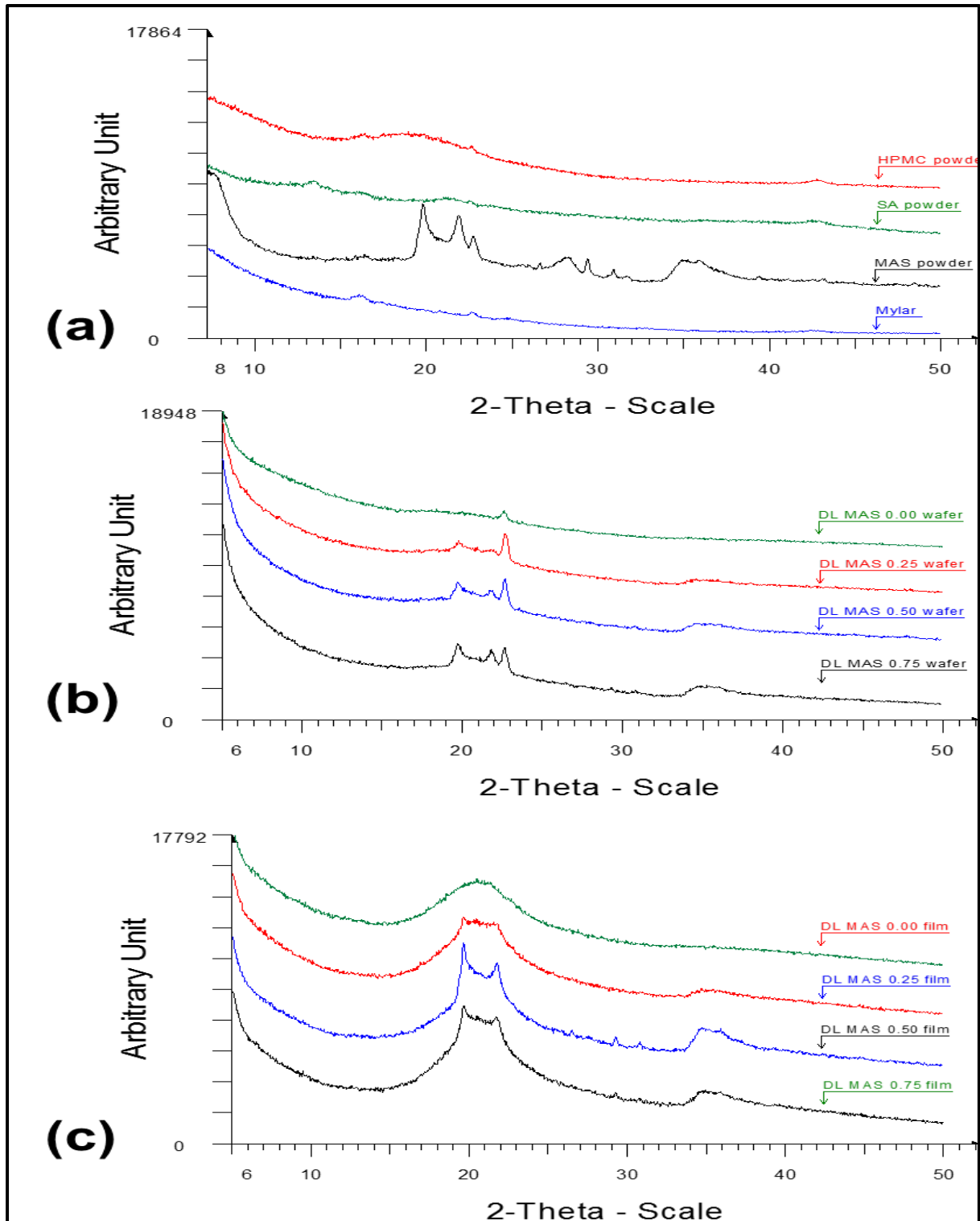


Figure 4.5: XRD diffractograms of (a) pure powders, (b) NIC loaded HPMC-SA-MAS wafers and (c) NIC loaded HPMC-SA-MAS films.

HPMC and SA demonstrated a broad peak at 2θ between $15^\circ - 24^\circ$ and $20^\circ - 23^\circ$ respectively suggesting amorphous structure. Unlike HPMC and SA powders, MAS demonstrated a crystalline form with diffraction peaks at 2θ values of 20° , 22° , 23° and 29° , and a broad amorphous peak from 2θ of $34^\circ - 38^\circ$. Figure 4.5(b) showed one crystalline peak at 2θ 23° in NIC loaded composite wafer without MAS (MAS 0.00) but showed three crystalline peaks at 20° , 22° , 23° for all other MAS formulations (i.e. MAS 0.25, 0.50 and 0.75), attributed to the presence of MAS. NIC loaded wafer also demonstrated a broad peak from 2θ $15-24^\circ$ and from 2θ $34^\circ - 38^\circ$. NIC loaded film without MAS showed a broad peak from 2θ $15-24^\circ$ while MAS loaded films (i.e. MAS 0.25, 0.50 and 0.75) showed broad peaks from $15-24^\circ$ with two crystalline shoulders at 2θ of 20° and 22° .

4.3.6 *ATR-FTIR spectroscopy*

ATR-FTIR spectra of SA, HPMC), GLY, NIC, MAS, NIC loaded composite wafers and films are shown in Figure 4.6. The characteristic peaks and band assignments of pure polymers, GLY, MAS, NIC, and NIC loaded composite wafers and films are summarised in Tables A1 and A2 respectively (appendix). NIC loaded wafers and films demonstrated a shift to higher wavenumber for O-H, O-C=O (asymmetric) and (symmetric) stretching bands. The Si-O-Al (octahedral Al), characteristic peak of MAS at 517cm^{-1} was demonstrated in MAS loaded wafers, with a shift to higher wavelength at 518cm^{-1} , but showed a shift to lower wavenumber at 516cm^{-1} for the corresponding films. However, films without MAS demonstrated a characteristic C-H peak of GLY with a shift to lower wavenumber and C-CH₃ characteristic peak of HPMC (1314cm^{-1}) with a shift to higher wavenumber (1319cm^{-1}).

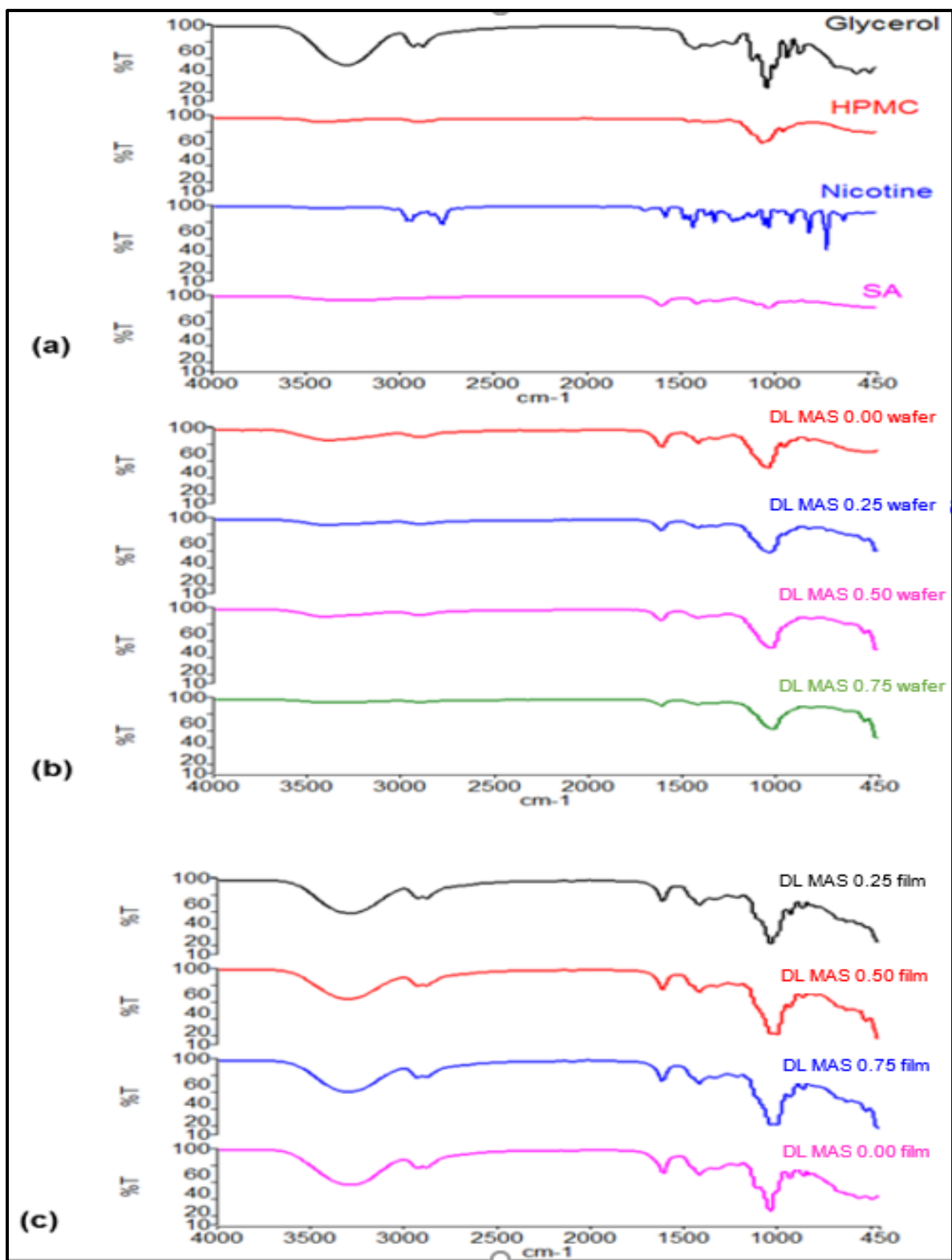


Figure 4.6: ATR-FTIR spectra of (a) pure polymers, GLY, MAS, and NIC, (b) Drug loaded (DL) MAS wafers and (c) Drug loaded (DL) MAS films.

4.3.7 Swelling studies

Figure 4.7 shows the swelling profiles of both composite wafers and films containing different concentrations of MAS. Wafers demonstrated a rapid and higher swelling profile (Figure 4.7a) compared to films (Figure 4.7b).

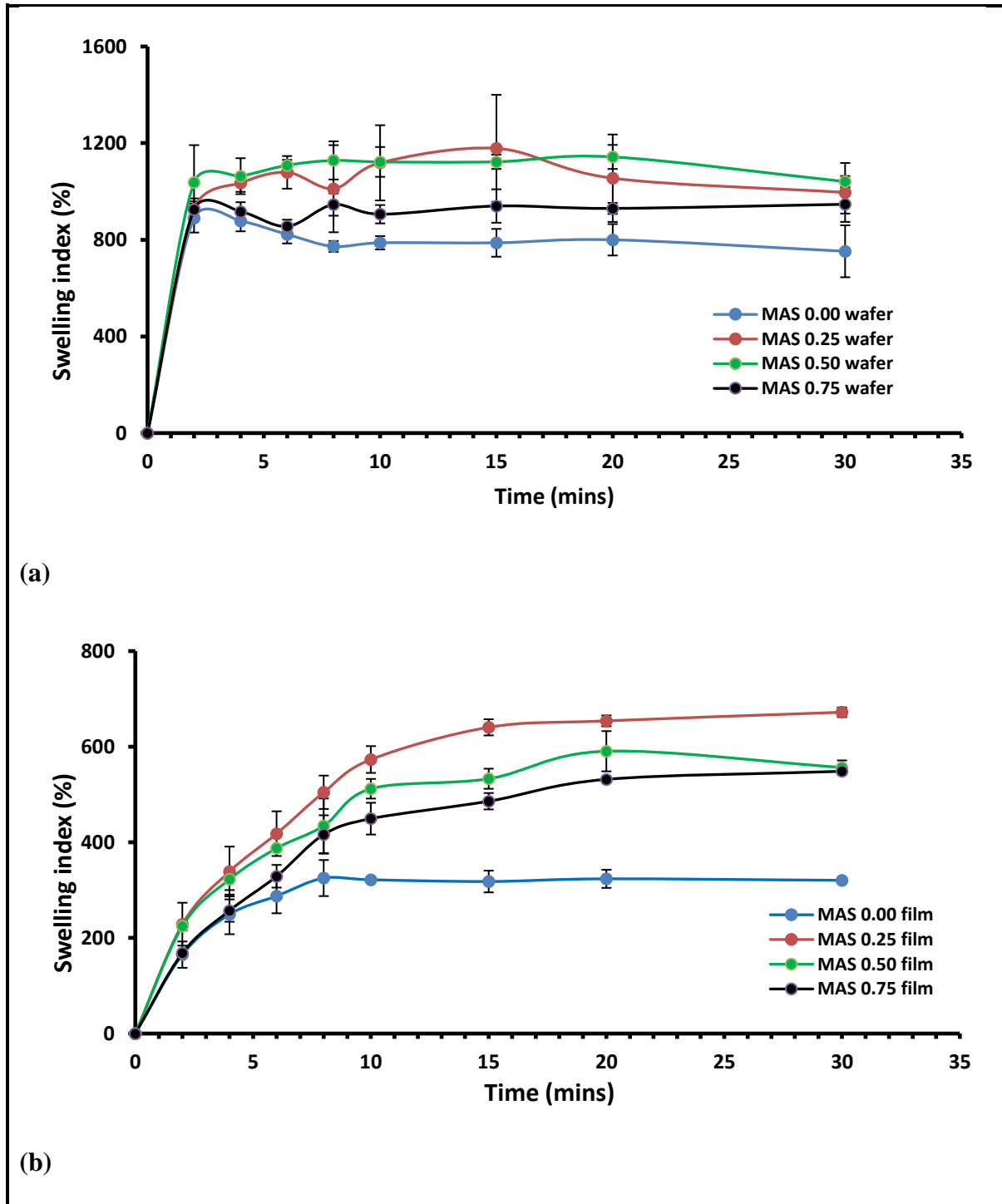


Figure 4.7: Swelling profiles (i.e. swelling index (%) against time) ($n = 3$, \pm SD) of (a) wafers and (b) films.

A swelling index between 700 - 1150% was observed in wafers and 150 - 700% in films after 2mins of contact with PBS solution. Increase in swelling index with incorporation of MAS was demonstrated in both wafers and films. Although MAS wafers (i.e. MAS 0.25, 0.50 and 0.75) showed higher swelling index than wafers with no MAS (i.e. MAS 0.00), wafers with MAS 0.75 concentration showed the lowest swelling index but was still significantly higher ($p = 0.0035$) than the wafers with no MAS present. In the same way, films with MAS 0.75 also showed the lowest swelling among the composite films but was still significantly higher ($p=0.0118$) than the films without MAS.

4.3.8 *Mucoadhesion studies*

Figure 4.8 shows the adhesive properties [(PAF, TWA and cohesiveness (stickiness)] of NIC loaded wafers and films. The wafers showed a significant ($p < 0.05$) decrease in PAF from $1.29 \pm 0.22\text{N}$ for MAS 0.00 wafer to $0.23 \pm 0.003\text{N}$ for MAS 0.25 wafer, representing about 82% decrease in adhesive force but remained constant with further increase in MAS concentration. NIC loaded films on the other hand, demonstrated an increase in PAF as MAS increased. Films showed an increase from $1.94 \pm 0.13\text{N}$ for MAS 0.00 formulation to $2.44 \pm 0.44\text{N}$ for MAS 0.75. In general, there was a significant difference ($p < 0.05$) in PAF between NIC loaded wafer and film, with the films showing higher PAF compared to their corresponding wafers (Figure 4.8a). The TWA (Figure 4.8b) of NIC loaded wafers also demonstrated an initial decrease from $1.01 \pm 0.21\text{Nmm}$ for MAS 0.00 to $0.17 \pm 0.025\text{Nmm}$ for MAS 0.25, and then remained constant as MAS concentration increased which was quite similar to the pattern observed for PAF. However, NIC loaded films showed an increase in TWA in the presence of MAS, increasing from $1.74 \pm 0.52\text{Nmm}$ for MAS 0.25 to $2.28 \pm 0.79\text{Nmm}$ for MAS 0.75. The cohesiveness (stickiness) profiles of NIC loaded wafers and films are shown in Figure 4.8c. The cohesiveness of wafers increased with the introduction of

MAS, with a value of 1.92 ± 0.51 mm for MAS 0.00 and 9.96 ± 0.71 mm for MAS 0.25. MAS can therefore significantly influence cohesiveness of NIC loaded wafers. However, in NIC film there was no influence, as cohesiveness remained relatively constant as MAS concentration increased.

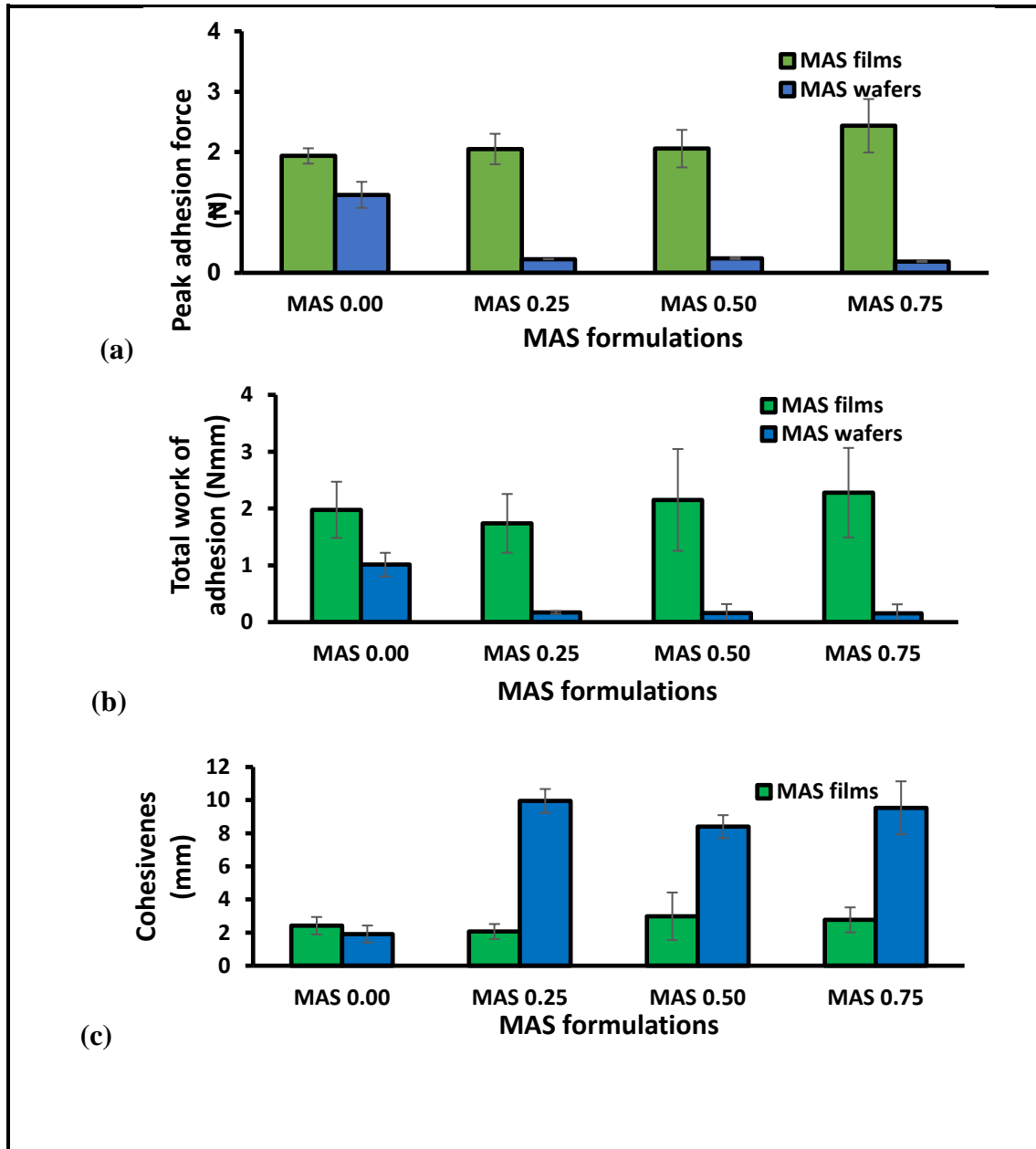


Figure 4.8: Mucoadhesive profiles of HPMC-SA-MAS wafers and films ($n = 3$, \pm SD): (a) peak adhesive force (N) (b) total work done (Nmm) (c) cohesiveness (mm).

Overall, though NIC loaded composite wafers demonstrated high cohesiveness (stickiness), NIC loaded MAS films demonstrated better mucoadhesive properties considering the PAF and TWA profiles which were both higher in films than the wafers.

4.3.9 Drug content (% loading / recovery)

Figure 4.9 shows the drug content of the composite wafers and films and calculated as percentage drug remaining in the dosage forms after the formulation process.

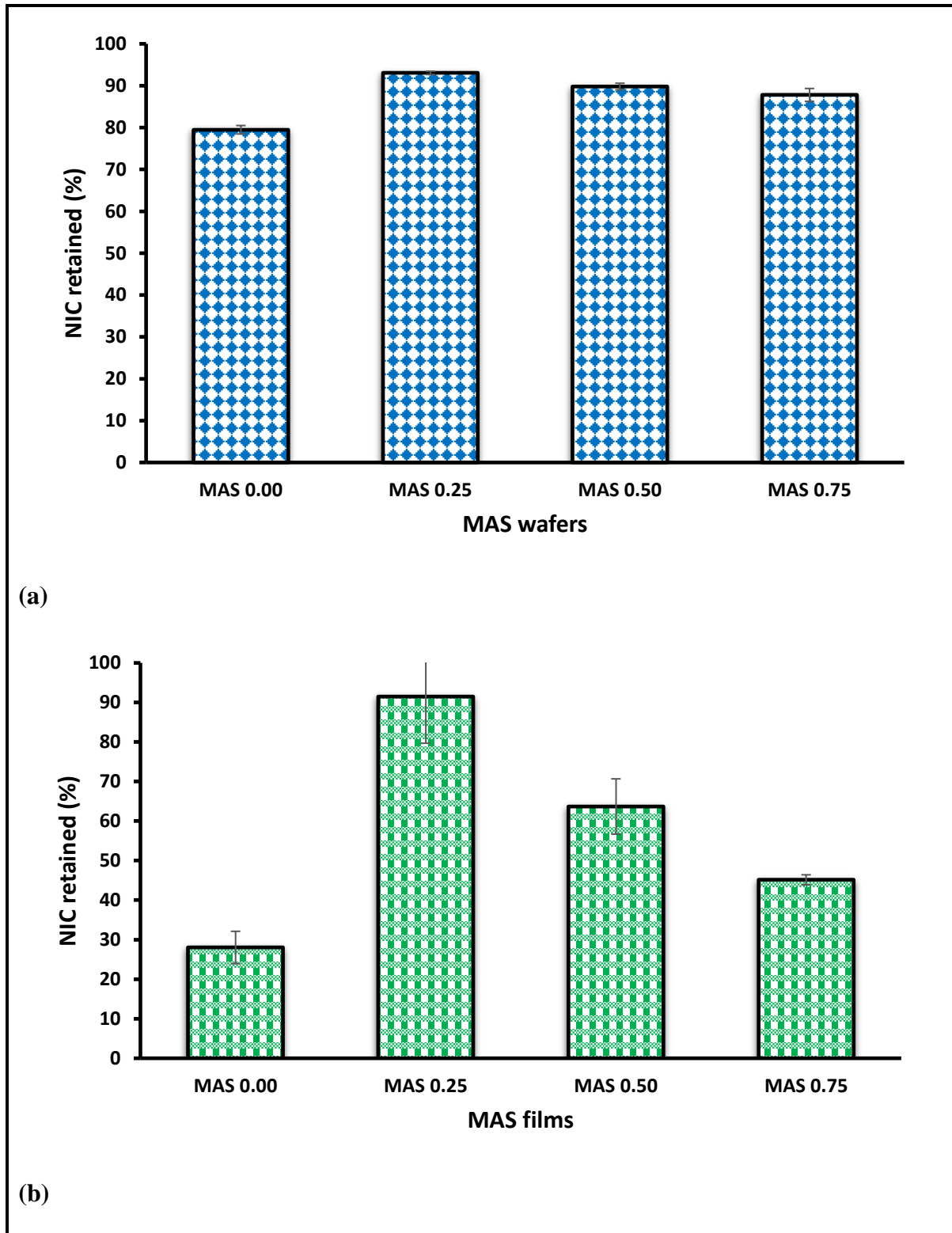


Figure 4.9: Percentage drug (NIC) assayed content for ($n = 3, \pm SD$) (a) HPMC-SA-MAS wafers and (b) HPMC-SA-MAS films at different MAS concentrations.

NIC content was $79 \pm 1\%$ and $28 \pm 4\%$ respectively for wafers and films containing no MAS, which increased to 93% and 92% respectively for wafers and films loaded with MAS 0.25, after which both showed a decrease in NIC content as MAS increased further. The increase in MAS from MAS 0.00 to 0.25 had the most significant effect on the NIC content of SA based composite films, with an increase of approximately 70% compared to wafers which increased by 15%. Further, the subsequent decrease in NIC content in composite films as MAS concentration increased, was more pronounced than the corresponding wafers. In the case of wafers, three formulations MAS 0.25 wafers, MAS 0.50 wafers and MAS 0.75 wafers maintained the NIC content above 85% whilst only MAS 0.25 films had values above 80%. Due to the very low drug content for MAS films at MAS 0.00, these films were not employed during *in vitro* drug dissolution studies.

4.3.10 *In vitro* drug dissolution

Figure 4.10 shows the drug dissolution profiles of MAS wafers and films. The wafers demonstrated a rapid drug release with about 80-100% of NIC released within 60 mins while films showed a much more sustained release profile with drug gradually released from the polymeric matrix. The different wafer formulations showed similar drug release profiles with no significant difference ($p > 0.05$) observed as MAS concentration increased. However, films demonstrated a significant difference ($p < 0.05$) in percentage cumulative drug release as MAS increased. Films containing MAS 0.25 showed the slowest release rate with a maximum cumulative drug release of $15.1 \pm 6.3\%$ at 120 mins followed by MAS 0.50 film ($26.1 \pm 0.1\%$) and increased slightly at MAS 0.75 film with a cumulative drug release of $35.6 \pm 2.7\%$.

The release parameters of NIC loaded SA based wafers and films have been summarised in Table 4.4 and Table 4.5 respectively. Based on the R^2 values, drug release from wafers fit the Korsmeyer-Peppas best compared to other models. However, the release data for

films fit the Korsmeier-Peppas equation for MAS 0.75 films ($R^2 = 0.8986$) and MAS 0.25 films ($R^2 = 0.9707$) whilst Hixson-Cromwell equation fit the release data for MAS 0.50 films ($R^2 = 0.9947$).

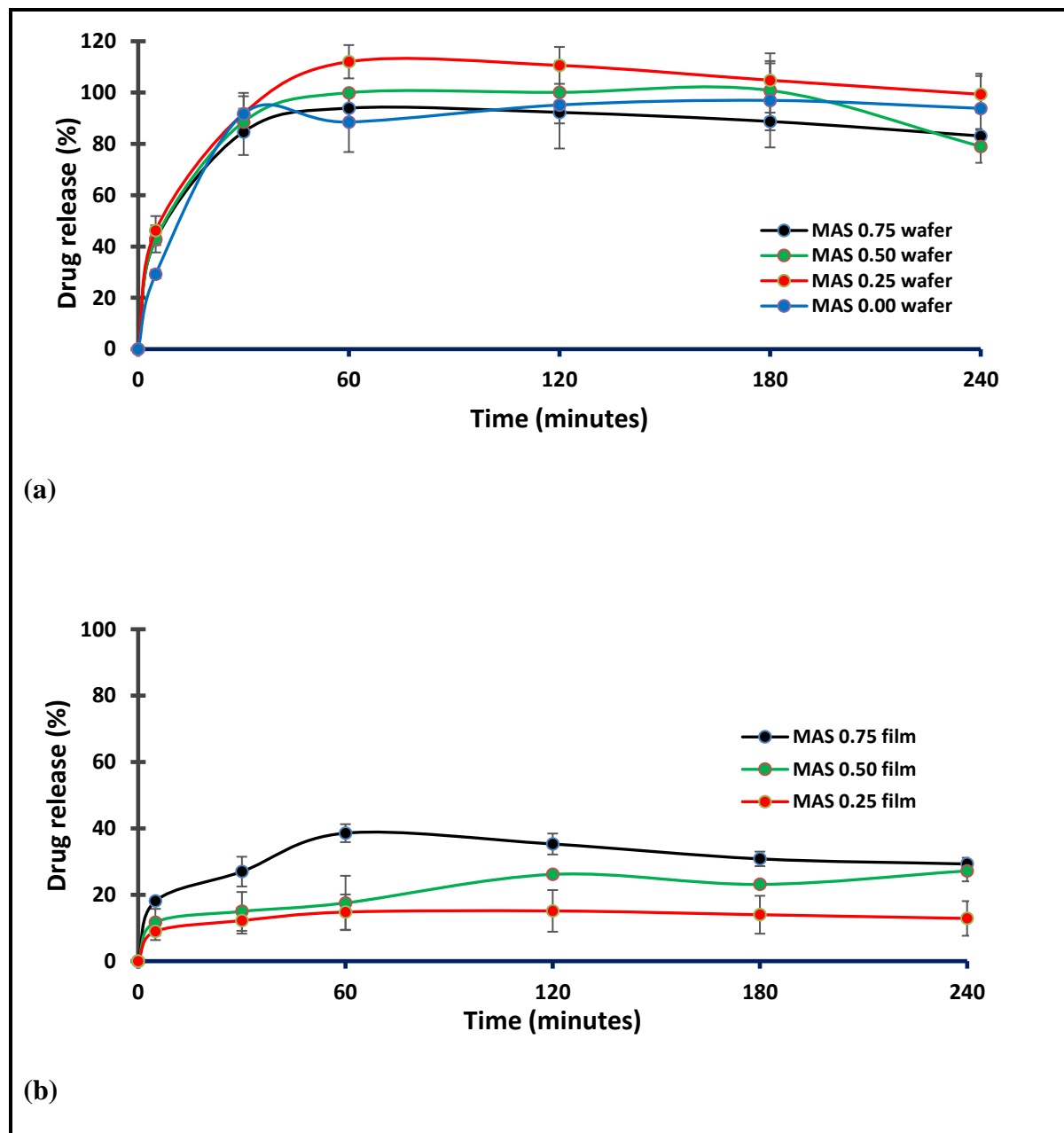


Figure 4.10: In vitro drug release profiles ($n = 3, \pm SD$) of NIC loaded (a) wafers and (b) films containing different MAS concentrations.

The n values of Korsmeier-Peppas equation in wafers ranged from 0.3306 - 0.4839 and decreased with increase in MAS in wafers and less than 0.45 except for MAS 0.00 wafers (0.4839). Similar to wafers, films demonstrated an n value of less than 0.50, which ranged from 0.1744 - 0.2363.

Table 4.4: Release parameters of NIC loaded HPMC-SA-MAS wafers developed by fitting experimental drug dissolution (release) data to different kinetic equations.

<i>Formulations</i>	<i>Zero-order</i>		<i>First order</i>		<i>Higuchi</i>		<i>Hixson-Crowell</i>		<i>Korsmeyer-Peppas</i>		
	<i>R</i> ²	<i>K</i> ₀ (<i>min</i> ⁻¹)	<i>R</i> ²	<i>K</i> ₁ (<i>min</i> ⁻¹)	<i>R</i> ²	<i>K</i> _H (<i>min</i> ^{-1/2})	<i>R</i> ²	<i>K</i> _{HC} (<i>min</i> ^{-1/3})	<i>R</i> ²	<i>n</i>	<i>K</i> _P (% <i>min</i> - <i>n</i>)
MAS 0.75	0.8442	0.9117	0.8071	0.0140	0.9379	9.5568	0.8189	0.0187	0.9770	0.3306	25.574
MAS 0.50	0.8582	1.0140	0.8162	0.0149	0.9471	10.5920	0.8297	0.0202	0.9803	0.3523	24.877
MAS 0.25	0.9280	1.1793	0.8757	0.0158	0.9862	12.0890	0.8935	0.0220	0.9967	0.3616	26.044
MAS 0.00	0.6614	1.0388	0.6783	0.0193	0.7973	11.3410	0.6733	0.0241	0.9123	0.4839	14.256

Table 4.5: Release parameters of NIC loaded HPMC-SA-MAS films developed by fitting experimental drug dissolution (release) data to different kinetic equations.

<i>Formulations</i>	<i>Zero-order</i>		<i>First order</i>		<i>Higuchi</i>		<i>Hixson-Crowell</i>		<i>Korsmeyer-Peppas</i>		
	<i>R</i> ²	<i>K</i> ₀ (<i>min</i> ⁻¹)	<i>R</i> ²	<i>K</i> ₁ (<i>min</i> ⁻¹)	<i>R</i> ²	<i>K</i> _H (<i>min</i> ^{-1/2})	<i>R</i> ²	<i>K</i> _{HC} (<i>min</i> ^{-1/3})	<i>R</i> ²	<i>n</i>	<i>K</i> _P (% <i>min</i> - <i>n</i>)
MAS 0.75	0.6011	0.1435	0.6111	0.0053	0.7613	2.1759	0.6099	0.0053	0.8986	0.2363	12.563
MAS 0.50	0.9917	0.124	0.991	0.0067	0.9303	1.6190	0.9947	0.0059	0.8710	0.2301	7.577
MAS 0.25	0.7526	0.0499	0.7178	0.0042	0.8980	0.7344	0.7299	0.0032	0.9707	0.1744	6.830

4.3.11 NIC Stability studies

Accelerated and intermediate stability studies were performed on MAS wafer, MAS film and non-MAS wafer, in accordance with ICH and FDA guidelines for stability studies. Figure 4.11 demonstrated the NIC content (%) stability study of optimized wafers and films at intermediate ($25^{\circ}\text{C} \pm 2^{\circ}\text{C}/60\% \text{RH} \pm 5\% \text{RH}$) and accelerated ($40^{\circ}\text{C} \pm 2^{\circ}\text{C}/75\% \text{RH} \pm 5\% \text{RH}$) for a period of 6 months.

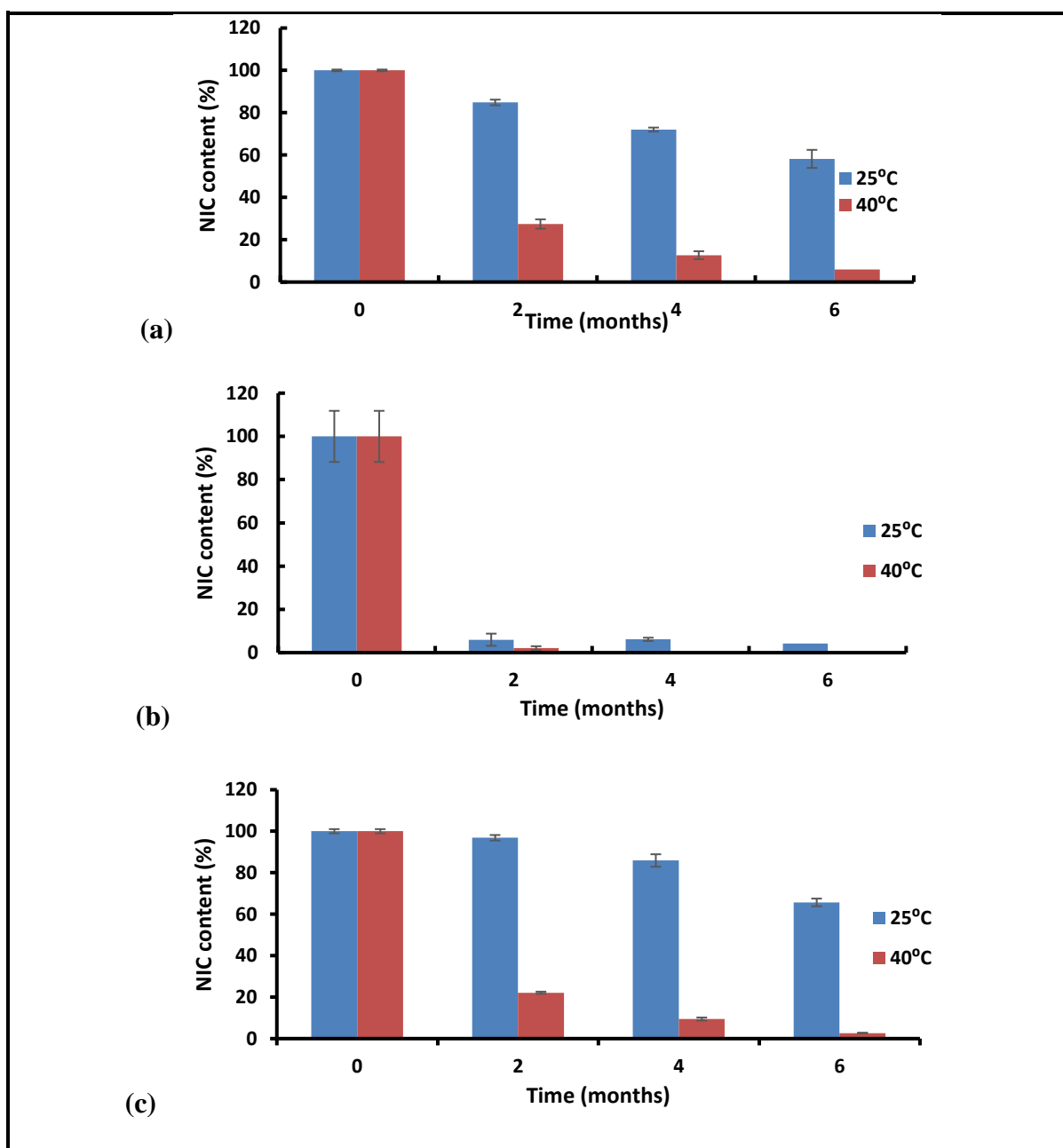


Figure 4.11: NIC content (%) for (a) MAS wafer (MAS 0.25), (b) MAS film (MAS 0.25) and (c) Non-MAS wafer (MAS 0.00) obtained at accelerated and intermediate stability temperatures ($n = 3, \pm SD$).

Optimized wafers (i.e. MAS wafer and Non-MAS wafer) demonstrated more NIC stability in intermediate stability than MAS film with more than 55% of NIC recovered after 6 months in MAS wafer (recovered NIC; $58\% \pm 4.26$) and Non-MAS wafer (recovered NIC; $66\% \pm 1.85$) but less than 5% of NIC was recovered in MAS film (recovered NIC; $4\% \pm 0.45$). However, in accelerated stability studies of optimized wafers and films, less than 10% of NIC was recovered in MAS wafer ($6\% \pm 0.01$), MAS film (0%) and Non-MAS wafer ($3\% \pm 0.11$) after 6 months accelerated stability studies.

4.4 Discussion

The introduction of MAS into wafers and film and the presence of SA was to overcome the challenges posed by NIC as regards to volatility (0.006 kPa at 20°C) and poor stability. The increase in surface stickiness, stringiness and gel strength with increase in MAS concentration was the result of decrease in free volume between the HPMC and SA polymers as the concentration of MAS increased.

The mechanical hardness of wafers is related to their handling and friability and therefore consistency of wafer structure can be demonstrated using hardness data as this shows their resistance to compressive deformation forces (Boateng & Areago, 2014). The consistency in the hardness for wafers containing MAS 0.00 to 0.50 was attributed to their constant porosities. The decrease in hardness of wafers at higher MAS concentration (MAS 0.75) is due to the increased porosity and low free volume between the polymers due to higher MAS solid particles leading to weaker sponge walls. The internal microstructure (SEM) also demonstrated weak sponge walls in wafers containing the highest MAS concentration (MAS 0.75). It's been reported that an increase in porosity can reduce hardness as a result of reduced interaction between polymer chains within the network (Boateng et al., 2010).

The tensile properties of films are very important as they affect ease of handling and application. Pongjanyakul and co-workers demonstrated the effect of MAS on elongation and

tensile strength, concluding that addition of solid particles usually decreases films' elongation (Pongjanyakul et al., 2005). The increase in visible solid particulates on the surface of the films with increase in MAS, could be the reason for the decreased elongation of the films. SA based films showed a decrease in percentage elongation with MAS because MAS reduces the free volume between SA and HPMC (Table 4.1) which further resulted in the increase in brittleness (tensile strength) and stiffness (elastic modulus). This could imply that MAS had an opposite effect to the known plasticising action of GLY.

The physical form of formulations (amorphous or crystalline) can influence functional characteristics such as water uptake and mucoadhesion (Prabaharan & Gong, 2008). The crystalline peaks demonstrated in both wafers and films were due to the crystalline nature of the montmorillonite and saponite clay structures of MAS. Although crystallinity generally decreases dissolution rate, incorporation of MAS increased the swelling index due to the interaction between MAS and SA as demonstrated in ATR-FTIR results and also previously reported (Pongjanyakul et al., 2005). MAS can interact with SA through the formation of hydrogen bonds between surface silanol groups of MAS and the carboxyl groups of SA and the extent of this interaction is responsible for the observed changes in characteristics with increase in MAS concentration.

Suitable hydration and swelling play a major role in mucoadhesion as well as drug release patterns (Pawar et al., 2013). In general, the rapid swelling profile of wafers compared to films was the result of the sponge-like pores in the wafers microstructure, enabling faster water ingress and making them hydrate faster than the films. (Pongjanyakul et al., 2005) suggested that the decrease in water uptake in SA films loaded with MAS was due to the interaction of SA and MAS, which produced a denser matrix structure and this could have occurred in the case of the films formulated in this study. The increase in swelling index as

MAS concentration increased up to MAS 0.5 was the result of increase in sponge-like porosity as MAS increased.

SA based films showed higher mucoadhesion than the corresponding wafers due to the presence of GLY. This allowed better contact stage via hydrogen bonding and van der Waals forces (adsorption theory of mucoadhesion) than wafers which were based on the diffusion theory (Smart, 2005). The increase in mucoadhesion in films as MAS concentration increased could be attributed to the exposure of weak positive and negatively charged forces. Upon contact with physiological fluids, the charged MAS interacts with mucin macromolecules leading to increased van der Waals forces and electrostatic interactions (Pongjanyakul & Suksri, 2009, Rowe et al., 2006). The decrease in mucoadhesion of wafers as MAS concentration increased could be due to the poor contact stage caused by gaps related to the sponge-like pores present in wafers (Smart, 2005). In addition, MAS can compete with SA and NIC for binding mucin. However, the increase in MAS showed no noticeable change in adhesion, as the freely available MAS after interaction with NIC, interacts with SA, therefore reducing the availability of the SA cationic group to interact with mucin.

The primary aim of incorporating MAS into HPMC-SA wafers and films was to stabilise NIC. The volatility of NIC base is one of the main reasons for its instability in formulations as NIC evaporates at high temperature (30°C) during the drying process (Nair et al., 1997). MAS can readily interact with amine based drugs through electrostatic interactions which can improve NIC stability (Pongjanyakul & Suksri, 2009) and improve the retention of NIC within the wafers and films. However, higher percentage NIC content was observed in wafers than in the films due to the lower temperatures used during freeze-drying, compared to oven drying. The decrease in percentage NIC content in MAS wafers and films at MAS 0.50 and 0.75 can be explained by the increase in repulsive forces which build-up as MAS concentration increased.

The release of drug from polymeric matrices such as wafers and films is dependent on factors such as hydration and eventual swelling of the polymeric dosage form (Siepmann & Peppas, 2012). As formulations come in contact with dissolution medium, they undergo hydration, swelling and erosion (dissolution), which was evident in the swelling behaviour of the various wafers and films which correlated with the respective drug dissolution profiles. The rapid release (80 - 100% in 60 mins) from the wafers corresponded to the high swelling index, due to the sponge-like porous internal structure of wafers (SEM and percentage porosity). Therefore, the use of SA based wafers can be efficient in achieving rapid release of NIC to the buccal mucosa to ensure rapid easing of the urge to smoke tobacco. The much slower release of NIC from the films, which corresponded to low swelling index, can be important in achieving sustained release of NIC, with an extended effect to reduce the need for frequent administration.

The release mechanism of HPMC-SA-MAS wafers and film was best described by Korsmeyer-Peppas model, suggesting that the drug release mechanism for these formulations was based on diffusion from a swollen polymeric system. The release exponents of MAS loaded formulations of less than 0.45 (wafer/cylinder) and 0.50 (thin film) was outside the limits of Korsmeyer-Peppas model and also highlights the limitations of the Korsmeyer-Peppas model in the understanding of drug release mechanisms (Shoib et al., 2006). However, the release exponent of 0.48 for wafers without MAS (MAS 0.00 wafers) shows that drug release from these wafers followed a Fickian diffusion transport mechanism (Nair et al., 2013). This implies that addition of MAS changed the release mechanism of NIC due to its interaction with MAS resulting in a complex release mechanism comprising swelling, diffusion and erosion.

The essence of stability studies is to assess the effect of the environmental factors such as temperature and humidity on the quality of a designed formulation. This can be applied in the prediction of the shelf life of the formulation, determine the storage conditions and develop

an instructional guide found on a product label (Bajaj et al., 2012). Stability studies at both accelerated and intermediate conditions were performed on optimized wafers and films for NIC content over 6 months. The loss of NIC was due to oxidative degradation of NIC upon exposure to air. Intermediate stability study demonstrated a much lower oxidative NIC degradation due to its relatively low temperature compared to accelerated stability study condition. Less oxidation was observed in freeze-dried wafers (i.e. MAS wafer and Non-MAS wafer) at intermediate stability studies condition than in film, which can be attributed to the formulation technique i.e. freeze-drying. Freeze-drying reduces oxidative degradation during storage due to its very low water content in its final product (Heinzelmann et al., 2000). NIC content remained above 85% after two months at intermediate condition but decreased in the fourth and sixth month of stability studies which implies that the shelf life of the formulation should not be more than 2 months when unprotected from environmental factors such as air and moisture. However, at accelerated stability studies condition, NIC readily evaporates off the formulation due to the volatile nature of NIC especially in MAS film formulation. This implies that optimized formulations cannot be stored at a temperature above 25°C. In order to improve stability of optimized wafers and films, an adequate protective packaging (that is resistant to moisture and air) needs to be adopted to protect NIC from degrading.

4.5 Conclusion

Composite SA based wafers and films, incorporating MAS were successfully formulated as potential buccal delivery systems for NRT. The two formulations demonstrated different behaviours in their functional physical characteristics (mechanical and surface/internal morphology, swelling index, mucoadhesion, drug loading capacity and drug release). The wafers showed a porous internal morphology which contribute to a higher swelling index than a continuous sheet of films. MAS improved the physical stability of NIC with an increase in drug loading capacity via molecular interaction between the inorganic clay and the alkaline drug. The release of drug from the wafers was rapid while release from the corresponding films was sustained. Furthermore, addition of MAS changed the release mechanism of NIC in both formulations with possible combination of swelling, diffusion and erosion. The MAS stabilized formulations have great potential as buccal delivery systems for NRT. Furthermore, the stability studies of the optimized formulations demonstrated low drug content within 6months, which can be attributed to oxidative degradation of NIC. However, optimized wafers demonstrated NIC content stability with 2-4months (above 85%) and in order to improve stability, an adequate packaging is recommended for the formulations.

**CHAPTER 5: EFFECT OF SIMULATED SALIVA ON MUCOADHESION,
SWELLING AND DISSOLUTION CHARACTERISTICS - A COMPARISON
OF OPTIMIZED FORMULATIONS WITH COMMERCIALY AVAILABLE
NRT PRODUCT (NIQUITIN®)**

5.1 Introduction

Human saliva is made up of approximately 99% water, with the presence of electrolytes such as sodium, calcium, potassium, chloride, phosphate, bicarbonate, magnesium. It also contains biological residues such as proteins (enzymes, mucosal glycoproteins, albumin, polypeptides and oligopeptides, immunoglobulins) and other antimicrobial features (Humphrey & Williamson, 2001). Numerous factors can impact salivary flow and composition such as the degree of hydration of an individual, smoking, medication, age, gender, body weight, salivary gland size, physical activities such as exercise, fasting and nausea, and disease (de Almeida et al., 2008).

In *in vitro* studies of oral transmucosal delivery systems, simulated saliva (SS) can play a vital role in understanding dosage form properties such as drug release and swelling. It is practically difficult to duplicate the properties of the human saliva because of its unique characteristics (Marques et al., 2011). However, several researchers have developed artificial (simulated) saliva for various applications including the study of corrosion behaviour in dental alloys (SS1 in Figure 5.1) (Duffó & Castillo, 2004) and to develop computational models for predicting local effects on the mouth from carcinogenic compounds present in tobacco smoke (SS2 in Figure 5.1) (Kartal et al., 2010). It has also been used to study the interaction of benzethonium-copolymer complex for dentifrices (SS3 in Figure 5.1) (Tavss et al., 1984), investigate the potential interactions between drug molecules and constituents of salivary secretions (SS4 in Figure 1). Finally, it has been used to observe the release of salbutamol

sulphate from oral fast dissolving films (SS5 in Figure 5.1) (Davis et al., 1971, Mashru et al., 2005).

Table 5.1: Simulated saliva (SS) compositions used in various studies (Marques et al., 2011)

<i>Composition</i>	<i>SS1 (g/L)</i>	<i>SS2 (g/L)</i>	<i>SS3 (g/L)</i>	<i>SS4 (g/L)</i>	<i>SS5 (g/L)</i>
<i>Potassium chloride</i>	0.720	0.720	-	0.149	
<i>Calcium chloride dehydrate</i>	0.220	0.220	0.228	-	
<i>Sodium chloride</i>	0.600	0.600	1.017	8.00	
<i>Potassium phosphate monobasic</i>	0.680	0.680	-	-	0.19
<i>Sodium phosphate dibasic</i>	0.866	0.866	0.204	-	2.38
	(dodecahydrate)	(dodecahydrate)	(heptahydrate)		
<i>Potassium bicarbonate</i>	1.500	1.500	-	-	
<i>Potassium thiocyanate</i>	0.060	0.060	-	-	
<i>Citric acid</i>	0.030	0.030	-	-	
<i>Magnesium chloride hexahydrate</i>	-	-	0.061		
<i>Potassium carbonate hemihydrate</i>	-	-	0.603	-	
<i>Sodium phosphate monobasic monohydrate</i>	-	-	0.273	-	
<i>Sodium bicarbonate</i>	-	-	-	2.00	
<i>Submaxillary mucin</i>	-	-	1.00	-	
<i>Alpha-amylase</i>	-	-	2.00	2.00	
<i>Mucin gastric</i>				1.00	
<i>Properties</i>					
<i>pH</i>	6.5	7.4	6.8	-	6.8

One commercially available NRT formulation related to this study is the NiQuitin® strip by GSK (Figure 5.1). NiQuitin® strips are designed to manage smoking craving or as a step-down method by a fast disintegration of the film strip followed by the rapid release of NIC within 3 minutes of contact with the tongue (GlaxoSmithKline, 2016). The comparison of the optimized formulations from previous chapters, to a related dosage form will allow the

demonstration of the effectiveness of the proposed composite wafers and films as potential NRT.



Figure 5.1: NiQuitin® strips for NRT.

In this study, artificial saliva (Table 5.1; SS 3) was developed and used as a dissolution medium for swelling and *in vitro* release of NIC from composite wafers and films in comparison to phosphate buffer saline (PBS). Furthermore, NiQuitin® was used as a commercially available NRT formulation to compare with swelling and dissolution profiles of optimized wafers and films.

5.2 Materials and methods

5.2.1 Materials

NiQuitin® was purchased from a local pharmacy (Gillingham, Kent). Submaxillary mucin was purchased from Sigma-Aldrich (Dorset, UK). Calcium chloride dehydrate, sodium chloride, sodium phosphate dibasic, magnesium chloride hexahydrate, potassium carbonate hemihydrate, sodium phosphate monobasic monohydrate, sodium acetate, and trimethylamine were all purchased from Fisher Scientific (Loughborough, UK).

5.2.2 Selected optimized formulations

The following formulations in Table 5.2 were selected for the investigation of the effect of SS (pH 6.8; ionic strength, 0.04) on swelling and *in vitro* drug dissolution characteristics.

The selection was based on previous studies on composite wafers and films (Chapter 2) and NIC stabilization using MAS (Chapter 4).

Table 5.2: Optimized wafers and films selected for this study.

<i>NIC loaded formulations</i>	<i>HPMC</i> (% w/v)	<i>SA</i> (% w/v)	<i>GLY</i> (% w/v)	<i>MAS</i> (% w/v)	<i>NIC</i> (g)
<i>MAS wafer</i>	1.25	0.75	-	0.25	0.20
<i>MAS film</i>	1.25	0.75	2.00	0.25	0.20
<i>Non-MAS wafer</i>	1.25	0.75	-	-	0.20

5.2.3 Swelling studies using SS.

The swelling capacities of optimized wafers and films were performed using the protocol described in chapter two (section 2.2.10). However, SS (pH 6.8; ionic strength, 0.04) was used as the dissolution medium to replace phosphate buffered saline (PBS). The swelling index (%) obtained was compared to previous swelling index (%) of optimized wafers and films obtained using PBS (pH 6.8; ionic strength, 0.07) from chapter two (section 2.3.8) and chapter four (section 4.3.7).

5.2.4 *In vitro* mucoadhesion studies using SS

The *in vitro* mucoadhesion studies of optimized wafers and films were performed using the protocol described in chapter two (2.2.12). However, SS (pH 6.8; ionic strength, 0.04) was used as the equilibration medium to represent moist buccal mucosa. An aliquot (0.5ml) of SS was evenly spread on the surface of the set gelatine gel. The TA analysis using TA analyser was performed as described in chapter two (2.2.12). The maximum adhesive force (F_{max}), total work of adhesion (TWA) and cohesion was compared to previous mucoadhesive studies of optimized wafers and films obtained using PBS (pH 6.8; ionic strength, 0.07) from chapters two (2.3.10) and four (4.3.8).

5.2.5 *In vitro drug dissolution studies using SS.*

The *in vitro* drug dissolution characteristics of optimized wafers and films were performed with the protocol described in chapter two (section 2.2.15). However, SS (pH 6.8; ionic strength, 0.04) was used as the dissolution medium to replace PBS (pH 6.8; ionic strength, 0.07). The drug release data obtained was compared with previous data for optimized wafers and films from chapter two (section 2.3.12) and chapter four (section 4.3.10).

5.2.6 *Swelling profile of commercial strip (NiQuitin®) versus optimized wafers and films*

The swelling capacities of commercial NiQuitin® strip was determined using the protocol described in section 5.2.3. The results were compared to the swelling profiles of optimized wafers and films using SS (pH 6.8; ionic strength, 0.04).

5.2.7 *In vitro mucoadhesion of commercial strip (NiQuitin®) versus optimized wafers and films*

The *in vitro* mucoadhesion of the commercial NiQuitin® strip was determined using the protocol described in section 5.2.4. The results were compared to the adhesive properties (PAF, TWA and cohesiveness) of optimized wafers and films using SS (pH 6.8; ionic strength, 0.04).

5.2.8 *Drug content (% loading / recovery) of commercial strip (NiQuitin®) versus optimized wafers and films*

The content of NIC in commercial strip (NiQuitin®) was assayed using the protocol in chapter two (section 2.2.14). The results were compared to that obtained for optimized wafers and films.

5.2.9 *In vitro drug dissolution of commercial strip (NiQuitin®) versus optimized wafers and films*

In vitro drug dissolution of commercial strip (NiQuitin®) was performed with the protocol described in chapter two (section 2.2.15). The drug release profiles of commercial strip (NiQuitin®) was compared to the drug release profiles of optimized wafers and films.

5.2.10 *HPLC analysis*

NIC was analysed by HPLC using an Agilent 1200 HPLC instrument (Agilent Technologies, Cheshire, UK) with an auto sampler. The stationary phase used was a C-18 reverse-phase column, 4.6 x 250mm (Phenomenex HPLC column, Cheshire, UK). Trimethylamine, methanol and sodium acetate (88:12:0.5 v/v) were used as mobile phase with pH adjusted to 5.8 using glacial acetic acid, at a flow rate of 1ml/min and UV detection at 259nm (Pongjanyakul & Suksri, 2010). The retention time of NIC was detected at approximately 5.1 min. A calibration curve was plotted using standards with NIC concentration ranging from 20µg/ml to 200µg/ml ($R^2=0.9995$).

5.2.11 *Statistical analysis*

Statistical analysis was performed using student t-test and / or one-way ANOVA to compare the results. The results were expressed as mean \pm standard deviation and significant differences were determined at a level of $p < 0.05$.

5.2.12 *Comparison of release profiles using difference and similarity factors*

Moore and Flanner (1996) equations were adopted in the calculation of the difference (f_1) and the similarity (f_2) factors in comparing the release profiles of optimized wafers and films in SS and PBS as well as optimized wafers and films, and NiQuitin strips. The difference factor value (f_1) measures the percent error between two curves over all time points, while the similarity (f_2) factors value is a logarithmic transformation of the sum-squared error of

differences between the test T_j and reference products R_j over all time points (Moore & Flanner, 1996).

The difference (f_1) and the similarity (f_2) factors was calculated using the equations below:

$$f_1 = \frac{\sum_{j=1}^n |R_j - T_j|}{\sum_{j=1}^n R_j} \times 100 \quad (6)$$

$$f_2 = 50 \times \log\left\{1 + \left(\frac{1}{n}\right) \sum_{j=1}^n |R_j - T_j|^2\right\} \times 100 \quad (7)$$

The drug release profiles are considered similar if the f_1 values is close to 0 and the f_2 values is close to 100 or if f_1 is lower than 15 and f_2 value is higher than 50. According to FDA recommendations, a similarity is declared on two drug release profiles if f_2 is between 50 and 100 ((Fda, 1997b, c, Fda, 1997a).

5.3 Results

5.3.1 Swelling studies of optimized wafer using simulated saliva

Figure 5.2 shows the swelling profiles (% swelling index against time) of optimized wafers (MAS wafer and Non-MAS wafer) and films (MAS film) in SS and PBS media. Optimized wafers (i.e. MAS and Non-MAS wafers) in general demonstrated higher swelling index in both SS (maximum swelling index; $1178 \pm 221.60\%$) and PBS (maximum swelling index; $897 \pm 26.52\%$) formulation than optimized film formulation (PBS and SS maximum swelling index; $600 \pm 243.68\%$, $672 \pm 10.06\%$ respectively). There was a difference in the swelling profile of all optimized formulations (both wafers and films) between SS and PBS medium. MAS wafer showed a statistically significant difference ($p = 0.0003$) between SS and PBS swelling profiles, while MAS film and Non-MAS wafer showed no statistically significant

difference ($p = 0.9056$ and $p = 0.8003$ respectively). However, the structural integrity of MAS films and Non-MAS wafers was observed to decrease after 10mins.

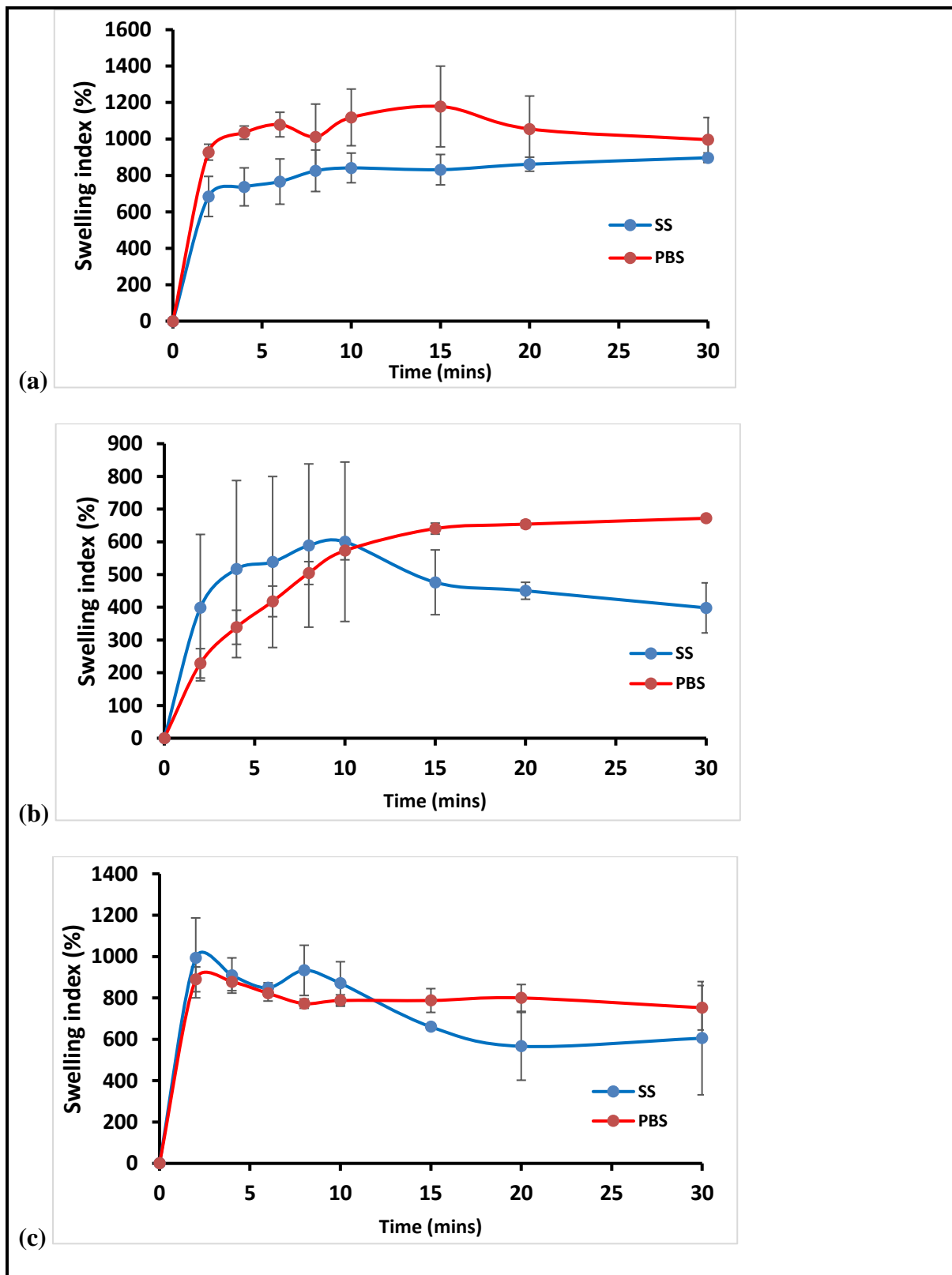


Figure 5.2: Swelling profiles (i.e. % swelling index against time) of (a) MAS wafer, (b) MAS film and (c) Non-MAS wafer in SS and PBS ($n = 3, \pm S.D.$).

5.3.2 *In vitro* mucoadhesion of optimized wafers and films using SS

Figure 5.3 showed the adhesive properties (PAF, TWA and cohesiveness) of optimized wafers and films.

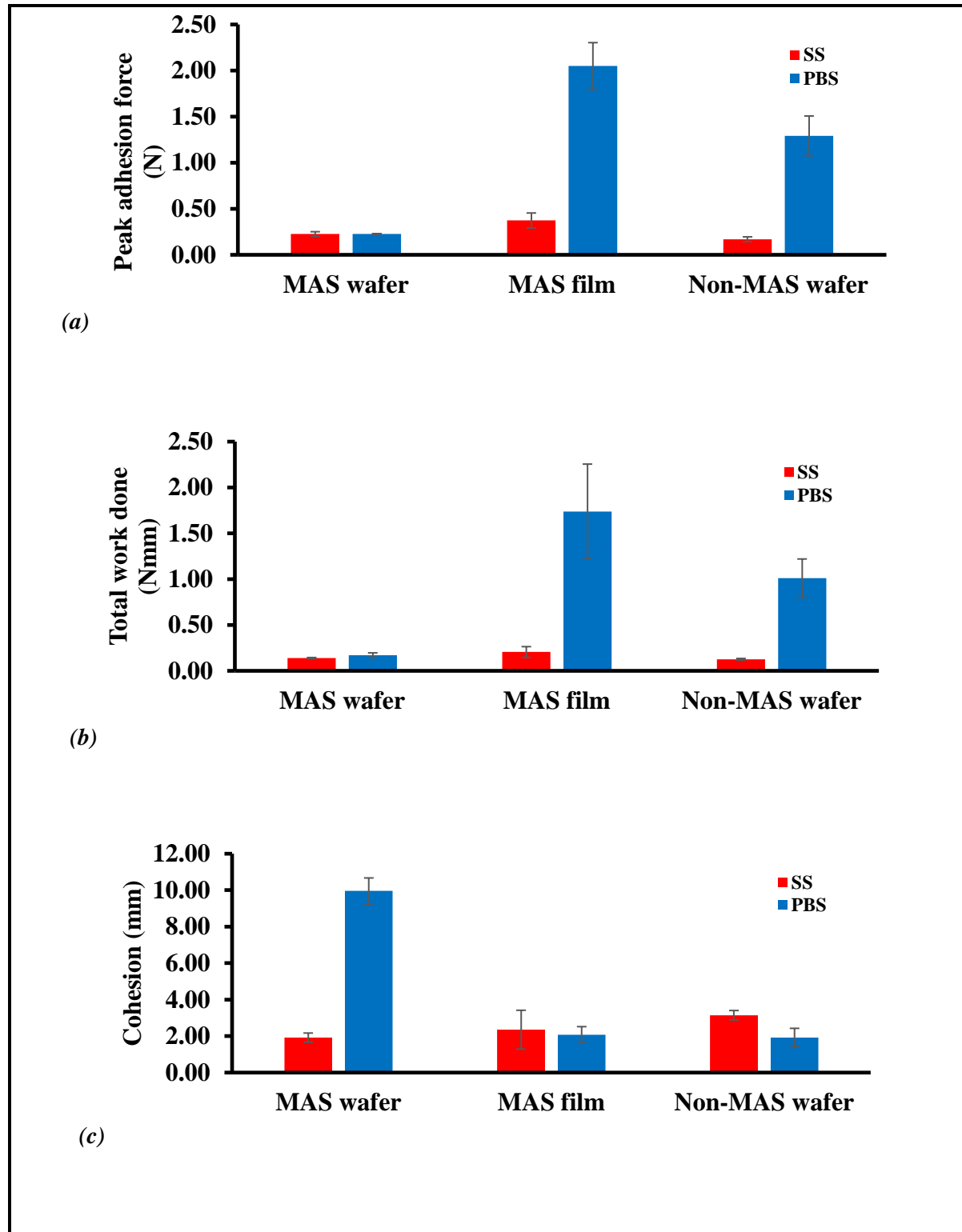


Figure 5.3: Mucoadhesive profiles of optimized wafers and films ($n = 3, \pm SD$): (a) peak adhesive force (N) (b) total work done (Nmm) (c) cohesiveness (mm).

The peak adhesion force (PAF) or F_{\max} of Optimized wafers and films (Figure 5.3a) were higher in PBS compared to SS. In PBS, the maximum value of $2.05 \pm 0.253\text{N}$ was observed in MAS film compared to MAS wafers and Non-MAS wafers with a PAF of $0.23 \pm 0.003\text{N}$ and $1.29 \pm 0.215\text{N}$ respectively. While in SS, the maximum value decreased but was also observed in MAS film ($0.37 \pm 0.081\text{N}$) compared to MAS wafers ($0.23 \pm 0.025\text{N}$) and Non-MAS wafers ($0.17 \pm 0.026\text{N}$). TWA and cohesiveness (Figure 5.3b and c) also follow similar trend as PAF with decrease in TWA and cohesiveness in SS. However, the maximum cohesiveness was observed in MAS wafers ($9.96 \pm 0.714\text{N}$) compared to MAS film ($2.07 \pm 0.452\text{N}$) and Non-MAS wafers ($1.92 \pm 0.510\text{N}$).

5.3.3 *In vitro drug dissolution of optimized wafers and films using SS*

Figure 5.4 demonstrates the drug release profiles of selected optimized formulations (i.e. MAS wafer, MAS film and Non-MAS wafer) in SS and PBS. The release profiles of selected optimized wafers (MAS wafer and Non-MAS wafer) showed a rapid drug release with about 80-100% of NIC released within 60mins in PBS (Figure 5.4(a) and (c)), while optimized film demonstrated a more sustained release profile as NIC was gradually released from the polymeric matrix in PBS (Figure 5.4(b)). NIC release from optimized wafers and films in SS on the other hand demonstrated a much slower NIC release profile for all optimized wafers and films (Figure 5.4(a), (b) and (c)). The NIC release from MAS wafer, MAS film and Non-MAS wafer in SS and PBS demonstrated a statistically significant difference ($p=0.0030$, $p=0.0015$ and $p=0.0054$ respectively).

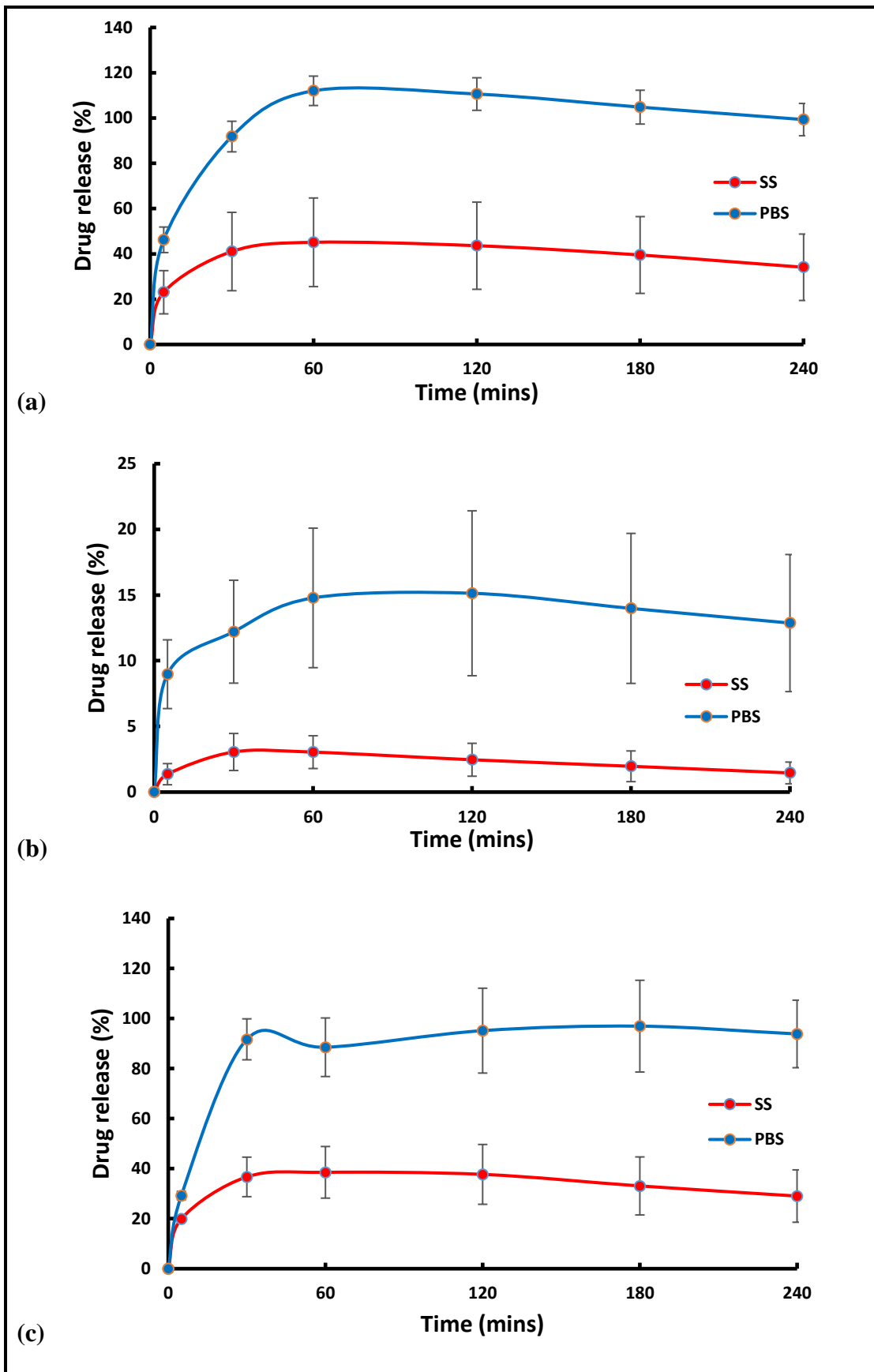


Figure 5.4: *in vitro* drug release profile ($n = 3, \pm S.D$) of NIC from optimized formulations; (a) MAS wafer (b) MAS film, and (c) Non-MAS wafer, in SS and PBS.

5.3.4 Drug release profiles comparison

The drug release profiles were compared using f_1 and f_2 values (i.e. similarity or difference respectively) relative to a selected reference formulation, are shown in Table 5.3 below.

Table 5.3: Similarity and difference factors for drug release profiles of optimized wafers and film (a) between optimized wafers and film in SS and (b) between optimized wafers and film in PBS.

(a)

<i>Optimized formulations (SS)</i>	<i>Similarity factor (f_2)</i>	<i>Difference factor (f_1)</i>
<i>MAS wafer</i>	22.07	1597.71
<i>MAS film</i>	Reference	Reference
<i>Non-MAS wafer</i>	25.53	1362.02

(c)

<i>Optimized formulations (PBS)</i>	<i>Similarity factor (f_2)</i>	<i>Difference factor (f_1)</i>
<i>MAS wafer</i>	3.87	624.56
<i>MAS film</i>	Reference	Reference
<i>Non-MAS wafer</i>	6.82	535.57

5.3.5 *Drug release kinetics in SS and PBS*

The release parameters of optimized wafers and films have been summarised in Tables 5.4 and 5.5 respectively. Based on the R^2 values, NIC released from optimized wafers and films best fits the Korsmeyer-Peppas compared to other models. The n values of Korsmeyer-Peppas equation in optimized wafers and films using PBS ranged from 0.362 - 0.484, which is less than 0.45 in MAS wafer and 0.50 in film but greater than 0.45 in Non-MAS wafer. While the n values of Korsmeyer-Peppas equation in optimized wafers and films, using SS range from 0.218 - 0.281, which is also less than 0.45 and 0.50 respectively.

Table 5.4: Release parameters of optimized wafers and films using PBS developed by fitting experimental drug dissolution (release) data to different kinetic equations.

<i>Media</i>	<i>Zero-order</i>		<i>First order</i>		<i>Higuchi</i>		<i>Hixson-Crowell</i>		<i>Korsmeyer-Peppas</i>		
	R^2	K_o (min^{-1})	R^2	K_I (min^{-1})	R^2	K_H ($\text{min}^{-1/2}$)	R^2	K_{HC} ($\text{min}^{-1/3}$)	R^2	n	K_P (% min^{-n})
<i>MAS wafer</i>	0.928	1.180	0.876	0.015	0.986	12.090	0.894	0.022	0.997	0.362	26.044
<i>MAS film</i>	0.753	0.050	0.718	0.004	0.898	0.734	0.730	0.003	0.971	0.174	6.830
<i>Non-MAS wafer</i>	0.661	1.039	0.678	0.019	0.797	11.34	0.673	0.024	0.912	0.484	14.256

Table 5.5: Release parameters of optimized wafers and films, and NiQuitin® using SS developed by fitting experimental drug dissolution (release) data to different kinetic equations.

<i>Media</i>	<i>Zero-order</i>		<i>First order</i>		<i>Higuchi</i>		<i>Hixson-Crowell</i>		<i>Korsmeyer-Peppas</i>		
	R^2	K_o (min^{-1})	R^2	K_I (min^{-1})	R^2	K_H ($\text{min}^{-1/2}$)	R^2	K_{HC} ($\text{min}^{-1/3}$)	R^2	n	K_P (% min^{-n})
<i>MAS wafer</i>	0.847	0.392	0.815	0.012	0.940	4.109	0.825	0.013	0.980	0.280	14.928
<i>MAS film</i>	0.134	0.006	0.196	0.003	0.299	0.118	0.175	0.001	0.611	0.218	1.109
<i>Non-MAS wafer</i>	0.782	0.330	0.762	0.012	0.894	3.503	0.768	0.012	0.958	0.281	12.977
<i>NiQuitin®</i>	0.565	0.1812	0.8396	0.00737	0.9498	4.6899	0.8471	0.0097	0.988	0.173	37.025

5.3.6 Swelling profile of commercial strip (NiQuitin®) versus optimized wafers and films

The swelling profile of NiQuitin® in SS was demonstrated in Figure 5.5. The swelling index demonstrated a maximum swelling index of $18118.84 \pm 943.86\%$ at 6mins but started to decline sharply after the maximum swelling index. NiQuitin® showed the highest swelling at maximum swelling in comparison to the optimized wafers and films. However, NiQuitin® formulation decrease rapidly after reaching its maximum swelling index and hence completely eroded within 20mins.

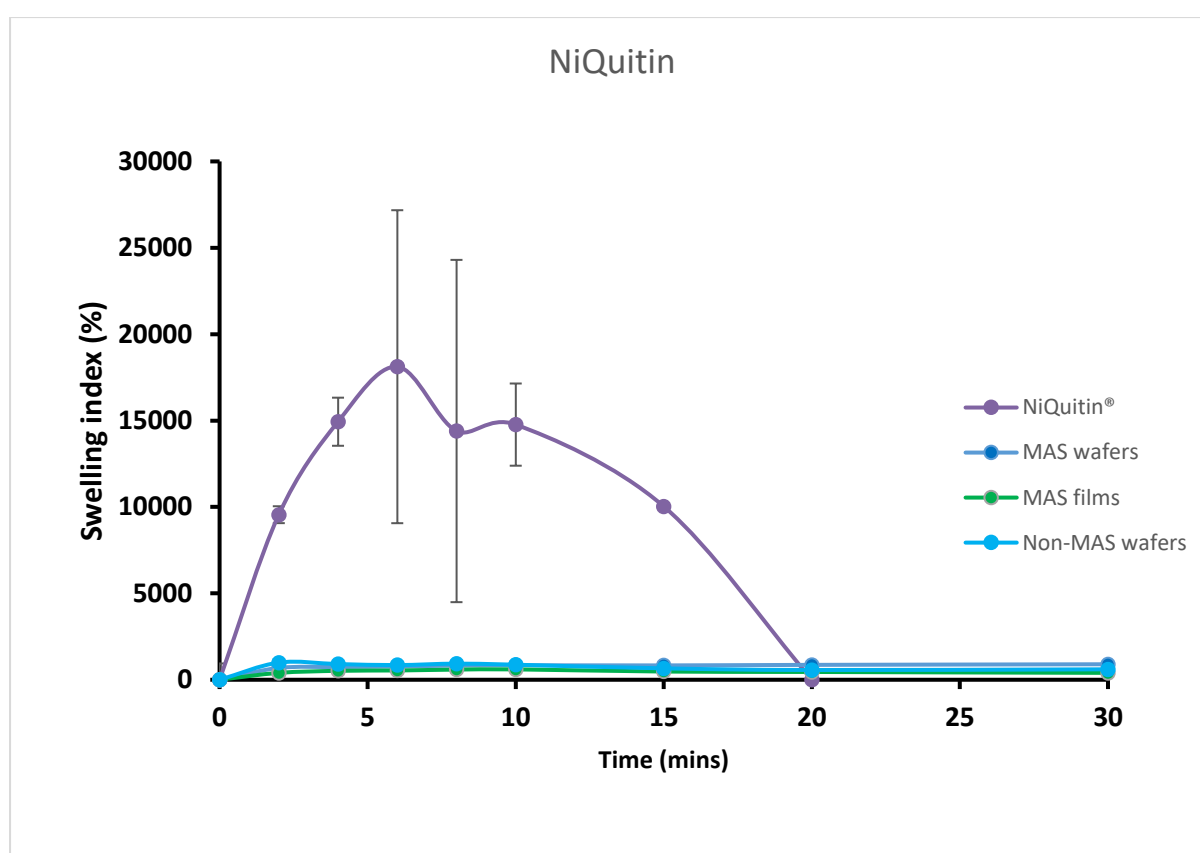


Figure 5.5: Swelling profile (i.e. % swelling index against time) ($n = 3, \pm S.D$) of NiQuitin®, optimized wafers and films.

5.3.7 *In vitro* mucoadhesion of commercial strip (NiQuitin®) versus optimized wafers and films

Figure 5.6 demonstrated the mucoadhesion profile of NiQuitin® and optimized wafers and films using SS.

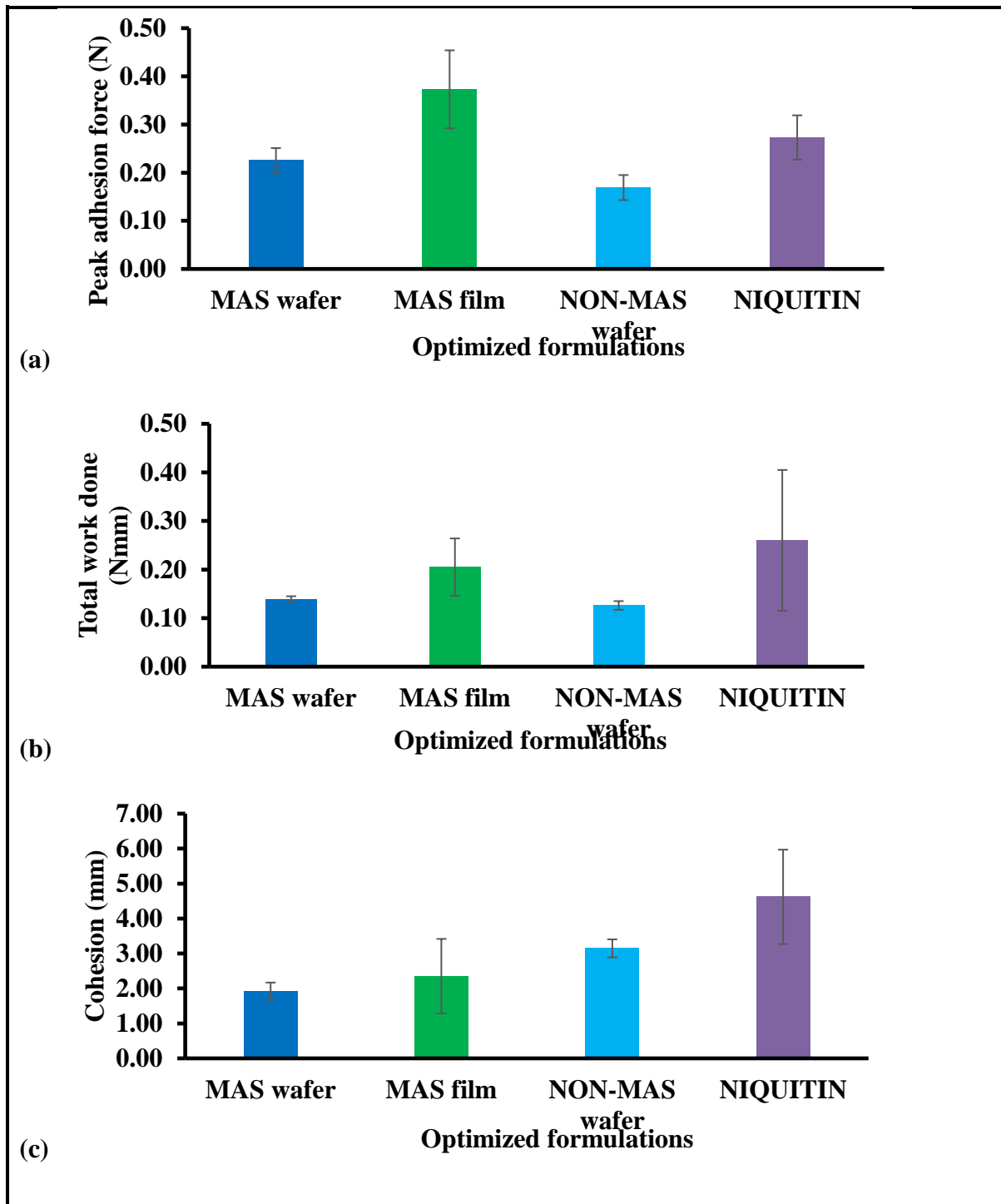


Figure 5.6: Mucoadhesive profiles of NiQuitin® and optimized wafers and films ($n = 3$, \pm SD): (a) peak adhesive force (N) (b) total work done (Nmm) (c) cohesiveness (mm).

The highest PAF value was demonstrated in MAS films ($0.37 \pm 0.081N$) in comparison with NiQuitin® ($0.27 \pm 0.046N$) and wafers (i.e. MAS and Non-MAS wafers; $0.23 \pm 0.025N$ and $0.17 \pm 0.026N$ respectively). However, NiQuitin® strips showed the maximum value in TWA and cohesion with $0.26 \pm 0.145Nmm$ and $4.62 \pm 1.35mm$ respectively, compared the optimized wafers and film formulation.

5.3.8 Drug content (% loading / recovery) of commercial strip (NiQuitin®) versus optimized wafers and films

Figure 5.7 demonstrates the percentage NIC in NiQuitin® and optimized wafers and films. NiQuitin® demonstrated the lowest NIC content (%) with 41 ± 5.10 % NIC. MAS wafer and film showed the highest NIC content with $93 \pm 0.40\%$ and $92 \pm 11.82\%$ of NIC respectively. MAS was also confirmed to have a significant effect on NIC content as well as the formulation technique as Non-MAS film demonstrated low NIC content in previous chapter (chapter two, section 2.3.11).

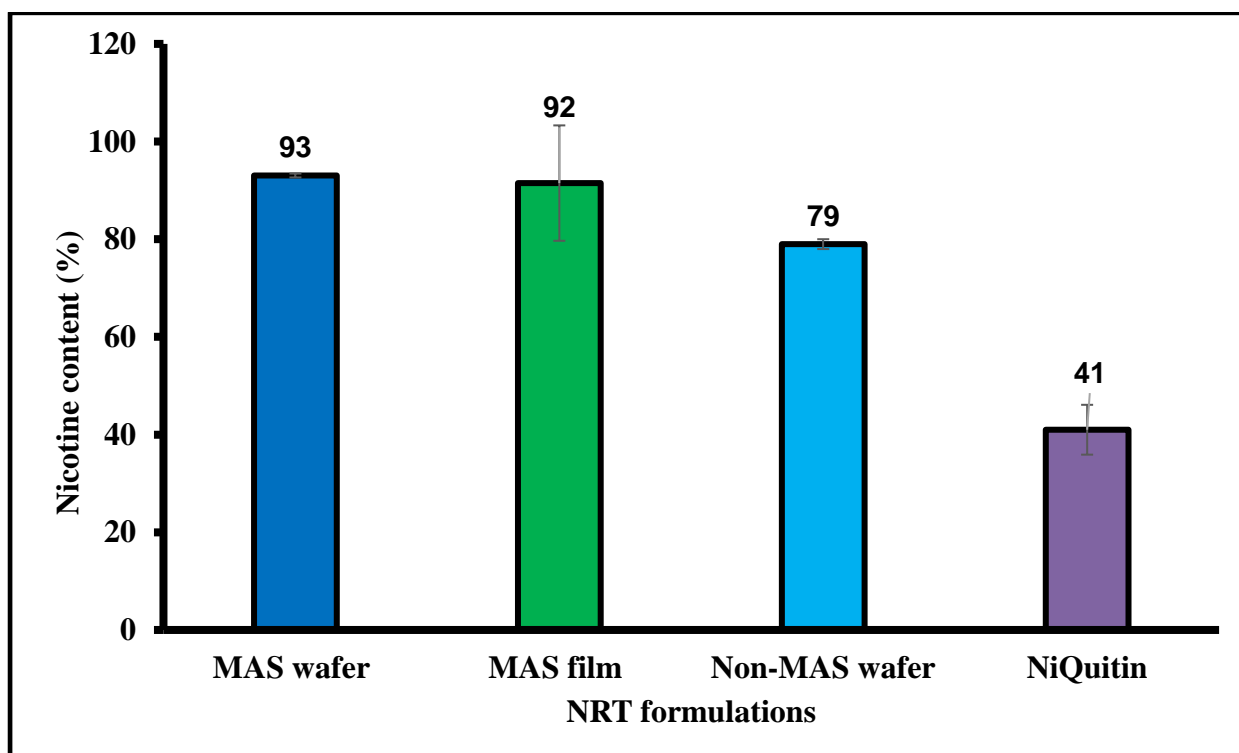


Figure 5.7: NIC content (%) in NiQuitin® and, optimized wafers and films ($n = 3, \pm SD$)

5.3.9 *In vitro* drug dissolution of commercial strip (NiQuitin®) versus optimized wafers and films in simulated saliva

Figure 5.8 demonstrates the *in vitro* drug release profile of NiQuitin® commercial strip and optimized formulations (i.e. MAS wafer, MAS film and Non-MAS wafer) in SS. The release profile of NiQuitin® showed a more rapid drug release from the polymer matrix into SS than optimized formulations. The *in vitro* release profiles of NiQuitin® and optimized wafers and films showed a statistically significant difference ($p = 0.00006$). However, NiQuitin® strips and MAS film demonstrated similarity in their release profile as showed in similarity and difference factor; $f_2 = 10.10$ and $f_1 = 96.54$ which is <15 and between $50 - 100$ respectively. While MAS wafers and film did not demonstrate similarity as f_2 and f_1 values were >15 and <50 respectively.

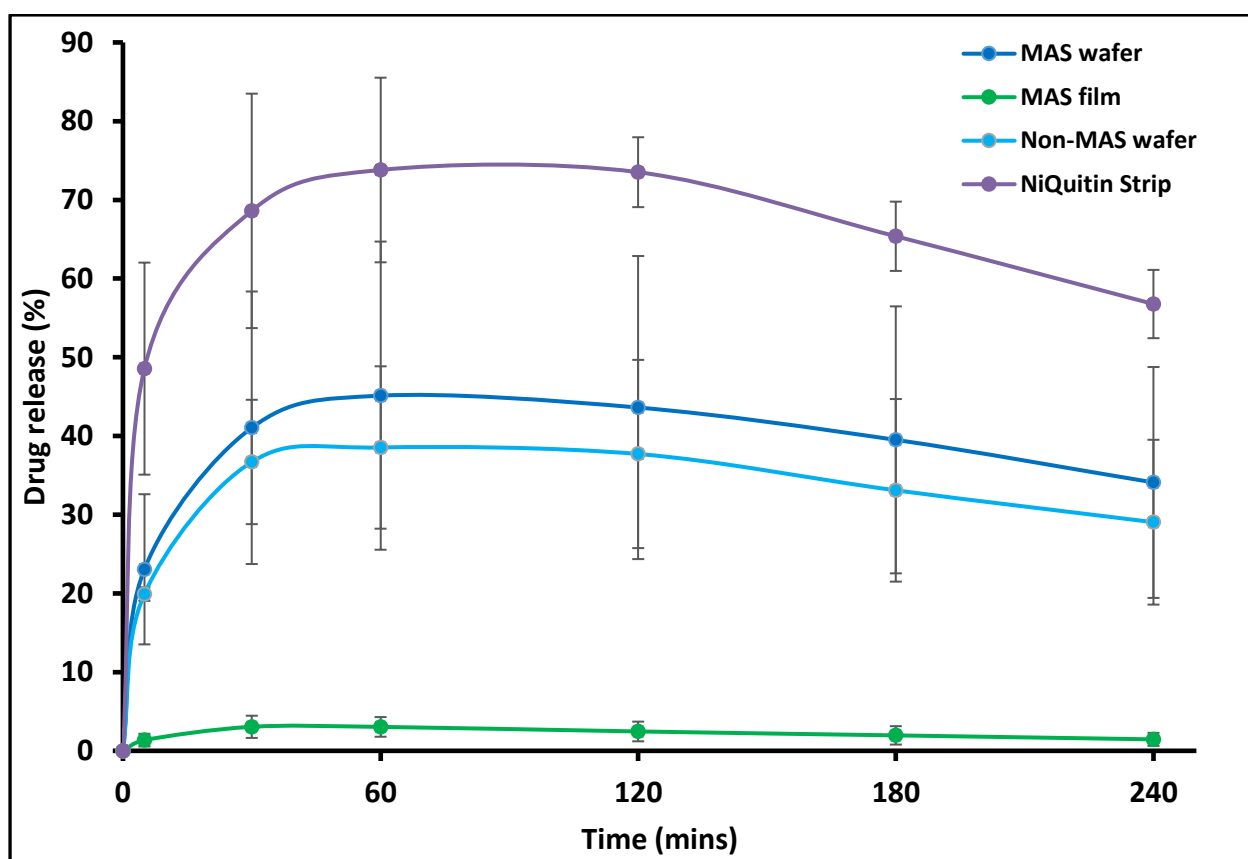


Figure 5.8: *In vitro* drug release profile of NiQuitin® strip and optimized wafers and films ($n = 3, \pm SD$).

Table 5.6: Similarity (f_2) and difference factor (f_1) of optimized wafers and films compared to NiQuitin® strips.

<i>Optimized formulations</i>	<i>Similarity factor (f_2)</i>	<i>Difference factor (f_1)</i>
<i>MAS wafer</i>	28.58	41.43
<i>MAS film</i>	10.10	96.54
<i>Non-MAS wafer</i>	24.68	49.56
<i>NiQuitin®</i>	Reference	Reference

5.3.10 Drug release kinetics of commercial strip (NiQuitin®) versus optimized wafers and films

The kinetic release parameters of NiQuitin® have been summarised in

Table 5.5. Based on the R^2 values (0.988), NIC released from NiQuitin® best fits the Korsmeyer-Peppas compared to other models. NiQuitin® demonstrated the highest release kinetics with a K_p value of $37.025\% \text{ min}^{-0.173}$ compared to MAS wafers, MAS film and Non-MAS wafer with a K_p values of $14.928\% \text{ min}^{-0.280}$, $1.109\% \text{ min}^{-0.218}$ and $12.977\% \text{ min}^{-0.281}$ respectively. The n value of Korsmeyer-Pappas equation in NiQuitin® was less than 0.50 (0.1733) which was similar to the n values of optimized formulation.

5.4 Discussion

The design of a buccal drug delivery system involves the application of the drug delivery system to the site of action (in this case the buccal mucosa) and the delivery of the drug either rapidly or in a controlled manner over a period. The immediate microenvironment of the buccal mucosa region plays a vital role in modulating the drug release with diffusion, swelling and erosion as the mechanism of a controlled release formulation (He et al., 2016, Siepmann & Peppas, 2012). Human saliva therefore plays a major role in the release mechanism of a buccal drug delivery system and it is vital in *in vitro* release studies to consider the components i.e. presence of electrolytes such as sodium, calcium, potassium, chloride, phosphate, bicarbonate, magnesium. The swelling results in section 5.3.1 demonstrated a higher swelling index in PBS than SS especially for MAS wafer (with a statistically significant difference). This implies that the presence of electrolytes and predominate negatively charged mucin increases ionic interaction, which affected the swelling capacity of both optimized wafers and films. The diffusion of PBS into MAS wafer can be attributed to electro-osmosis i.e. generation of an electric field by mobile ions in MAS (silicate, magnesium and aluminium) with accelerated flow, which induces high diffusivity of water molecules associated to these ions. This could also explain why MAS wafers demonstrated higher swelling capacity than Non-MAS wafers. However, the presence of SS electrolytes reduced swelling capacity of optimized formulations by creating an ionic pressure gradient. This excess pressure was introduced with the difference in concentrations of ions in formulation and in SS, which decreases the diffusion rate of SS into the formulations (Drozdov & deClaville Christiansen, 2015). Furthermore, the ions (although lower in ionic strength (0.04) than PBS) and mucin present in SS competes for available ionic interaction with SA and MAS in optimized MAS wafers and films and SA in optimized Non MAS wafer hence reducing the rate of hydration (Khan et al., 2016). The general increase in hydration and swelling

capacity in optimized wafers can be attributed to the pore size which increases the rate of diffusion of solution into the formulation as described in previous chapter (chapter two and four). The mucoadhesion of optimized wafers and films depends on mechanisms of interaction with the mucosa surface such as adsorption, wetting, diffusion and mechanical theories (Rahamatullah Shaikh et al., 2011). The decrease in mucoadhesion with SS suggested that the presence of higher ionic interactions in SS components such as sodium, calcium, potassium, chloride, phosphate, bicarbonate, magnesium and mucin which could potentially interact with SA and MAS negatively charged group. This limited the ionic interaction as well as hydrogen bonding with the mucin in the mucoadhesive model system used as the ions and mucin present in SS competes for bonding site on optimized wafers and film polymeric metrics (Grabovac et al., 2005). The high mucoadhesion in optimized films compared to optimized wafers could be attributed to adhesion based on liquid to solid affinity (wetting theory), of which film's large adhesive surface area played a role in adhesion compared to optimized wafers with lower adhesive surface area and lesser contact because of the presence of sponge-like pores. NiQuitin® strips also uses similar principle as MAS films in mucoadhesion since it is basically a film, however the ionic effect from the high concentration of charged components in SS is minimal in mucoadhesion with only methyl acrylic acid – ethyl acrylate copolymer (anionic) in NiQuitin® strips as a competing site for ionic interaction of SS components compared to MAS film with both SA (anionic polymer) and MAS (amphoteric clay). In addition, the high hydration and swelling properties of methyl acrylic acid – ethyl acrylate copolymer in NiQuitin® improved the diffusion properties which encouraged chain entanglement (diffusion theory of mucoadhesion).

The *in vitro* drug release from optimized wafers and films depends heavily on the hydration which leads to swelling of the polymeric dosage form and eventual drug diffusion from the swollen matrix (Siepmann & Peppas, 2012). As described above, the presence of electrolyte

and mucin in SS caused a decrease in the swelling capacity of optimized formulation. These components create an ionic pressure between the high concentration of charged components such as mucin and electrolyte in the SS and the ions in the formulation. The results of the *in vitro* drug release studies also demonstrated a similar trend with a decrease in the release profile of optimized wafers and films in SS as compared to the release profile of PBS. This implies that the presence of electrolyte and mucin results in the slower release rate over time in optimized formulations, hence avoiding dumping of NIC in the buccal mucosa (Khan et al., 2016). The drug release mechanism of optimized wafers and films did not change with the presence of electrolytes and mucin in SS. The drug release kinetics of optimized wafers and films fits into Korsmeyer-Peppas model which is based on diffusion from a swollen polymeric system. The NIC release kinetics of optimized wafers and film was shown to be higher in PBS than in SS. The decrease in release kinetics of optimized wafers and films in SS can again be attributed to the presence of high concentration of ions present in SS which influenced hydration and swelling by creating an ionic pressure which decreases the process of diffusion and hence decreasing the release kinetics. However, the release exponents of MAS formulations (MAS wafer and MAS film) in PBS as well as all optimized formulations (MAS wafer, MAS film and Non-MAS wafer) in SS demonstrated a value less than 0.45 for wafers (cylinders) and 0.50 for films which was outside the limits of Korsmeyer-Peppas model. This also highlights the limitations of the Korsmeyer-Peppas model in the understanding of drug release mechanisms (Shoaib et al., 2006). This release mechanism of optimized wafers and films was therefore not influenced by the presence of higher concentration of ions in comparison to PBS as the release mechanism remained the same.

NiQuitin® strip is composed mainly of anionic copolymers i.e. methacrylic acid – ethyl acrylate copolymer used in the formulation for rapid release of NIC. These copolymers contribute to the fast dissolution properties of NiQuitin formulation and the rapid release of

NIC upon contact with the saliva as described the formulation instruction manual. Other components of NiQuitin include triethyl citrate used as a plasticizer, peppermint flavour and sucralose for taste masking and sodium hydrogen carbonate used as a buffer.

The swelling profile (% swelling index against time) observed in NiQuitin® strips demonstrated in Figure 5.4 showed that the maximum swelling profile of NiQuitin® strips was attained within 6 min of contact with the SS medium. The rapid swelling of NiQuitin can be attributed to its composite polymer composition i.e. methyl acrylic acid – ethyl acrylate copolymer. Methyl acrylic acid – ethyl acrylate is an anionic based copolymer that respond to environmental pH. Anionic hydrogels are usually ionized at higher pH above its pK_a and un-ionized below its pK_a . The rapid dissolving process of the copolymer used in NiQuitin® strips was activated with an increase in pH upon contact with the SS solution by the neutralizing base (sodium hydrogen carbonate) which then creates an osmotic swelling force in the copolymer network by the presence of hydroxyl ions (Gupta et al., 2002). The rapid ingress of SS into the polymeric matrix results in the eventual rapid erosion of the polymer matrix at its optimum swelling capacity as observed in NiQuitin swelling profile (Figure 5.4).

One of the major challenges of dealing with NIC free base is its volatility. NIC readily evaporates in an unstable formulation. Based on the conditions used in the analysis of optimised wafers and film formulation, the low NIC content in NiQuitin® strips can be attributed to loss of NIC over time. This suggests that the hydrogen bonding between the copolymer and NIC was not stable enough to stabilise NIC within the NiQuitin® strips. The high NIC content in MAS formulation can be attributed to strong ionic interaction between the negatively charged silicate and the partially positively charged NIC in combination with hydrogen bonding between NIC and the composite polymers in the formulation hence stabilising NIC in the formulation.

NiQuitin® strips also showed a rapid release of NIC in less than 30min in comparison with optimized wafers and films. This can be attributed to the rapid swelling of the strips in response to environmental pH triggered by the neutralising base. However, the decrease in swelling rate after the maximum swelling point at 6mins to approximately 30mins can be attributed to low concentration (8mL of medium in receiving chamber) of sodium hydrogen carbonate to impact on osmotic swelling force with a high ionic strength of the SS. The limitations of using Franz diffusion cell to assess the release of NIC from NiQuitin® is that the formulation is designed to be placed on the tongue and then pressed by the roof of the mouth according to the patient information leaflet. This reduces the drug release time as the pressure applied on the strip by the roof of the mouth increases the disintegration of the polymer matrix and hence result in higher dissolution rate compared to the experimental results obtained in this research. The Franz diffusion cell used in this project is limited in modelling the pressure applied on the NiQuitin® by the tongue and the roof of the mouth but did demonstrate the dissolution of NiQuitin® upon contact with PBS and SS. The determination of similarity (f_2) and difference (f_1) factor using FDA definition of similarity between two dissolution profiles, similarity was demonstrated between NiQuitin® and MAS films with f_2 similarity factor >15 and between f_1 difference factor 50 – 100. However, the optimized wafers demonstrated a difference in dissolution with NiQuitin® as the optimized wafers (MAS wafers and Non-MAS wafers) showed f_2 similarity factor <15 and f_1 difference factor <50 . Furthermore, the drug release mechanism of NiQuitin® also fits the Korsmeyer-Peppas model but showed similar challenge of a n -value less than 0.50 which was outside the limitations of the Korsmeyer-Peppas models. The fit with Korsmeyer-Peppas showed that mechanism by which NIC is released from NiQuitin is based on diffusion from a swollen polymeric system (Dash et al., 2010). However, in comparison with optimized wafers and films in terms of release kinetics, NiQuitin® demonstrated a higher release kinetics than optimized wafers and films. Since the release

mechanism is controlled by hydration and swelling, the high release kinetics can be related to the swelling profile of NiQuitin® strips with a rapid hydration, swelling and dissolution properties. In general, although NiQuitin® strips possess a higher mucoadhesive, hydration and swelling, and rapid release properties, however, it could result in NIC dumping in the saliva which will result to swallowing.

5.5 Conclusion

Selected optimized wafers and films were analysed for swelling and NIC release properties using SS and PBS as medium to demonstrate the effect of the constituents of SS such as electrolytes and mucin, on the optimized formulations. The optimized formulations demonstrated reduced swelling properties in SS which is attributed to the ionic pressure created by the high concentration of ion and mucin present in simulated saliva which can potentially affect the release profile of the formulations in the human buccal mucosa. The drug release profile of the optimized formulations demonstrated a slow release profile within 30 mins as predicted by the swelling profile. The swelling profile of NiQuitin strips demonstrated a rapid swelling within 6mins and also a higher swelling compared to optimized wafers and films but eroded rapidly after reaching its optimum swelling capacity. NIC content in NiQuitin® strips also demonstrated the lowest content of NIC in comparison to optimized wafers and films whilst optimized wafers and films demonstrated a higher NIC content attributed to the ionic interaction between the silicate and NIC in combination with hydrogen bond of NIC with the composite polymers in stabilising NIC in the formulations. Furthermore, the rapid swelling rate of NiQuitin® strips was demonstrated in the release studies as NIC showed a rapid release from the polymer matrix (Korsmeyer-Peppas model) in comparison with optimized wafers and films swelling and release. However, the swallowing effect in the mouth poses a challenge in the rapid release of NIC in the tongue. In conclusion, optimized wafer and film showed better optimized properties, better stability of NIC with slow release suitable for the buccal mucosa.

CHAPTER 6: *EX VIVO* PERMEATION AND TISSUE VIABILITY STUDIES OF OPTIMIZED WAFERS AND FILM USING PORCINE BUCCAL TISSUE AND ENGINEERED HUMAN BUCCAL TISSUE (EPIORAL™).

6.1 Introduction

The successful delivery of a drug to the systemic circulation relies on the diffusion of the target drug across the oral mucosa. In comparison to GI mucosa and transdermal routes, the buccal mucosa demonstrates better permeability owing to its anatomical and physiological properties as discussed in chapter 1, sections 1.4.1 and 1.4.2. The degree of keratinization of cells in the buccal mucosa membrane plays a vital role in terms of its higher permeability compared to the skin epidermis, since human buccal mucosa is composed mostly of non-keratinized cells (Gimeno et al., 2014, Patel et al., 2011).

The ready permeability of NIC across the buccal mucosa has been attributed to its high solubility in both water and organic solvents (Log P of 1.17) and its low molecular weight (162.2g/mol) (Hansch et al., 1995, Zorin et al., 1999). As reviewed in chapter 1, section 1.6, the permeability of NIC species depends on pH, however, all species of nicotine can readily permeate mucosal membranes including the buccal mucosa with higher permeation for un-ionized species than ionized species (Nair et al., 1997). NIC is considered a toxic substance with a lethal dose of 30-60mg upon ingestion and causes poisoning with skin contact as a result of its high permeability leading to vomiting, illness and other symptoms (Mayer, 2014, Zorin et al., 1999).

Porcine buccal mucosa has been commonly used as a suitable model membrane for buccal delivery systems as its properties such as morphology and permeation are comparable to the human buccal mucosa in terms of its non-keratinized cells and enzymatic activities (Gimeno et al., 2014). Several reported studies involving buccal permeation have utilized porcine buccal mucosa as a model for permeation of drugs such as naratriptan (Sattar et al.,

2015), NIC (Marxen et al., 2016), buspirone (Birudaraj et al., 2005), omeprazole (Figueiras et al., 2009) and doxepin (Gimeno et al., 2014). Other buccal mucosa models such as sheep buccal mucosa have been reported in permeation studies (Kumar et al., 2011, S Boateng et al., 2014).

EpiOral™ buccal tissue comprises typical human derived epithelial cells developed by MatTeK (MatTek, Ashland, MA, USA) and has recently been engineered and commercialized for a better controlled permeation studies due to uniform and reproducible *in vivo*-like morphology and growth characteristics (www.mattek.com [Accessed 17 October 2016]). The multi-layered tissue is made up of a structured basal layer and several non-cornified layers similar to the human buccal tissue and cultured in a serum free medium on the surface of collagen-coated inserts to form a three dimensional differentiated tissue. Several researchers have utilized EpiOral™ buccal tissue as a model in permeation studies (Koschier et al., 2011, Giovino et al., 2013, Boateng et al., 2014).

The aim of this chapter was to investigate the permeation of NIC released from wafers and films using porcine buccal tissue and a human equivalent EpiOral™ buccal tissue. Furthermore, the tissue viability of the human equivalent EpiOral™ buccal tissue after coming in contact with the NIC loaded wafers and films, was investigated using MTT assay.

6.2 Materials and methods

6.2.1 Materials

The materials used in this study included: EpiOral™ buccal tissue kit (ORL-200) purchased from MatTek (Ashland MA, USA), PBS tablets (pH 7.4), MTT (3-(4,5-Dimethylthiazol-2-yl)-2,5-Diphenyltetrazolium Bromide), Krebs-Ringer Bicarbonate buffer and Dimethyl sulfoxide (DMSO) were all purchased from Sigma-Aldrich (Dorset, UK).

6.2.2 Optimized formulations for permeation studies

The following formulations in Table 6.1 were investigated for NIC permeation across porcine and EpiOral™ buccal tissues. Non-treated EpiOral™ tissue was used as a negative control in MTT assay for tissue integrity studies.

Table 6.1: Optimized formulations selected for permeation studies.

<i>NIC loaded formulations</i>	<i>HPMC</i> (% w/v)	<i>SA</i> (% w/v)	<i>GLY</i> (% w/v)	<i>MAS</i> (% w/v)	<i>NIC</i> (g)
<i>MAS wafer</i>	1.25	0.75	-	0.25	0.20
<i>MAS film</i>	1.25	0.75	2.00	0.25	0.20
<i>Non-MAS wafer</i>	1.25	0.75	-	-	0.20

6.2.3 Ex vivo buccal permeation studies (Porcine buccal tissue)

Ex vivo buccal permeation studies of NIC released from optimized wafers (MAS and Non-MAS wafers) and films (MAS films) were carried out using Franz diffusion cell with a diffusional surface area of 0.6cm². Fresh porcine buccal tissue was obtained from a local slaughterhouse and was immediately stored in a container containing Krebs-Ringer bicarbonate buffer (modified with sodium bicarbonate) and used within 2hrs of slaughter (Boateng et al., 2014, Patel et al., 2007). The tissues were trimmed with a scalpel to a thickness of 1-3mm and washed with physiological PBS (pH 6.8) at 37°C.

Membranes were mounted on a Franz diffusion cell between the donor and the receiver (8mL of 0.01 M PBS; pH 6.8) compartments with the epithelial side facing the donor compartment. The receiver compartment was allowed to equilibrate at 37°C for 30mins while stirring at 200-400rpm. After the equilibration period, 0.5mL of 0.01M PBS was poured into the donor compartment and 20-30mg of optimized wafers or films was placed in the donor compartment with the mucoadhesive layer in contact with the epithelial surface. The donor and the receiver chambers were held tight with a cell clamp and sealed with parafilm to limit evaporation. Samples (0.5mL) were collected at time intervals from the port of the receiver compartment and replaced with the same amount of PBS in order to maintain a steady volume for 4hrs. The collected samples were analysed using HPLC. Permeation flux (J) were determined using equation 1.

$$J = \frac{dQ}{dt} \cdot \frac{1}{A} \quad (1)$$

J = steady state flux

dQ/dt = amount of drug permeated

A = effective diffusion area

6.2.4 *In vitro buccal permeation studies (EpiOral™ buccal tissue)*

EpiOral™ assay medium (MatTek, Ashland MA, USA) was pre warmed to 37°C for 30 mins. Using a sterile technique, 0.3mL/well of EpiOral™ assay medium were pipetted into 4 wells of a 24 well plate and labelled 1hr equilibration. The remaining wells were labelled as 0.5, 1, 2, 3 and 4 hrs. The EpiOral™ samples were transferred into the 1 hr equilibration wells containing the pre-warmed assay medium and placed in a 37°C, 5% CO₂ incubator for 1hr. After 1 hr equilibration, the EpiOral™ was transferred into the 0.5 hr labelled well, treated with 0.5mL donor solution (0.01M PBS) into which 15mg of wafers and/or film was added with the mucoadhesive layer in contact with the apical surface of the EpiOral™ buccal tissue

and returned to the incubator. After the elapsed time point (0.5hrs) the tissue was moved to the next time point (i.e. 1, 2, 3 and 4hrs) till the total elapsed time (4hrs). 50 μ L of the receiver fluid was collected at predetermined time intervals and transferred to a vial for HPLC analysis. Permeation flux (J) were determined using equation 1.

6.2.5 *Permeation correlation between buccal permeation using Porcine and EpiOral™ buccal tissues.*

The permeability of NIC across the porcine buccal tissue and EpiOral™ engineered human buccal tissue epithelium was further investigated to determine the correlation using a correlation curve of EpiOral™ cumulative permeation against the porcine cumulative permeation curve of wafers and film. Linear regression (R^2) obtained from the curve of film and wafers was compared.

6.2.6 *Tissue viability (MTT assay) of EpiOral tissues after permeation studies*

Following the permeation studies using EpiOral™ buccal tissues, the tissue inserts used were transferred into a 24 well plate filled with MTT solution (0.3mL) dissolved in PBS (5mg/mL) and incubated for 3hrs. After incubation, the MTT was gently extracted from all well plates and the cultures were extracted in 2mL of DMSO for 2hrs with gentle shaking (120rpm). The aliquots ($n = 3$) of the extracts (200 μ L) were placed in a 96 well plate and the absorbance of the extracted (purple coloured) formazan was determined using a Multiskan EX microplate photometer at 540nm.

The viable cells had the greatest amount of MTT reduction and hence the highest absorbance values. Relative cell viability was calculated for each tissue used during permeation as a percentage of the mean negative control tissues ($n = 3$). The average percentage of optimized wafers and films was plotted using the negative non-treated control which is a 100% viable tissue.

6.3 Results

6.3.1 *Ex vivo buccal permeation studies (Porcine buccal tissue)*

The cumulative permeation curve of optimized wafers (MAS and Non-MAS wafers) and films (MAS films) using porcine buccal tissues are shown in figure 6.1. The permeation flux (J) of the formulations are shown in Table 6.2. NIC permeation in optimized wafers and films demonstrated a high cumulative permeation above $100\mu\text{g}/\text{cm}^2$. Optimized wafers (MAS and Non-MAS wafers) in general demonstrated higher cumulative permeation than optimized film formulation (MAS films).

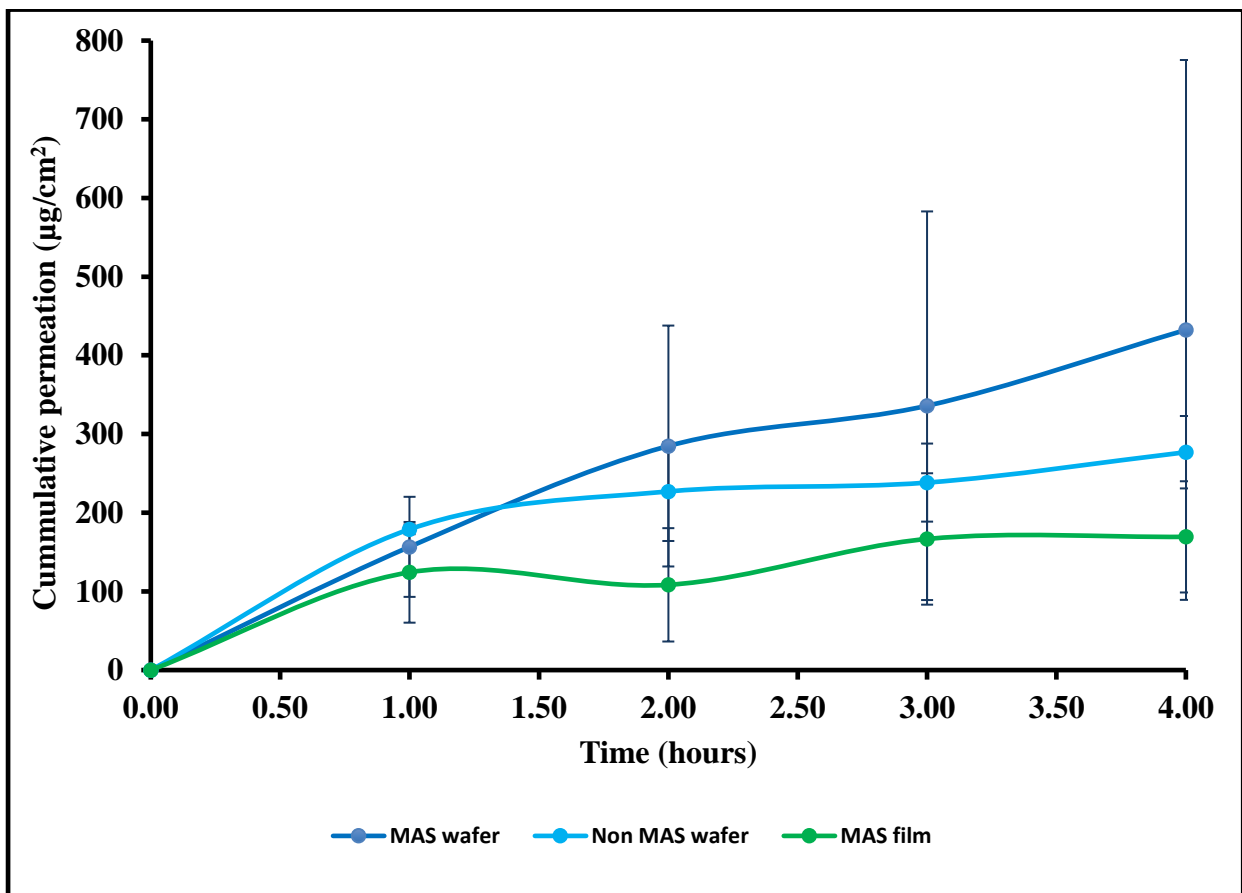


Figure 6.1: Cumulative permeation curve of optimized wafers and films using porcine buccal tissue ($n = 3$, \pm SD).

The highest cumulative permeation and permeation flux (J) was shown in MAS wafers with the maximum cumulative permeation of $432.30\pm 343.04\mu\text{g}/\text{cm}^2$ within 4hrs and permeation flux (J) of $108.08\pm 85.76\mu\text{g}/\text{cm}^2/\text{h}$ while the lowest cumulative permeation and

permeation flux (J) was shown in optimized films (MAS films) with the maximum cumulative permeation of $169.30 \pm 70.67 \mu\text{g}/\text{cm}^2$ within 4hrs and permeation flux (J) of $42.33 \pm 17.67 \mu\text{g}/\text{cm}^2/\text{h}$.

Table 6.2: Permeation flux (J) for optimized wafers and films from EpiOral™ tissue construct.

	<i>Formulation</i>	<i>Flux (J) ($\mu\text{g}/\text{cm}^2/\text{h}$)</i> <i>(mean \pm SD, n = 3)</i>
<i>Porcine tissue</i>	MAS wafers	108.08 \pm 85.76
	MAS films	42.33 \pm 17.67
	Non-MAS wafers	69.22 \pm 11.50
<i>EpiOral™ tissue</i>	MAS wafers	139.74 \pm 22.29
	MAS films	42.31 \pm 5.22
	Non-MAS wafers	140.55 \pm 47.55

6.3.2 *In vitro buccal permeation studies (EpiOral™ buccal tissue)*

The cumulative permeation curves of optimized wafers and films using EpiOral™ buccal tissue are shown in Figure 6.2. The permeation flux (J) of NIC from optimized wafers and films are shown in Table 6.2. The permeation of NIC from optimized wafers and films demonstrated a lag-time of 30mins. The highest cumulative permeation within 4hrs and permeation flux (J) was observed for optimized wafers with the maximum cumulative permeation of $562.22 \pm 190.20 \mu\text{g}/\text{cm}^2$ (Non-MAS wafers) and permeation flux (J) of $140.55 \pm 47.55 \mu\text{g}/\text{cm}^2/\text{hr}$. Optimized MAS films demonstrated a lower cumulative permeation within 4hrs and permeation flux, with a maximum cumulative permeation of $169.234 \pm 20.89 \mu\text{g}/\text{cm}^2$ and permeation flux (J) of $42.31 \pm 5.22 \mu\text{g}/\text{cm}^2/\text{hr}$. EpiOral™ buccal tissues demonstrated a higher flux than porcine buccal tissues.

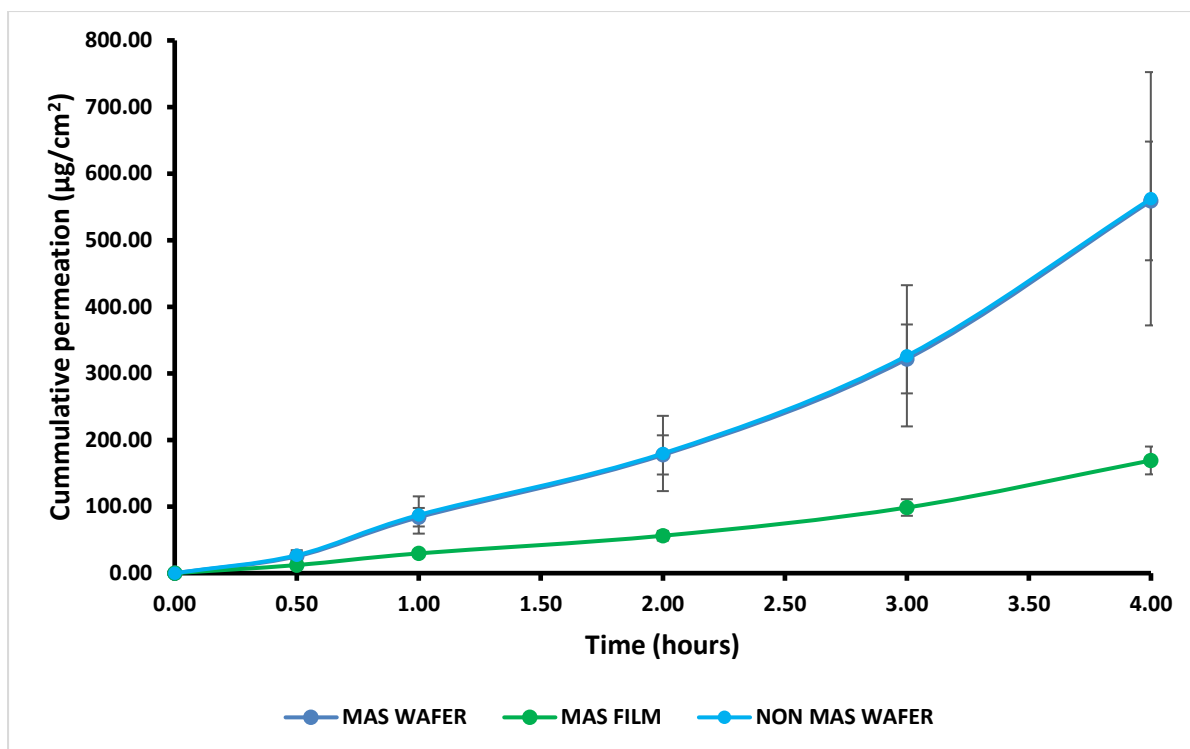


Figure 6.2: Cumulative permeation of optimized wafers and films using EpiOral™ engineered buccal tissue ($n = 3, \pm SD$).

6.3.3 Permeation correlation between *in vitro* porcine buccal tissue and EpiOral™ engineered buccal tissue

The correlation between the cumulative permeation curve of NIC in optimized wafers (i.e. MAS and Non-MAS wafers) and films using a porcine buccal tissue and EpiOral™ buccal engineered tissue is shown in figure 6.3. The correlation of cumulative permeation between the porcine buccal tissue and the EpiOral™ human engineered buccal tissue showed a positive correlation in optimized wafers and films, with an increase in cumulative permeation using EpiOral™ human engineered buccal tissue as cumulative permeation using porcine buccal tissue increases. Optimized wafers generally showed higher regression than optimized films. MAS wafers (Figure 6a) demonstrated the highest linear regression coefficient (0.935) while MAS films (Figure 6b) demonstrated the least linear regression coefficient (0.675).

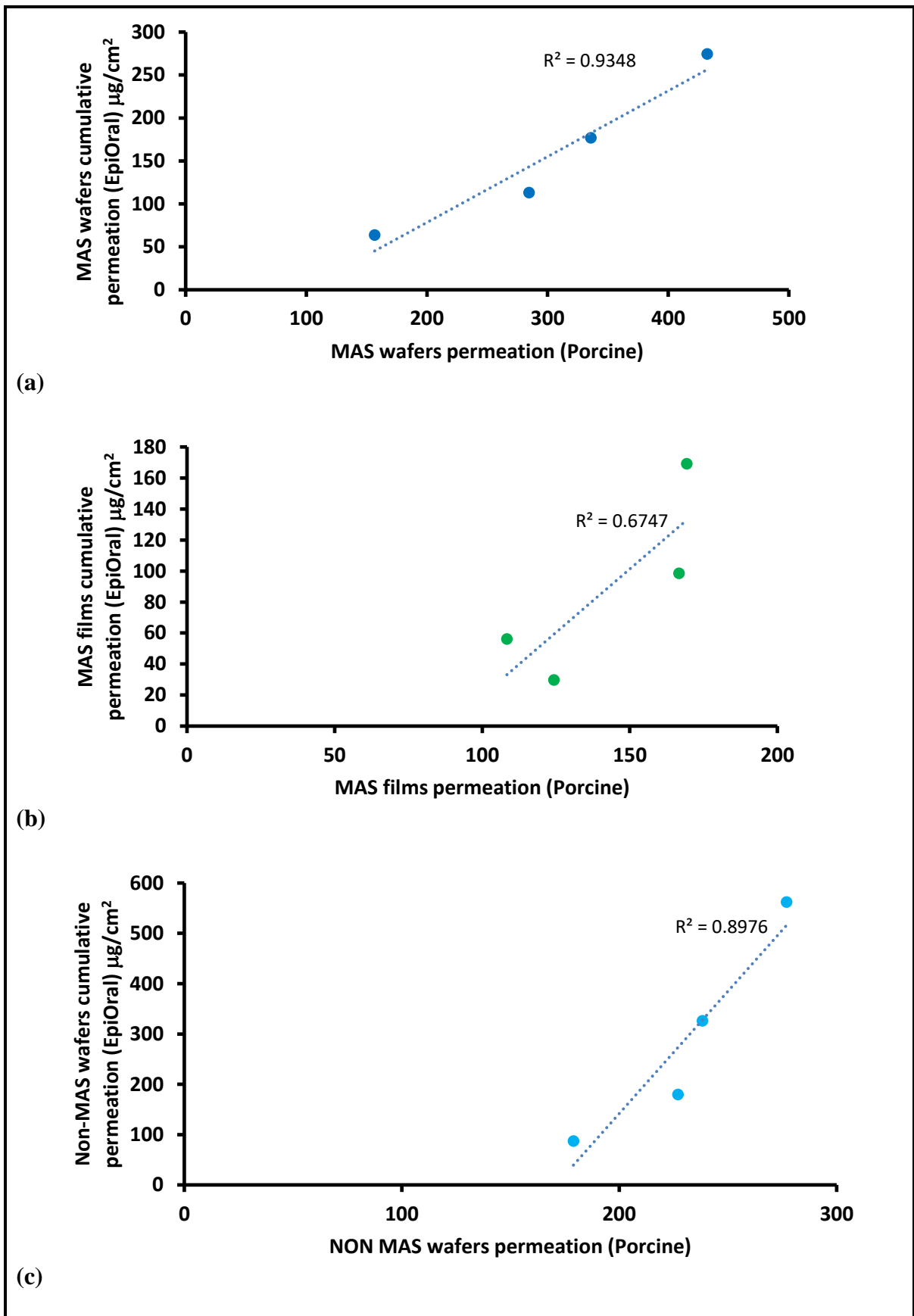


Figure 6.3: Correlation between porcine and EpiOralTM cumulative permeation curve for (a) MAS wafers, (b) MAS films and (c) Non-MAS wafers.

6.3.4 Tissue viability (MTT assay) of EpiOral™ tissues after permeation studies

MTT was utilized to assess the tissue viability of EpiOral™ after contact with the optimized wafers and films. The assay investigates the reduction of yellow MTT to an insoluble purple formazan predominantly by enzymes (mitochondrial succinate dehydrogenase) found in the mitochondria of viable cells (van Meerloo et al., 2011, Riss et al., 2015, Zeng et al., 2015). Cell viability of EpiOral™ engineered buccal tissue used for permeation studies of optimized wafers and films measured with MTT assay is shown in Figure 6.4. There was a reduction in the activity of cell enzymes (mitochondrial succinate dehydrogenase) in all optimized wafers (i.e. MAS and Non-MAS wafers) and films (MAS films) formulations as there was lesser percentage cell viability in comparison to negative non-treated control (100% viability). However, MAS films demonstrated a high percentage cell viability ($91 \pm 13.34\%$) in comparison with wafers (MAS wafers; $86 \pm 4.70\%$ and Non-MAS wafers; $81 \pm 21.15\%$).

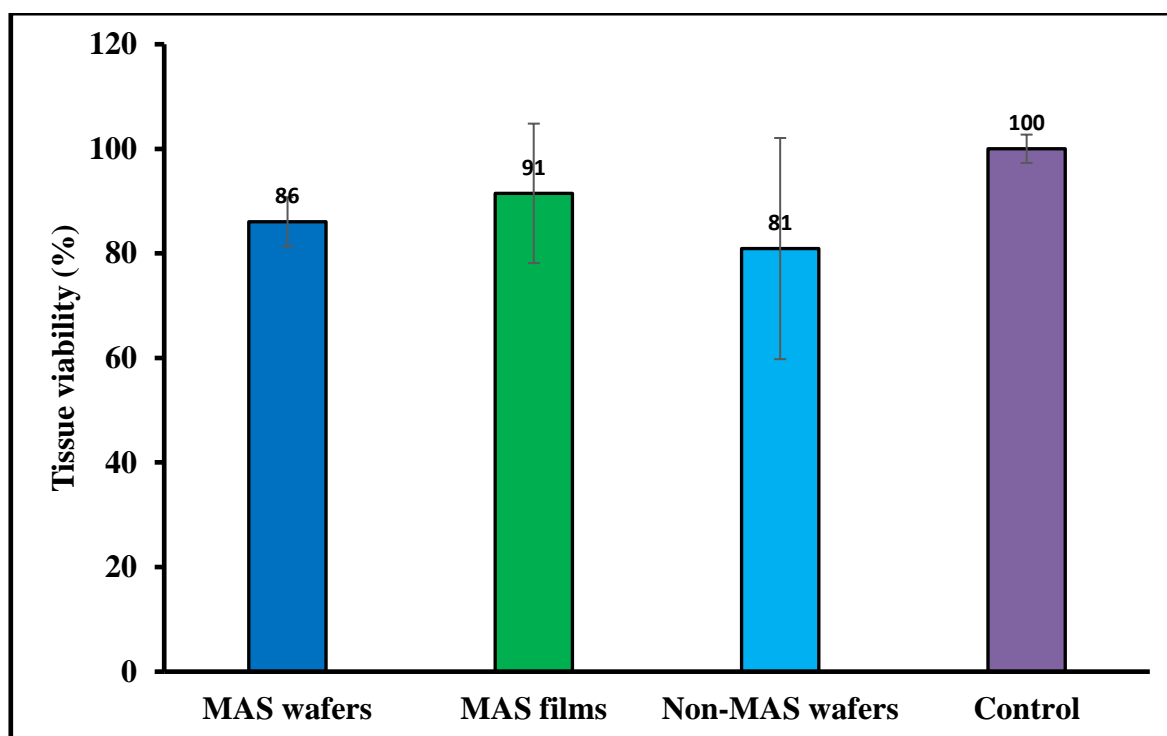


Figure 6.4: EpiOral™ tissue viability after permeation studies of MAS wafers, MAS films, Non-MAS wafers and negative (non-treated) control ($n = 3$, $\pm SD$).

6.4 Discussion

This study was aimed at investigating NIC permeability when released from optimized wafers and films using porcine and human engineered EpiOral™ buccal tissues as a model buccal mucosa membrane. As already discussed in previous chapters, the buccal route offers an admirable opportunity for NIC drug delivery as it bypasses NIC degradation (such as hepatic first-pass effect) when administered by conventional oral route as well as NICs ability to easily penetrate the buccal route than the skin (Nair et al., 1997, Adrian et al., 2006). The buccal permeability of optimized wafers and films with different physicochemical properties and attributes such as swelling and release properties was necessary as it is essential to achieve the required bioavailability for eventual therapeutic action. Furthermore, in order to assess the reliability of the permeation results of both porcine and human engineered EpiOral™ buccal tissues were utilized and compared. The toxicity of the buccal cells was assessed as the mucoadhesive formulations were loaded with NIC which could be toxic at high dose (Chang et al., 2002).

The most important properties that affects the permeability of a drug compound through a tissue membrane is its lipophilicity and molecular weight (Dahan et al., 2016). Lipophilicity however is usually expressed in terms of octanol-water partition coefficient ($\log P$). NIC possesses a low $\log P$ value (1.17) and a low molecular weight of 162.23g/mol which make it highly permeable at physiological pH (6.8) via the buccal mucosa, with un-ionized NIC permeation via transcellular pathway, while ionized NIC via the paracellular pathway (Patel et al., 2011). The permeation of NIC via porcine and EpiOral™ buccal tissue in this study demonstrated a high flux value (between 40 $\mu\text{g}/\text{cm}^2/\text{h}$ - 150 $\mu\text{g}/\text{cm}^2/\text{h}$) at elapse time (4hrs). Similar high flux values of NIC has been observed in previous studies using porcine oesophageal mucosa as a model membrane (Pongjanyakul et al., 2013) and human skin (Zorin et al., 1999). Pongjanyakul et al. demonstrated in his permeation studies a high permeation

curve of NIC between $400\mu\text{g}/\text{cm}^2$ - $800\mu\text{g}/\text{cm}^2$ within 480mins and also showed decrease in film permeation rate as MAS ratio in film increases, which was a similar case in this study as NIC permeation decreased in optimized film formulation (MAS films). The use of porcine and EpiOral™ buccal tissue in these studies demonstrated a good correlation. However, EpiOral™ buccal tissue demonstrated a higher permeation flux (J) than porcine buccal tissue which can be attributed to fatty tissues beneath the buccal mucosa tissue.

Hydration, swelling and release rate of NIC from the formulations played a role on the permeation flux via porcine and EpiOral™ buccal tissue. Wafer formulations (MAS and Non-MAS wafers) showed higher swelling index as discussed in previous chapters, which can be attributed to the its sponge-like pores and therefore high porosity, which allows rapid inflow of buffered solution into the polymer matrix (Okeke & Boateng, 2016). The increased hydration and swelling of wafers played a role in the release rate of NIC from the polymer matrix leading to a rapid release of NIC. These influenced the permeation flux in both porcine and EpiOral™ buccal tissue models with higher flux in comparison to film as shown in figure 6.1 and 6.2. The increased NIC release from optimized wafers formulation allows a higher concentration diffusion gradient towards absorption across the buccal membrane compared to the films.

Film formulations (MAS films) on the other hand, demonstrated a lower permeation flux in both porcine and EpiOral™ buccal tissue models which can be attributed to lower rates of hydration, swelling and release (Okeke & Boateng, 2016, Boateng et al., 2009). The diffusion of buffered solution into film formulation is relatively slow owing to the continuous polymeric sheet and absence of pores in films (SEM data) which therefore affects the hydration and swelling of the formulations and subsequent release rate of NIC from the swollen gels with low concentration diffusion gradient towards absorption across the buccal membrane. This

implies that optimized wafers can provide a more rapid action while optimized films can provide a prolonged action.

The reduction of yellow MTT to purple formazan by viable cell enzyme demonstrated cytotoxicity of NIC with non-viable cell's inability to of reducing yellow MTT to purple formazan. NIC has been reported by Chang et al. to suppress the growth of periodontal ligament fibroblast (PDLF) as well inhibit cell proliferation and decrease protein synthesis with increase in NIC concentration (Chang et al., 2002). NIC induced cytotoxicity was shown in the studies with optimized wafers demonstrating 14% non-viable cells in MAS wafers and 19% non-viable cells in Non-MAS wafers, however lesser non-viable cells (8%) was shown in optimized films (MAS films). The increase in NIC induced cytotoxicity in optimized wafer formulations was as a result of increased concentration of NIC with increased hydration and swelling of optimized wafers which resulted to rapid release of NIC from the polymeric matrix. Similar phenomenon was the case with film formulation, which demonstrated slow hydration and swelling leading to slow NIC release with low concentration diffusion gradient towards absorption across the buccal mucosa whereby leading to lower numbers of non-viable cells in EpiOral™ buccal tissue. The results of cell viability of optimized wafers and films demonstrated that the formulations can be considered safe of toxicity as the percentage viable cells were more than 70% after exposure (Moritz et al., 2014).

6.5 Conclusion

The study demonstrated a readily cumulative permeability of NIC via the buccal route modelled by porcine buccal tissue and EpiOral™ engineered human buccal tissue. NIC released from optimized wafers demonstrated a higher permeation flux than optimized films for both porcine and EpiOral buccal tissue which can be attributed to the formulation properties such as hydration, swelling and release properties of optimized wafers and films. A good linear correlation was achieved for NIC cumulative permeation in porcine and EpiOral buccal tissues with optimized wafers (MAS wafers) showing the highest correlation coefficient. However, as a result of the high concentration of NIC release from optimized wafers, the percentage of viable cells in EpiOral buccal tissue reduced the most in optimized wafers with 14% reduction in MAS wafer and 19% reduction in Non-MAS wafers than optimized films (9% reduction). The optimized wafers and films however can be considered safe as percentage viable cells were >70%.

CHAPTER 7: SUMMARY COMMENTS, KEY FINDINGS AND FUTURE WORK

7.1 Summary comments

The aim of this project was to develop, optimise and characterise composite freeze dried wafers and solvent evaporated films for novel NRT buccal dosage form successfully loaded with NIC. The developed dosage forms involved the use of composite mucoadhesive polymers to target and deliver NIC to the buccal mucosa through the controlled release of NIC from the dosage forms (Figure 7.1). In this section, a summary of the conclusions on the composite formulation design, optimisation and physicochemical properties including hydration and swelling capacity, mucoadhesion, in vitro release profile and kinetics, and permeation characterisation of wafers and films as potential NRT buccal dosage forms.

Composite wafers and films were formulated using GRAS mucoadhesive polymers that are selected based on their ability to adhere to the buccal mucosa, ability to demonstrate a controlled release profile and ability to interact with NIC via ionic interaction and hydrogen bonding. The combination of HPMC and SA as selected polymer at optimum concentration demonstrated improved cake structure, porosity and mechanical properties of freeze dried wafers while film demonstrated improved surface morphology and transparency. Mechanical properties (flexibility) of films were however improved by incorporating GLY in HPMC-SA films. Optimized GLY concentration (2% w/v) in HPMC-SA films was selected by evaluating its mechanical properties (tensile strength, elastic modulus and elongation) and surface morphology using TA and SEM which met the criteria of an ideal film mechanical properties in term of handling. Wafers on the did not require the use of GLY to improve the mechanical properties as the freeze drying annealing treatment optimized the mechanical properties by improving porosity of wafers to form a sponge-like structure which gave wafers its unique property. The interaction between HPMC-SA was showed to be via hydrogen bonding as demonstrated using ATR-FTIR. Increase in SA concentration in BK demonstrated an increase

in wafers hardness and also increased brittleness (tensile strength) in films. This is due the hydrogen bonding between COO⁻ groups of SA and OH groups of HPMC hence reducing the free volume of HPMC. However, the incorporation of NIC in BK HPMC-SA composite wafer and film increased the free volume between HPMC and SA hence improving its mechanical properties by decreasing hardness of wafers and increasing elongation while decreasing stiffness of film. Furthermore, higher SA concentration increased porosity.

The amorphous properties of wafers and films was vital in hydration and swelling capacity. However, their structural morphology demonstrated difference in terms of hydration and swelling capacity which played a vital role in vitro NIC release profile of wafers and films. Freeze drying demonstrated high drug loading capacity as wafers showed higher NIC than films. However, the formulations demonstrated a low NIC content which can be attributed to the evaporation of liquid free based NIC from the formulations. MAS was hence studied as an adsorbent to stabilize NIC in wafers and films. The formulation of MAS-NIC complex demonstrated a cationic exchange, hydrogen bonding and water bridging interaction when freeze dried and/or dried via solvent evaporation. These interactions were demonstrated by analysing the particle size, surface charge, surface morphology, physical properties (amorphous/crystalline) and molecular interactions was performed using Mastersizer, Zetasizer, SEM, XRD, ATR-FTIR and NMR respectively. This demonstrated an interaction between the negatively charged silicate of MAS and the amine group of NIC.

The incorporation of MAS into composite HPMC-SA wafers and films was successful in stabilizing NIC. Although, the two formulations demonstrated different behaviours in their functional physical properties such as mechanical and surface/internal morphology, swelling index, mucoadhesion, drug loading capacity and drug release. In general, MAS loaded wafers demonstrated higher swelling index, improved NIC stability with increase in drug loading capacity and demonstrated a rapid release compared to MAS loaded films with a moderate

swelling index, improved NIC stability with increased drug loading capacity and sustained NIC release. The release mechanism of MAS loaded wafers and films demonstrated a swelling, diffusion and erosion mechanism. However, selected optimized wafers and films (MAS wafers, MAS film and Non-MAS wafers) were subjected to intermediate and accelerated stability studies over the period of 6 months which demonstrated a low NIC content as a result of oxidative degradation. The result implies that in order to improve stability of product adequate packaging is recommended.

The effect of SS on optimized wafers and films was demonstrated by comparing mucoadhesion, swelling and NIC release in SS and PBS medium. The result demonstrated a decrease in mucoadhesion, swelling and release rate attributed to ionic pressure created by the high concentration of ion present in simulated saliva. The result was also compared to commercially available NRT (NiQuitin®) which demonstrated higher mucoadhesion, rapid hydration and swelling (fast dissolving), and rapid release of NIC from the polymeric matrix. However, low NIC content was observed compared to optimized wafers and films, with a possibility of dumping of NIC in the saliva resulting in swallowing effect. Optimized wafers and films were also investigated for permeability of NIC using porcine buccal tissue and EpiOral™ engineered human buccal tissue models as well as buccal cell viability. The study demonstrated a correlation between NIC cumulative permeation in porcine and EpiOral™ buccal tissues from optimized wafers and films. However, optimized wafers demonstrated higher permeation flux than optimized film for both porcine and EpiOral™ buccal tissue which can be attributed to their functional properties such as hydration, swelling and release properties. The cell viability study demonstrated low reduction in viable cells upon exposure with more than 70% viable cells. This implies that the optimized wafers and films can be considered safe.

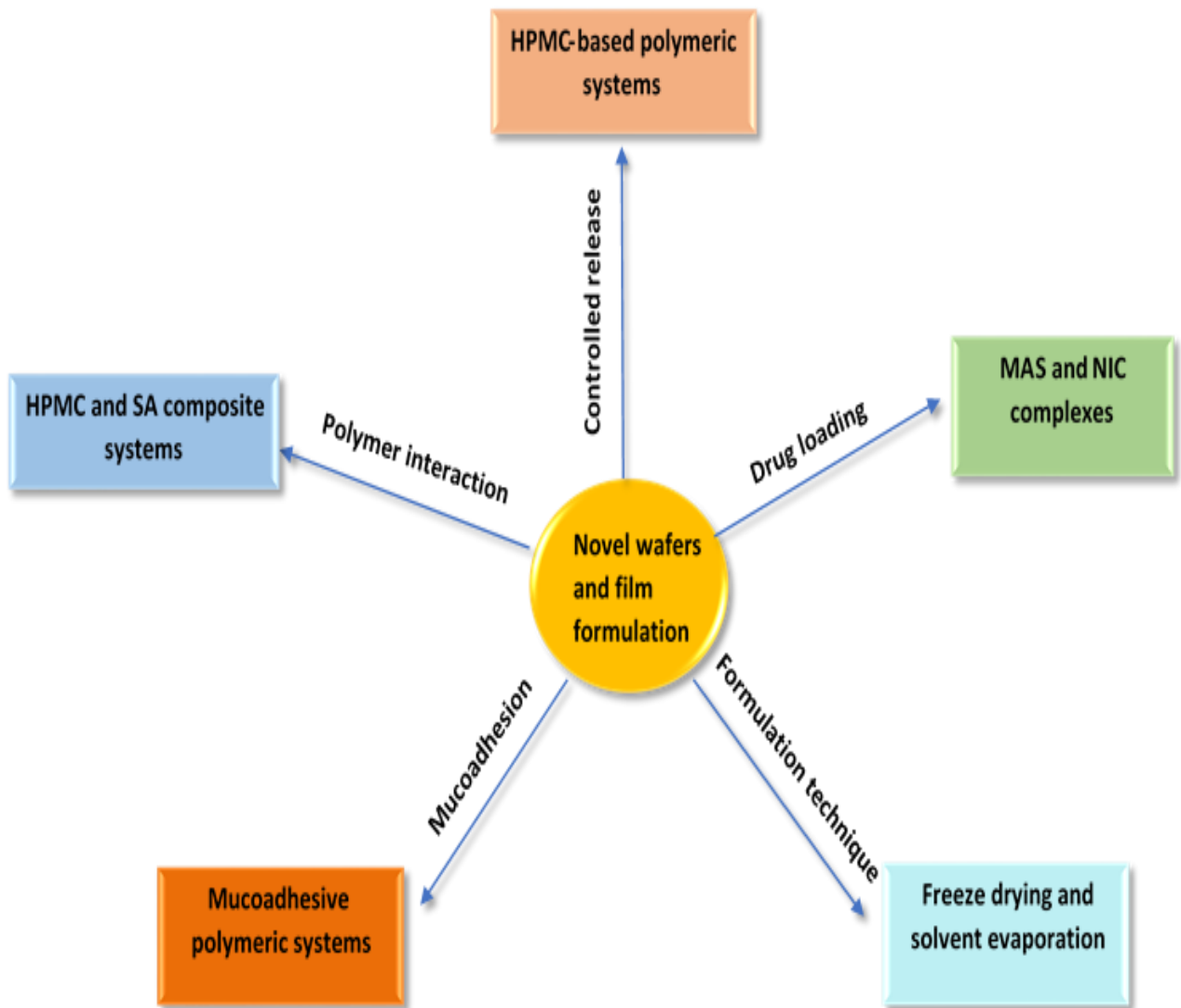


Figure 7.1: Summary of wafers and films mechanisms.

7.2 Key research findings

- Novel buccal mucosal drug delivery system has been developed for NRT using both freeze-drying and solvent evaporated method with optimal hydration and swelling, mucoadhesion and drug release properties.
- Composite HPMC-SA wafers have demonstrated the potential to be utilised as a NRT dosage form using NIC base form with better drug efficiency than composite HPMC-SA films. In addition, the formulation technique utilised in the formulation of wafers can resolve the challenges posed by using NIC base form.
- Interactions between NIC and MAS have been studied by the formulation of MAS-NIC complexes using freeze-drying and solvent evaporation method.
- MAS has successfully been utilised as a NIC stabiliser in both wafers and film formulation. For the first time, MAS has been incorporated in wafer formulation to stabilise NIC.
- Constitutes of SS can affect the functional properties of optimized wafers and films such as mucoadhesion, hydration and swelling, and drug release.
- Optimised wafers and films can be effective in buccal delivery of NIC compare to commercially available NiQuitin®.
- Ex vivo permeation demonstrated good permeation in both porcine buccal tissue and EpiOral™ engineered human buccal tissue, and can be considered safe.

7.3 Future work

- The stability studies undertaken suggests the need to develop adequate protective packaging and hence, re-evaluation of stability studies on optimized wafers and films stored in appropriately designed package will need to be undertaken. This will reduce chances of degradation and evaporation of NIC during storage hence improve stability.
- Long-term (12 months) stability evaluation of optimized wafers and films stored under ICH stability conditions would be carried out in order to establish the stability of optimized wafers and films over the full-expected duration of storage in order to inform the appropriate product shelf life. Furthermore, the long-term stability will be investigated under conditions that represent different geographical environment conditions.
- Further optimization of wafers and films to deal with taste issues encountered with oral NIC based formulations. This will resolve the problem of patient non-compliance due to its bitter taste.
- There are currently other non-NIC based pharmacotherapies used in smoking cessation therefore an optimized freeze-dried wafer and film loaded with bupropion and varenicline will need to be formulated and compared with the optimized NIC loaded wafers and films developed in current study.

CHAPTER 8: REFERENCES

- Abruzzo, A., Bigucci, F., Cerchiara, T., Cruciani, F., Vitali, B. and Luppi, B. (2012): Mucoadhesive chitosan/gelatin films for buccal delivery of propranolol hydrochloride. *Carbohydrate Polymers*, **87**, 581-588.
- Adrian, C.L., Olin, H.B.D., Dalhoff, K. and Jacobsen, J. (2006): In vivo human buccal permeability of nicotine. *International Journal of Pharmaceutics*, **311**, 196-202.
- Agarwal, S. and Aggarwal, S. (2015): Mucoadhesive Polymeric Platform for Drug Delivery; A Comprehensive Review. *Current Drug Delivery*, **12**, 139-156.
- Aguzzi, C., Cerezo, P., Viseras, C. and Caramella, C. (2007): Use of clays as drug delivery systems: Possibilities and limitations. *Applied Clay Science*, **36**, 22-36.
- Ahsan, H., Ali, A. and Ali, R. (2003): Oxygen free radicals and systemic autoimmunity. *Clinical & Experimental Immunology*, **131**, 398-404.
- Allen Jr, L.V. (2008): Dosage form design and development. *Clinical Therapeutics*, **30**, 2102-2111.
- Allen, L.V. and Popovich, N.G. (2005): *Ansel's pharmaceutical dosage forms and drug delivery systems*. Lippincott Williams & Wilkins Baltimore.
- Ambrose, J.A. and Barua, R.S. (2004): The pathophysiology of cigarette smoking and cardiovascular disease: an update. *Journal of the American College of Cardiology*, **43**, 1731-1737.
- Andrews, G.P., Lavery, T.P. and Jones, D.S. (2009): Mucoadhesive polymeric platforms for controlled drug delivery. *European Journal of Pharmaceutics and Biopharmaceutics*, **71**, 505-518.
- Anselmo, A.C. and Mitragotri, S. (2014): An overview of clinical and commercial impacts of drug delivery systems. *Journal of Controlled Release*, **190**, 15-28.
- Aulton, M.E. and Taylor, K.M.G. (2013): *Aulton's Pharmaceutics: the design and manufacture of medicines*. Elsevier Health Sciences.
- Ayensu, I., Mitchell, J.C. and Boateng, J.S. (2012a): Development and physico-mechanical characterisation of lyophilised chitosan wafers as potential protein drug delivery systems via the buccal mucosa. *Colloids and Surfaces B: Biointerfaces*, **91**, 258-265.
- Ayensu, I., Mitchell, J.C. and Boateng, J.S. (2012b): In vitro characterisation of chitosan based xerogels for potential buccal delivery of proteins. *Carbohydrate Polymers*, **89**, 935-941.

- Azagury, A., Khoury, L., Enden, G. and Kost, J. (2014): Ultrasound mediated transdermal drug delivery. *Advanced Drug Delivery Reviews*, **72**, 127-143.
- Bajaj, S., Singla, D. and Sakhuja, N. (2012): Stability Testing of Pharmaceutical Products, **3**, 129-138
- Beaglehole, R., Bonita, R., Yach, D., Mackay, J. and Reddy, K.S. (2015): A tobacco-free world: a call to action to phase out the sale of tobacco products by 2040. *The Lancet*, **385**, 1011-1018.
- Benowitz, N.L., Hukkanen, J. and Jacob Iii, P. (2009): Nicotine chemistry, metabolism, kinetics and biomarkers. In: *Nicotine Psychopharmacology*), pp. 29-60, Springer.
- Benowitz, N.L., Jacob, P., Jones, R.T. and Rosenberg, J. (1982): Interindividual variability in the metabolism and cardiovascular effects of nicotine in man. *Journal of Pharmacology and Experimental Therapeutics*, **221**, 368-372.
- Benowitz, N.L., Jacob, P. and Savanapridi, C. (1987): Determinants of nicotine intake while chewing nicotine polacrilex gum. *Clinical Pharmacology & Therapeutics*, **41**, 467-473.
- Benowitz, N.L., Porchet, H., Sheiner, L. and Jacob, P. (1988): Nicotine absorption and cardiovascular effects with smokeless tobacco use: comparison with cigarettes and nicotine gum. *Clinical Pharmacology & Therapeutics*, **44**, 23-28.
- Birudaraj, R., Berner, B., Shen, S. and Li, X. (2005): Buccal permeation of buspirone: mechanistic studies on transport pathways. *Journal Of Pharmaceutical Sciences*, **94**, 70-78.
- Blagden, N., De Matas, M., Gavan, P.T. and York, P. (2007): Crystal engineering of active pharmaceutical ingredients to improve solubility and dissolution rates. *Advanced Drug Delivery Reviews*, **59**, 617-630.
- Boateng, J.S. and Areago, D. (2014): Composite Sodium Alginate and Chitosan Based Wafers for Buccal Delivery of Macromolecules. *Austin J Anal Pharm Chem*, **1**, 1022.
- Boateng, J.S., Auffret, A.D., Matthews, K.H., Humphrey, M.J., Stevens, H.N.E. and Eccleston, G.M. (2010): Characterisation of freeze-dried wafers and solvent evaporated films as potential drug delivery systems to mucosal surfaces. *International Journal Of Pharmaceutics*, **389**, 24-31.
- Boateng, J.S. and Okeke, O. (2014): Chitosan-based films for the sustained release of peptides: a new era in buccal delivery? *Therapeutic Delivery*, **5**, 497-500.
- Boateng, J.S., Stevens, H.N.E., Eccleston, G.M., Auffret, A.D., Humphrey, M.J. and Matthews, K.H. (2009): Development and mechanical characterization of solvent-cast

- polymeric films as potential drug delivery systems to mucosal surfaces. *Drug Development and Industrial Pharmacy*, **35**, 986-996.
- Boddupalli, B.M., Mohammed, Z.N.K., Nath, R.A. and Banji, D. (2010): Mucoadhesive drug delivery system: An overview. *Journal Of Advanced Pharmaceutical Technology & Research*, **1**, 381.
- Britton, J. and Bogdanovica, I. (2013): Tobacco control efforts in Europe. *The Lancet*, **381**, 1588-1595.
- Brown, J., Hajek, P., McRobbie, H., et al. (2013): Cigarette craving and withdrawal symptoms during temporary abstinence and the effect of nicotine gum. *Psychopharmacology*, **229**, 209-218.
- Bruce, C. and Manning, M. (2009): Melt extruded nicotine thin strips.), Google Patents.
- Carretero, M.I. and Pozo, M. (2009): Clay and non-clay minerals in the pharmaceutical industry: Part I. Excipients and medical applications. *Applied Clay Science*, **46**, 73-80.
- Chang, Y.C., Huang, F.M., Tai, K.W., Yang, L.C. and Chou, M.Y. (2002): Mechanisms of cytotoxicity of nicotine in human periodontal ligament fibroblast cultures in vitro. *Journal Of Periodontal Research*, **37**, 279-285.
- Chaplin, S. (2011): Nicorette QuickMist: rapidly absorbed NRT mouthspray. *Prescriber*, **22**, 26-28.
- Cheng, Y.-H., Watts, P., Hinchcliffe, M., et al. (2002): Development of a novel nasal nicotine formulation comprising an optimal pulsatile and sustained plasma nicotine profile for smoking cessation. *Journal of Controlled Release*, **79**, 243-254.
- Cho, H. and Lee, K. (2014): A new assessment method of outdoor tobacco smoke (OTS) exposure. *Atmospheric Environment*, **87**, 41-46.
- Choi, J.H., Dresler, C.M., Norton, M.R. and Strahs, K.R. (2003): Pharmacokinetics of a nicotine polacrilex lozenge. *Nicotine & Tobacco Research*, **5**, 635-644.
- Choices, N.H.S. (2015): E-cigarettes may make lungs vulnerable to infection-Health News-NHS Choices.
- Church, D.F. and Pryor, W.A. (1985): Free-radical chemistry of cigarette smoke and its toxicological implications. *Environmental Health Perspectives*, **64**, 111.
- Colombo, P. (1993): Swelling-controlled release in hydrogel matrices for oral route. *Advanced Drug Delivery Reviews*, **11**, 37-57.

- Conway, B.R. (2008): Solid dosage forms. *Pharmaceutical Manufacturing Handbook: Production and Processes*, 233-265.
- Costa, I.d.S.M., Abranches, R.P., Garcia, M.T.J. and Pierre, M.B.R. (2014): Chitosan-based mucoadhesive films containing 5-aminolevulinic acid for buccal cancer's treatment. *Journal of Photochemistry and Photobiology B: Biology*, **140**, 266-275.
- Cummings, K.M., Giovino, G., Jaén, C.R. and Emrich, L.J. (1985): Reports of smoking withdrawal symptoms over a 21 day period of abstinence. *Addictive Behaviors*, **10**, 373-381.
- Czogala, J., Goniewicz, M.L., Fidelus, B., Zielinska-Danch, W., Travers, M.J. and Sobczak, A. (2014): Secondhand exposure to vapors from electronic cigarettes. *Nicotine & Tobacco Research*, **16**, 655-662.
- Dahan, A., Beig, A., Lindley, D. and Miller, J.M. (2016): The solubility–permeability interplay and oral drug formulation design: Two heads are better than one. *Advanced Drug Delivery Reviews*, **101**, 99-107.
- Dash, S., Murthy, P.N., Nath, L. and Chowdhury, P. (2010): Kinetic modeling on drug release from controlled drug delivery systems. *Acta Pol Pharm*, **67**, 217-223.
- Date, A.A. and Nagarsenker, M.S. (2008): Parenteral microemulsions: An overview. *International Journal of Pharmaceutics*, **355**, 19-30.
- Davis, R.E., Hartman, C.W. and Fincher, J.H. (1971): Dialysis of ephedrine and pentobarbital from whole human saliva and simulated saliva. *Journal Of Pharmaceutical Sciences*, **60**, 429-432.
- de Almeida, P.D.V., Gregio, A.M., Machado, M.A., De Lima, A.A. and Azevedo, L.R. (2008): Saliva composition and functions: a comprehensive review. *J Contemp Dent Pract*, **9**, 72-80.
- Dempsey, D.A. and Benowitz, N.L. (2001): Risks and benefits of nicotine to aid smoking cessation in pregnancy. *Drug Safety*, **24**, 277-322.
- Dixit, R.P. and Puthli, S.P. (2009): Oral strip technology: Overview and future potential. *Journal of Controlled Release*, **139**, 94-107.
- Djordjevic, M. V., Hoffmann, D., & Hoffmann, I. (1997). Nicotine regulates smoking patterns. *Preventive medicine*, 26(4), 435-440.
- Dolovich, M.B. and Dhand, R. (2011): Aerosol drug delivery: developments in device design and clinical use. *The Lancet*, **377**, 1032-1045.

- Dow, T. C. (2000): Using methocel cellulose ethers for controlled release of drugs in hydrophilic matrix systems. Midland (MI): The Dow Chemical Company.
- Dreher, D. and Junod, A.F. (1996): Role of oxygen free radicals in cancer development. *European Journal Of Cancer*, **32**, 30-38.
- Drozдов, A.D. and deClaville Christiansen, J. (2015): Modeling the effects of pH and ionic strength on swelling of polyelectrolyte gels. *The Journal Of Chemical Physics*, **142**, 114904.
- Duffó, G.S. and Castillo, E.Q. (2004): Development of an artificial saliva solution for studying the corrosion behavior of dental alloys. *Corrosion*, **60**, 594-602.
- Elmore, A. R. (2002): Final report on the safety assessment of aluminum silicate, calcium silicate, magnesium aluminum silicate, magnesium silicate, magnesium trisilicate, sodium magnesium silicate, zirconium silicate, attapulgite, bentonite, Fuller's earth, hectorite, kaolin, lithium magnesium silicate, lithium magnesium sodium silicate, montmorillonite, pyrophyllite, and zeolite. *International Journal of Toxicology*, **22**, 37-102.
- FDA, U.S. (1997a): Guidance for Industry: SUPAC-MR: Modified Release Solid Oral Dosage Forms; Scale-Up and Post-Approval Changes: Chemistry, Manufacturing and Controls. Vitro Dissolution Testing, and In Vivo Bioequivalence Documentation.
- FDA, U.S. (1997b): Guidance for Industry: Dissolution testing of immediate-release solid oral dosage forms. Food and Drug Administration, Center for Drug Evaluation and Research (CDER).
- FDA, U.S. (1997c): Guidance for Industry: Extended release oral dosage forms: Development, evaluation, and application of in vitro/in vivo correlations. Food and Drug Administration, Center for Drug Evaluation and Research (CDER).
- Figueiras, A., Hombach, J., Veiga, F. and Bernkop-Schnürch, A. (2009): In vitro evaluation of natural and methylated cyclodextrins as buccal permeation enhancing system for omeprazole delivery. *European Journal of Pharmaceutics and Biopharmaceutics*, **71**, 339-345.
- Fortuna, A., Alves, G., Serralheiro, A., Sousa, J. and Falcão, A. (2014): Intranasal delivery of systemic-acting drugs: Small-molecules and biomacromolecules. *European Journal of Pharmaceutics and Biopharmaceutics*.
- Gad, S.C. (2008): *Pharmaceutical manufacturing handbook: production and processes*. John Wiley & Sons.
- Ganem-Quintanar, A., Falson-Rieg, F. and Buri, P. (1997): Contribution of lipid components to the permeability barrier of oral mucosa. *European Journal of Pharmaceutics and Biopharmaceutics*, **44**, 107-120.

- Ganguly, I., Abraham, S., Bharath, S. and Madhavan, V. (2014): Development of Fast Dissolving Sublingual Wafers of Promethazine Hydrochloride. *Iranian Journal of Pharmaceutical Sciences*, **10**, 71-92.
- Ghulaxe, C. and Verma, R. (2015): A review on transdermal drug delivery system.
- Gilman, J.W. (1999): Flammability and thermal stability studies of polymer layered-silicate (clay) nanocomposites. *Applied Clay Science*, **15**, 31-49.
- Gimeno, A., Calpena, A.C., Sanz, R., Mallandrich, M., Peraire, C. and Clares, B. (2014): Transbuccal delivery of doxepin: Studies on permeation and histological investigation. *International Journal of Pharmaceutics*, **477**, 650-654.
- Giovino, C., Ayensu, I., Tetteh, J. and Boateng, J.S. (2013): An integrated buccal delivery system combining chitosan films impregnated with peptide loaded PEG-b-PLA nanoparticles. *Colloids and Surfaces B: Biointerfaces*, **112**, 9-15.
- GlaxoSmithKline (2016): NiQuitin strips., <http://www.niquitin.co.uk/product/niquitin-strips>.
- Grabovac, V., Guggi, D. and Bernkop-Schnürch, A. (2005): Comparison of the mucoadhesive properties of various polymers. *Advanced Drug Delivery Reviews*, **57**, 1713-1723.
- Grim, R. E. (1968). *Clay mineralogy*.
- Gryczke, A., Schminke, S., Maniruzzaman, M., Beck, J. and Douroumis, D. (2011): Development and evaluation of orally disintegrating tablets (ODTs) containing Ibuprofen granules prepared by hot melt extrusion. *Colloids and Surfaces B: Biointerfaces*, **86**, 275-284.
- Guideline, I.C.H.H.T. (2003): Stability testing of new drug substances and products. Q1A (R2), current step, **4**.
- Gupta, P., Vermani, K. and Garg, S. (2002): Hydrogels: from controlled release to pH-responsive drug delivery. *Drug Discovery Today*, **7**, 569-579.
- Gurny, R., Meyer, J.-M. and Peppas, N.A. (1984): Bioadhesive intraoral release systems: design, testing and analysis. *Biomaterials*, **5**, 336-340.
- Gutniak, M.K., Larsson, H., Heiber, S.J., Juneskans, O.T., Holst, J.J. and Ahrén, B. (1996): Potential therapeutic levels of glucagon-like peptide I achieved in humans by a buccal tablet. *Diabetes Care*, **19**, 843-848.
- Hacker, M., Messerli, W.S. and Bachmann, K.A. (2009): *Pharmacology: principles and practice*. Academic Press.

- Handa, S. (2013): [Nicotine replacement therapy]. *Nihon rinsho. Japanese Journal Of Clinical Medicine*, **71**, 482-486.
- Hansch, C., Leo, A. and Hoekman, D.H. (1995): *Exploring QSAR: fundamentals and applications in chemistry and biology*. American Chemical Society Washington, DC.
- He, W.-S., Xiong, H.-W., Xi, D., et al. (2016): Buccal Transmucosal Delivery System of Enalapril for Improved Cardiac Drug Delivery: Preparation and Characterization. *Tropical Journal of Pharmaceutical Research*, **15**, 13-18.
- Hearnden, V., Sankar, V., Hull, K., et al. (2012): New developments and opportunities in oral mucosal drug delivery for local and systemic disease. *Advanced Drug Delivery Reviews*, **64**, 16-28.
- Hecht, S.S. (2006): Cigarette smoking: cancer risks, carcinogens, and mechanisms. *Langenbeck's Archives of Surgery*, **391**, 603-613.
- Heinzelmann, K., Franke, K., Velasco, J. and Marquez-Ruiz, G. (2000): Microencapsulation of fish oil by freeze-drying techniques and influence of process parameters on oxidative stability during storage. *European Food Research and Technology*, **211**, 234-239.
- Henningfield, J.E., Fant, R.V., Buchhalter, A.R. and Stitzer, M.L. (2005): Pharmacotherapy for Nicotine Dependence. *CA: A Cancer Journal for Clinicians*, **55**, 281-299.
- Hirlekar, R.S. and Kadam, V.J. (2009): Design of buccal drug delivery system for a poorly soluble drug. *Asian Journal of Pharmaceutical and Clinical Research*, **2**, 49-53.
- Huang, Y., Leobandung, W., Foss, A. and Peppas, N.A. (2000): Molecular aspects of muco- and bioadhesion:: Tethered structures and site-specific surfaces. *Journal Of Controlled Release*, **65**, 63-71.
- Hughes, J.R., Higgins, S.T. and Bickel, W.K. (1994): Nicotine withdrawal versus other drug withdrawal syndromes: similarities and dissimilarities. *Addiction*, **89**, 1461-1470.
- Humphrey, S.P. and Williamson, R.T. (2001): A review of saliva: normal composition, flow, and function. *The Journal Of Prosthetic Dentistry*, **85**, 162-169.
- Ikinci, G., Şenel, S., Tokgözoğlu, L., Wilson, C.G. and Şumnu, M. (2006): Development and in vitro/in vivo evaluations of bioadhesive buccal tablets for nicotine replacement therapy. *Die Pharmazie-An International Journal of Pharmaceutical Sciences*, **61**, 203-207.
- Jannin, V., Lemagnen, G., Gueroult, P., Larrouture, D. and Tuleu, C. (2014): Rectal route in the 21st Century to treat children. *Advanced Drug Delivery Reviews*, **73**, 34-49.

- Jones, A.M., Laporte, A., Rice, N. and Zucchelli, E. (2015): Do public smoking bans have an impact on active smoking? Evidence from the UK. *Health Economics*, **24**, 175-192.
- Kartal, A., Marvola, J., Matheka, J., Peltoniemi, M. and Sivén, M. (2010): Computational prediction of local drug effect on carcinogenic acetaldehyde in the mouth based on in vitro/in vivo results of freely soluble L-cysteine. *Drug Development And Industrial Pharmacy*, **36**, 715-723.
- Kasper, J.C. and Friess, W. (2011): The freezing step in lyophilization: Physicochemical fundamentals, freezing methods and consequences on process performance and quality attributes of biopharmaceuticals. *European Journal of Pharmaceutics and Biopharmaceutics*, **78**, 248-263.
- Keane, H. (2013): Making smokers different with nicotine: NRT and quitting. *International Journal of Drug Policy*, **24**, 189-195.
- Khan, S., Trivedi, V. and Boateng, J. (2016): Functional physicochemical, ex vivo permeation and cell viability characterization of omeprazole loaded buccal films for paediatric drug delivery. *International Journal Of Pharmaceutics*, **500**, 217-226.
- Khutoryanskiy, V.V. (2011): Advances in Mucoadhesion and Mucoadhesive Polymers. *Macromolecular Bioscience*, **11**, 748-764.
- Kianfar, F., Ayensu, I. and Boateng, J.S. (2014): Development and physico-mechanical characterization of carrageenan and poloxamer-based lyophilized matrix as a potential buccal drug delivery system. *Drug Development And Industrial Pharmacy*, **40**, 361-369.
- Kianfar, F., Chowdhry, B.Z., Antonijevic, M.D. and Boateng, J.S. (2012): Novel films for drug delivery via the buccal mucosa using model soluble and insoluble drugs. *Drug Development And Industrial Pharmacy*, **38**, 1207-1220.
- Koschier, F., Kostrubsky, V., Toole, C. and Gallo, M.A. (2011): In vitro effects of ethanol and mouthrinse on permeability in an oral buccal mucosal tissue construct. *Food And Chemical Toxicology*, **49**, 2524-2529.
- Kumar, V., Aggarwal, G., Zakir, F. and Choudhary, A. (2011): Buccal bioadhesive drug delivery—a novel technique. *International Journal of Pharmacy and Biological Sciences*, **1**, 89-102.
- Lam, J.K.W., Xu, Y., Worsley, A. and Wong, I.C.K. (2014): Oral transmucosal drug delivery for pediatric use. *Advanced Drug Delivery Reviews*.
- Lam, P.L. and Gambari, R. (2014): Advanced progress of microencapsulation technologies: *In vivo* and *in vitro* models for studying oral and transdermal drug deliveries. *Journal of Controlled Release*, **178**, 25-45.

- Lerner, C.A., Sundar, I.K., Watson, R.M., et al. (2015): Environmental health hazards of e-cigarettes and their components: Oxidants and copper in e-cigarette aerosols. *Environmental Pollution*, **198**, 100-107.
- Levendoski, E.E., Leydon, C. and Thibeault, S.L. (2014): Vocal fold epithelial barrier in health and injury: a research review. *Journal of Speech, Language, and Hearing Research*, **57**, 1679-1691.
- Lorist, M. and Snel, J. (2013): *Nicotine, caffeine and social drinking: behaviour and brain function*. Routledge.
- López-Galindo, A., Viseras, C. and Cerezo, P. (2007): Compositional, technical and safety specifications of clays to be used as pharmaceutical and cosmetic products. *Applied Clay Science*, **36**, 51-63.
- Mamatha, Y., Selvi, A., Prasanth, V.V., Sipai, M. and Yadav, V. (2012): Buccal drug delivery: a technical approach. *Journal of Drug Delivery and Therapeutics*, **2**.
- Marques, M.R.C., Loebenberg, R. and Almukainzi, M. (2011): Simulated biological fluids with possible application in dissolution testing. *Dissolution Technol*, **18**, 15-28.
- Martin, L., Wilson, C.G., Koosha, F. and Uchegbu, I.F. (2003): Sustained buccal delivery of the hydrophobic drug denbufylline using physically cross-linked palmitoyl glycol chitosan hydrogels. *European Journal of Pharmaceutics and Biopharmaceutics*, **55**, 35-45.
- Marxen, E., Axelsen, M.C., Pedersen, A.M.L. and Jacobsen, J. (2016): Effect of cryoprotectants for maintaining drug permeability barriers in porcine buccal mucosa. *International Journal of Pharmaceutics*, **511**, 599-605.
- Mashru, R.C., Sutariya, V.B., Sankalia, M.G. and Parikh, P.P. (2005): Development and evaluation of fast-dissolving film of salbutamol sulphate. *Drug Development and Industrial Pharmacy*, **31**, 25-34.
- Mayer, B. (2014): How much nicotine kills a human? Tracing back the generally accepted lethal dose to dubious self-experiments in the nineteenth century. *Archives of Toxicology. Archiv für Toxikologie*, **88**, 5.
- Mihranyan, A., Andersson, S.-B. and Ek, R. (2004): Sorption of nicotine to cellulose powders. *European Journal of Pharmaceutical Sciences*, **22**, 279-286.
- Mitchell, J. R., & Blanshard, J. M. V. (1976): Rheological properties of alginate gels. *Journal of texture studies*, **7**(2), 219-234.
- Moore, J.W. and Flanner, H.H. (1996): Mathematical comparison of dissolution profiles. *Pharmaceutical Technology*, **20**, 64-74.

- Morales, J.O. and McConville, J.T. (2011): Manufacture and characterization of mucoadhesive buccal films. *European Journal of Pharmaceutics and Biopharmaceutics*, **77**, 187-199.
- Moritz, S., Wiegand, C., Wesarg, F., et al. (2014): Active wound dressings based on bacterial nanocellulose as drug delivery system for octenidine. *International Journal Of Pharmaceutics*, **471**, 45-55.
- Moser, K., Kriwet, K., Naik, A., Kalia, Y.N. and Guy, R.H. (2001): Passive skin penetration enhancement and its quantification in vitro. *European Journal of Pharmaceutics and Biopharmaceutics*, **52**, 103-112.
- Nair, A.B., Kumria, R., Harsha, S., Attimarad, M., Al-Dhubiab, B.E. and Alhaider, I.A. (2013): In vitro techniques to evaluate buccal films. *Journal of Controlled Release*, **166**, 10-21.
- Nair, M.K., Chetty, D.J., Ho, H. and Chien, Y.W. (1997): Biomembrane permeation of nicotine: Mechanistic studies with porcine mucosae and skin. *Journal of Pharmaceutical Sciences*, **86**, 257-262.
- Newman, S.P. (2006): AEROSOLS. In: *Encyclopedia of Respiratory Medicine* (Laurent, G.J. and Shapiro, S.D., eds.), pp. 58-64, Academic Press, Oxford.
- Okeke, O.C. and Boateng, J.S. (2016): Composite HPMC and sodium alginate based buccal formulations for nicotine replacement therapy. *International Journal of Biological Macromolecules*, **91**, 31-44.
- Okeke, O.C. and Boateng, J.S. (2017): Nicotine stabilization in composite sodium alginate based wafers and films for nicotine replacement therapy. *Carbohydrate Polymers*, **155**, 78-88.
- O'Brien, A.P. (2013): MERGER WAVE. *Routledge Handbook of Major Events in Economic History*, 32.
- Paderni, C., Compilato, D., Giannola, L.I. and Campisi, G. (2012): Oral local drug delivery and new perspectives in oral drug formulation. *Oral Surgery, Oral Medicine, Oral Pathology And Oral Radiology*, **114**, e25-e34.
- Pani, N.R. and Nath, L.K. (2014): Development of controlled release tablet by optimizing HPMC: Consideration of theoretical release and RSM. *Carbohydrate Polymers*, **104**, 238-245.
- Pastore, M.N., Kalia, Y.N., Horstmann, M. and Roberts, M.S. (2015): Transdermal patches: history, development and pharmacology. *British Journal Of Pharmacology*.
- Patel, V., Prajapati, B. and Patel, M. (2007): Design and characterization of chitosan-containing mucoadhesive buccal patches of propranolol hydrochloride. *Acta Pharmaceutical*, **57**, 61-72.

- Patel, V.F., Liu, F. and Brown, M.B. (2011): Advances in oral transmucosal drug delivery. *Journal of Controlled Release*, **153**, 106-116.
- Pavlidou, S. and Papaspyrides, C.D. (2008): A review on polymer-layered silicate nanocomposites. *Progress in Polymer Science (Oxford)*, **33**, 1119-1198.
- Pawar, H.V., Boateng, J.S., Ayensu, I. and Tetteh, J. (2014): Multifunctional Medicated Lyophilised Wafer Dressing for Effective Chronic Wound Healing. *Journal Of Pharmaceutical Sciences*, **103**, 1720-1733.
- Pawar, H.V., Tetteh, J. and Boateng, J.S. (2013): Preparation, optimisation and characterisation of novel wound healing film dressings loaded with streptomycin and diclofenac. *Colloids and Surfaces B: Biointerfaces*, **102**, 102-110.
- Perioli, L., Ambrogi, V., Rubini, D., et al. (2004): Novel mucoadhesive buccal formulation containing metronidazole for the treatment of periodontal disease. *Journal of Controlled Release*, **95**, 521-533.
- Pongjanyakul, T., Khunawattanakul, W. and Puttipipatkachorn, S. (2009): Physicochemical characterizations and release studies of nicotine–magnesium aluminum silicate complexes. *Applied Clay Science*, **44**, 242-250.
- Pongjanyakul, T., Khunawattanakul, W., Strachan, C.J., Gordon, K.C., Puttipipatkachorn, S. and Rades, T. (2013): Characterization of chitosan–magnesium aluminum silicate nanocomposite films for buccal delivery of nicotine. *International Journal of Biological Macromolecules*, **55**, 24-31.
- Pongjanyakul, T., Priprem, A. and Puttipipatkachorn, S. (2005): Investigation of novel alginate–magnesium aluminum silicate microcomposite films for modified-release tablets. *Journal Of Controlled Release*, **107**, 343-356.
- Pongjanyakul, T. and Suksri, H. (2009): Alginate-magnesium aluminum silicate films for buccal delivery of nicotine. *Colloids and Surfaces B: Biointerfaces*, **74**, 103-113.
- Pongjanyakul, T. and Suksri, H. (2010): Nicotine-loaded sodium alginate–magnesium aluminum silicate (SA–MAS) films: Importance of SA–MAS ratio. *Carbohydrate Polymers*, **80**, 1018-1027.
- Prabaharan, M. and Gong, S. (2008): Novel thiolated carboxymethyl chitosan-g- β -cyclodextrin as mucoadhesive hydrophobic drug delivery carriers. *Carbohydrate Polymers*, **73**, 117-125.
- Rahamatullah Shaikh, T.R.R.S., Garland, M.J., Woolfson, A.D. and Donnelly, R.F. (2011): Mucoadhesive drug delivery systems. *Journal of Pharmacy and Bioallied Sciences*, **3**, 89.

- Rakić, V., Damjanović, L., Rac, V., Stošić, D., Dondur, V. and Auroux, A. (2010): The adsorption of nicotine from aqueous solutions on different zeolite structures. *Water Research*, **44**, 2047-2057.
- Regan, A.K., Promoff, G., Dube, S.R. and Arrazola, R. (2013): Electronic nicotine delivery systems: adult use and awareness of the 'e-cigarette' in the USA. *Tobacco control*, **22**, 19-23.
- Rhim, J.-W. (2004): Physical and mechanical properties of water resistant sodium alginate films. *LWT-Food Science and Technology*, **37**, 323-330.
- Riggleman, R.A., Lee, H.-N., Ediger, M.D. and De Pablo, J.J. (2007): Free volume and finite-size effects in a polymer glass under stress. *Physical Review Letters*, **99**, 215501.
- Rioux, L.E., Turgeon, S.L. and Beaulieu, M. (2007): Characterization of polysaccharides extracted from brown seaweeds. *Carbohydrate Polymers*, **69**, 530-537.
- Riss, T.L., Moravec, R.A., Niles, A.L., Benink, H.A., Worzella, T.J. and Minor, L. (2015): Cell viability assays.
- Rojtanatanya, S., & Pongjanyakul, T. (2010): Propranolol–magnesium aluminum silicate complex dispersions and particles: Characterization and factors influencing drug release. *International journal of pharmaceutics*, **383**(1), 106-115.
- Rong, L., Frontera, A.T. and Benbadis, S.R. (2014): Tobacco smoking, epilepsy, and seizures. *Epilepsy & Behavior*, **31**, 210-218.
- Rowe, R.C., Sheskey, P.J., Owen, S.C. and American Pharmacists, A. (2006): *Handbook of Pharmaceutical Excipients*. Pharmaceutical Press.
- Ruff, L.K., Volmer, T., Nowak, D. and Meyer, A. (2000): The economic impact of smoking in Germany. *European Respiratory Journal*, **16**, 385-390.
- S Boateng, J., C Mitchell, J., Pawar, H. and Ayensu, I. (2014): Functional characterisation and permeation studies of lyophilised thiolated chitosan xerogels for buccal delivery of insulin. *Protein And Peptide Letters*, **21**, 1163-1175.
- Salamat-Miller, N., Chittchang, M. and Johnston, T.P. (2005): The use of mucoadhesive polymers in buccal drug delivery. *Advanced Drug Delivery Reviews*, **57**, 1666-1691.
- Salústio, P.J., Feio, G., Figueirinhas, J.L., Cabral-Marques, H.M., Costa, P.C. and Pinto, J.F. (2012): Release profile of ibuprofen in β -cyclodextrin complexes from two different solid dosage forms. *Powder Technology*, **221**, 245-251.
- Sankar, V., Hearnden, V., Hull, K., et al. (2011): Local drug delivery for oral mucosal diseases: challenges and opportunities. *Oral Diseases*, **17**, 73-84.

- Sattar, M., Hadgraft, J. and Lane, M.E. (2015): Preparation, characterization and buccal permeation of naratriptan. *International Journal of Pharmaceutics*, **493**, 146-151.
- Sattar, M., Sayed, O.M. and Lane, M.E. (2014): Oral transmucosal drug delivery – Current status and future prospects. *International Journal of Pharmaceutics*, **471**, 498-506.
- Services, U.S.D.o.H.a.H. (2004): The health consequences of smoking: a report of the Surgeon General. Atlanta, GA: US Department of Health and Human Services, Centers for Disease Control and Prevention, National Center for Chronic Disease Prevention and Health Promotion, Office on Smoking and Health, **62**.
- Services, U.S.D.o.H.a.H. (2006): The health consequences of involuntary exposure to tobacco smoke: a report of the Surgeon General. Atlanta, GA: US Department of Health and Human Services, Centers for Disease Control and Prevention, Coordinating Center for Health Promotion, National Center for Chronic Disease Prevention and Health Promotion, Office on Smoking and Health, **709**.
- Services, U.S.D.o.H.a.H. (2014): The health consequences of smoking—50 years of progress: a report of the Surgeon General. Atlanta, GA: US Department of Health and Human Services, Centers for Disease Control and Prevention, National Center for Chronic Disease Prevention and Health Promotion, Office on Smoking and Health, **17**.
- Shiffman, S., Elash, C. A., Paton, S. M., Gwaltney, C. J., Paty, J. A., & Clark, D. B. (2000). Comparative efficacy of 24-hour and 16-hour transdermal nicotine patches for relief of morning craving. *Addiction*, 95(8), 1185-1195.
- Shiffman, S., Gwaltney, C.J., Balabanis, M.H., et al. (2002): Immediate antecedents of cigarette smoking: an analysis from ecological momentary assessment. *Journal Of Abnormal Psychology*, **111**, 531.
- Shoib, M.H., Tazeen, J., Merchant, H.A. and Yousuf, R.I. (2006): Evaluation of drug release kinetics from ibuprofen matrix tablets using HPMC. *Pakistan Journal of Pharmaceutical Sciences*, **19**, 119-124.
- Shojaei, A.H. (1998): Buccal mucosa as a route for systemic drug delivery: a review. *J Pharm Pharm Sci*, **1**, 15-30.
- Siepmann, J. and Peppas, N.A. (2012): Modeling of drug release from delivery systems based on hydroxypropyl methylcellulose (HPMC). *Advanced Drug Delivery Reviews*, **64**, **Supplement**, 163-174.
- Silagy, C., Lancaster, T., Stead, L., Mant, D. and Fowler, G. (2004): Nicotine replacement therapy for smoking cessation. *The Cochrane Library*.
- Singhvi, G. and Singh, M. (2011): Review: in-vitro drug release characterization models. *Int J Pharm Stud Res*, **2**, 77-84.

- Smart, J. (2015): Principles of Bioadhesion. *Bioadhesion and Biomimetics: From Nature to Applications*, 3.
- Smart, J.D. (2005): The basics and underlying mechanisms of mucoadhesion. *Advanced Drug Delivery Reviews*, **57**, 1556-1568.
- Sosnik, A., das Neves, J. and Sarmiento, B. (2014): Mucoadhesive polymers in the design of nano-drug delivery systems for administration by non-parenteral routes: A review. *Progress in Polymer Science*, **39**, 2030-2075.
- Stead, L.F., Perera, R., Bullen, C., et al. (2012): Nicotine replacement therapy for smoking cessation. *The Cochrane Library*.
- Stead, L.F., Perera, R., Bullen, C., Mant, D. and Lancaster, T. (2008): Nicotine replacement therapy for smoking cessation. *The Cochrane Library*.
- Steinberg, M.L., Williams, J.M. and Ziedonis, D.M. (2004): Financial implications of cigarette smoking among individuals with schizophrenia. *Tobacco Control*, **13**, 206-206.
- Stuber, J., Galea, S. and Link, B.G. (2008): Smoking and the emergence of a stigmatized social status. *Social Science & Medicine*, **67**, 420-430.
- Sudhakar, Y., Kuotsu, K. and Bandyopadhyay, A.K. (2006): Buccal bioadhesive drug delivery — A promising option for orally less efficient drugs. *Journal of Controlled Release*, **114**, 15-40.
- Swamy, M. and Ramaraj, B. (2009): Thermal and morphological properties of SA/HPMC blends. *Journal of Applied Polymer Science*, **112**, 2235-2240.
- Tang, J.L., Law, M. and Wald, N. (1994): How effective is nicotine replacement therapy in helping people to stop smoking? *Bmj*, **308**, 21-26.
- Tavss, E.A., Gaffar, A. and King, W.J. (1984): Studies on the formation of electrostatic complexes between benzethonium chloride and anionic polymers. *Journal Of Pharmaceutical Sciences*, **73**, 1148-1152.
- Taylor Jr, D.H., Hasselblad, V., Henley, S.J., Thun, M.J. and Sloan, F.A. (2002): Benefits of smoking cessation for longevity. *American Journal Of Public Health*, **92**, 990-996.
- Tønnesen, H.H. and Karlsen, J. (2002): Alginate in Drug Delivery Systems. *Drug Development and Industrial Pharmacy*, **28**, 621-630.
- Uddin, M.J., Scoutaris, N., Klepetsanis, P., Chowdhry, B., Prausnitz, M.R. and Douroumis, D. (2015): Inkjet printing of transdermal microneedles for the delivery of anticancer agents. *International Journal Of Pharmaceutics*, **494**, 593-602.

- Ugwoke, M.I., Agu, R.U., Verbeke, N. and Kinget, R. (2005): Nasal mucoadhesive drug delivery: Background, applications, trends and future perspectives. *Advanced Drug Delivery Reviews*, **57**, 1640-1665.
- van Meerloo, J., Kaspers, G.J.L. and Cloos, J. (2011): Cell sensitivity assays: the MTT assay. *Cancer cell culture: methods and protocols*, 237-245.
- Vieira, M. G. A., da Silva, M. A., dos Santos, L. O., & Beppu, M. M. (2011): Natural-based plasticizers and biopolymer films: A review. *European Polymer Journal*, **47**, 254-263.
- Vinayak, V., Annigeri, R.G., Patel, H.A. and Mittal, S. (2013): Adverse affects of drugs on saliva and salivary glands. *Journal of Orofacial Sciences*, **5**, 15.
- Weidner, J. (2002): A novel nasal nicotine formulation for smoking cessation. *Drug Discovery Today*, **7**, 833-835.
- Wittaya-areekul, S., Krueenate, J. and Prahsarn, C. (2006): Preparation and in vitro evaluation of mucoadhesive properties of alginate/chitosan microparticles containing prednisolone. *International Journal Of Pharmaceutics*, **312**, 113-118.
- Wu, J., Yang, C., Rong, Y. and Wang, Z. (2012): Preparation and Nutritional Characterization of Perilla Chewable Tablet. *Procedia Engineering*, **37**, 202-207.
- Xiao, Q., Gu, X. and Tan, S. (2014): Drying process of sodium alginate films studied by two-dimensional correlation ATR-FTIR spectroscopy. *Food Chemistry*, **164**, 179-184.
- Yang, M.Y., Chan, J.G.Y. and Chan, H.-K. (2014): Pulmonary drug delivery by powder aerosols. *Journal of Controlled Release*.
- Zeng, N., Mignet, N., Dumortier, G., et al. (2015): Poloxamer bioadhesive hydrogel for buccal drug delivery: Cytotoxicity and trans-epithelial permeability evaluations using TR146 human buccal epithelial cell line. *International Journal of Pharmaceutics*, **495**, 1028-1037.
- Zorin, S., Kuylenstierna, F. and Thulin, H. (1999): *In vitro* test of nicotine's permeability through human skin. Risk evaluation and safety aspects. *Annals of Occupational Hygiene*, **43**, 405-413.
- İkinci, G., Şenel, S., Wilson, C.G. and Şumnu, M. (2004): Development of a buccal bioadhesive nicotine tablet formulation for smoking cessation. *International Journal of Pharmaceutics*, **277**, 173-178.
- Şenel, S. and Hıncal, A.A. (2001): Drug permeation enhancement via buccal route: possibilities and limitations. *Journal of Controlled Release*, **72**, 133-144.

CHAPTER 9: APPENDIX

APPENDIX A: List of publications

1. **Okeke O.C.**, Boateng, J.S., (2017). Nicotine stabilization in composite HPMC-sodium alginate wafers for nicotine replacement therapy. *Carbohydrate Polymers* 155, 78-88.
2. **Okeke, O. C.**, & Boateng, J. S. (2016). Composite HPMC and sodium alginate based buccal formulations for nicotine replacement therapy. *International Journal of Biological Macromolecules*, 91, 31-44.
3. Boateng, J.S., **Okeke, O.**, & Khan, S. (2015). Polysaccharide based formulations for mucosal drug delivery: a review. *Current Pharmaceutical Design*, 21(33), 4798-4821.
4. Boateng, J.S., Burgos-Amador, R., **Okeke, O.**, & Pawar, H. (2015). Composite alginate and gelatin based bio-polymeric wafers containing silver sulfadiazine for wound healing. *International Journal of Biological Macromolecules*, 79, 63-71.
5. Boateng, J.S., & **Okeke, O.** (2014). Chitosan-based films for the sustained release of peptides: a new era in buccal delivery? *Therapeutic Delivery*, 5(5), 497-500.

APPENDIX B: List of abstract and posters from conference proceedings

1. **Obinna Okeke**, Joshua Boateng. (2016). Functional Properties of Mucoadhesive Composite Wafer and Film for Buccal Nicotine Replacement Therapy (NRT). Academy of Pharmaceutical Sciences 7th APS International PharmSci 2016. Technology and Innovation Centre, University of Strathclyde, Glasgow
2. **Obinna Okeke**, Joshua Boateng. (2016). Comparative Study of Functional Properties and Stability Studies of Wafers and Film for Buccal Delivery of Nicotine. Proceedings of the American Association of Pharmaceutical Scientists (AAPS) Annual Meeting and Exposition, Denver, Colorado, November 2015.
3. **Obinna Okeke**, Joshua Boateng. (2015). Nicotine Stabilization in mucoadhesive composite wafers for buccal nicotine replacement therapy (NRT). Academy of Pharmaceutical Sciences UKPHARMSCI Conference, 2015. Nottingham Conference Centre, UK.
4. **Obinna Okeke**, Joshua Boateng. (2015). Development of hydropropylmethylcellulose based composite wafers for buccal delivery of nicotine. Proceedings of the American Association of Pharmaceutical Scientists (AAPS) Annual Meeting and Exposition, Orlando, Florida, Oct 2015, W4055.
5. **Obinna Okeke**, Joshua Boateng. (2015). Composite hydroxypropylmethyl cellulose based films and wafers for buccal drug delivery. Academy of Pharmaceutical Sciences UKPHARMSCI Conference, 2015. Nottingham Conference Centre, UK.
6. **Obinna Okeke**, Joshua Boateng. (2014). Hydroxypropyl methylcellulose based film with sodium alginate for buccal drug delivery system. Academy of Pharmaceutical Sciences UKPHARMSCI Conference, 2014. Hertfordshire University, UK.

APENDIX C: Conference posters

Comparative Study of Functional Properties and Stability Studies of Wafers and Film for Buccal Delivery of Nicotine.

O.C. Okeke, J.S. Baskin
 Department of Pharmaceutical, Chemical & Environmental Sciences, Faculty of Engineering and Science, University of Greenwich, Medway Campus,
 Central Avenue, Chatham Maritime, Kent ME4 4TB, UK
 O.C.Okeke@greenwich.ac.uk

2016 AAPS
 ANNUAL MEETING AND EXPOSITION
 NOVEMBER 15-17 2016
 COLLEGE CONVENTION CENTER, SANTA
Poster Number
AM-16-0701

Introduction

Buccal drug delivery of nicotine (NIC) has been recognised as an effective route for successful delivery of NIC with the most popularly used NIC replacement therapy formulations (such as chewing gum, buccal spray). Wafer and film dosage forms have been recognised as a novel dosage form for buccal drug delivery to improve the conventional NIC replacement therapy dosage forms. As a result of challenges such as volatility and oxidative degradation, materials such as magnesium aluminum silicate (MAS) and cation exchange resins have been utilised in different formulations to overcome these challenges. The purpose of this research was to develop and compare the functional properties as well as NIC stability in wafer and film formulations.

Results

Physicochemical properties
 Table 1: mechanical properties of Wafers and film formulation (n=3, ± SD).

Sample	Porosity (%)	Porosity to Puckiness Ratio	Tensile strength (N/cm ²)	Tensile strength (lb/in ²)	Pliability at break (%)
MAS wafer	62.45 ± 6.85	1.18 ± 0.15	-	-	-
MAS film	-	-	12.30 ± 2.77	5.80 ± 0.68	22.50 ± 3.87

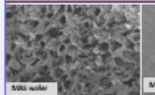


Figure 1: SEM images of MAS wafers and film

Results

NIC assay content

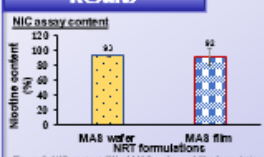


Figure 3: NIC content (%) of MAS wafer and film formulation (n=3, ± SD).

Both formulation however demonstrated (Figure 3) a high NIC loading with a drug assayed content of 93±0.40% for wafer formulation and 92±11.82% for film formulation. This implies less volatility and oxidative degradation of NIC in the presence of MAS.

Results

Stability



Figure 6: Stability curve of nicotine content in MAS film over 8 months/ time period (n=3, ± SD).

Water formulation demonstrated a better stability of NIC within 6 months (Figure 5) at room temperature (25°C) in comparison to film formulation which demonstrated a very rapid decrease in NIC content at both room temperature (25°C) and extreme temperature (40°C) (Figure 6). This is as a result of less exposure of NIC to volatility in wafer than film formulation.

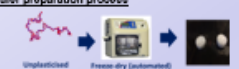
Methods

NIC (0.2%) loaded polymeric gel formulations containing HPMC (1.25% w/v), Sodium alginate (SA) (0.75% w/v) and glycerol (2% w/v, for film) incorporated with MAS (0.25% w/v) were prepared. Gels (1g of gel per well) were poured into 24 well moulds (diameter: 15.5mm) and freeze dried using a Virtis Advantage XL 70 freeze dryer to obtain wafers. Films were prepared by solvent evaporation in a Petri-dish. The formulations were characterised for mechanical properties, swelling capacity, drug loading (assay content) and drug loading (assay content) stability (HPLC) and in vitro drug dissolution (HPLC).

Film preparation process



Wafer preparation process



Results

Swelling capacity

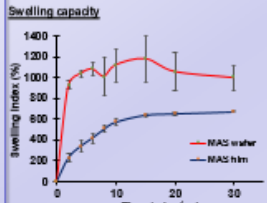


Figure 2: Swelling profiles (%) of MAS-wafers and film (n=3, ± SD).

MAS wafer (swelling index: 928-1119%) demonstrated a higher swelling profile as compared to MAS film (swelling index: 229-472%) as a result of its sponge-like structure which allows rapid inflow of solvent.

Results

NIC In vitro dissolution profile

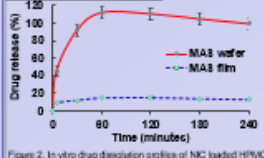


Figure 2: In vitro drug dissolution profiles of NIC loaded HPMC-SA-MAS wafers and films (n=3, ± SD).

Figure 2 showed rapid NIC release from MAS wafers and slow release from MAS films with both release profiles corresponding to their swelling profiles.

Conclusion

Composite HPMC-SA-MAS wafer and film formulation have been developed and can be utilised as a buccal nicotine replacement therapy. The use of MAS as an adsorbent can be a promising approach for stabilising nicotine in wafers and film formulation. However, the method of formulation can play a vital role in maintaining the stability of NIC in formulation. Wafer demonstrated better stability of NIC in nicotine than film formulation due to its process procedure which involves a very low temperature. Furthermore, HPMC-SA-MAS wafer and film can be utilised as rapid and slow release drug delivery system respectively as a result of their functional properties.

References

1. Mathews, A. D., Ayub, M. J., Humphrey, H. N., Stevens, and G. M. *Comparison of in vitro drug release studies of polymeric hydrogels wafers and solvent-cast films using ginseng as a model soluble drug* International journal of pharmaceutics, 378 (2009) 66-72.
2. T. Pongyanyai, and H. Sakai, "Alginata-magnesium aluminum silicate films for buccal delivery of nicotine" Colloids and Surface B: Biointerfaces, 74 (2009) 103-113.



Functional Properties of Mucoadhesive Composite Wafer and Film for Buccal Nicotine Replacement Therapy (NRT).



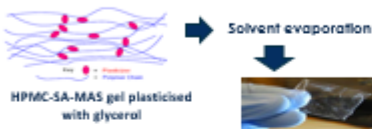
O. Okeke¹, J.S. Boateng¹

¹ Department of Pharmaceutical, Chemical & Environmental Sciences, Faculty of Engineering and Science, University of Greenwich, Medway Campus, Central Avenue, Chatham Maritime, Kent ME4 4TB, UK
O.O.okeke@greenwich.ac.uk

The difference in functional properties of composite HPMC and sodium alginate (SA) wafers and films such as drug release properties can be utilised in the delivery of nicotine (NIC). Magnesium aluminium silicate (MAS) was introduced into both formulations to enhance NIC stability. The results demonstrate improved NIC loading efficiency within both formulations by MAS incorporation as well as yielding different functional characteristics.

MATERIALS AND METHODS

FILM



WAFER



Formulation

NIC (0.2g) loaded polymeric gel formulations containing HPMC (1.25% w/v) and SA (0.75% w/v) incorporating MAS (0.25% w/v) were prepared. Glycerol (GLY) was used as a plasticizer to improve the mechanical properties of films. Gels (1g per well) were poured into 24 well moulds (diameter 15.5mm) and freeze dried using a Virtis Advantage XL 70 freeze dryer to obtain wafers. Films were prepared by solvent evaporation in a Petri-dish.

Characterisation

The formulations were characterised for internal/surface morphology, mechanical properties, swelling capacity, drug loading (assay content) and *in vitro* drug dissolution (HPLC).

Formulation composition

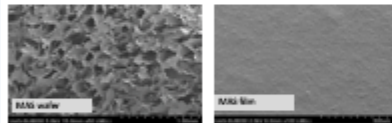
Sample name	HPMC (% w/v)	SA (% w/v)	MAS (% w/v)	GLY	NIC (g)
MAS wafer	1.25	0.75	0.25	-	0.20
MAS film	1.25	0.75	0.25	2.00	0.20

Gel properties

	Surface stickiness (g)	Stringiness (mm)	Gel strength (g)
MAS Gels	18.98 ± 1.64	0.88 ± 0.08	981.45 ± 112.59

MAS LOADED WAFER AND FILM CHARACTERIZATION

Scanning electron microscopy



Physico-mechanical properties

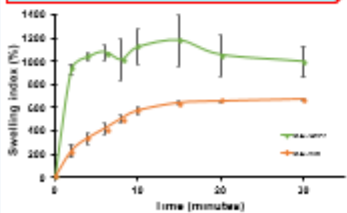
Sample name	Porosity (%)	Resistance to compression (N)	Young's modulus (N/mm ²)	Tensile strength (N/mm ²)	Elongation at break (%)
MAS wafer	62.45±0.95	1.19±0.15	-	-	-
MAS film	-	-	15,20±2.77	4.98±0.68	22.66±3.07

Swelling capacity

The swelling capacity of MAS wafer and film were determined by measuring the increase in the final diameter (mm) of the wafer/film. The swelling index (SI) was calculated using the following equation: $SI = \frac{D_f - D_d}{D_d} \times 100$. The wafer/film was placed in a beaker containing distilled water and allowed to swell for 24 hours. The swelling index was determined at 0, 5, 10, 15, 20, and 24 hours. The average swelling index was calculated for each formulation.

Swelling index = $\frac{D_f - D_d}{D_d} \times 100$

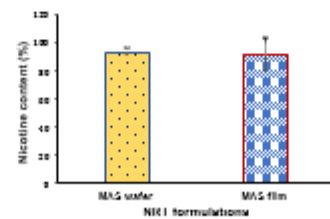
Where: D_f = final diameter of wafer/film
 D_d = diameter of wafer/film after drying



- Higher swelling profile in MAS wafer than MAS film
- Swelling driven by sponge-like structure and higher porosity.

NIC assay content

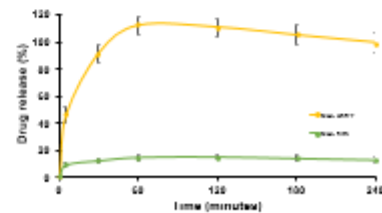
The amount of NIC (0.20g) loaded into each wafer and film was determined by measuring the amount of nicotine (NIC) released from the wafer/film. The nicotine content was determined using a HPLC method. The average nicotine content was calculated for each formulation.



- High NIC loading in MAS wafers and films
- Drug assay content above 90%
- Less volatility and oxidative degradation

NIC *in vitro* drug dissolution profile

In vitro drug dissolution of the MAS wafer and film were determined using a USP dissolution apparatus. The dissolution apparatus was filled with 250 ml of phosphate buffer (pH 6.8) with a paddle on the rotation. The MAS wafer and film were placed in the apparatus and allowed to dissolve. The drug release was determined at 0, 5, 10, 15, 20, 30, 45, 60, 90, 120, 180, and 240 minutes. The average drug release was calculated for each formulation.



- Rapid NIC release in MAS wafer; slower release in MAS film
- Drug release driven by water uptake (swelling profile)
- Release profile of MAS wafer and film followed Korsmeyer-Peppas equation.

Stabilisation of NIC using MAS in composite wafers and films can be a promising approach for buccal NRT. HPMC-SA-MAS wafers and films can also be utilised in both rapid and slow release drug delivery systems as a result of their unique functional properties.

O. Okeke, K. H. Mofenson, A. D. J. L. Boateng, H. S. Boateng, and G. M. Boateng, "Stabilisation of nicotine in composite wafers and films for buccal nicotine replacement therapy," *International Journal of Pharmaceutics*, 579 (2019) 68-72.

O. Okeke, K. H. Mofenson, A. D. J. L. Boateng, H. S. Boateng, and G. M. Boateng, "Stabilisation of nicotine in composite wafers and films for buccal nicotine replacement therapy," *Colloid and Interface Science*, 546 (2019) 103-110.

HYDROPROPYLMETHYLCELLULOSE BASED COMPOSITE FILMS AND WAFERS FOR BUCCAL DRUG DELIVERY.

O. Okeke¹, J.S. Boateng² Department of Pharmaceutical, Chemical and Environmental Sciences, Faculty of Engineering and Science, University of Greenwich, Chatham Maritime, Kent, UK, ME4 4TB
(O.C.Okeke@gre.ac.uk)

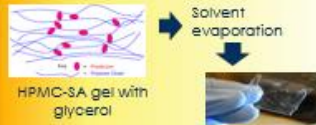
Introduction

HPMC is a hydrophilic polymer, widely used in pharmaceutical dosage forms including mucoadhesive formulations [1]. Wafers and films have been recognised as appropriate dosage form for buccal drug delivery [2].

The aim of this project is to develop composite dosage forms (films and wafers) via the buccal mucosa.

Method

Film



Wafers



Formulation

Gels (2% w/v) containing different ratios (2:0, 7:1, 3:1 and 5:3) of HPMC and sodium alginate (SA) respectively, were prepared by dissolving the polymers in deionised water with NiC. Glycerol (2% w/v) was used for films.

Characterisation

The formulations were characterised for tensile properties (films), hardness (wafers), SEM, and swelling properties

Results and discussion

The HPMC-SA composite films showed constant tensile strength in BK and DL films, decrease in elastic modulus and increase in % elongation at break with increase in SA content which can be attributed to hydrogen bonding between SA and HPMC.

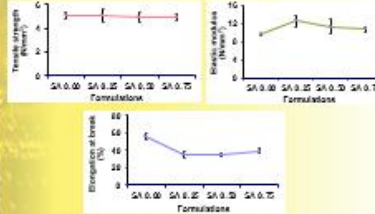


Fig. 1. Tensile properties of HPMC-SA films at different concentration ratios of both polymers.

Hardness decreased at the lowest concentration of SA but gradually increased as SA increased (Fig. 2). SEM showed a sponge-like porous wafers due to the freeze drying technique used (Fig. 3a) whilst the films showed a smooth topography (Fig. 3b). Fig. 4 shows higher swelling index (%) in optimised HPMC-SA wafers compared with HPMC only wafers and films and optimised HPMC-SA film. This is due to the wafer porosity compared to film thus increasing the hydration and resulting in higher swelling index.

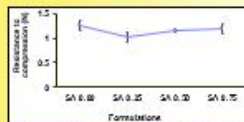


Fig. 2. Hardness profiles of HPMC-SA wafer at different concentration ratios of both polymers.

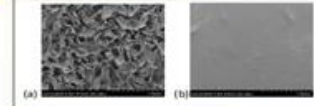


Fig. 3. SEM (x50) images of optimized (a) wafer and (b) film.

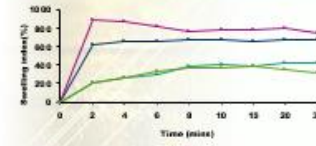


Fig. 4. Swelling profiles of HPMC wafers and films

CONCLUSIONS

Composite films and wafers with HPMC optimised with SA show potential as buccal drug delivery devices. Wafers which were porous due to the freeze-drying process showed better swelling rate and capacity which are expected to have a direct impact on drug release profiles.

REFERENCES

- [1] J. Siermann and N. A. Peppas, "Modeling of drug release from delivery systems based on hydroxypropyl methylcellulose (HPMC)." *Adv. Drug Del. Rev.* 48 (2001) 139 - 157.
- [2] J. K. Lam, Y. Xu, A. Worsley, I. C. Wong, "Oral transmucosal drug delivery for pediatric use." *Adv. Drug Del. Rev.* 73 (2013) 50 - 62.

NICOTINE STABILIZATION IN MUCOADHESIVE COMPOSITE WAFERS FOR BUCCAL NICOTINE REPLACEMENT THERAPY (NRT).

O. Okeke¹, J.S. Boateng¹, Department of Pharmaceutical, Chemical and Environmental Sciences, Faculty of Engineering and Science, University of Greenwich, Chatham Maritime, Kent, UK, ME4 4TB
(O.C.Okeke@gre.ac.uk)

Introduction

The properties of nicotine (NIC) include volatility and oxidative degradation, which poses a challenge in its formulation development [1]. Materials such as cation exchange resins [2], cellulose powder [3] and magnesium aluminum silicate (MAS) [1] have been utilised in different formulations to overcome these challenges.

Method

Formulation technique



NIC loaded polymer gel formulations (total 2% w/v) contained HPMC (1.25% w/v) and SA (0.75% w/v) with different concentrations of MAS (0.00, 0.25, 0.50 and 0.75% w/v) were prepared. Gels were poured in a 24 well moulds (diameter 15.5mm) by weight 1g of gel per well in a well mould (24g of gel per well mould). Wafers were obtained by freeze drying using a Virtis Advantage XL 70 freeze dryer with automated freeze drying cycle. The wafers were characterised for 'hardness', mucoadhesion (texture analysis) and drug content (HPLC).

Fig. 1 demonstrated a consistency in hardness as MAS concentration in HPMC-SA-MAS wafers increased from 0.00 - 0.50% w/v but decreased at 0.75% w/v as a result of polymer network interruption by MAS.

Results and discussion

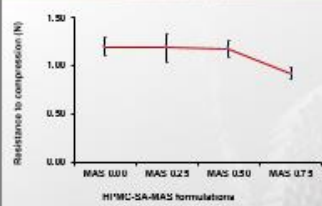


Fig. 1. Hardness studies of different MAS concentrations of NIC loaded HPMC-SA-MAS composite wafers.

Fig 2 demonstrated a decrease in peak adhesive force as MAS concentration increased in NIC loaded HPMC-SA-MAS wafers. The decrease in mucoadhesion of the wafers can be attributed to the amphoteric nature of MAS within the composite system. Fig 3 shows an increase in NIC content (loading) as MAS concentration increased. HPMC-SA-MAS wafers with lowest MAS concentration resulted in the highest NIC recovering (% drug loading content) within the formulation. The stabilization can be attributed to the ionic interaction of MAS and NIC as well as the hydrogen bond between NIC and SA.

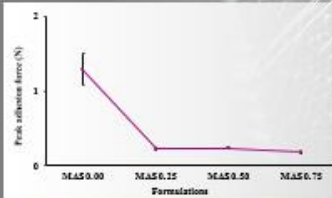


Fig. 2. Peak adhesive force of NIC loaded HPMC-SA-MAS composite wafers.

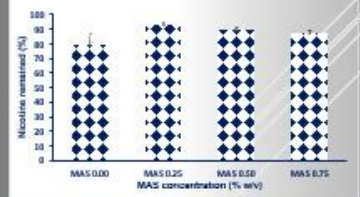


Fig. 3. Drug content of different MAS concentrations of NIC loaded HPMC-SA-MAS composite wafers.

CONCLUSIONS

Stabilisation of NIC using composite freeze-dried wafers containing HPMC, SA and MAS can be a promising potential as a buccal NRT. Though MAS loaded formulations showed a decrease in hardness and mucoadhesion it demonstrated an increased NIC content in formulation which fell within the USP specification.

ACKNOWLEDGMENTS

The authors are grateful to Mrs Devyani Amin for help with HPLC analysis.

REFERENCES

- [1] I. Pongpanyakul, and H. Sakrri, "Alginate-magnesium aluminum silicate films for buccal delivery of nicotine" Coll. Surf. B: Biointerf. 74 (2009) 103 - 113.
- [2] V. Rakic, L. Damjanovic, V. Rac, D. Stojic, V. Dondur, and A. Auresek, "The adsorption of nicotine from aqueous solutions on different zeolite structures" Water Res. 44 (2010) 2047 - 2057.
- [3] A. Mithranjan, A. P. Llagostera, R. Karmhan, M. Sussanne, and R.E.H., "Moisture sorption by cellulose powders of varying crystallinity" Int. J. Pharm. 269 (2004) 433 - 442.

HYDROXYLPROPYLMETHYLCELLULOSE AND SODIUM ALGinate BASED FILMS FOR BUCCAL MUCOSA DRUG DELIVERY

O. Okeke¹, J.S. Boateng¹.

¹ Department of Pharmaceutical, Chemical and Environmental Sciences, Faculty of Engineering and Science, University of Greenwich, Chatham Maritime, Kent, UK, ME4 4TB
(O.C.Okeke@gre.ac.uk)



INTRODUCTION

Hydroxypropylmethylcellulose (HPMC) is a hydrophilic polymer widely used in various delivery systems including mucoadhesive formulations [1]. Its mucoadhesive properties can be modified by using plasticizers and/or combining with other hydrophilic polymers [2].

MATERIALS AND METHODS

HPMC (2%w/v) gel was initially prepared using glycerol (GLY) (0-4%w/v) as plasticizer. The optimized plasticized gel was combined with sodium alginate (SA) in different ratios (HPMC: SA 2:0, 7:1, 3:1, 5:3 and 1:1). The films were obtained by pouring gels into Petri dishes (90mm) and drying at 40°C (18 hours). The tensile/mucoadhesive properties and surface morphology of the formulated films were investigated using a texture analyser and scanning electron microscope (SEM).

RESULTS AND DISCUSSION

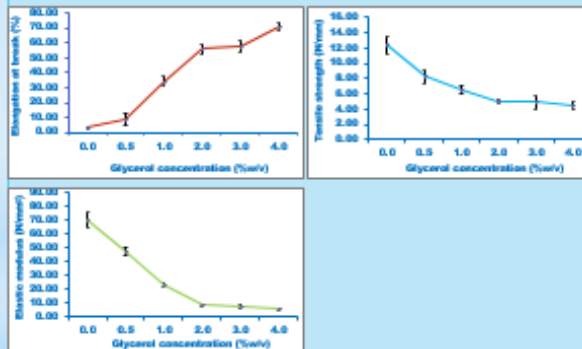


Fig. 1. Tensile profiles of HPMC films from gels with different GLY concentrations.

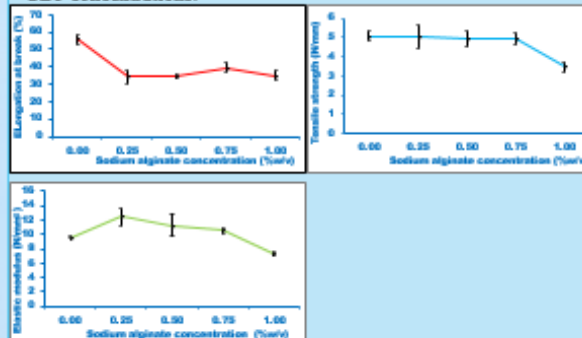


Fig. 2. Tensile profiles of HPMC-SA films showing effect of SA

Elongation at break of HPMC films increased while tensile strength and elastic modulus decreased with increase in GLY content (Fig. 1). Highly plasticised films were sticky and difficult to handle, while films with no GLY or low amounts were brittle. Therefore 2%w/v of GLY was selected as optimum plasticizer concentration.

SA decreased the elongation at break of the film, while tensile strength and elastic modulus remained fairly constant except HPMC: SA 1:1. Films with 1:1 ratio of HPMC: SA showed a sudden reduction in tensile strength compared to the other films with lower SA ratio (Fig. 2). SEM also showed irregularity on the surface of films with high GLY content (Fig. 3). Texture analysis showed increase in mucoadhesive properties of the composite films with increasing SA concentration.

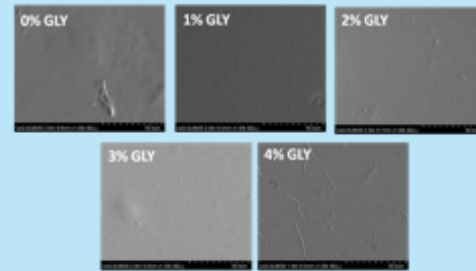


Fig. 3. SEM images (magnification x1000) of HPMC films with different concentrations of GLY (0 – 4% w/v).

% w/v	Peak adhesive force (PAF) (N)	Total work of adhesion (TWA) (Nmm)	Cohesiveness (mm)
SA 0.00	0.162±0.00	0.078±0.00	0.583±0.00
SA 0.25	0.176±0.02	0.148±0.01	0.947±0.02
SA 0.50	0.191±0.00	0.257±0.10	1.820±0.65
SA 0.75	0.227±0.02	0.308±0.09	1.512±0.40

CONCLUSIONS

The mechanical (tensile), mucoadhesive characteristics and surface morphology of HPMC films can be influenced by the concentration of GLY and SA. This can be utilised in improving the functional properties of HPMC based delivery systems for potential buccal drug delivery.

ACKNOWLEDGMENTS

The authors thank Dr Ian Slipper for the SEM analysis.

REFERENCES

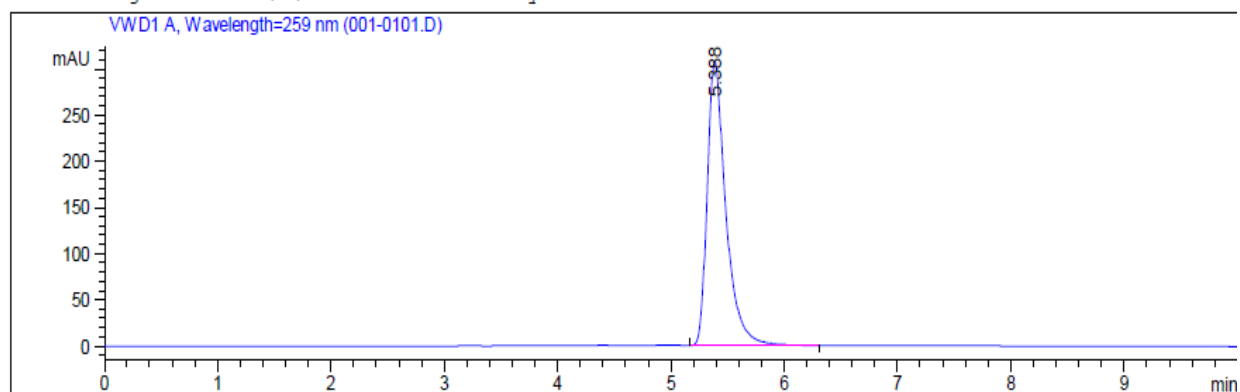
- [1] J. Siepmann and N.A. Peppas, "Modeling of drug release from delivery systems based on hydroxypropyl methylcellulose (HPMC)" Adv. Drug Del. Rev., 64 (2012) Supplement(0):163-174.
- [2] E. Karavas, E. Georgarakis and D. Bikiaris, "Application of PVP/HPMC miscible blends with enhanced mucoadhesive properties for adjusting drug release in predictable pulsatile chronotherapeutics." Eur. J. Pharm. Biopharm. 64 (2006) 115-126.

APPENDIX D: Sample Chromatograms

```

-----
Acq. Operator   : OBI                               Seq. Line :    1
Acq. Instrument : Instrument 9                       Location  : Vial 1
Injection Date  : 12/3/2015 6:22:39 PM             Inj       :    1
                                                    Inj Volume: 20.000 µl

Sequence File   : C:\Chem32\1\DATA\STABILITY WITH CALIBRATION 2015-12-03 18-21-22\STABILITY
                  WITH CALIBRATION.S
Method          : C:\CHEM32\1\DATA\STABILITY WITH CALIBRATION 2015-12-03 18-21-22\DEF_
                  LCNICOTINE.M (Sequence Method)
Last changed    : 12/3/2015 6:21:22 PM by OBI
  
```



```

=====
                          Area Percent Report
=====
  
```

```

Sorted By           :      Signal
Multiplier:         :      1.0000
Dilution:           :      1.0000
Use Multiplier & Dilution Factor with ISTDs
  
```

Signal 1: VWD1 A, Wavelength=259 nm

Peak #	RetTime [min]	Type	Width [min]	Area [mAU*s]	Height [mAU]	Area %
1	5.388	VB	0.1697	3515.04810	307.67166	100.0000

```
Totals :                3515.04810  307.67166
```